Empa
Materials Science and Technology

Scanning Probe Methods (SPM)

Hans J. Hug[1,2]
[1] Empa: Swiss Federal Laboratories for Material Testing and Research,
Laboratory for Nanoscale Materials Science
Überlandstrasse 129, CH-8600 Dübendorf, Switzerland
&
[2] NCCR on Nanoscale Science, Department of Physics,
University of Basel, Klingelbergstrasse 82, CH-4056 Basel, Switzerland

Contents 1

Contents 2

1.

Principles & Instrumentational Issues

The Scanning Probe Microscopy Family

Empa
Materials Science and Technology

Scanning Probe Microscopy (SPM)

- The starting point of SPM was the invention of the *scanning tunneling microscope* (STM) by G. Binnig and H. Rohrer in 1982 [1,2] (Nobel prize in physics in 1986).

The family present family of scanning probe microscopes is based on a variety of tip-sample interactions:

- The first and most important extension of the STM was the scanning force microscope (SFM) or atomic force microscope (AFM), invented in 1986 by Binnig, Quate, and Gerber [3].

- Most of the present scanning probe instrumentation is based on the AFM often combined with other techniques mapping/controlling properties not accessible by AFM.

Refs.: [1] G. Binnig and H. Rohrer et al. Helv. Phys. Acta 55, 726 (1982)
[2] G. Binnig and H. Rohrer et al. Phys. Rev. Lett. 50, 120 (1983)
[3] G. Binnig, C.F: Quate, CH. Gerber, Phys. Rev. Lett. 56, 930 (1986)
see also R. Wiesendanger and H.-J. Güntherodt, Vols. 20, 28, 29
Springer Series in Surface Science 1992, 1993, 1994 R. Colton et al., Wiley-VCM, Weinheim 1998

Block Diagram of an STM

Empa
Materials Science and Technology

Basic setup of an STM (but also any other type of SPM)

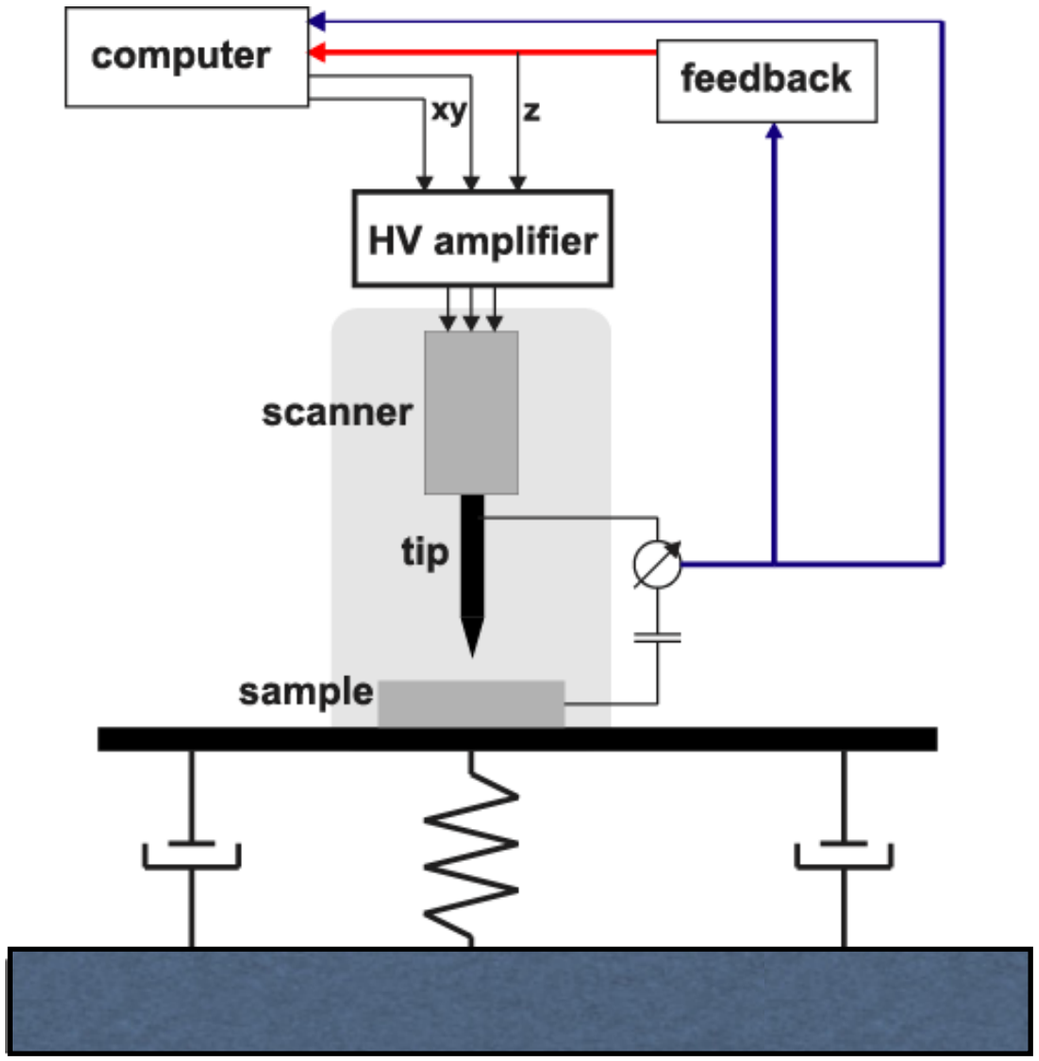

- tip-sample gap stability < 1pm in best instruments
  ➜ stiff, high resonance frequency instrument
  ➜ vibration isolation system
- tip can be scanned in x,y, z (tip-sample distance) with pm precision
  ➜ piezo electric scanners
- tip-sample interaction (tunnel current) is measured
  ➜ current amplifier for 1pA - 10nA range needed
  ➜ log I is used for the feedback
- PI-feedback adjusts z to keep log I constant
  ➜ maximum feedback speed depends on resonance frequency of instrument and bandwidth of current amplifier
  ➜ feedback speed & toleratable errors determine maximum scan speed.
- Computer controlled electronics is used for scan-generation, feeback, data recording, displaying and user GUI
- in other types of SPM other tip-surface interactions are used to control the tip-sample distance

In an STM typically two signals are acquired, namely the z-coordinate (topography) and the tunneling current, or more generally the measured tip sample interaction (error signal)

Vibration Isolation

Empa
Materials Science and Technology

Transfer Function of SPM
(harmonic oscillator transfer function)

$$T_{SPM}(\omega) = \frac{1}{1 - (\frac{\omega}{\omega_{SPM}})^2 + i\frac{\omega}{Q_{SPM}\omega_{SPM}}}$$

$$\omega_{SPM} => 1\,\mathrm{kHz} \quad \text{and} \quad Q_{SPM} < 10$$

not relevant

~~$x_T(t) = x_{SPM}(t) \cdot T_{SPM}(\omega)$~~

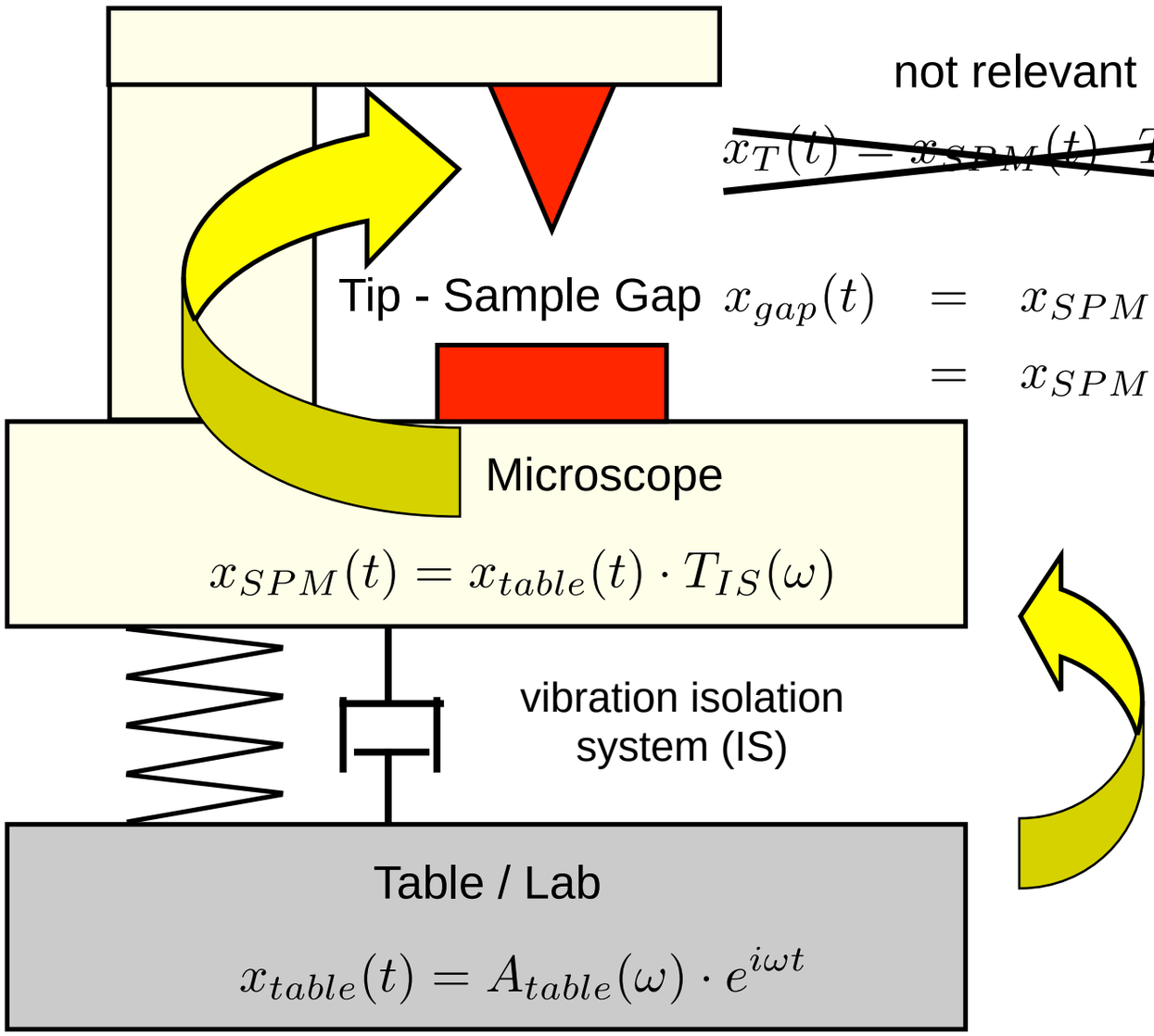

$$\begin{aligned} x_{gap}(t) &= x_{SPM}(t) \cdot T_{SPM}(\omega) - x_{SPM}(t) \\ &= x_{SPM}(t) \cdot [1 - T_{SPM}] \end{aligned}$$

Transfer Function of Table
(harmonic oscillator transfer function)

$$T_{IS}(\omega) = \frac{1}{1 - (\frac{\omega}{\omega_{IS}})^2 + i\frac{\omega}{Q_{IS}\omega_{IS}}}$$

$$\omega_{IS} = 1\,\mathrm{Hz} \quad \text{and} \quad Q_{IS} = 2$$

low resonance and Q required !
➜ good damping @ higher frequencies

Note: Use multiple damping stages for optimal results !

Ref.: O. Züger, H.P. Ott, and U. Dürig, Rev. Sci. Instrum. 63 (1992) 5634

1/2-Stage Vibration Isolation

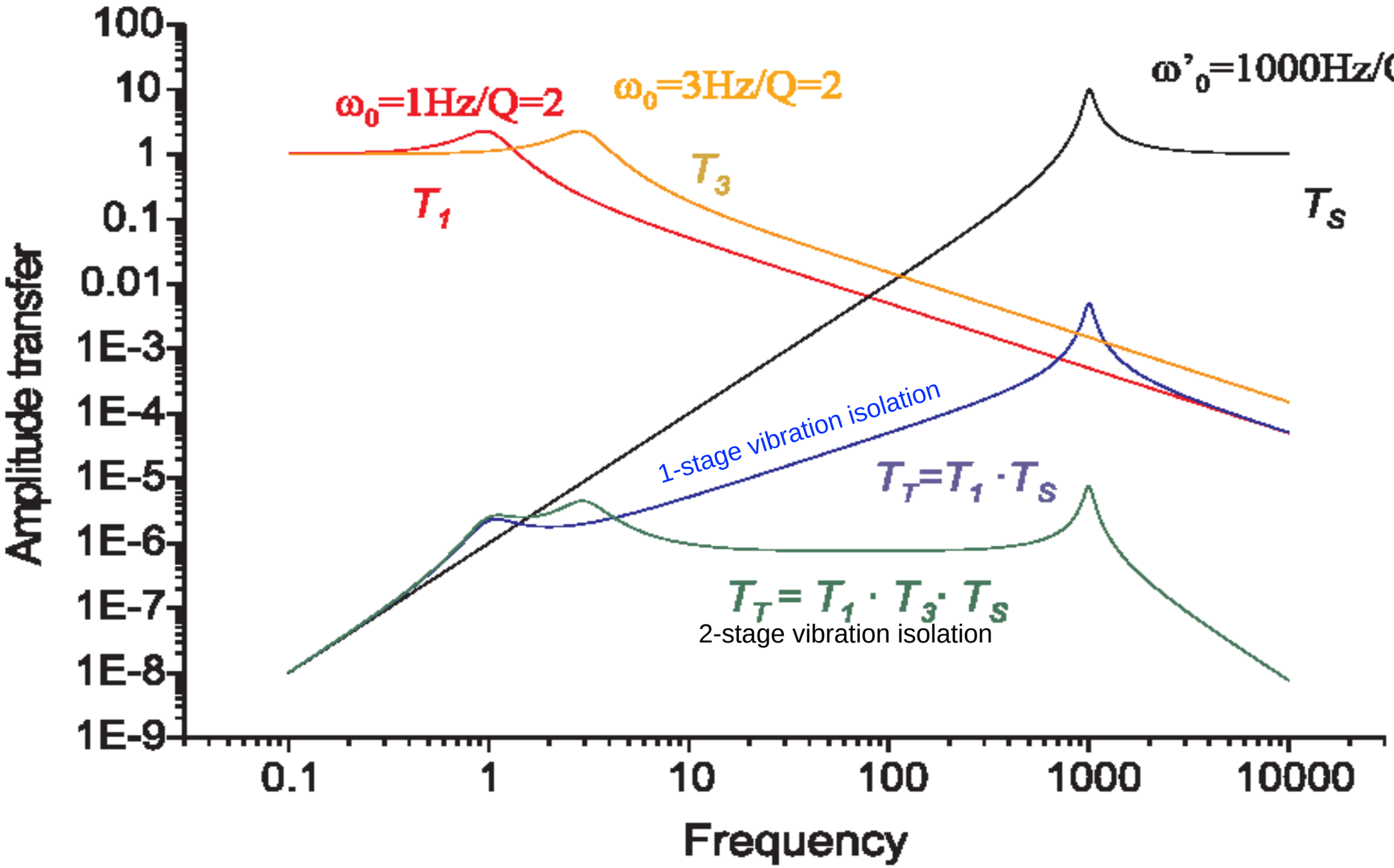

Only the double vibration isolation stage can provide sufficient isolation @ the resonance frequency of the microscope. Assume floor vibrations < 100nm.
Then the tip-sample vibration will be less than 10^{-3}nm !

Piezoelectric Actuators

Since the piezo effect exhibited by natural materials (e.g. quartz) is very small, polycrystalline ferroelectric ceramic materials such as barium titanate and lead zirconate titanate (PZT) with improved properties (e.g. PZT-5H: *d31*=-2.62Å/V) have been developed. These ferroelectric ceramics become piezoelectric when poled.

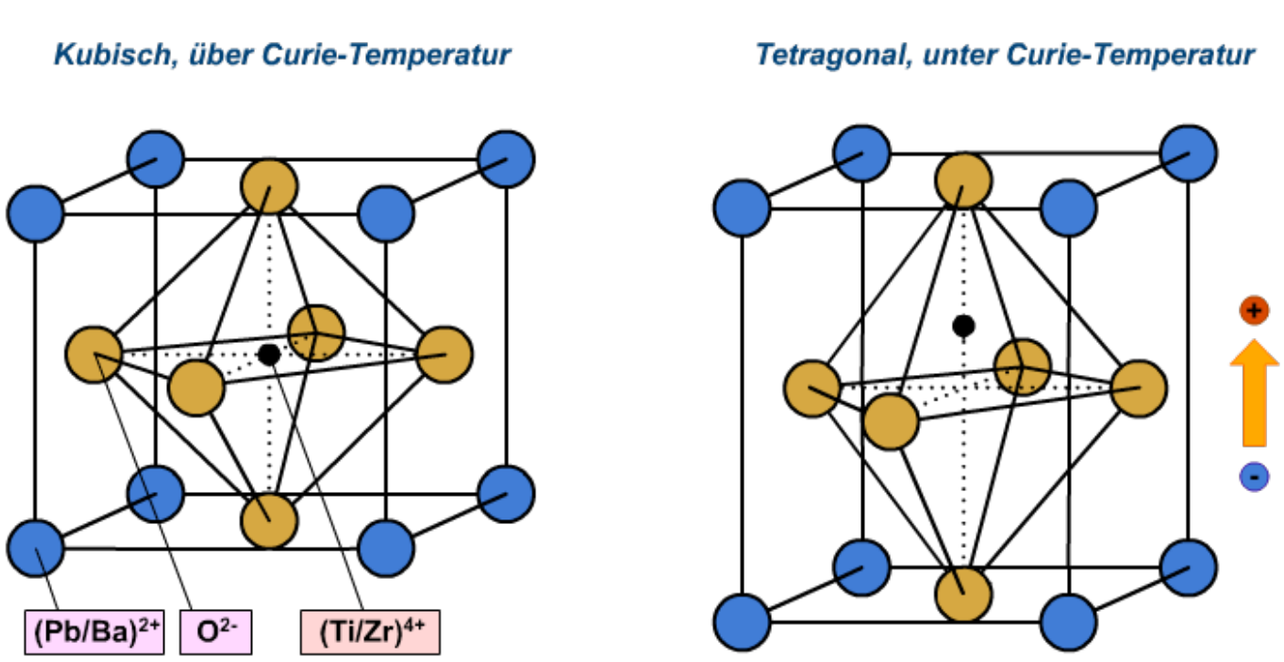

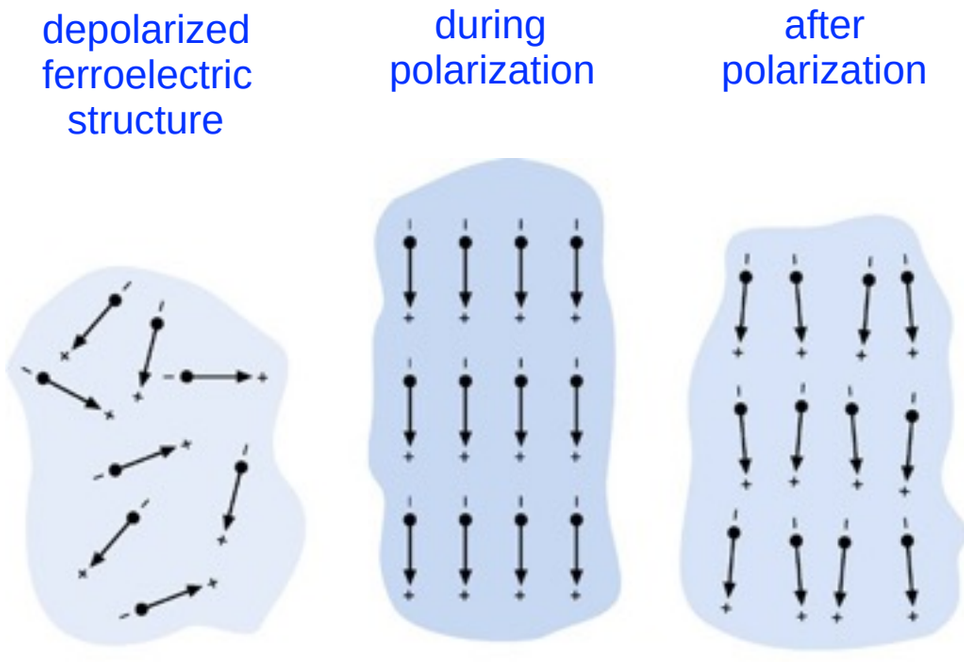

$$\Delta L = d_{31} \cdot L \cdot E$$

E eletric field, *L* lengths, ΔL change in length
d_{31} transversal piezoelectric coefficient

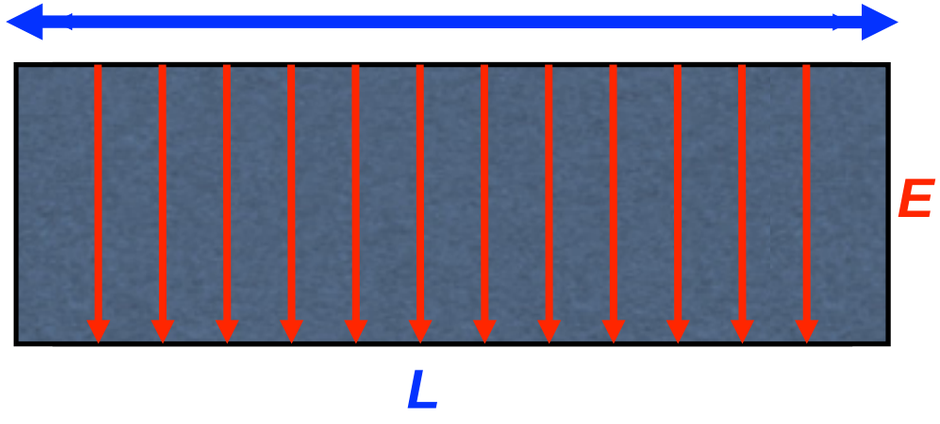

Stick-Slip Piezomotors

Empa
Materials Science and Technology

Mechanical Challenges

- Approach & Positioning
  - over distances of mm - cm
  - with <100nm precision

- high stiffness & high resonance frequency of the SPM

Principle slip-stick piezomotor

Implementation of a piezo motor in a low temperature SFM

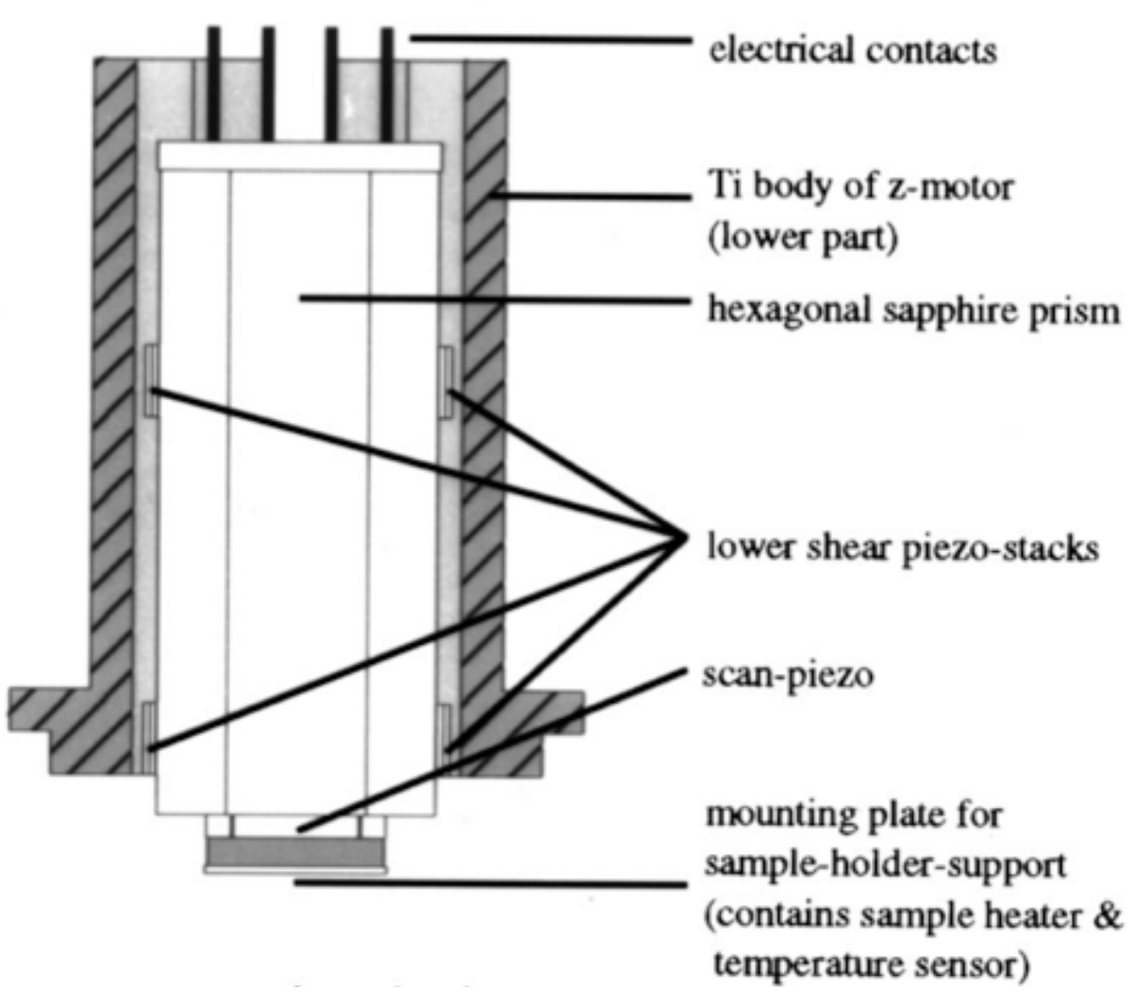

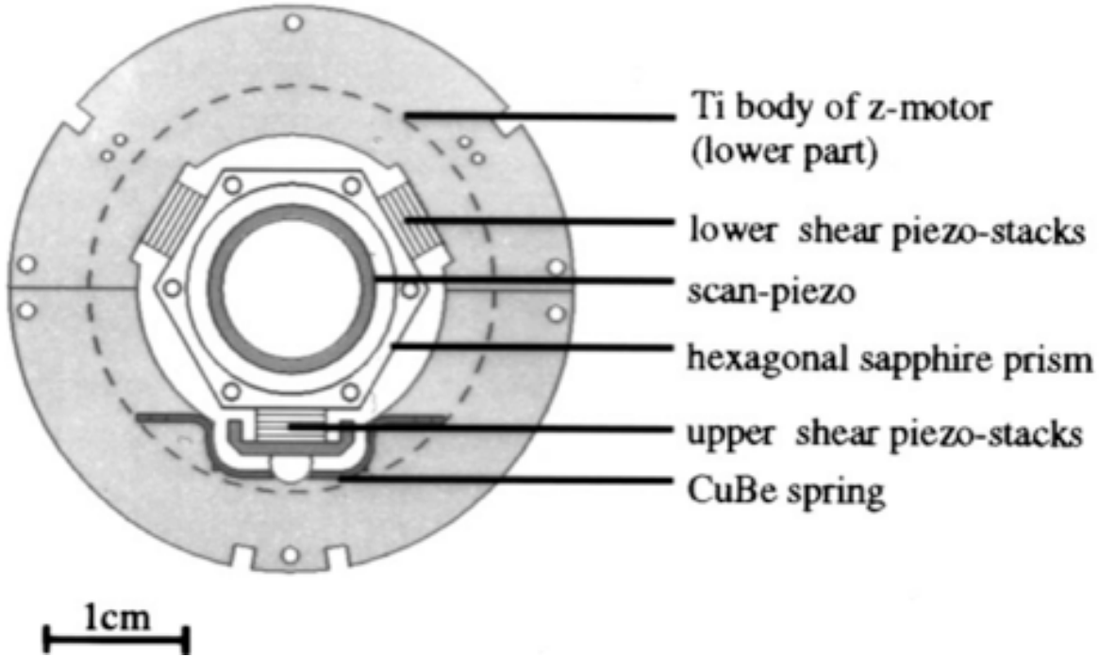

Tunneling Current Preamplifier or Current-Voltage Converter

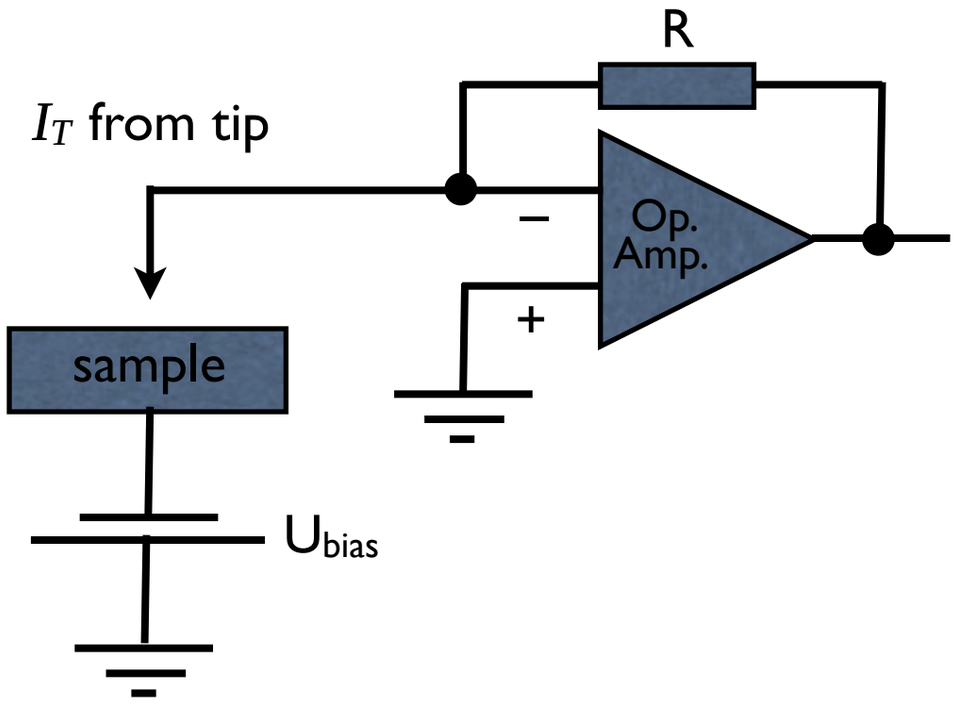

$U(I_T) = I_T * R$

typically 10^9 gain, i.e. I_T = 1nA ➜ 1V @ output

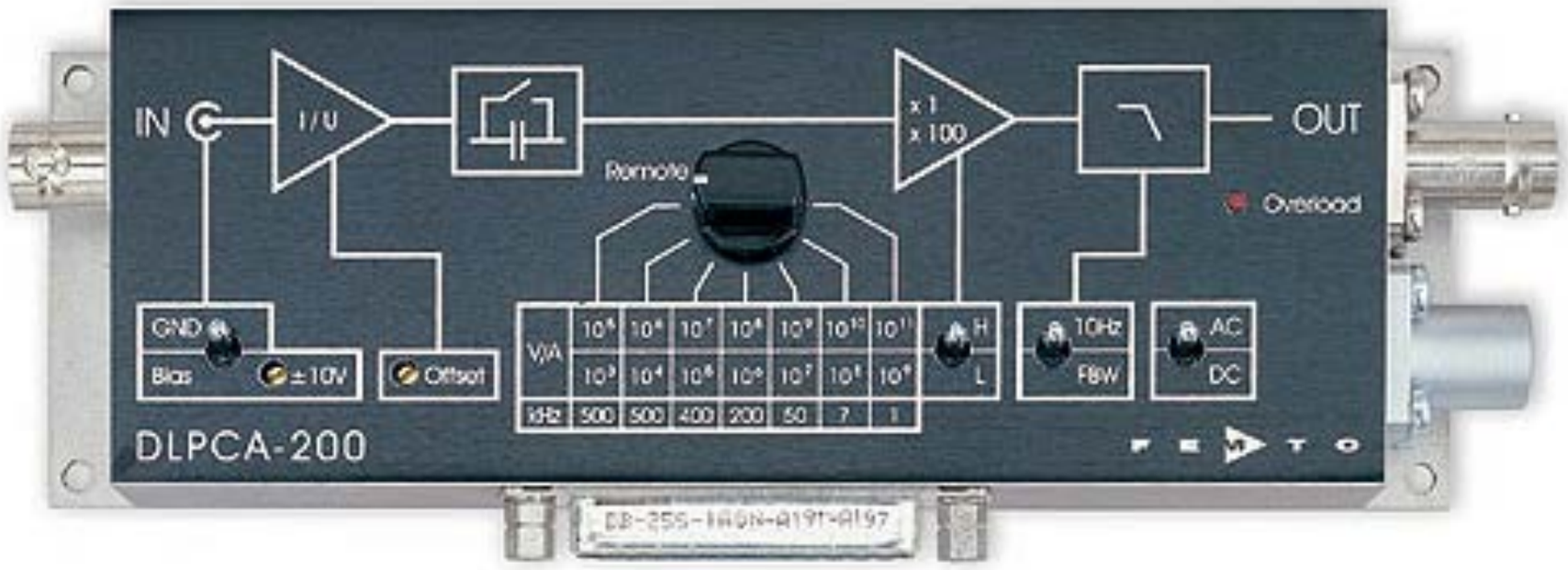

- **Transimpedance Gain from 10^3 to 10^{11} V/A**
- **Input Noise down to 4.3 fA/√Hz**
- **Bandwidth up to 500 kHz**
- **Rise Time down to 700 ns**
- **Adjustable Bias Voltage**
- **Manual and Remote Control**

PI(D)-Feedback

P: proportional gain, I: integral gain, D: differential gain

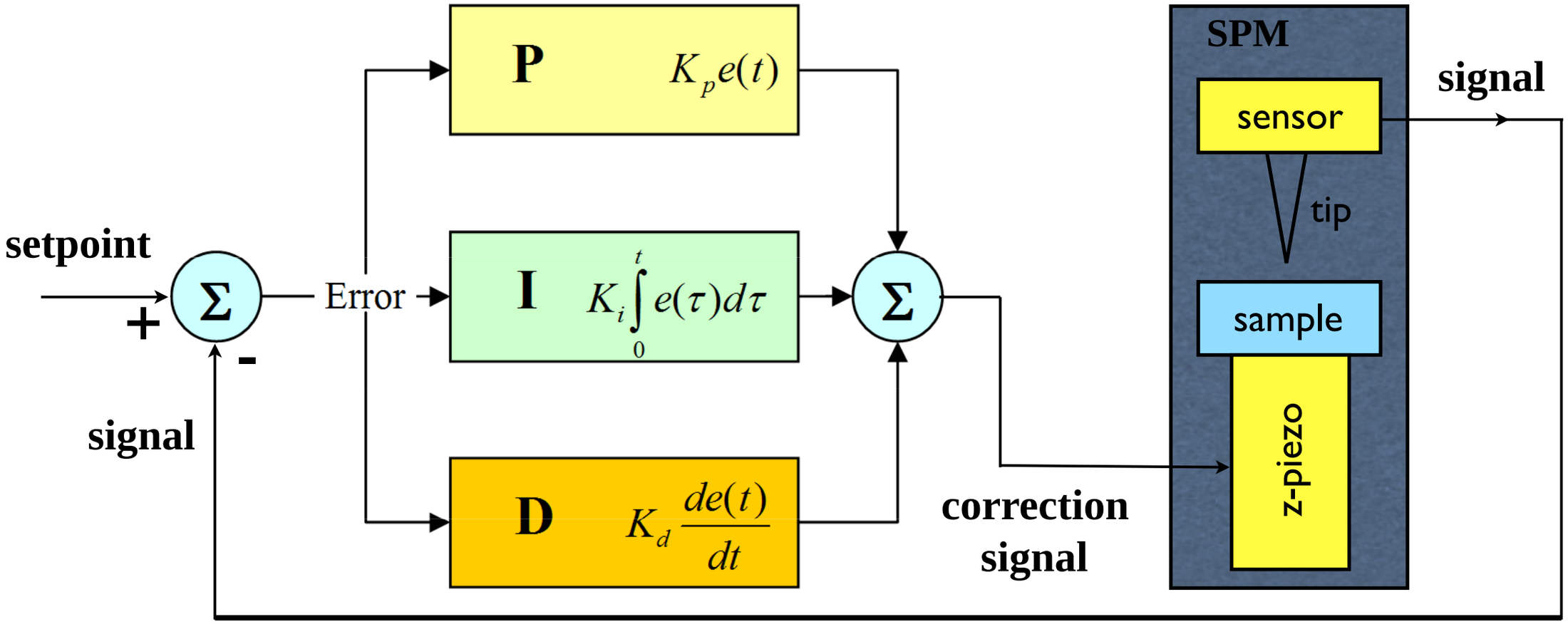

$$\mathrm{MV(t)} = P_{\mathrm{out}} + I_{\mathrm{out}} + D_{\mathrm{out}} \qquad \mathrm{u(t)} = \mathrm{MV(t)} = K_p e(t) + K_i \int_0^t e(\tau)\, d\tau + K_d \frac{de}{dt}$$

Feedback Setup:

1. experience / trial & error
2. Ziegler-Nichols procedure [1,2]:
   - increase P-part until small oscillations of the current are observed.
   - reduce P-part to 0.45P_{krit}.
   - measure oscillation period (T_{krit}) and set I-part to 0.85T_{krit}.

[1] J. Ziegler, N. Nichols: Trans. ASME **64**, 759 (1942)
[2] H. Unbehauen: *Regelungstechnik I* (Friedr. Vieweg und Sohn, Braunschweig/ Wiesbaden, 1982)

Feedback and Error Signals

Empa
Materials Science and Technology

Si(111)-7x7, 10x10nm²

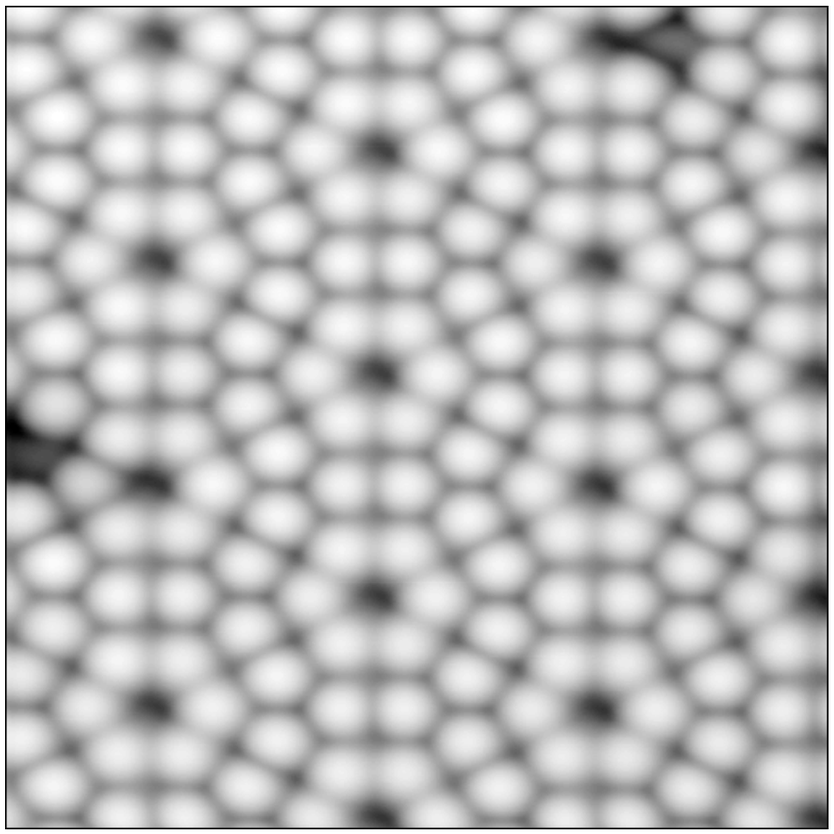

topography Δz = 0.2nm
„image“

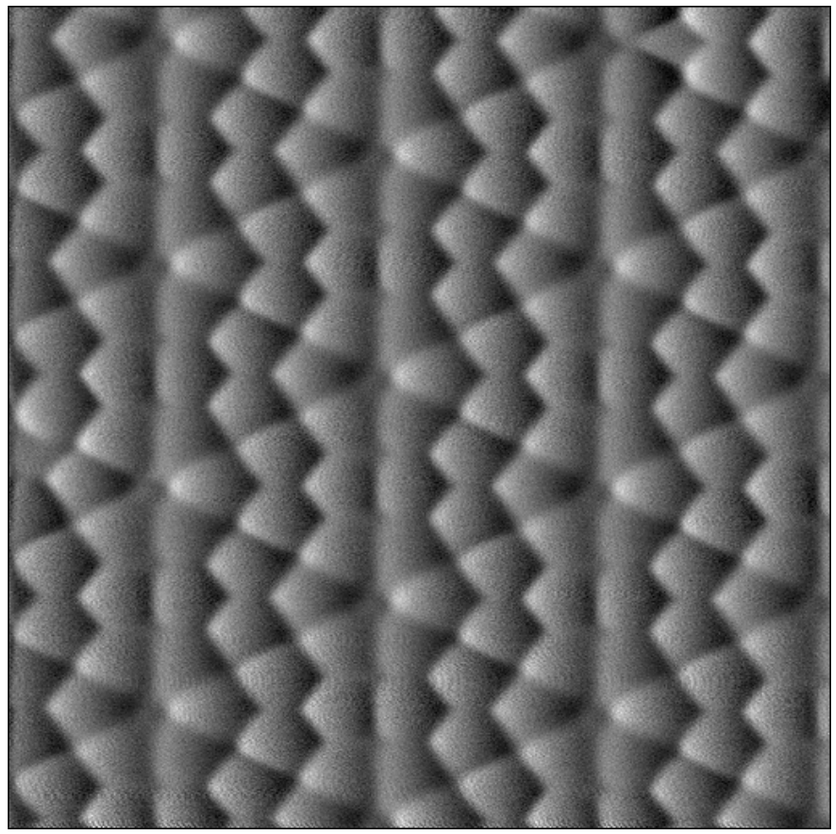

I_T = 0.5nA; ΔI_T = 0.18nA;
„error signal“

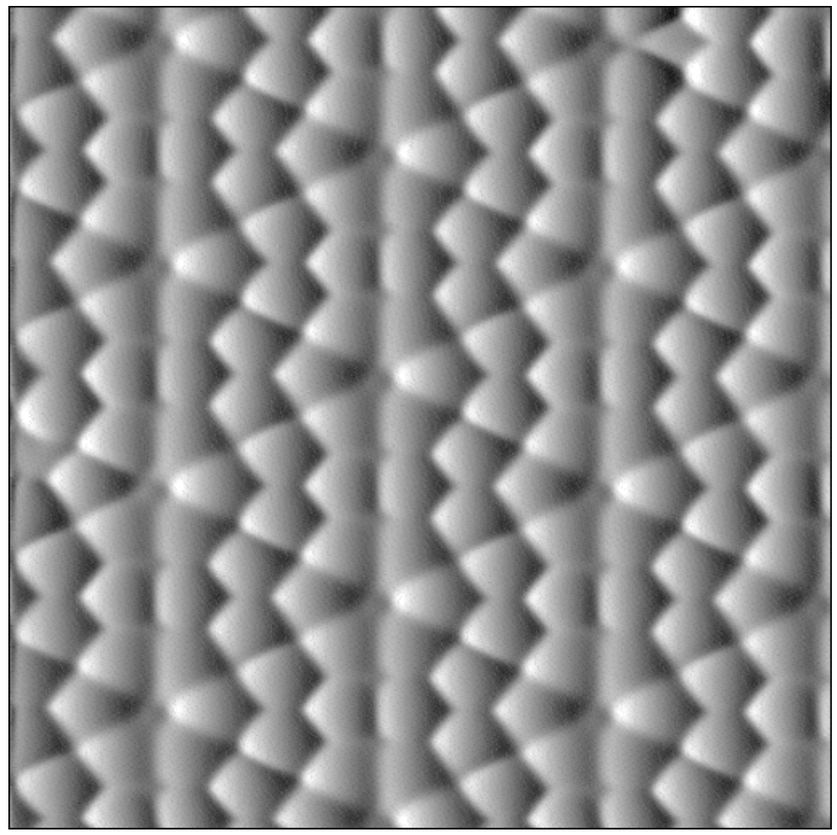

dz/dx derivative
„simulated error signal“

Note:

1. a feedback is like a low-pass filter, filtering away the high frequency signals.
   The latter appear in the error signal.
2. Faster scanning or slower feedback generates larger errors.
3. maximum feedback speed is limited by the systems responce time.
4. Feedback errors look like the d/dx derivative of the image

Preparation of Tunneling Tips

Empa
Materials Science and Technology

- Electrochemical etching:
  - a 0.25mm tungsten wire is immersed in 1M acqueous solution of NaOH.
  - the counterelectrode is a piece of stainless steel or platinum
  - a positive voltage of 4-12V is applied to the wire.
  - etching occurs at the liquid-air interface and a neck is formed
  - the weight of the lower part of the wire pulls the neck and naturally fractures it.
  - cutoff time after the tip has fractured is important parameter

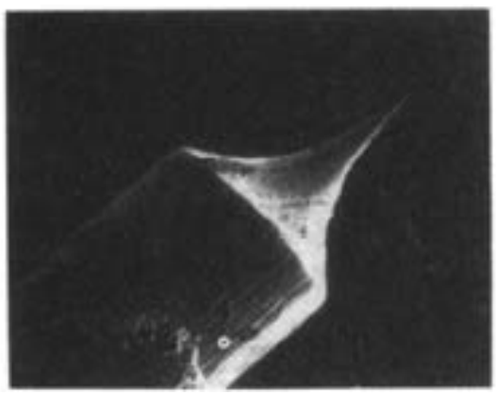

600ns, with 32nm

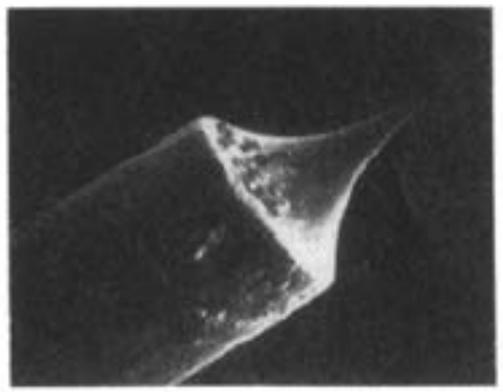

140ms, with 58nm

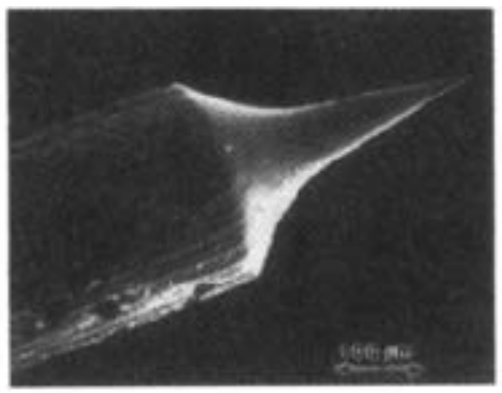

640ms, with 100nm.

  - cleaning in boiling water to remove residuals of NaOH.
  - problem: formation of a surface oxide during etching, which has to be removed before tunneling.
  - remove the oxide by resistive heating or electron bombardment

- Mechanical methods: cut PtIr wire with scissors !

- Field evaporation: in combination with FIM atomically sharp tips

- Controlled collision with surface

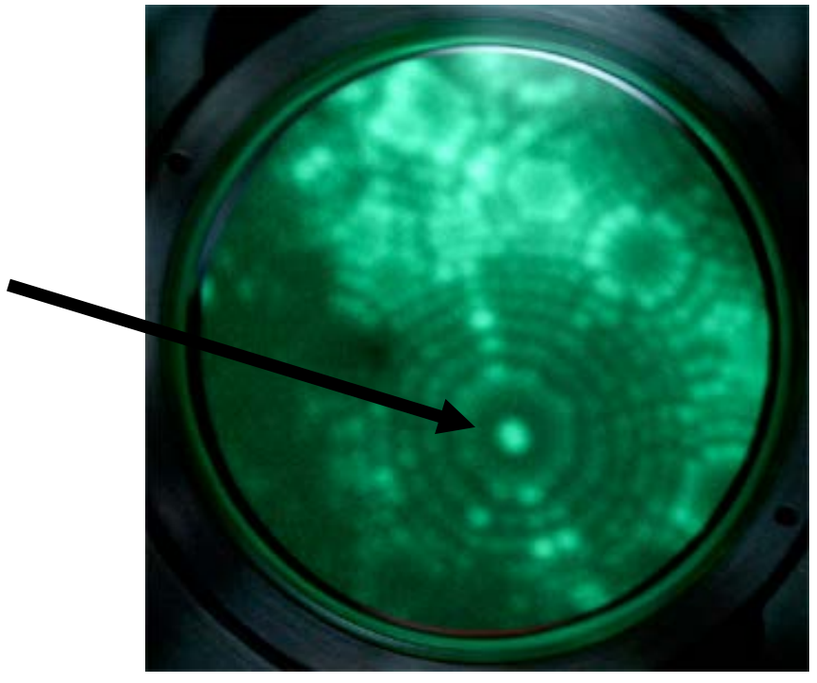

Influence of the Tip Geometry on Imaging Surface Features

tip artifacts

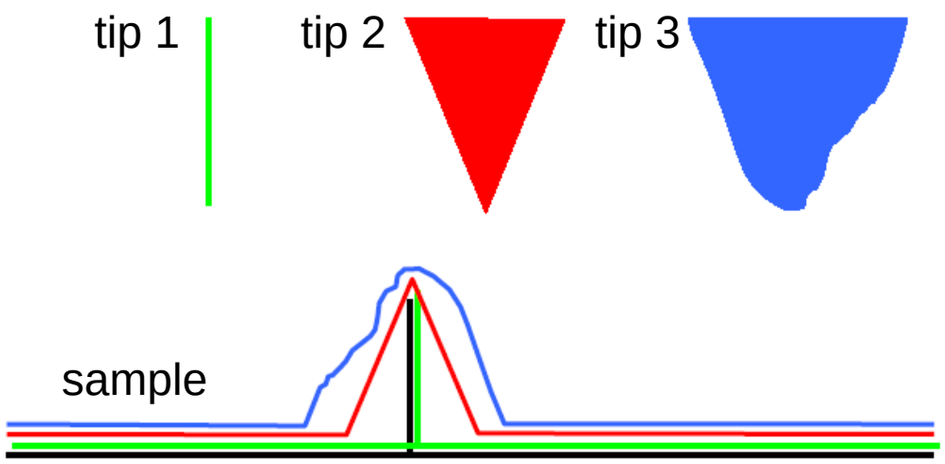

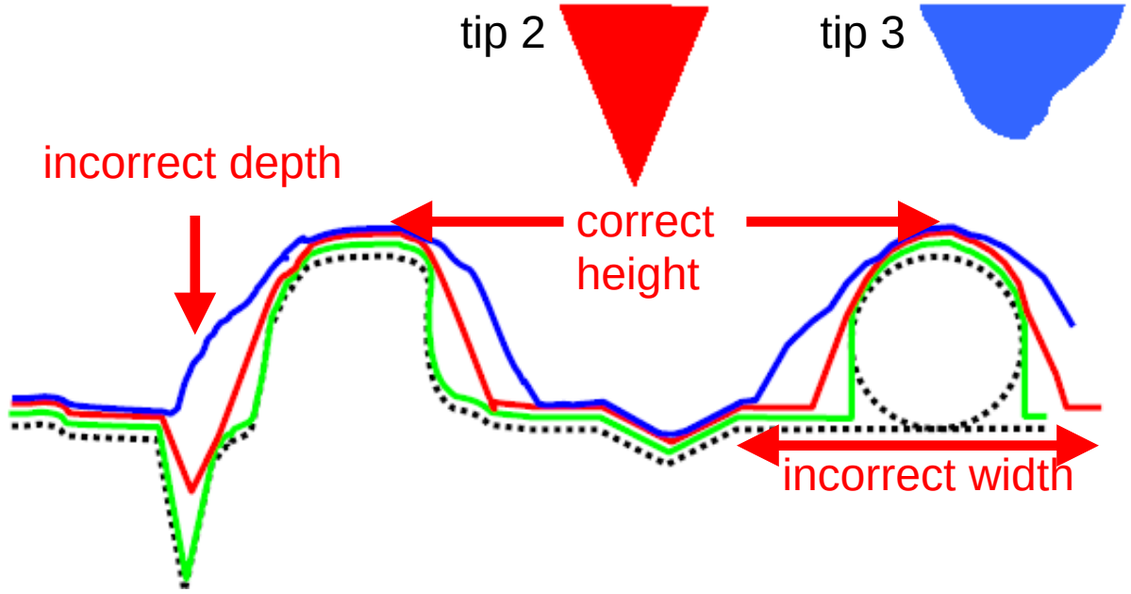

PRINCIPLE OF DETECTION OF THE AFM-TIP SHAPE AND TIP RADIUS

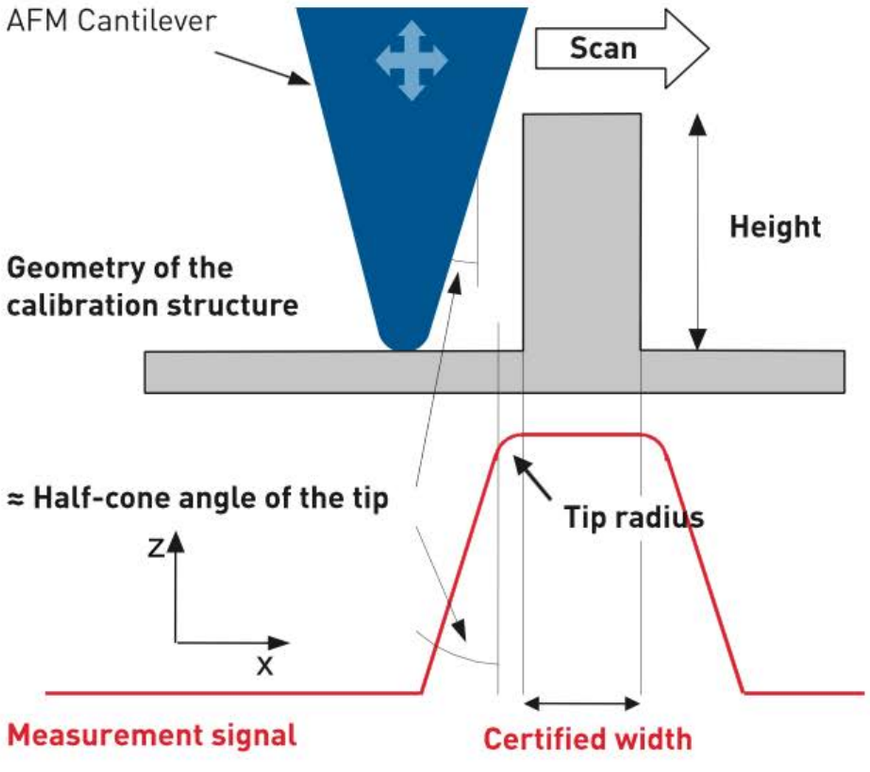

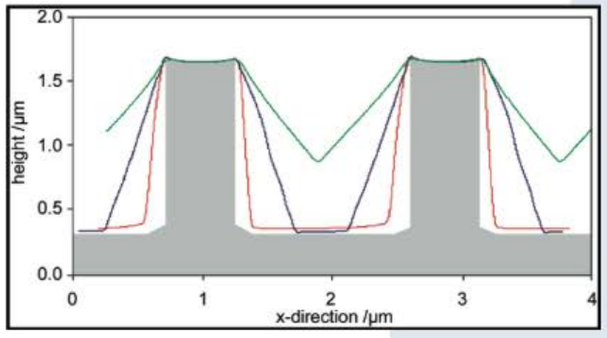

AFM-measurements of the calibration structures with three different tip shapes (the cross section of the calibration structure is shaded). The extracted tip shapes are visualized on the SEM-images of the tips.

red: high aspect ratio tip (NanoSensors AR5-NCHR)

blue: silicon tip (NanoSensors NCH)

green: silicon nitride tip

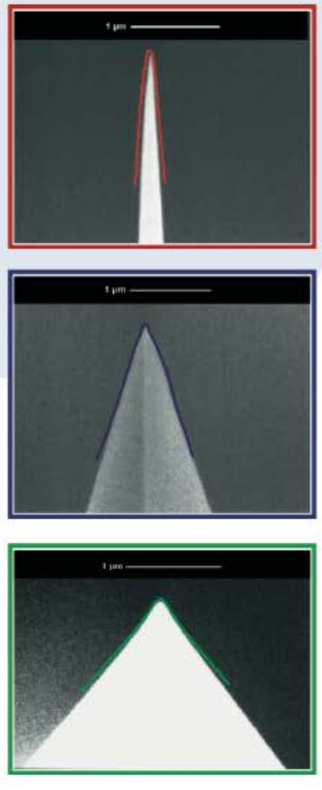

AFM-pictures: Courtesy of Th. Sulzbach, Nanoworld GmbH

Supracon AG | An der Lehmgrube 11 | 07751 Jena | Germany
Tel. +49 [3641] 23 28 100 | Fax +49 [3641] 23 28 109
info@supracon.com | www.supracon.com

Hübner et al., Appl. Phys. A 76, 913–917 (2003)

Tip Artifacts - an Example

„epitaxial“ Pt on Sapphire

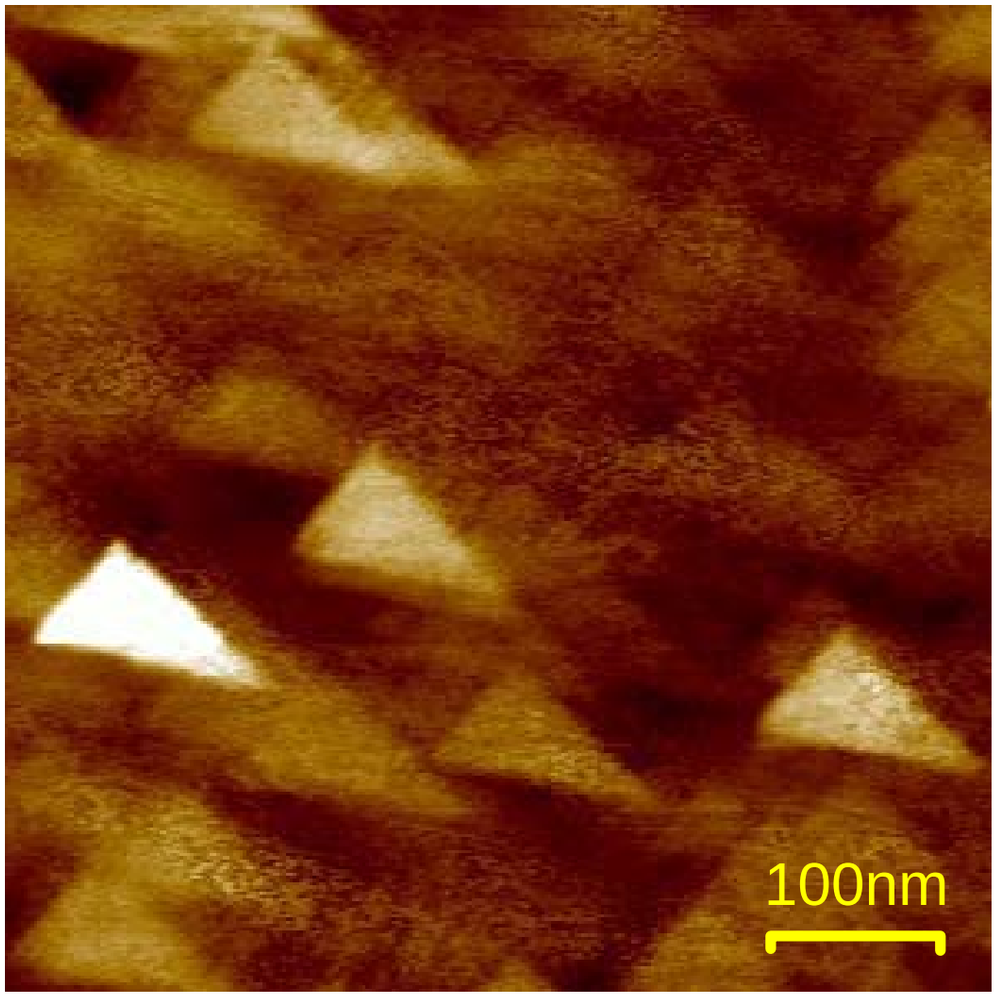

pieces of cake

1st STM by G. Binnig, H. Rohrer & Ch. Gerber (1998)

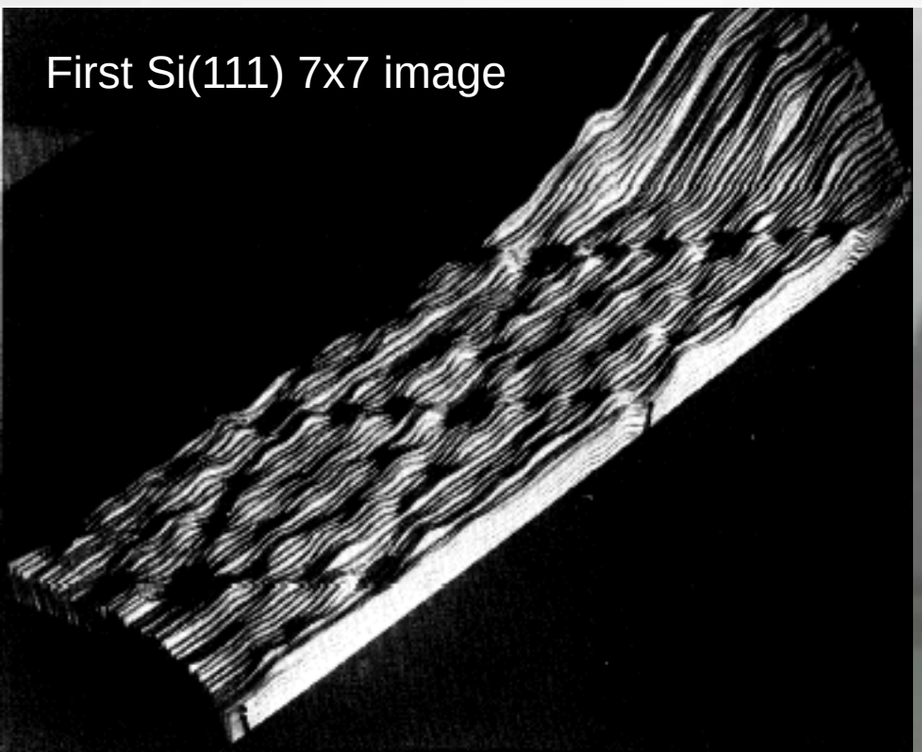

The Nanosurf STM … an effective Simplification

2.

Scanning Tunneling Microscopy (STM)

2.1. Principles of STM

Tunneling: a Quantum mechanical Effect

1d tunneling junction

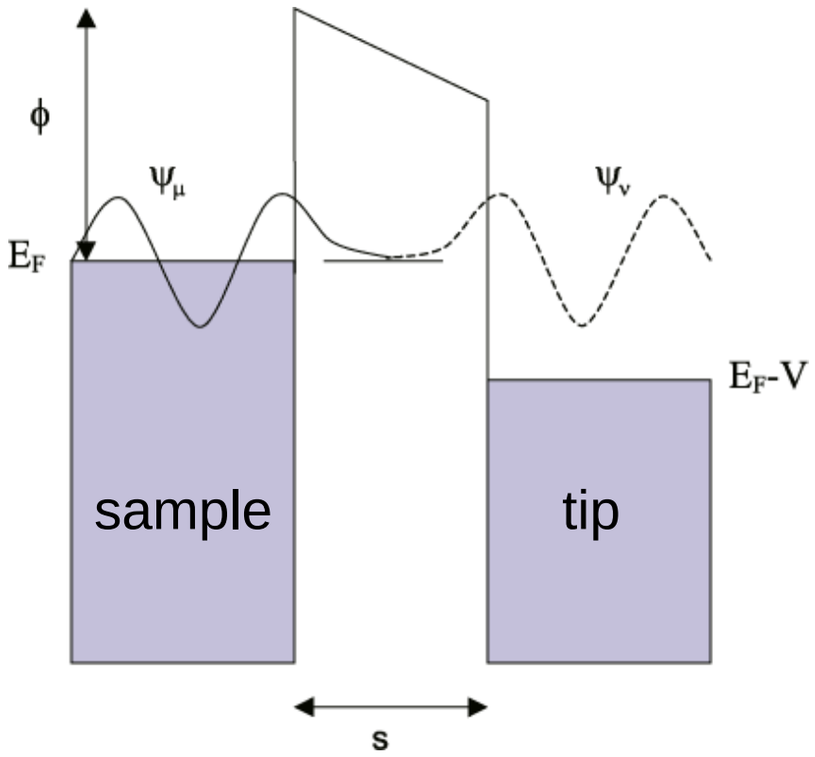

According to quantum mechanics, a particle with an energy *E* can penetrate a barrier ∅ > *E*. In the classically forbidden region, the wave function *ψ* decays exponentially

$$I_T \propto e^{-2\frac{\sqrt{2m\phi}}{\hbar}z}$$

where the barrier height *Φ* is in eV and *z* in Angstrom. **With a typical barrier height of *Φ* = 5*eV*** , which corresponds to the work function of gold, **the tunneling current decays by an order of magnitude when the vacuum gap is changed by 0.1nm !**

Refs.: Theoretical: Frenkel: Phys. Rev. B 36, 1604 (1930) & Bardeen, J. PRL, vol. 6, no.2, pp.57-59, 1961
First experiments: R. Young, J. Ward, F. Scire: Phys. Rev. Lett. 27, 922 (1971)
First experiments: R. Young, J. Ward, F. Scire: Rev. Sci. Instr. 43(7), 999–1011 (1972)
First clear demonstration of vacuum tunneling: G. Binnig, H. Rohrer: Appl. Phys. Lett. 40, 178 (1982)

Tunneling: a Quantum mechanical Effect

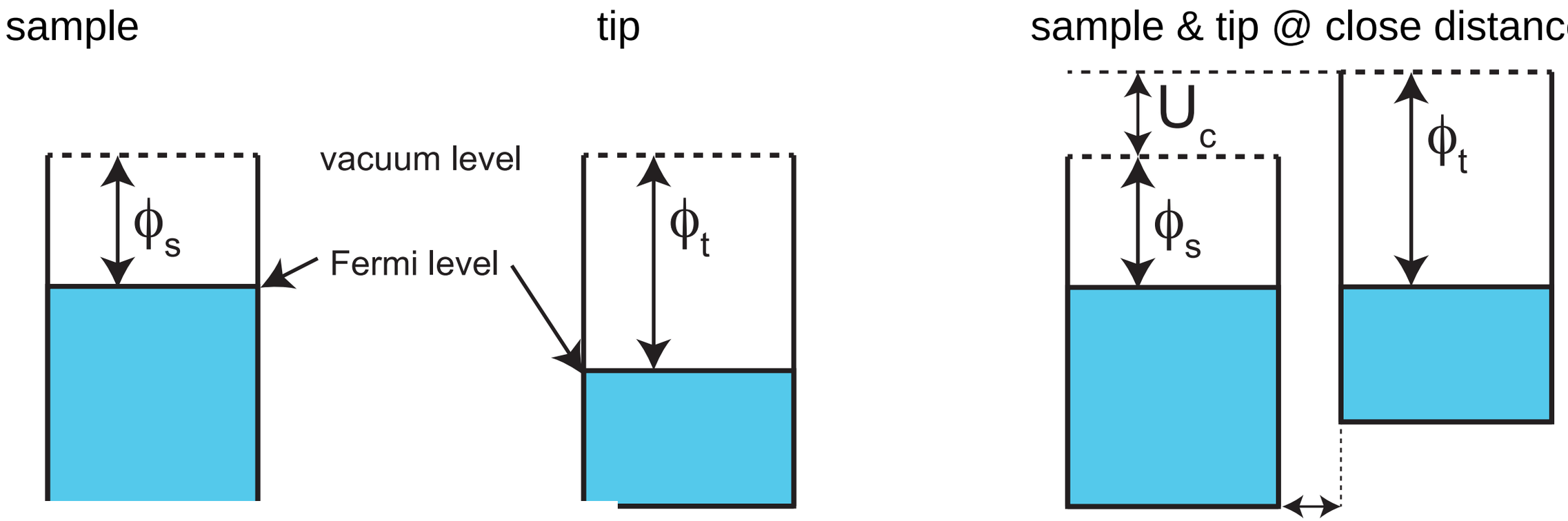

electrons tunnel
- from sample to tip
  (or vice versa if $-U_b$ is applied)
- out of filled states
- into empty states

tunnel current depends on
- distance z
- overlap of wave functions
- density of filled and empty states
- ... „sligthly“ on temperature

Bardeen‘s tunnel current formalism [1]

Based on Bardeen, the tunneling current between two electrodes, separated by an insulator, is given by

$$I_t = \frac{4\pi e}{\hbar}\int_{-\infty}^{\infty}[f(E_F - eV + \varepsilon) - f(E_F + \varepsilon)] \times \rho_s(E_F - eV + \varepsilon)\rho_t(E_F + \varepsilon)M^2 d\varepsilon$$

$$f(E) = \frac{1}{1 + e^{(E - E_F)/k_B T}}$$

Fermi function

ρ_s, ρ_t are the density of states of sample and tip. The tunneling matrix element M is given by

$$M = \frac{\hbar}{2m}\int_{surface}\left(\psi_s^* \frac{\partial \psi_t}{\partial z} - \psi_s \frac{\partial \psi_t^*}{\partial z}\right) dS$$

where ψ_t, ψ_t are the wave functions of the sample and of the tip. For low voltages the integral simplifies to

$$I_t = \frac{4\pi e}{\hbar}\int_0^{eV} \rho_s(E_F - eV + \varepsilon)\rho_t(E_F + \varepsilon)M^2 d\varepsilon$$

performing the integration in 1d (plane wave wave functions)

$$\psi_s(z) = \psi_s^0 e^{-Kz}, \quad \psi_t(z) = \psi_t^0 e^{-K(d-z)}, \text{ with: } K = \frac{\sqrt{2m\phi}}{\hbar}$$

we obtain

$$I \propto |\psi_s^0|^2 |\psi_t^0|^2 e^{-2Kd}$$

[1] Bardeen, J. PRL, vol. 6, no.2, pp.57-59, 1961.

Basic Operation Modes

imaging:

- constant current mode, i.e. feedback adjusts z to keep I_T constant
- constant height mode z = const. ➜ I_T varies

in reality: $I_T \approx$ constant, because z-feedback cannot adjust z infinitely fast
so in addition to the „topography“ image *z(x,y)* an „error signal“ image $I_T(x,y)$ exists.

Si(111)-7x7, 10x10nm²

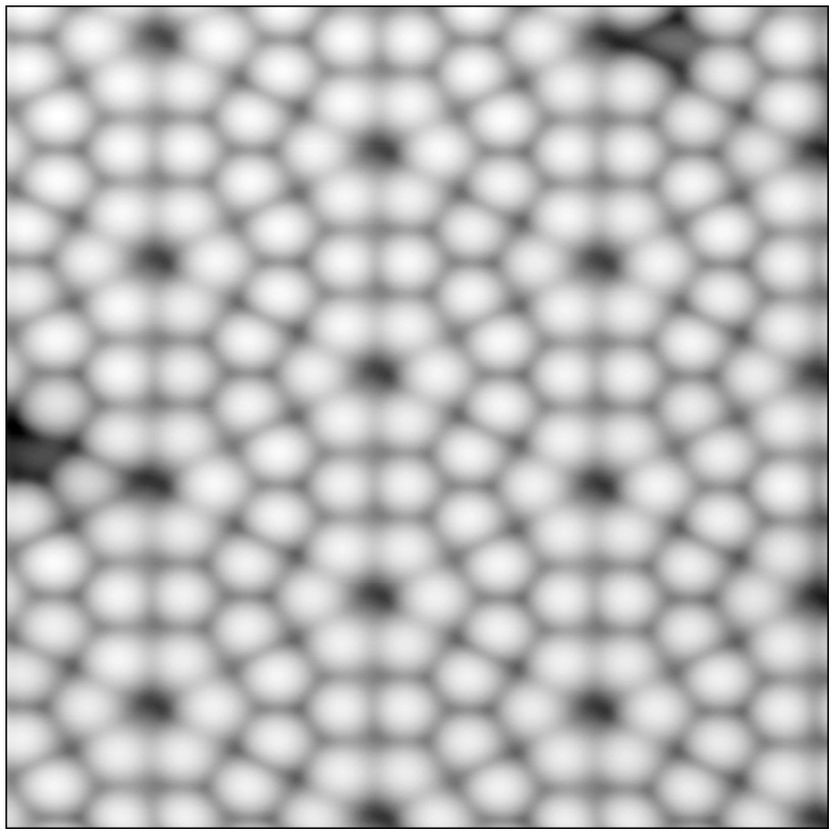

topography Δz = 0.2nm
„image“

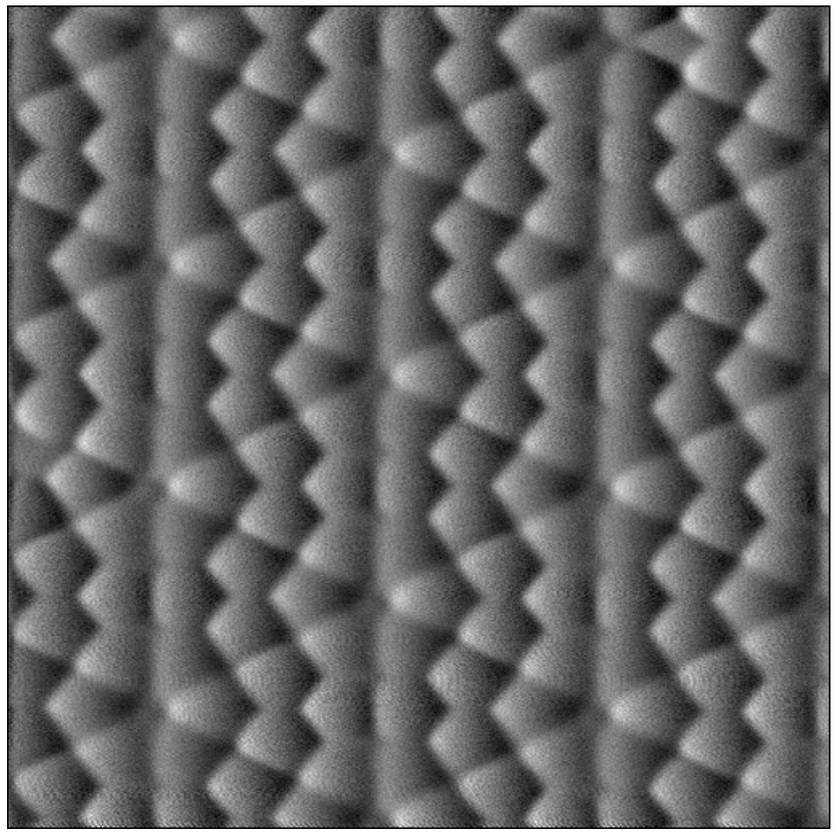

I_T = 0.5nA; ΔI_T = 0.18nA;
„error signal“

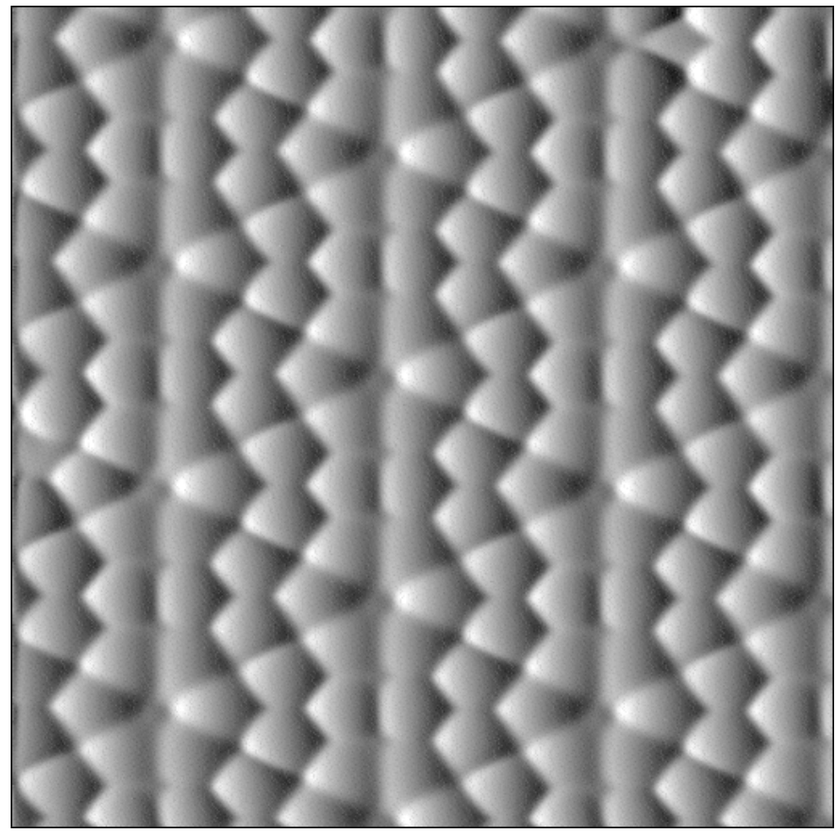

dz/dx derivative
„simulated error signal“

2.2. STM Imaging of Semiconductors, Metals & Layered Materials

STM on Semiconductors

First Si(111) 7x7 image [1]

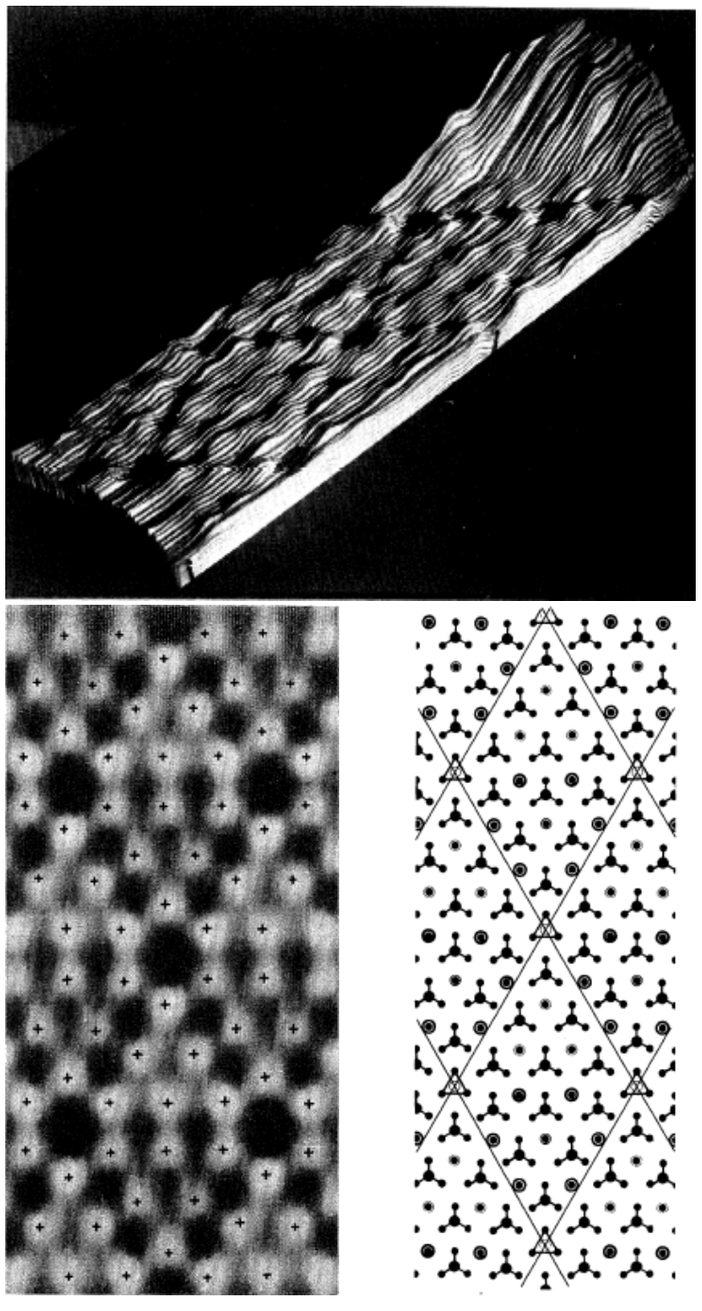

First Si(100) 2x1 [2] and
STM @ various tip-sample potentials an GaAs

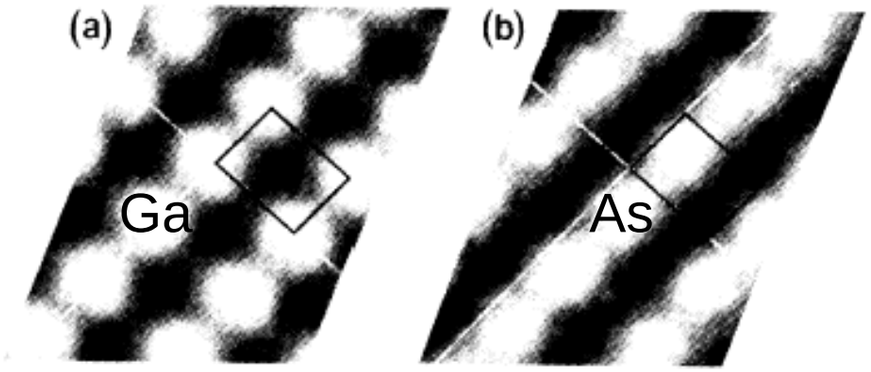

Us = +1.9V Us = -1.9V

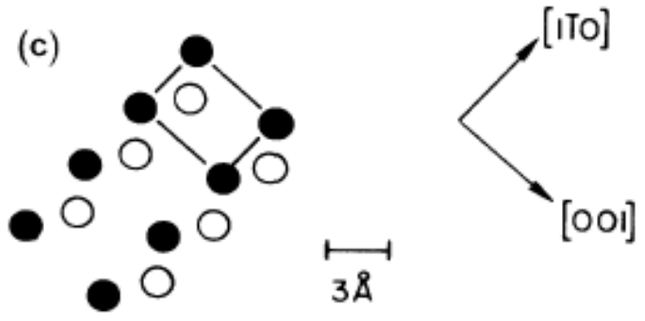

FIG. 2. Constant-current STM images acquired at sample voltages of (a) +1.9 and (b) −1.9 V. The surface height is given by a grey scale, ranging from 0 (black) to (a) 0.83 and (b) 0.65 Å (white). (c) Top view of the surface atoms. As atoms are represented by open circles and Ga atoms by closed circles. The rectangle indicates a unit cell, whose position is the same in all three figures.

Refs.:[1] G. Binnig et al. PRL50 120 (1983)
[2] R. Feenstra Surf Sci. 181, 295 (1987) and PRL58 1192 (1987)

STM on Metals

- first resolved by Binnig and Rohrer 1982 [1] (Au(110)-2x1 and Au(110)3x1 reconstructions)
- atomic resolution on a close-packed Au(111) by Hallmark et al. [2] in 1987
- today, a large number of clean metal surfaces could be resolved, such as Cu(111), Cu(110), Cu(001), Pt(111), Pt(001), Ru(0001), Ni(001) and Ni(110)
- spacing between the atoms of the close-packed surfaces is 2-3Å.
- corrugation heights are found to be rather large of the order of tenths of Å
- corrugation in contradiction with results from He scattering (STM shows larger corrugations)
- contradiction explained by force induced variation of tip-sample distance

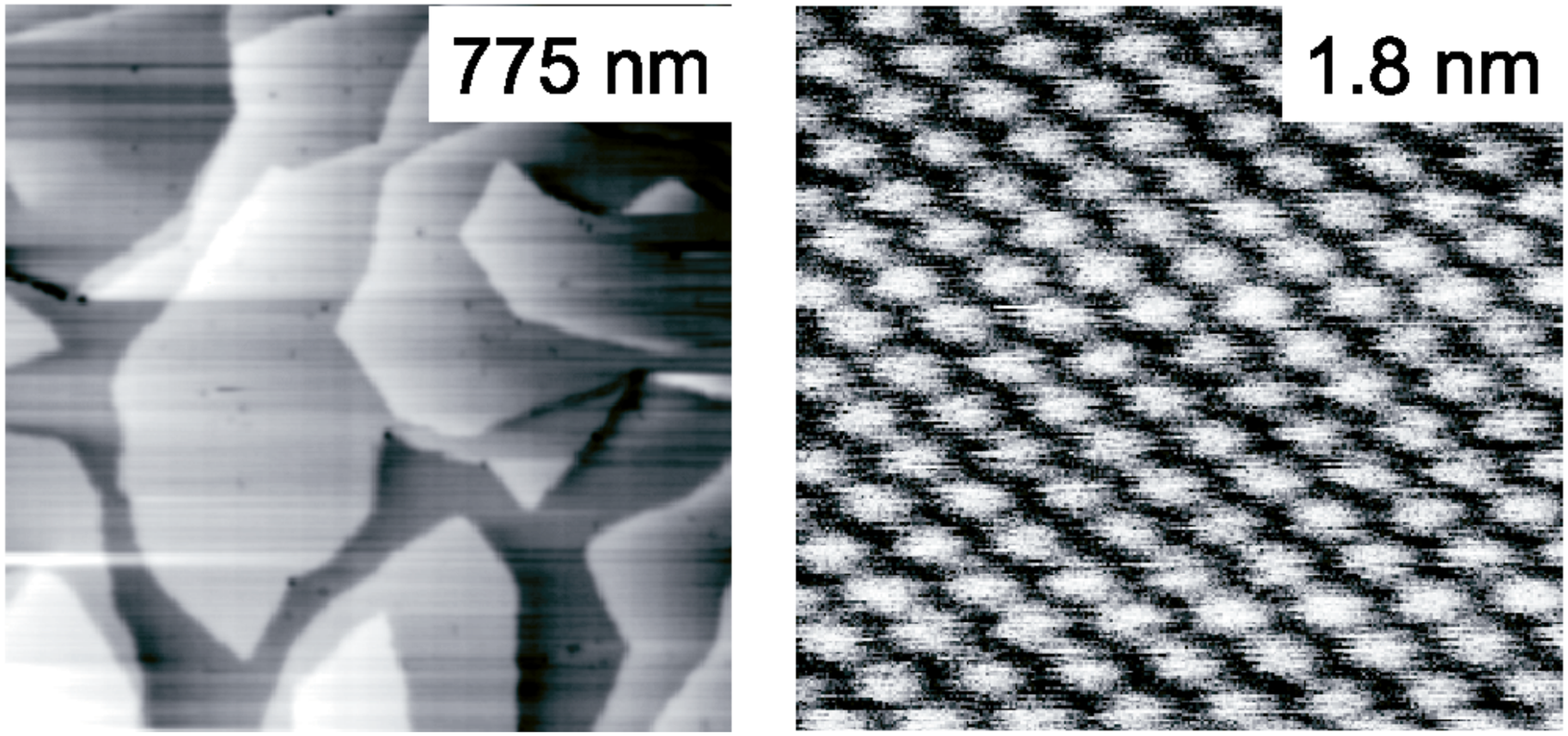

STM images of the Cu(111) surface in constant current mode. (left) Overview image with monatomic steps (right) Atomic resolution on Cu(111). The spacing between the protrusions is 2.5Å.

Refs.:[1] G. Binnig et al. Rev. Mod. Phys. 56 615 (1987)
[2] V. M. Hallmark et al. PRL59 2879 (1987)

Super-resolution on Metals

An impressive example of the resolution capabilities is given by Schmid et al. [1], where Pt-atoms and Ni-atoms could be distinguished on a $Pt_{25}Ni_{75}$(111)-surface.

The best resolution was observed with small tunnel resistances of (50-300kOhms), which was attributed to the interaction between adsorbates at the tunneling tip and the surface atoms.

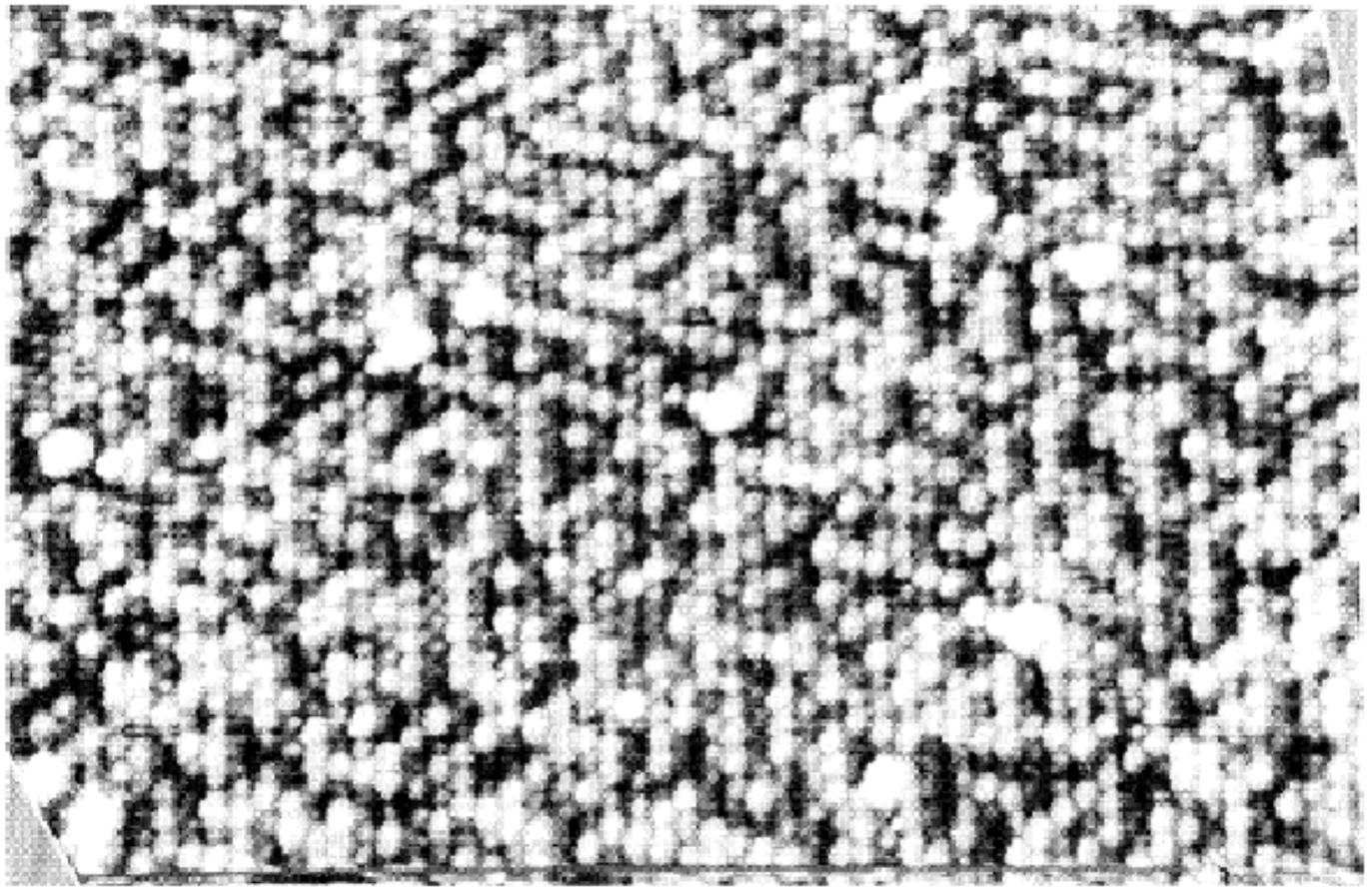

After extensive surface preparation, atomically resolved STM images on this surface [Fig. 1(a)] are routinely achieved at rather low tunneling resistance (50 to 300 kΩ). These images show atomic corrugation of 0.1 to 0.2 Å, with very little variation between individual atoms. Tip conditions leading to such images are usually rather stable; subsequent images of the same surface region are virtually identical. At higher tunneling resistance, the atomic corrugation gradually disappears.

If the surface is prepared less thoroughly, but still sufficiently to achieve "clean" Auger spectra, tunneling conditions are less stable. We often observe sudden changes in image quality, especially when the tip reaches a step. We attribute this to adsorbates hopping between sample and tip or between tip sites. Adsorbates often show a preference for step edges (we have also observed this for sulfur on the same sample [12]), which easily explains why tip conditions are most unstable near steps.

D. Eigler (IBM Almaden Research Lab) calls these adsorbates "Behm amplifiers". He often uses a Xe-atom that is picked up by the tip. Such adsorbates are only weakly bound to the tip. The strong force field between the tip and the sample leads to a modulation of the position of the adsorbate within the tip-sample gap. This causes an enhancement of the corrugation and superresolution.

Refs.:[1] M. Schmid et al. PRL70 1141 (1993)

STM on Layered Materials

- A number of layered materials, such as graphite or MoS_2, could be resolved.
- Especially, graphite has attracted a lot of attention, because of the giant corrugation heights.
- transition metal dichalcogenides, such as 1T-TaS_2 or 1T-$TaSe_2$, with atomic structure and charge density waves (CDW).
- A review of the STM work of layered materials with CDW has been published by Coleman et al. [2]

Forces between tip and sample were attributed to play an important role [1].

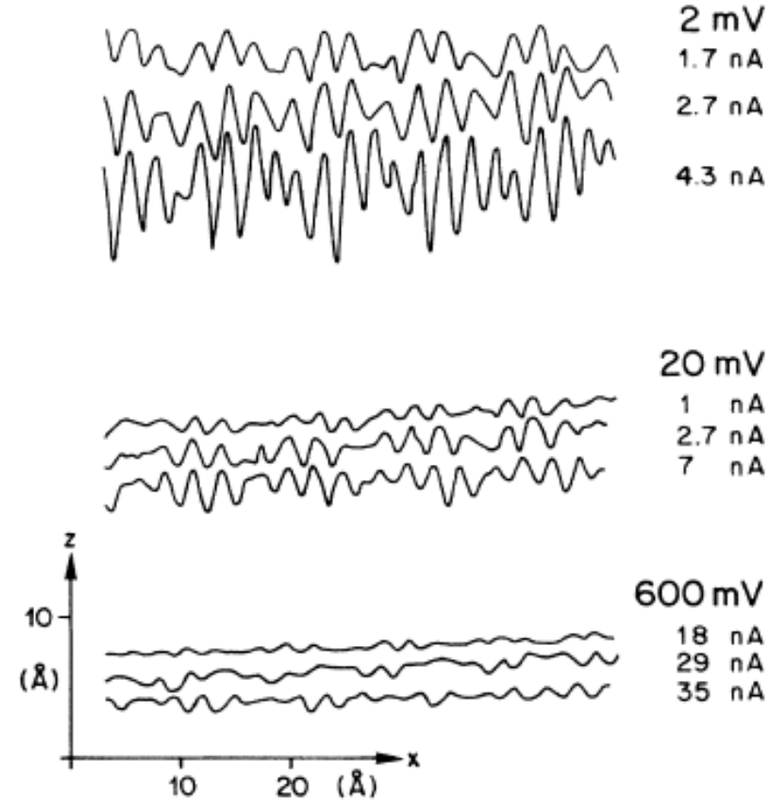

FIG. 1. Graphite STM traces obtained at ambient-air pressure and room temperature with a "pocket-size" STM (Ref. 14) with scanning speeds between 1 and 5 sec per scan. The varying corrugation within a scan is due to the mismatch between crystallographic and scanning directions (Ref. 3); plateaus in the traces indicate the saddle points in the LDOS (Refs. 3 and 11).

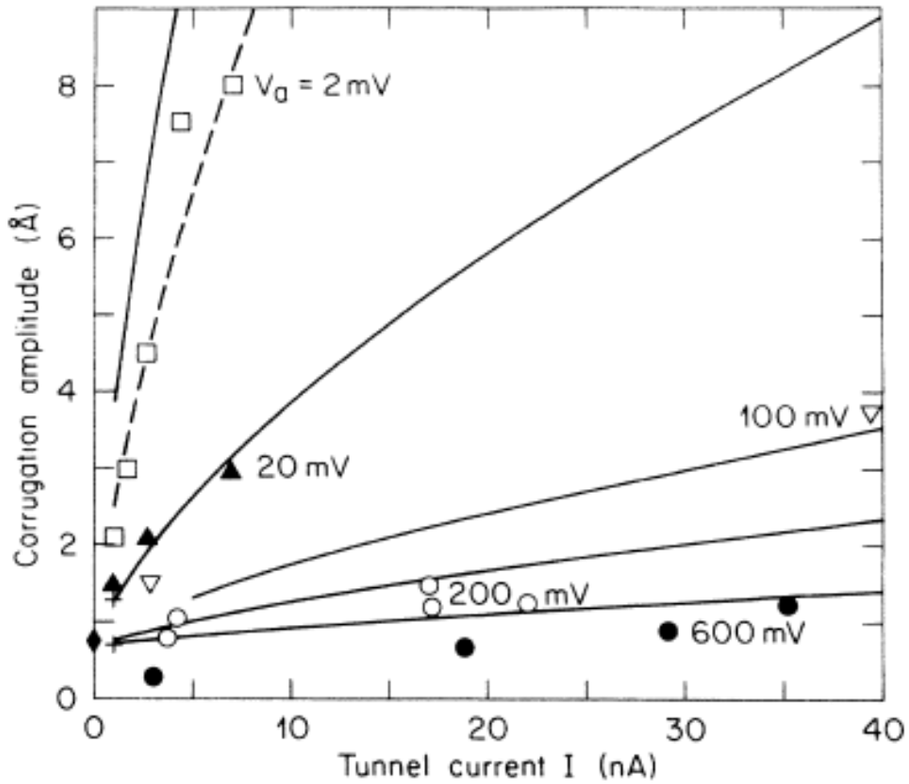

FIG. 4. Measured (symbols) and calculated (solid lines) corrugations as a function of tunneling current and voltage. The dashed line was obtained with $d^* = 0.4$ Å. The two crosses at 1 nA correspond to the measured corrugations at 50 and 400 mV, respectively, of Ref. 3; the diamond at zero current indicates the corrugation of the LDOS at the Fermi level (Ref. 11).

Refs.:[1] Soler et al. PRL57 444 (1987)
[2] R.V. Colemann et al. Adv. Phys. 37 559 (1988)

2.3. Scanning Tunneling Spectroscopy (STS)

2.3.1. Principles of STS

Spectroscopic Measurements

spectroscopy:

- barrier height measurements: $\frac{d \ln I_T}{dz} \propto \sqrt{\phi}$ because $I_T \propto e^{-2\frac{\sqrt{2m\phi}}{\hbar}z}$

- density of states mapping

  neglecting the density of states in the tip (or assuming a flat density of states) we have

$$I_T \propto \int_0^{eU_{bias}} \rho_s(E_F - eU_{bias} + \epsilon) d\epsilon$$

  differentiation gives

$$\frac{dI_T}{dU_{bias}}(U_{bias}) \propto \rho_s(E_F - eU_{bias})$$

Example: W tip on Si(111)-7x7

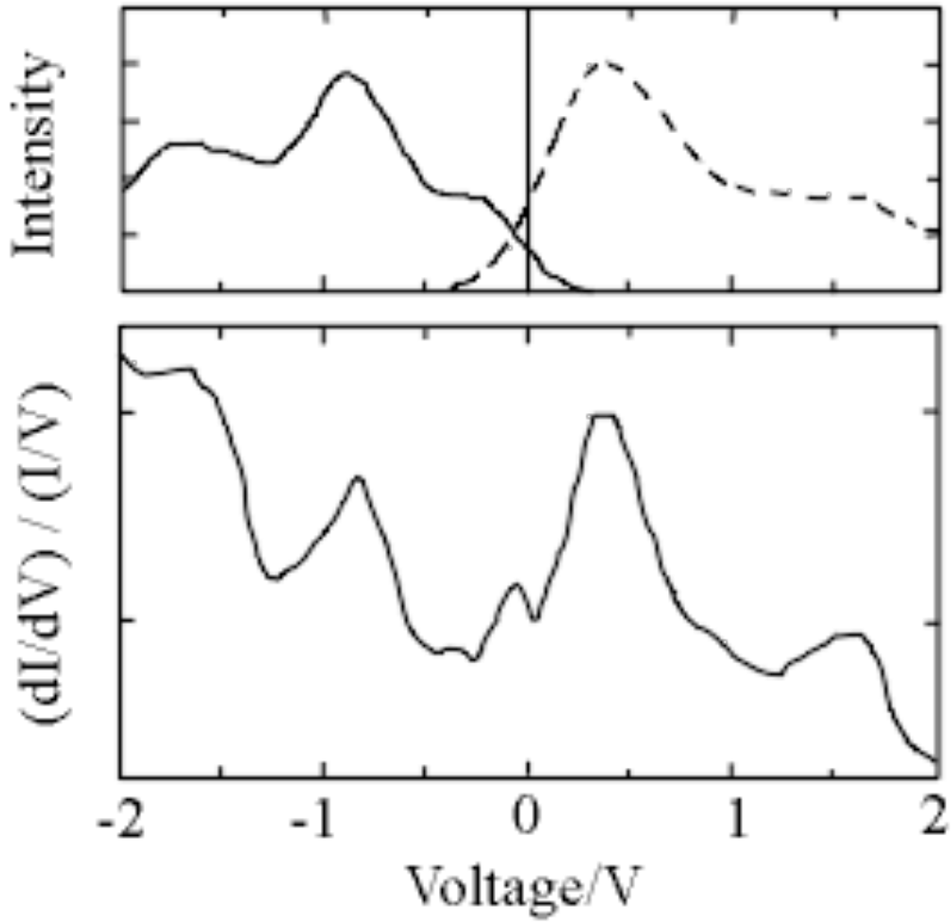

Refs.:[1] Collma al. PRL50 120 (1983)
[2] R. Feenstra Surf Sci. 181, 295 (1987) and PRL58 1192 (1987)

How to measure Derivatives with a Lock-in Amplifier (LIA)

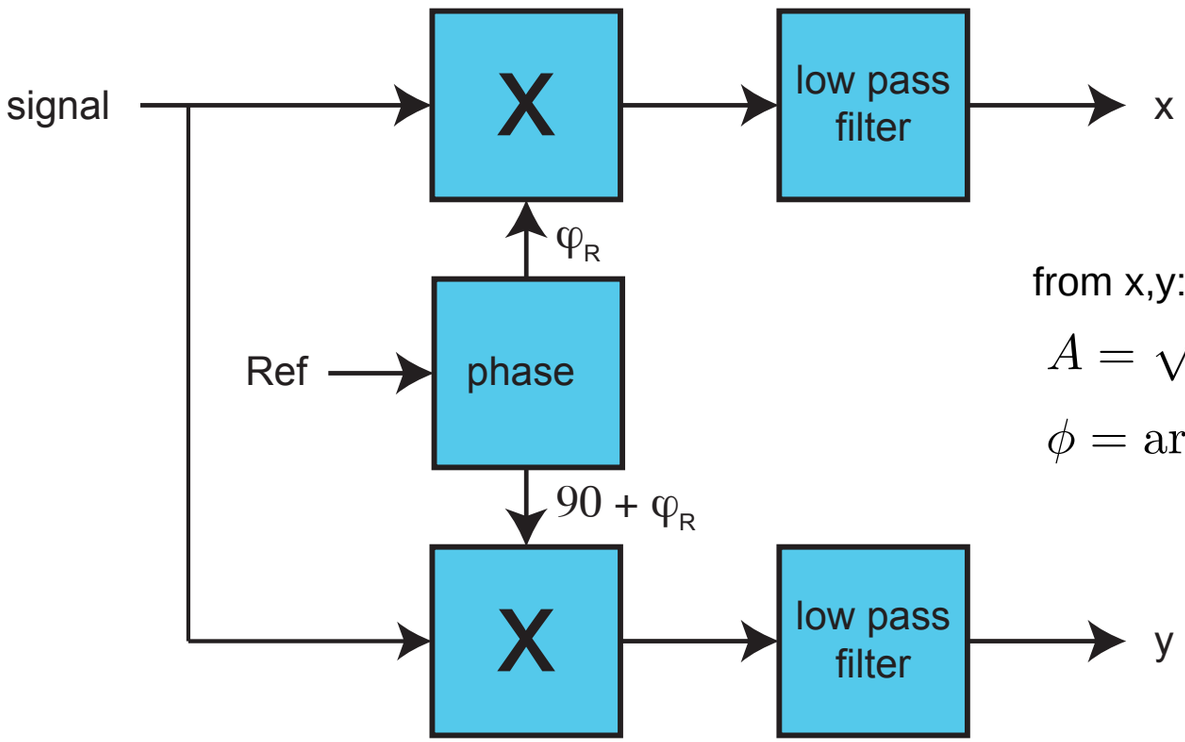

from x,y:

$$A = \sqrt{x^2 + y^2}$$

$$\phi = \arctan \frac{y}{x}$$

signal, e.g.

$$U_s(t) = U_s^0 \cos((\omega_s)t + \phi_s)$$

reference

$$U_R(t) = \cos(\omega_R t + \phi_R)$$

principle of lock-in

assume incoming signal is sinusoidal $U_s(t) = U_s^0 \cos((\omega_s)t + \phi_s)$ with $\omega_R = \omega_s \quad \text{and} \quad \phi_R = \phi_s$

and reference signal is $U_R(t) = \cos(\omega_R t + \phi_R)$

then
$$\begin{aligned} U_x(t) &= U_s^0 \cos(\omega_s t + \phi_s) \cdot \cos(\omega_R t + \phi_R) \\ &= \frac{1}{2} U_s^0 \cdot \cos[(\omega_s + \omega_R)t + \phi_s + \phi_R] + \frac{1}{2} U_s^0 \cdot \cos[(\omega_s - \omega_R)t + \phi_s - \phi_R] \\ &= \frac{1}{2} U_s^0 \cdot \cos[2\omega_s t + 2\phi_s] + \frac{1}{2} U_s^0 \cdot \cos[0] \end{aligned}$$

$$\mathrm{LPF}[U_x(t)] = \frac{1}{2} U_s^0$$ half of amplitude *A* of signal

$$\mathrm{LPF}[U_y(t)] = 0$$

Scanning Tunneling Spectroscopy on Carbon Nanotubes

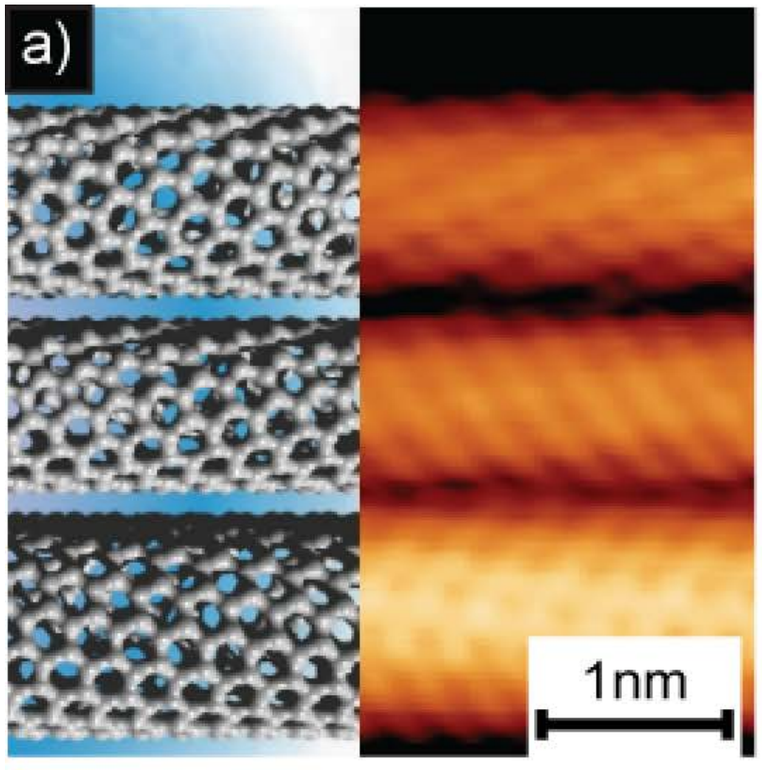

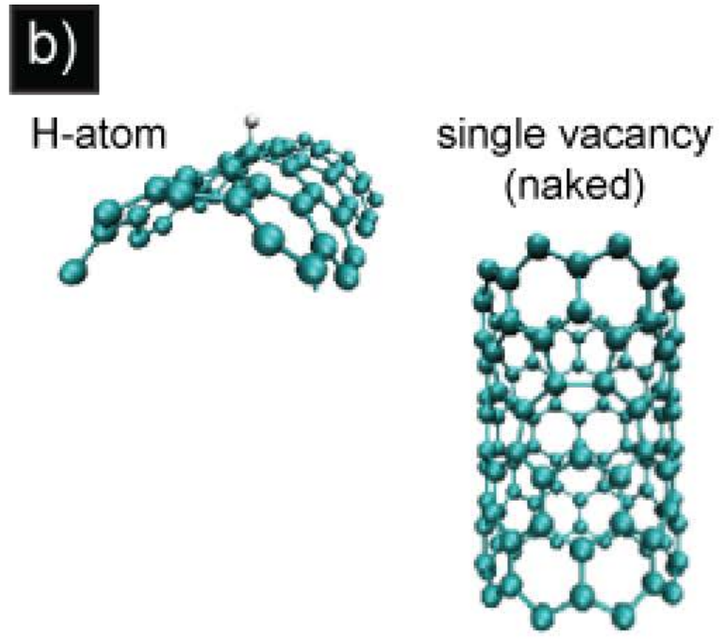

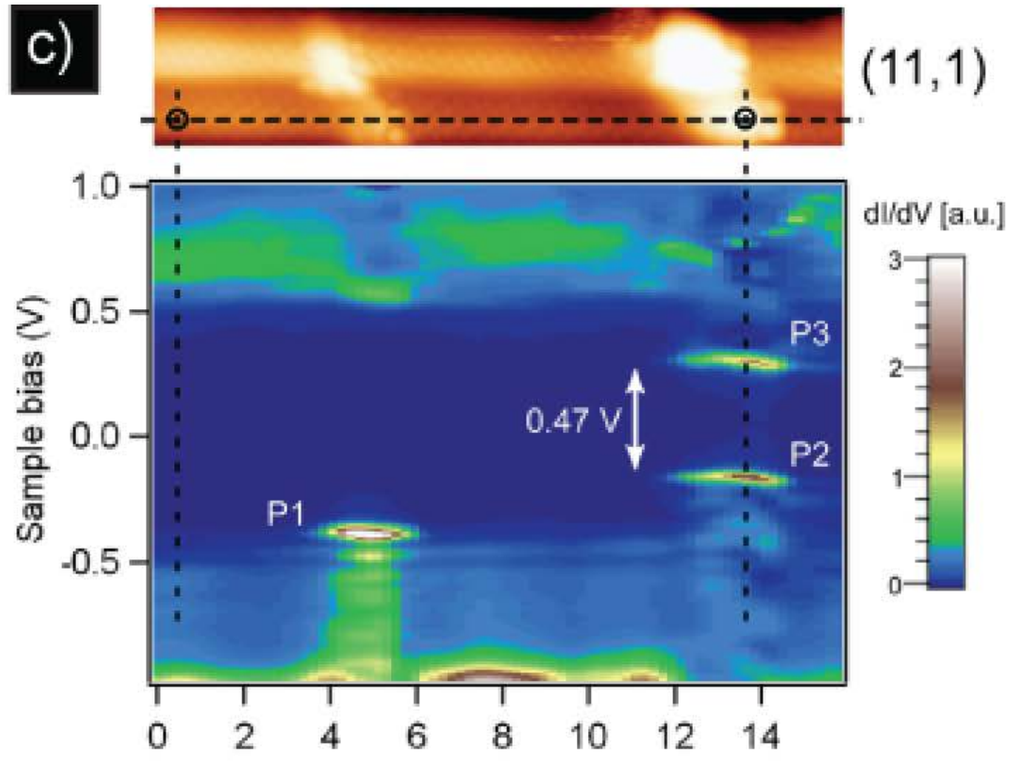

a) Right hand side: Experimental STM image with atomic resolution of three single walled carbon nanotubes (SWNT) with different chiralities. Left hand side: Atomic model representation of the three SWNTs.

b) Ball-and-Stick model of a hydrogen chemisorption and a vacancy type defect on a (10,0) semiconducting SWNT.

c) Upper panel: STM topography image of a (11,1) SWNT with two hydrogen-plasma induced defect sites. Lower panel: Corresponding scanning tunneling spectroscopy (STS) line scan on the dashed horizontal line in the topography image showing the band gap of the SWNT and localized (spatially as well as energetically) states of the defect sites. The paired gap states of the right defect is characteristic of a chemisorbed hydrogen-dimer [1,2].

Refs.: [1] G. Buchs, et al., Appl. Phys. Lett 90 (2007) 013104
[2] G. Buchs, et al., New J. of Physics 9 (2007) 275

2.3.2. Spin Polarized Tunneling

Spin-polarized Tunneling

in ferromagnetic metals:

split density of states for **up** and **down** spins

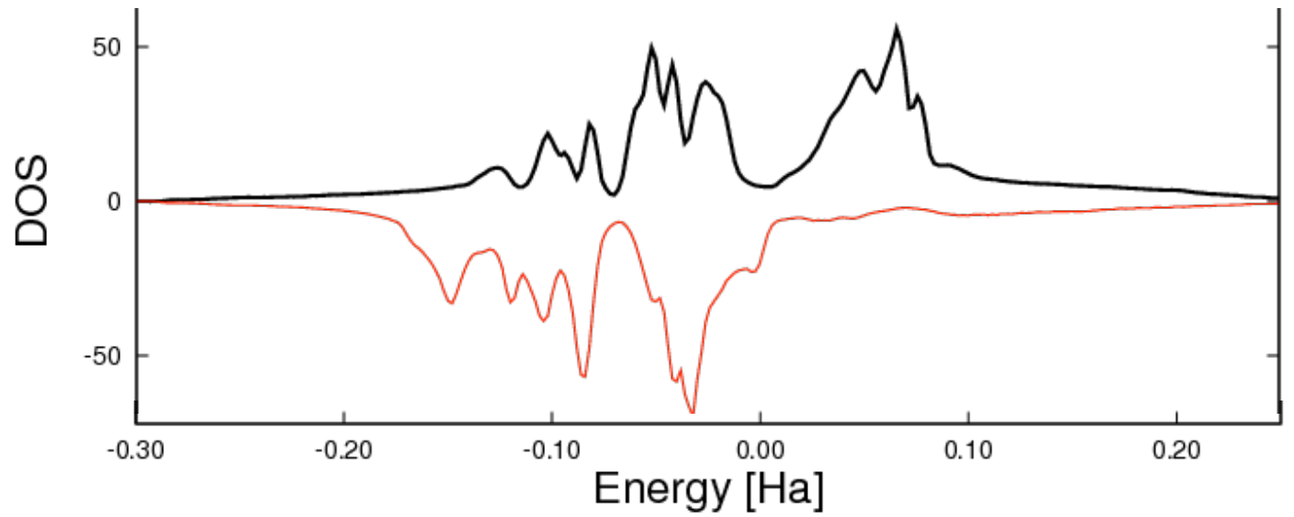

Select tip magnetization by:

- Fe-coated W tips: in plane (perpendicular to tip axis) –> in-plane component [1]
- FeGd coated W tips: perpendicular (along tip axis) –> perpendicular component [2]
- for samples with low coercivity use antiferromagnetic coatings (Cr) [3]

Fe-coated W tip: in-plane component

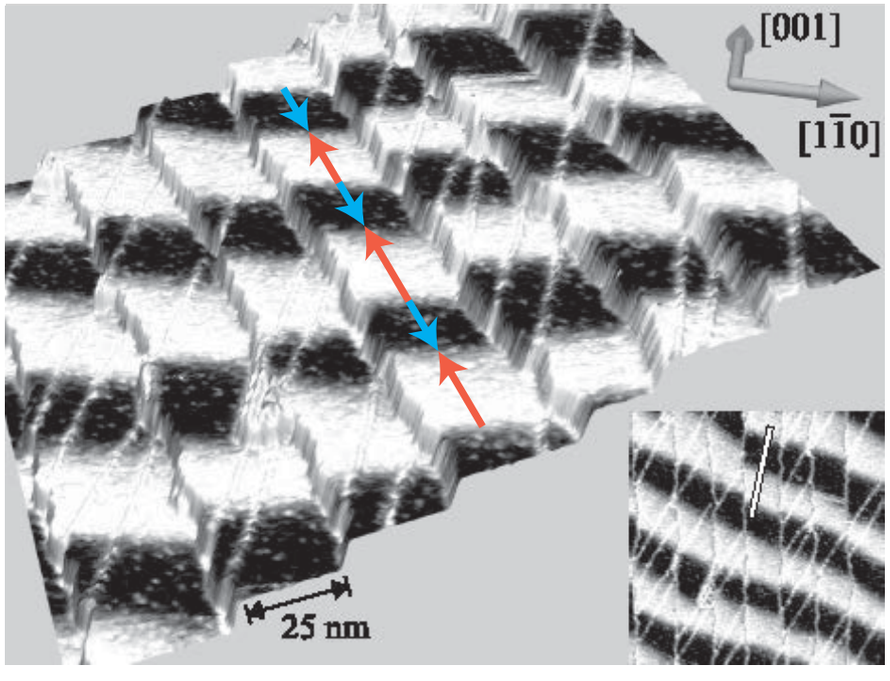

FeGd coated W tips: perp. component

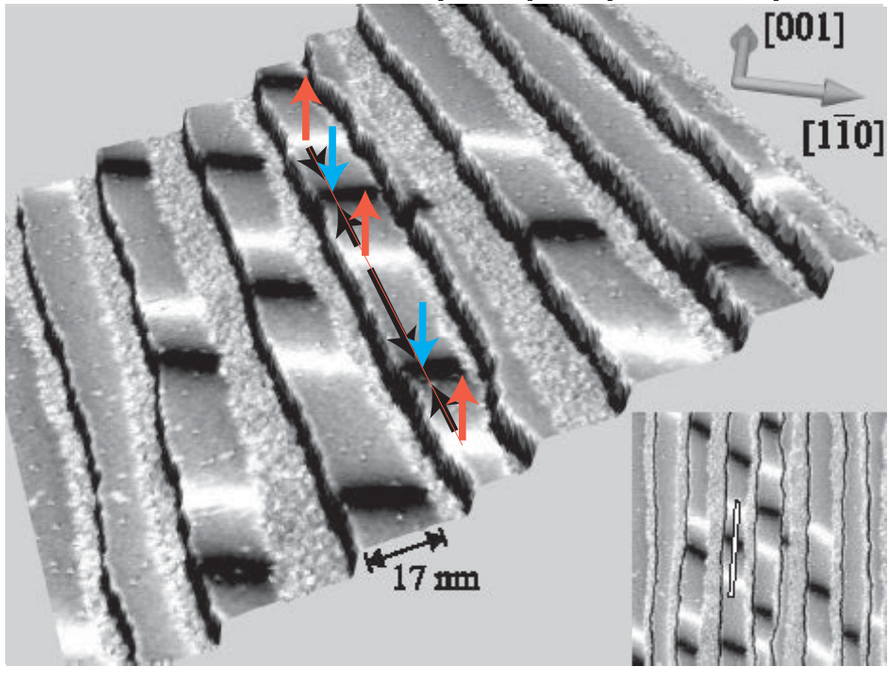

2 ML of Fe on W(110) crystal

Refs.: [1] M. Bode, et al. PRL81 4256 (1998)
A. Kubetzka, et al. PRL88 057201 (2002)
[2] A. Kubetzka, et al. PRL88 057201 (2002)
[3] S. Heinze et. al. Science 288 1805 (2000) and A. Wachowiak,Science 298 577 (2002)
Note: other SPT-methods described in Meyer, Hug, Bennewitz „Scanning Probe Microscopy“ Springer ISBN 3-540-43180-2 (2004)

sp-STM: Revealing Magnetic Interactions from Single-Atom Magnetization Curves

STM topograph colored with spin-pol. dI/dV map

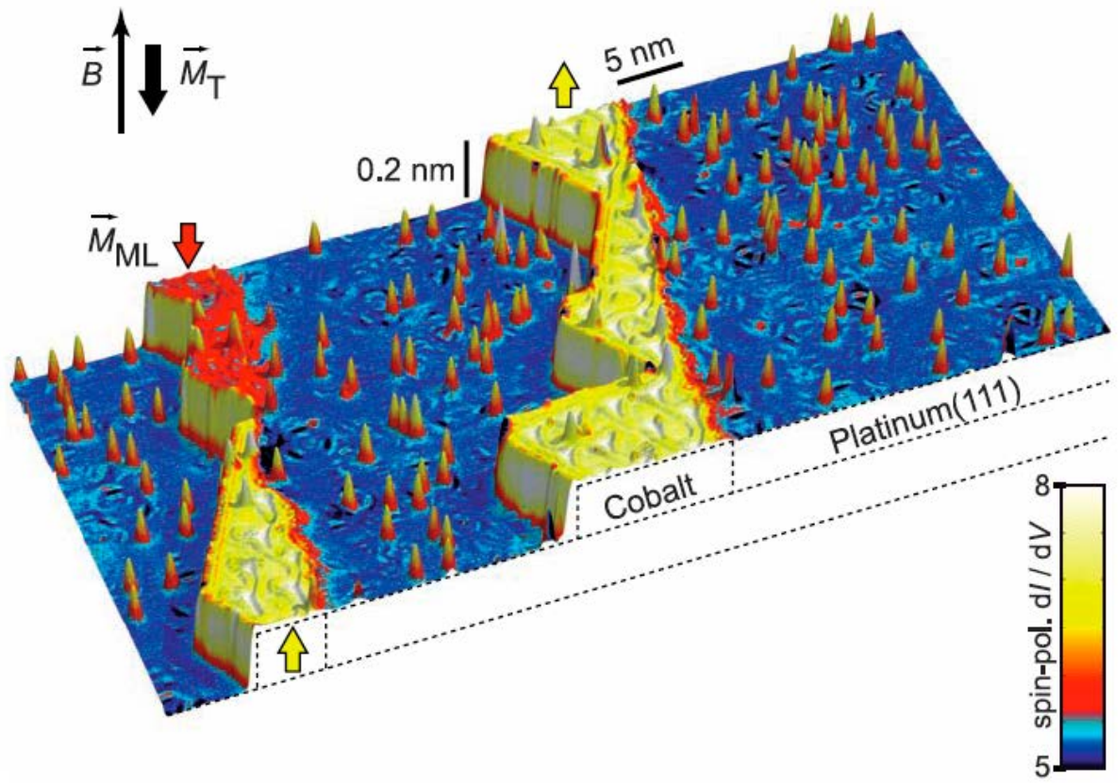

Individual Co adatoms on the Pt(111) surface (blue) and Co ML stripes (red and yellow) attached to the step edges
An external ***B*** can be applied perp. to the sample surface to change the magnetization of adatoms ***M***, ML stripes ***M***, or tip $\boldsymbol{M_T}$ at different *T*.
The ML appears red when ***M*** ML is parallel to $\boldsymbol{M_T}$ and yellow when ***M*** ML is antiparallel to $\boldsymbol{M_T}$.
(Tunneling parameters are as follows: *I* = 0.8 nA, *V* = 0.3 V, modulation voltage V_{mod} = 20 mV, *T* = 0.3 K.)

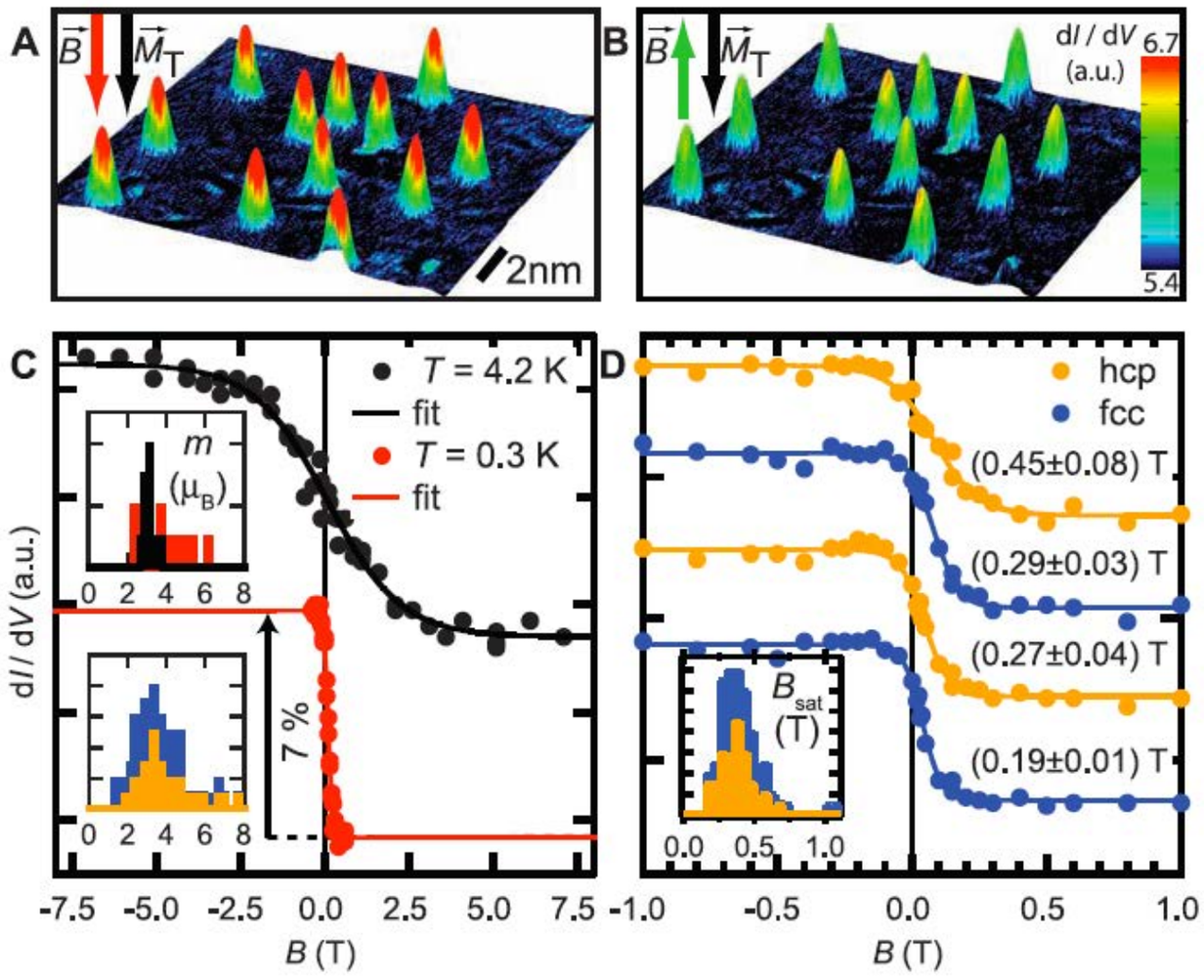

(A and B) Topographs of an area with several adatoms colorized with the spin-pol. dI/dV map at ***B*** = −0.5 T parallel to the tip magnetization $\boldsymbol{M_T}$ (A)
and B = +0.5 T antiparallel to $\boldsymbol{M_T}$ (B) (T = 0.3 K).
(C) ***M(B)*** curves from the same adatom taken at different temperatures as indicated (dots). Reversal of $\boldsymbol{M_T}$ is corrected.
(D) Magnetization curves of four adatoms at 0.3 K with fit curves and resulting $\boldsymbol{B_{sat}}$ of 99% saturation.

Refs.: F. Meier et al., Science **320** (2008) 82

2.3.3. Inelastic Tunneling

Inelastic Tunneling

Schematic showing the emergence of inelastic tunneling at the threshold for vibrational excitation. The change in the tunneling current due to vibrational excitation is too small to be measured from the *I*–*V* curve. While a change in the differential conductance, dI/dV, can be seen for strong modes, more often vibrational features needs to be extracted from d^2I/dV^2. An important characteristic of vibrational inelastic electron tunneling spectroscopy is the occurrence of a peak of the opposite sign on the negative bias side. Lacking an isotope shift analysis, the assignment of a feature to vibrational excitation needs to be confirmed by a corresponding feature with the opposite polarity at the opposite bias. This schematic depicts an increase in the conductance, associated with a positive/negative peak for positive/negative sample bias. In contrast, electronic spectra arise from elastic tunneling peaks are positive and occur on either positive (unoccupied) states or negative (occupied) states !

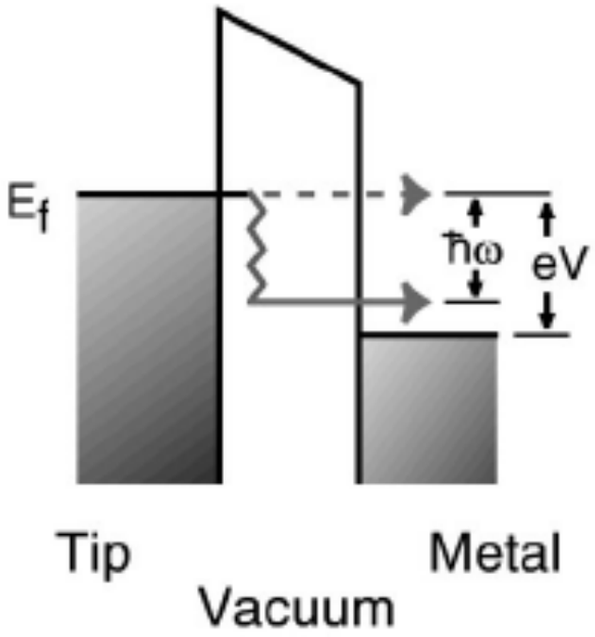

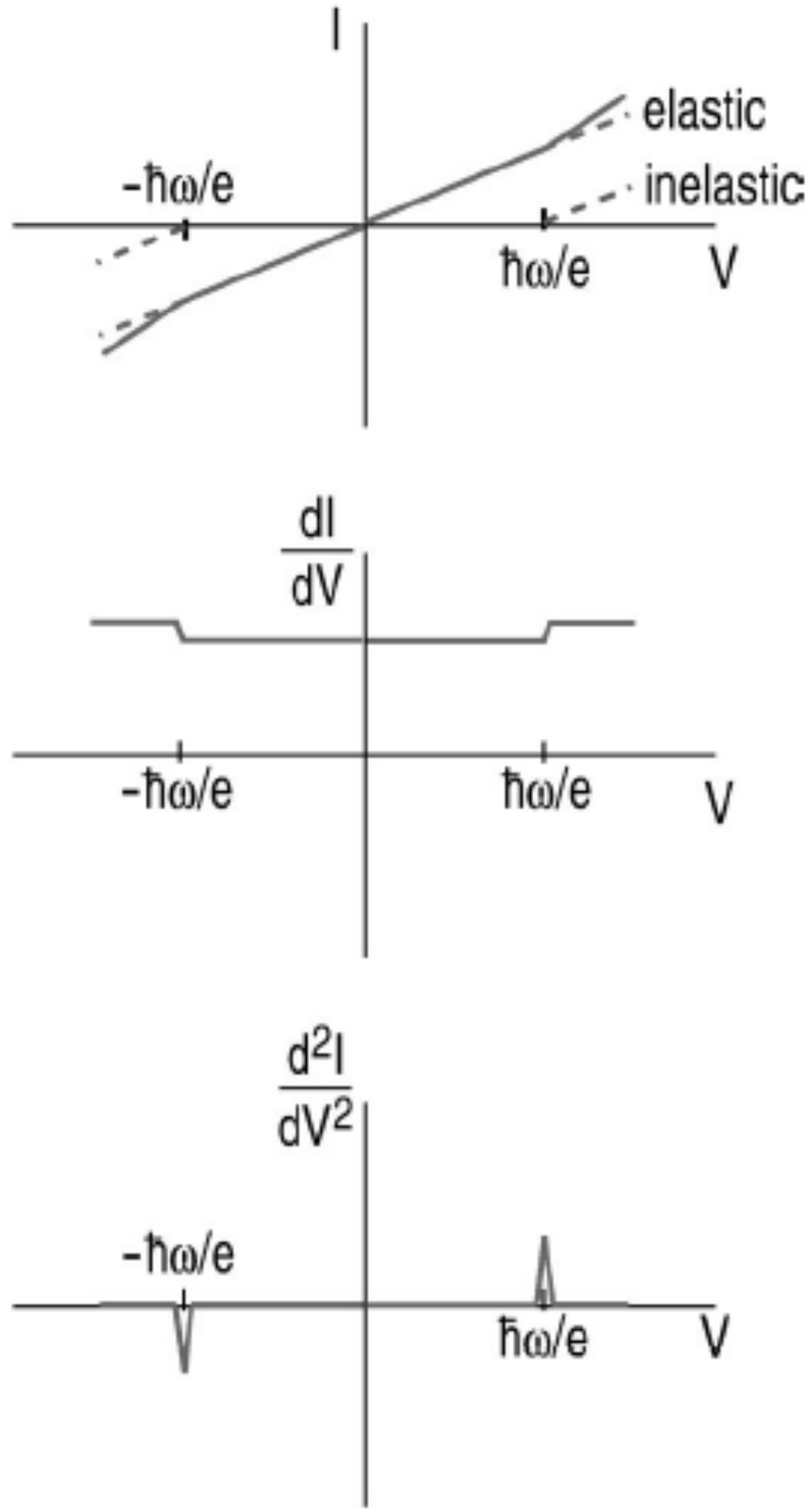

Ref.: W. Ho, J. Chem. Phys.117, 11033 (2002)

Vibrational Spectroscopy

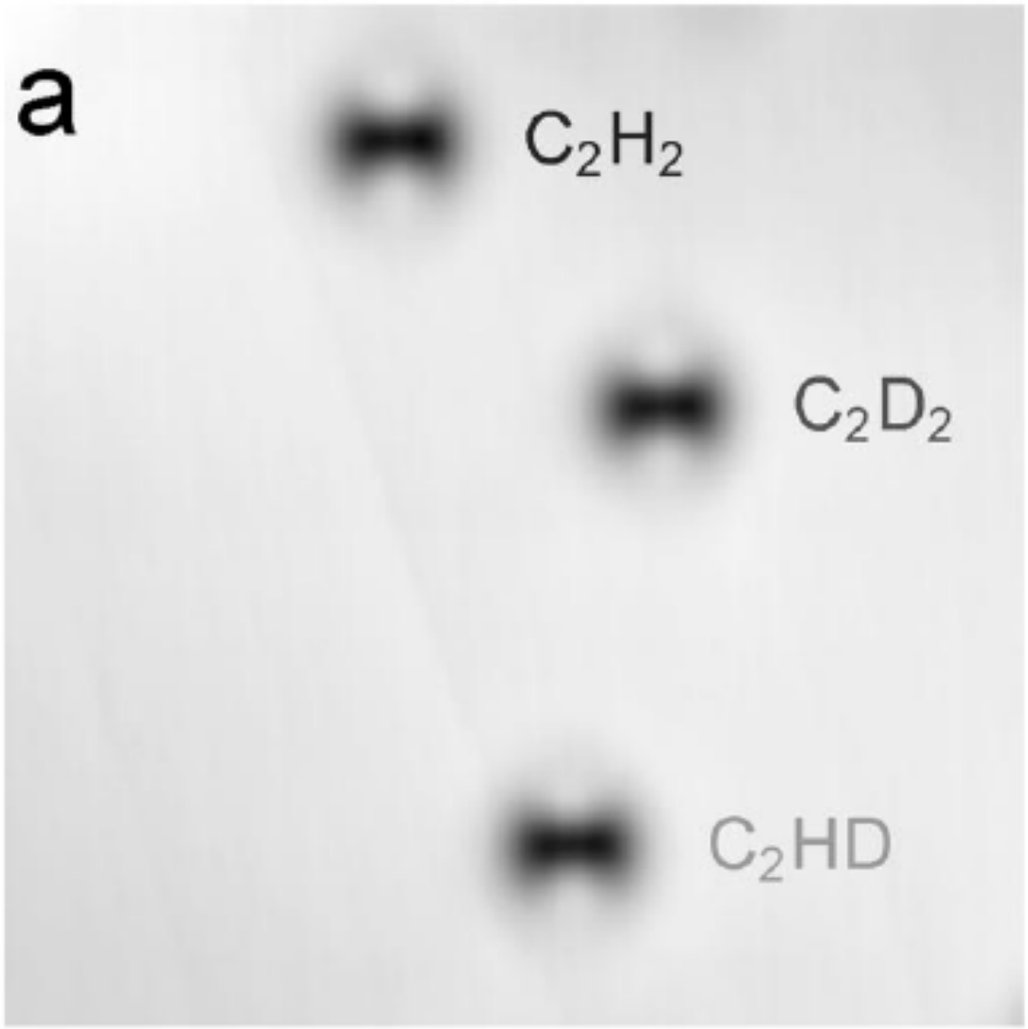

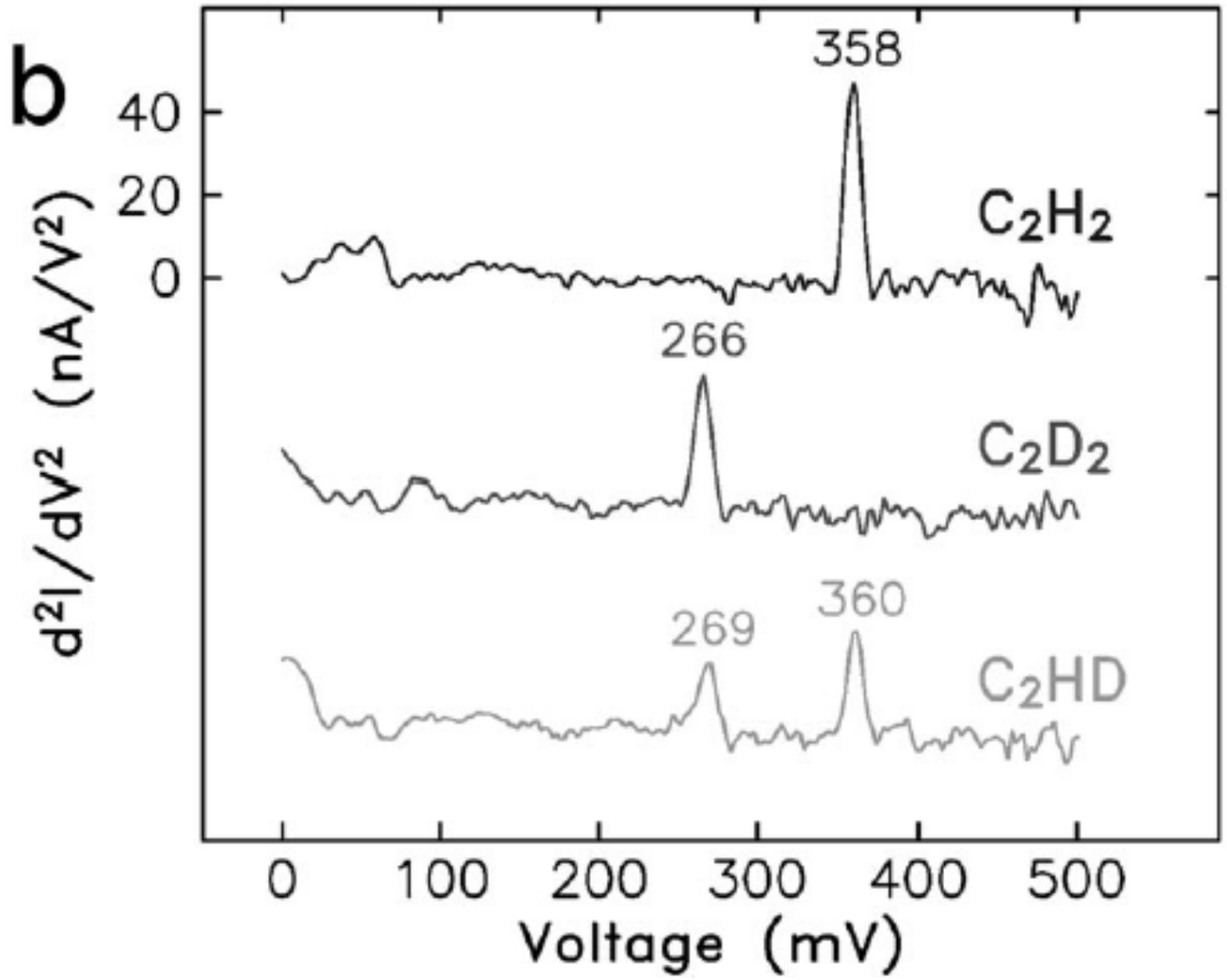

56 Å x 56 Å STM topographical images and single-molecule vibrational spectra via STM-IETS of three acetylene isotopes on Cu(001) at 8 K. The two protrusions bright in the image of each isotope are due to the presence of the C–H and C–D bonds while the central depression dark is attributed to the C–C bond. The C–H stretch is observed at 358 meV for C_2H_2 and the C–D stretch is observed at 266 meV for C_2D_2. Small upshifts are found for the C–H and C–D stretches of C_2HD. The C_2HD spectrum demonstrated for the first time single bond sensitivity with STM-IETS.

Ref.: W. Ho, J. Chem. Phys.117, 11033 (2002)

2.3.4. Arrhenius Analysis & Action Spectroscopy

Dynamics of Molecules on Surfaces

Empa
Materials Science and Technology

J. K. Gimzewski, et al., Science 281 (1998) 531: hexa-*tert*-butyl deca-cyclene (HB-DC) on Cu(111) @ RT

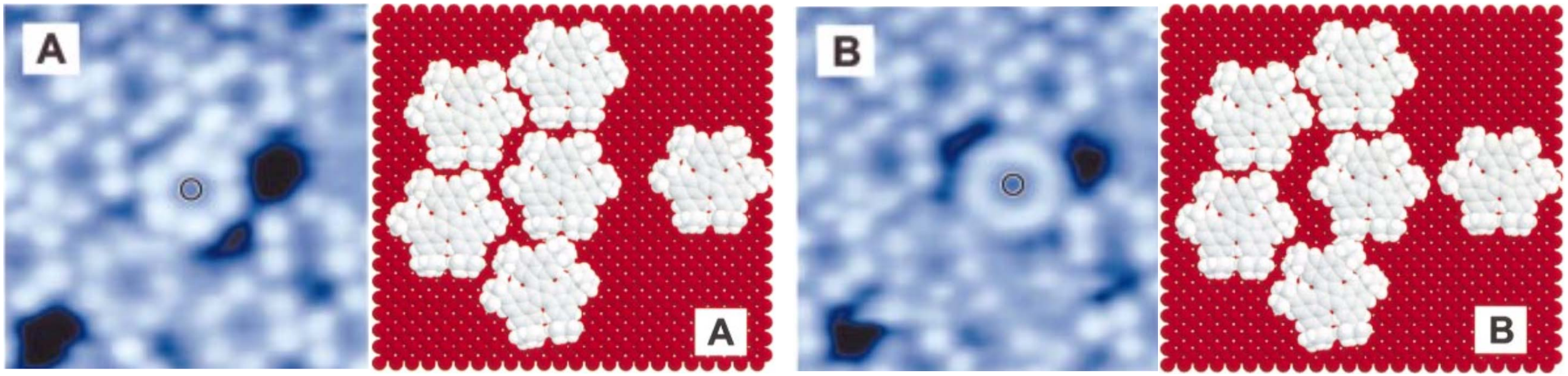

Rotation of a single hexa-tert-butyl deca-cyclene (HB-DC) molecule within a supramolecular bearing on Cu(111) @ RT

B.C. Stipe, M.A. Rezaei and W. Ho, Science 279 (1998) 5358: rotation of O_2 molecule on Pt(111)

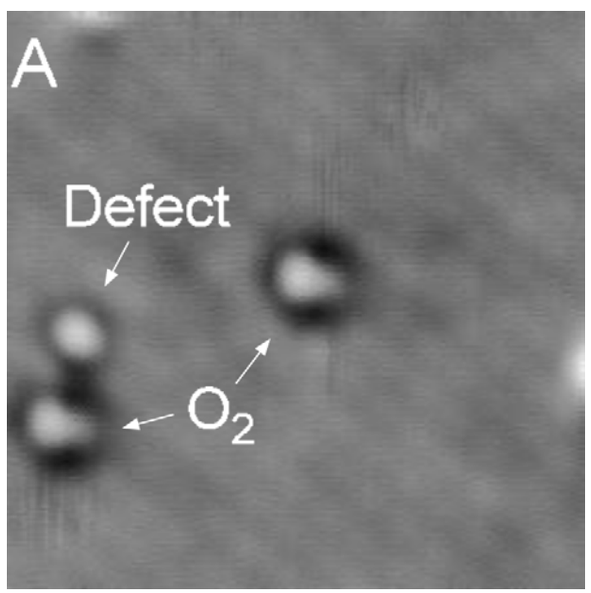

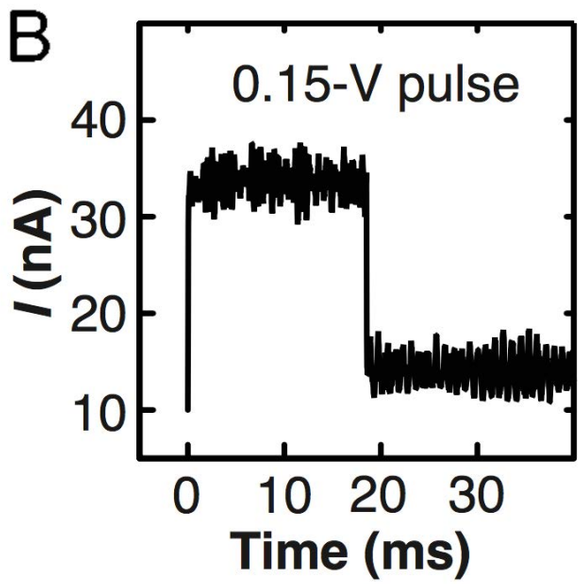

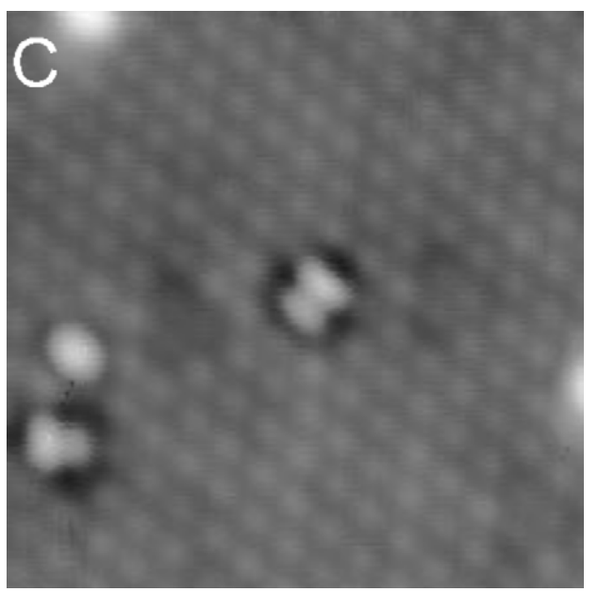

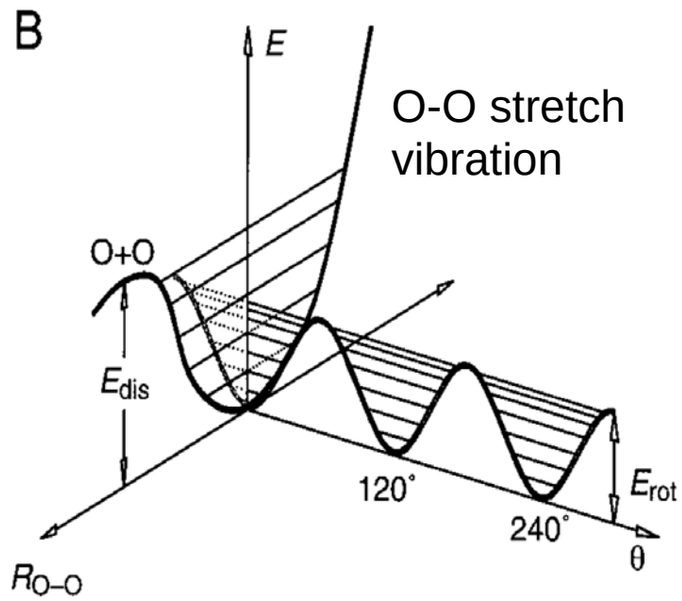

tip-induced rotation of O_2 molecule on Pt(111) @ 8K

O-O stretch vibration barrier:
$0.15\text{eV} < E_{rot} < 0.175\text{eV}$

Dynamics of Molecules on Surfaces

Empa
Materials Science and Technology

L. J. Lauhon, & W. Ho, Journal of Chemical Physics 111 (1999) 5633.

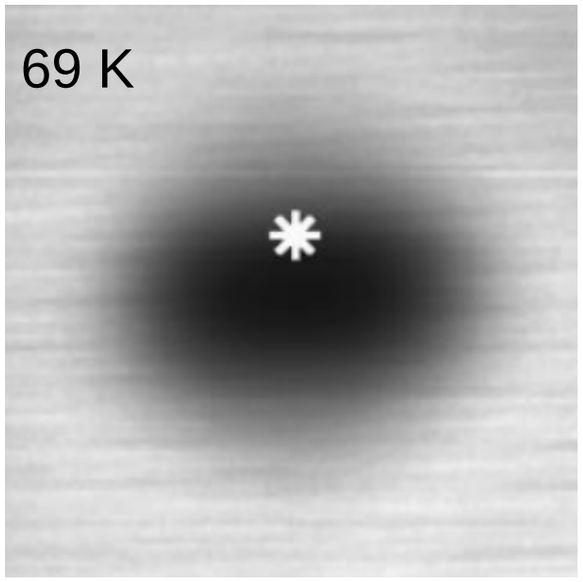

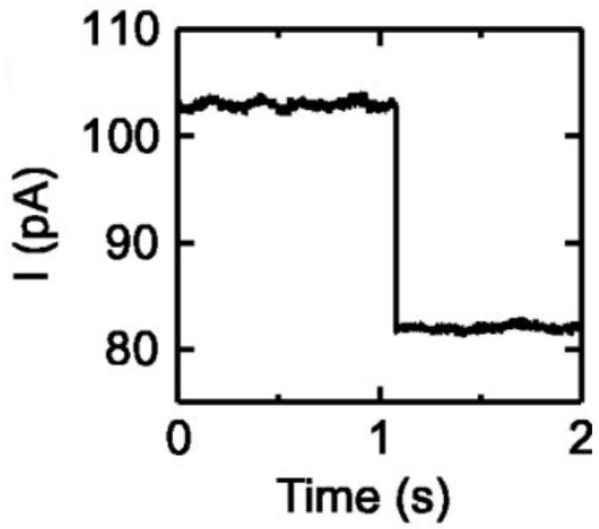

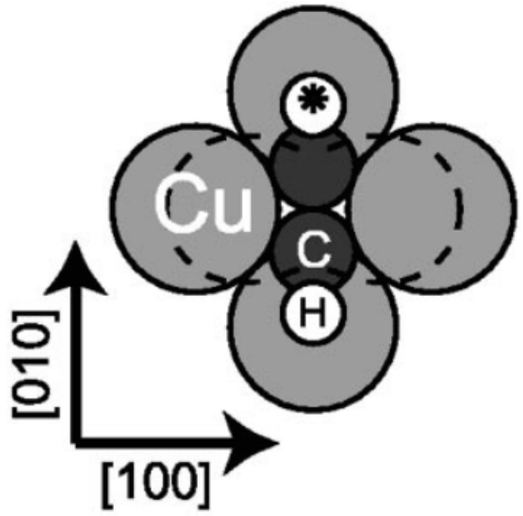

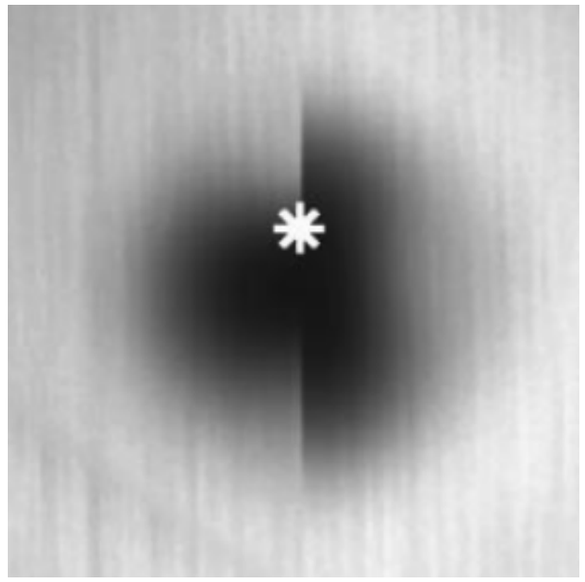

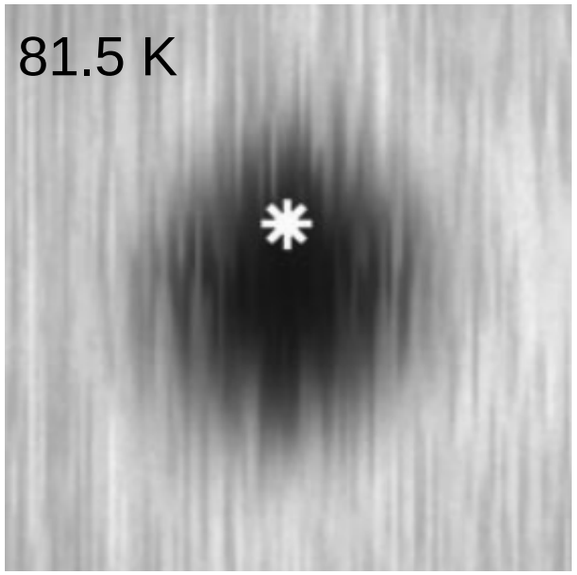

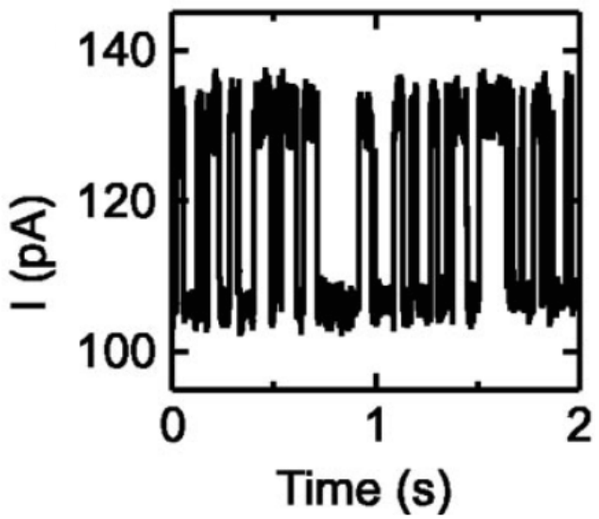

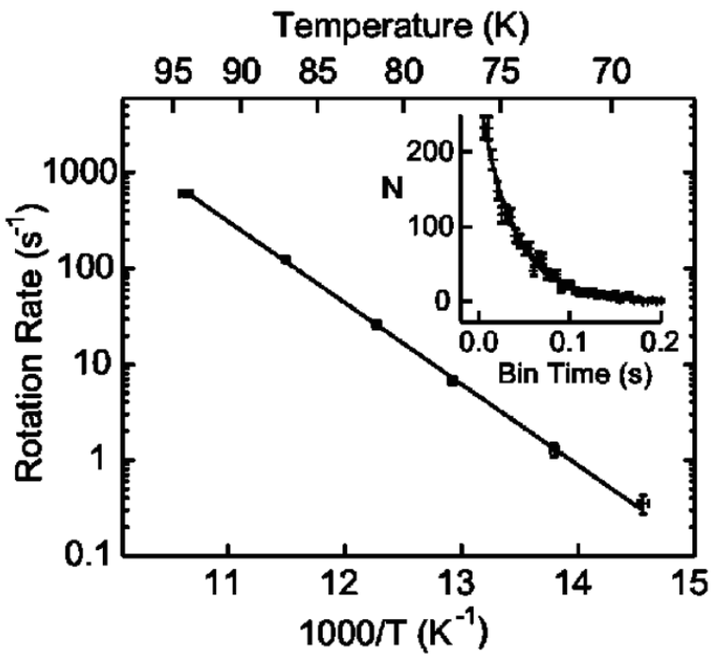

$$R_r = \nu_r \exp(-E_r/kT)$$
$$E_r = 169 \pm 3\,\mathrm{meV}$$
$$\nu_r = 10^{11.8\pm0.2}\,\mathrm{s}^{-1}$$

Single molecule C_2H_2 thermal rotation and diffusion: Acetylene on Cu(001).

2.4. Manipulation by STM

STM Manipulation of single Atoms

a) Vertical manipulation (transfer of the surface atom to the tip and back to the sample):
The transfer of the adsorbate atom from the surface to the tip, or vice versa, is achieved by approaching the tip into contact or near-contact. The application of voltage pulses can be used to set the direction. Eigler [1] found that Xe atoms moved in the same direction as the tunneling electrons, which was related to heating-assisted electromigration.

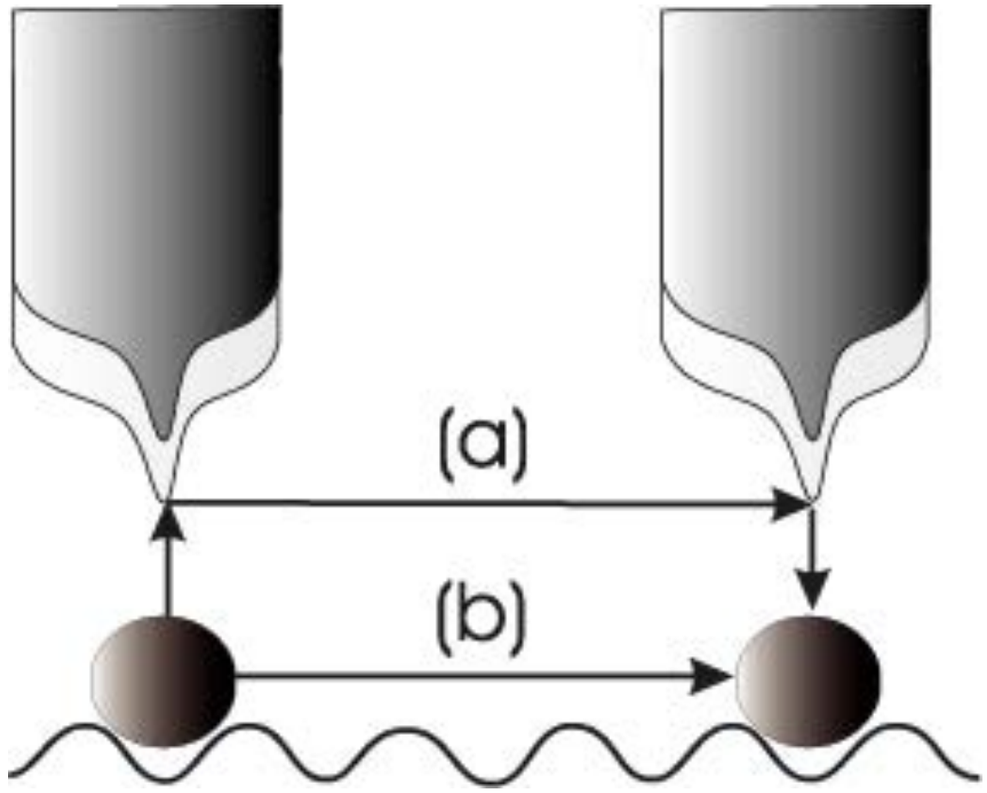

b) Lateral manipulation mode (adsorbate is kept adsorbed to the surface and moved laterally along surface): The tip is moved to the initial point, the set point is increased by about 2 orders of magnitude, which corresponds to a decrease of the distance of several Angstrom. The tip forms a weak bond with the adsorbate atom or molecule. The tip is then moved along the line of manipulation.
Typical threshold resistances to slide an adsorbate are 5MOhm for sliding Xe along rows of Ni(110), 200kOhm for sliding CO along Pt(111) and 20kOhm to move Pt adatoms along Pt(111).

Ref.: [1] D. Eigler, E. Schweizer: Nature 344, 524 (1990)

STM Manipulation of single Atoms and Molecules

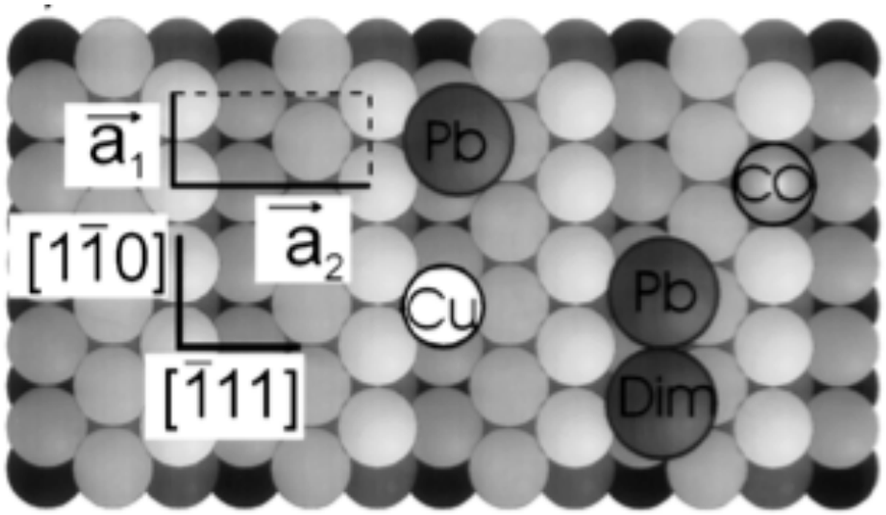

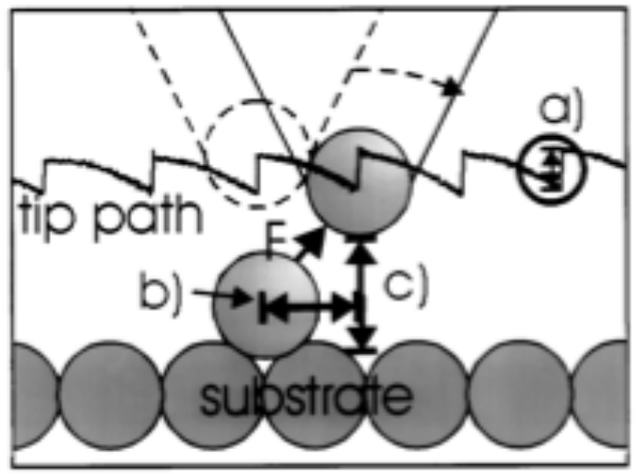

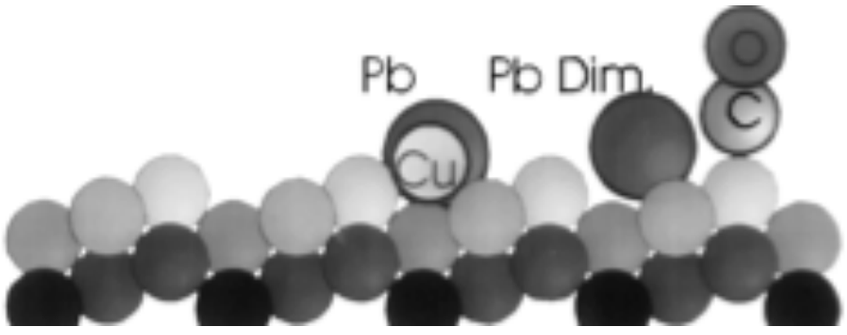

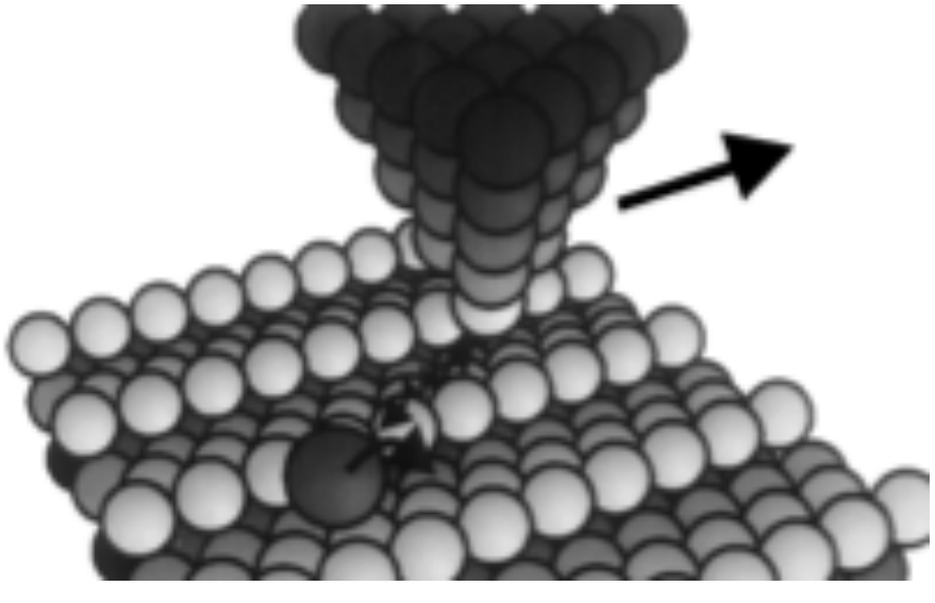

stick-slip motion (pulling)

continuous motion (pulling)

stick-slip motion (pushing)

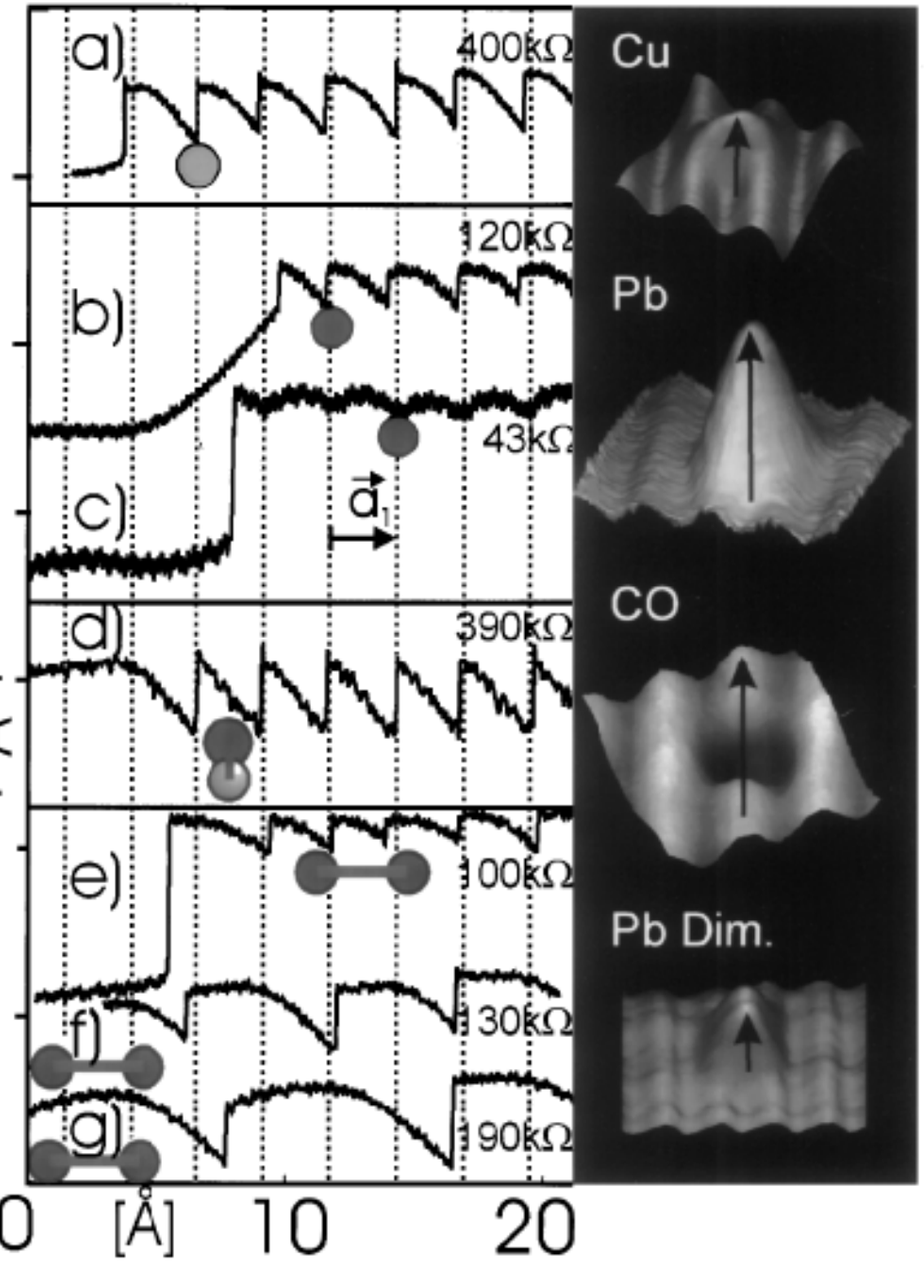

Ref.: [1] L. Bartels et al., Phys. Rev. Lett. 79, 697 (1997)

STM Manipulation of single Fe-Atoms on Cu(111)

Don Eigler, IBM Almaden Research Center

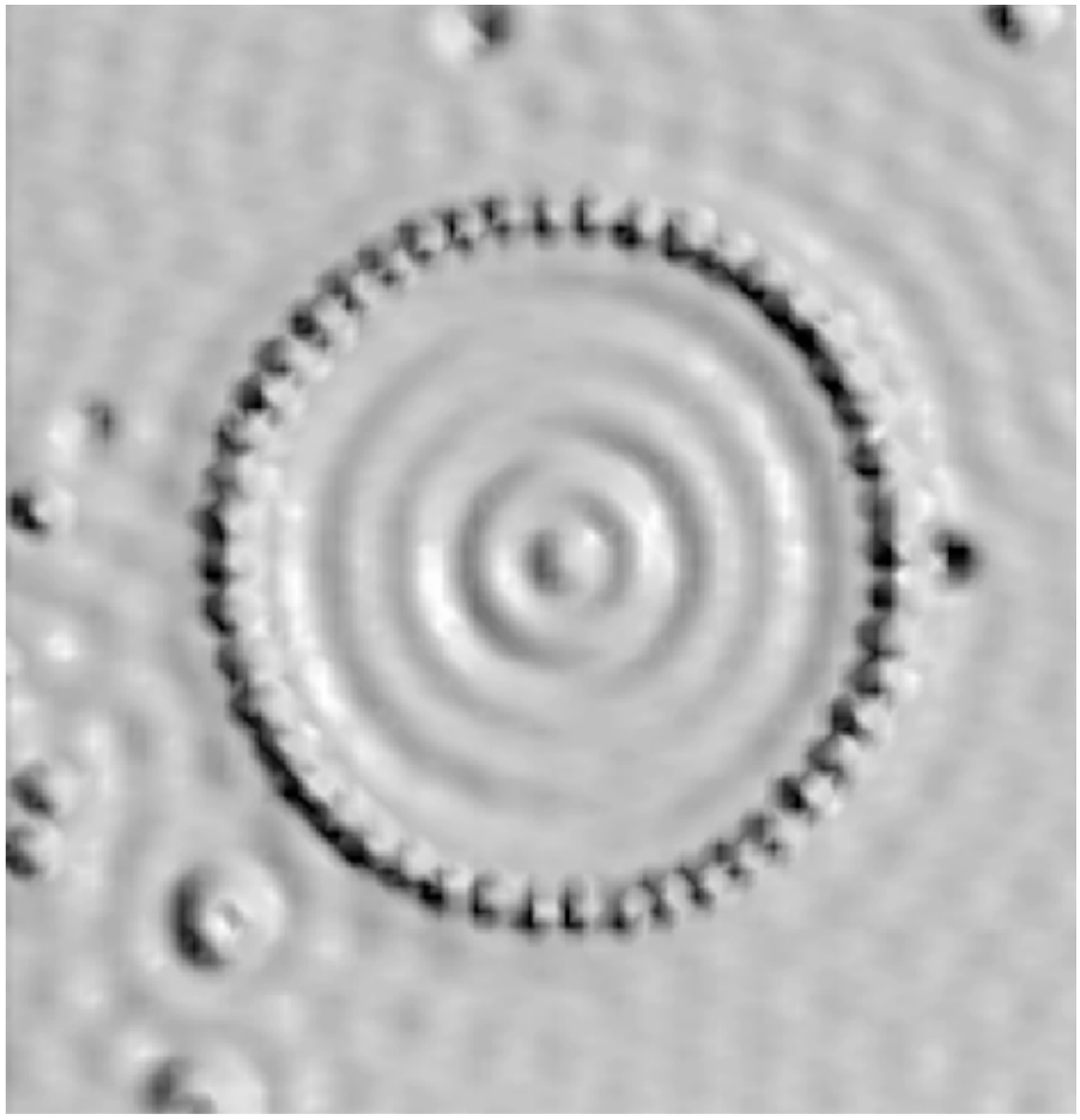

3.

Scanning Force Microscopy (SFM)
Atomic Force Microscopy (AFM)

3.1. Instrumentation

Force Effects in STM

Forces between tip and sample were attributed to play an important role [1].

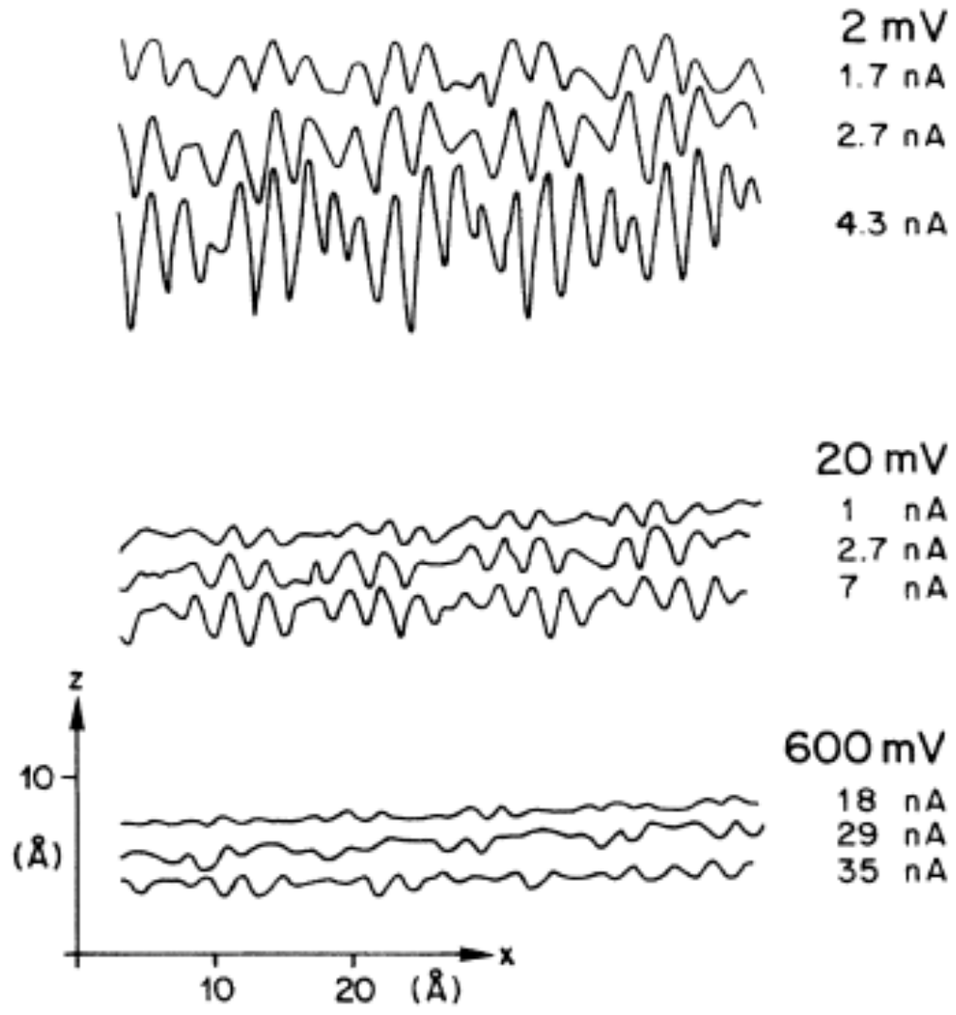

FIG. 1. Graphite STM traces obtained at ambient-air pressure and room temperature with a "pocket-size" STM (Ref. 14) with scanning speeds between 1 and 5 sec per scan. The varying corrugation within a scan is due to the mismatch between crystallographic and scanning directions (Ref. 3); plateaus in the traces indicate the saddle points in the LDOS (Refs. 3 and 11).

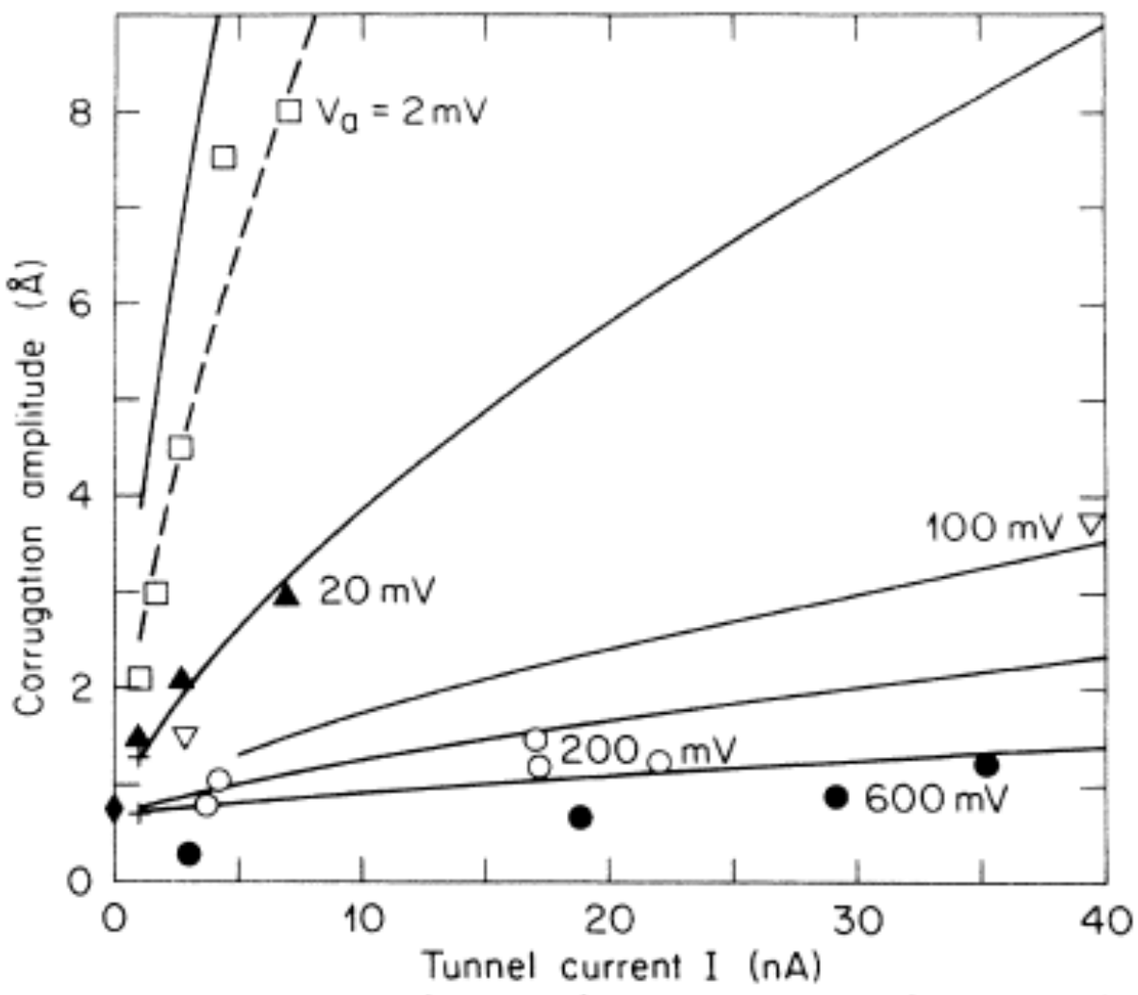

FIG. 4. Measured (symbols) and calculated (solid lines) corrugations as a function of tunneling current and voltage. The dashed line was obtained with $d^* = 0.4$ Å. The two crosses at 1 nA correspond to the measured corrugations at 50 and 400 mV, respectively, of Ref. 3; the diamond at zero current indicates the corrugation of the LDOS at the Fermi level (Ref. 11).

Refs.:[1] Soler et al. PRL57 444 (1987)
[2] R.V. Colemann et al. Adv. Phys. 37 559 (1988)

The First AFM by G. Binnig, C. Quate and Ch. Gerber (1986)

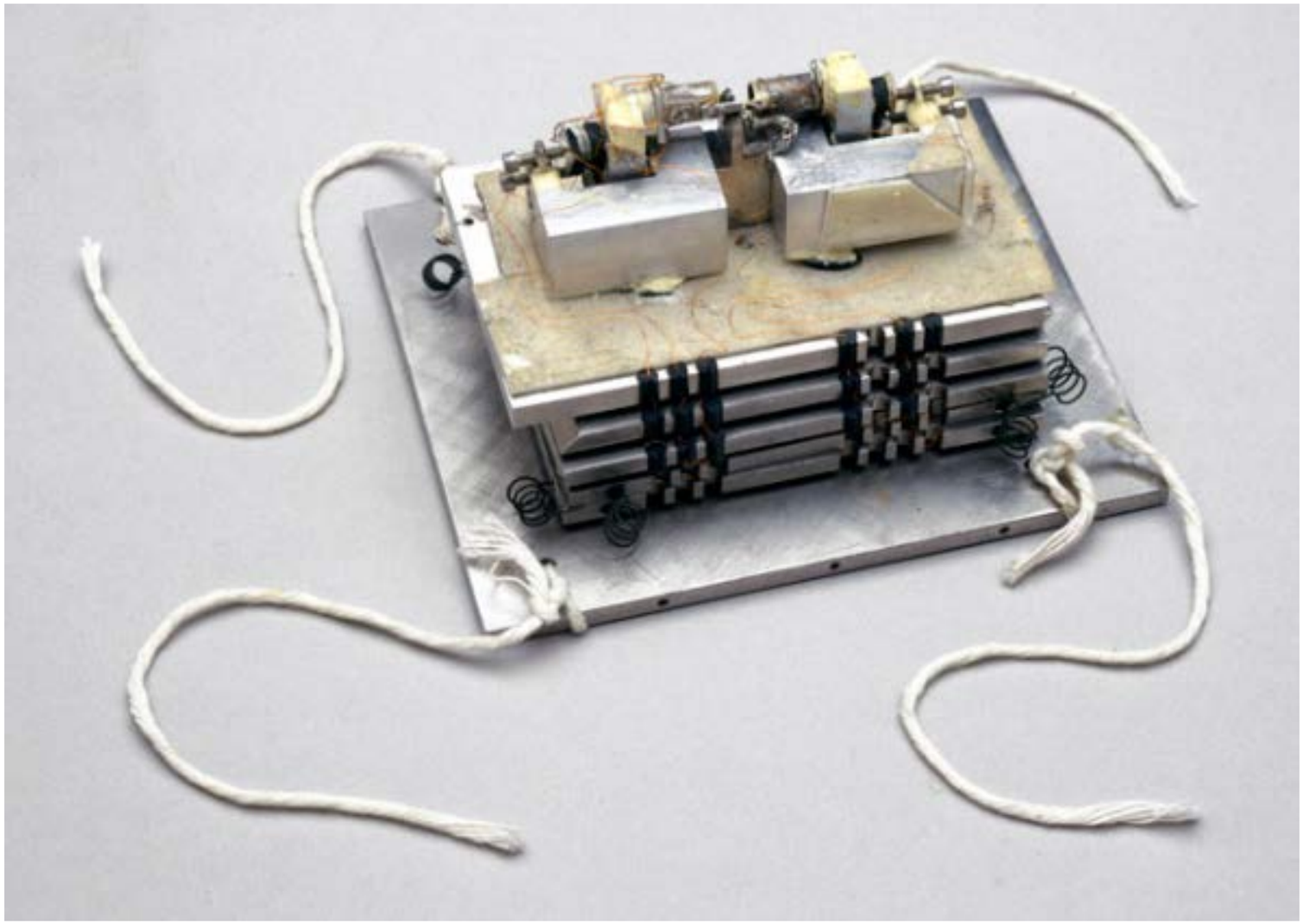

2016:

THE KAVLI PRIZE IN NANOSCIENCE is shared between **Gerd Binnig,** Former Member of IBM Zurich Research Laboratory, Switzerland, **Christoph Gerber**, University of Basel, Switzerland, and **Calvin Quate**, Stanford University, USA. They receive the prize “for the invention and realization of atomic force microscopy, a breakthrough in measurement technology and nanosculpting that continues to have a transformative impact on nanoscience and technology”.

The First AFM by G. Binnig, C. Quate and Ch. Gerber (1986)

The scanning tunneling microscope is proposed as a method to measure forces as small as 10^{-18} N. As one application for this concept, we introduce a new type of microscope capable of investigating surfaces of insulators on an atomic scale. The atomic force microscope is a combination of the principles of the scanning tunneling microscope and the stylus profilometer. It incorporates a probe that does not damage the surface. Our preliminary results *in air* demonstrate a lateral resolution of 30 Å and a vertical resolution less than 1 Å.

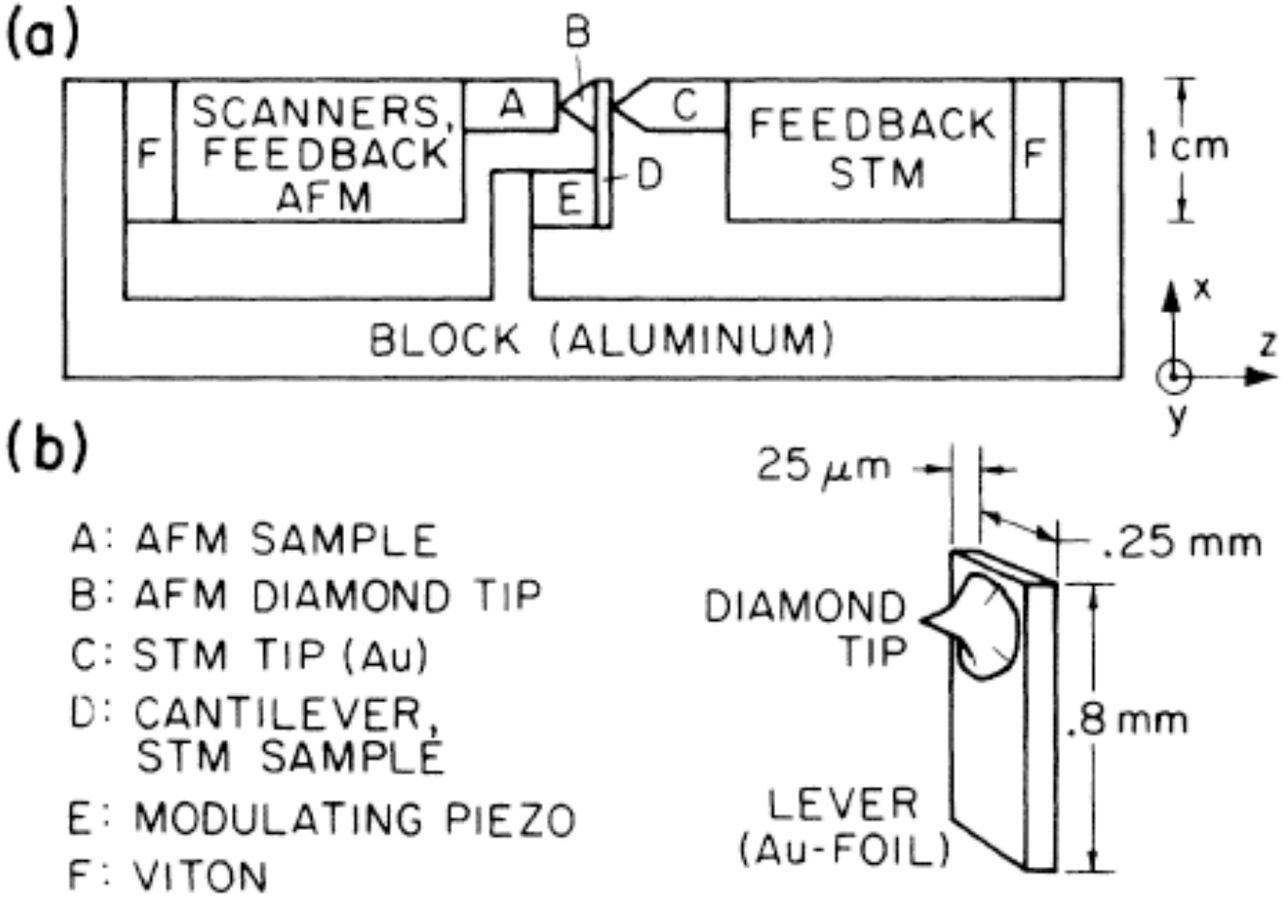

FIG. 2. Experimental setup. The lever is not to scale in (a). Its dimensions are given in (b). The STM and AFM piezoelectric drives are facing each other, sandwiching the diamond tip that is glued to the lever.

G. Binnig, C. Quate, Ch. Gerber, Phys. Rev. Lett. **56**, 930 (1986)

An AFM consists of:

- a 3d-scanner (similar to that of an STM)
- a force sensor (cantilever)
- a deflection sensor
- in most cases a sensor-cantilever positioning unit

AFM - SFM - or? - Possible Classification Schemes

1. operation mode bases schemes

   measured cantilever property per imaged xy (z, other parameter) point:

   a) Static Modes: (dc) deflection (flexural or torsional) of cantilever
   b) Dynamic Modes: dynamic cantilever properties
      i. oscillation amplitude, phase
      ii. required drive amplitude, frequency shift
      iii. overtones (harmonic & non-harmonic), intermodulation products

2. tip-sample interaction based schemes

   a) physical nature of force
      i. frictional forces (FFM),
      ii. magnetic (MFM), electrostatic (EFM), contact potential (Kelvin)
      iii. energy-loss: dissipation force microscopy
   b) „mechanics“ of tip-sample interaction
      i. contact mode
      ii. pulsed force mode
      iii. intermittent contact mode (tapping)
      iv. non-contact mode

- be aware that you just measure forces or force gradients ...
- differentiate between
  - instrumentation physics (how to measure) and
  - physics of tip-sample interaction (what you measure)

3.1.1. relevant Forces

Relevant Forces

typical long-range forces (> 1nm):
- van der Waals
- electrostatic, magnetic, Casimir

forces in liquids:
- hydrophobic / hydrophilic forces
- steric forces
- solvation forces

typical short-range forces (contact / near contact):
- short-range repulsive forces (Pauli exclusion) or ionic repulsion forces
- short-range chemical binding forces

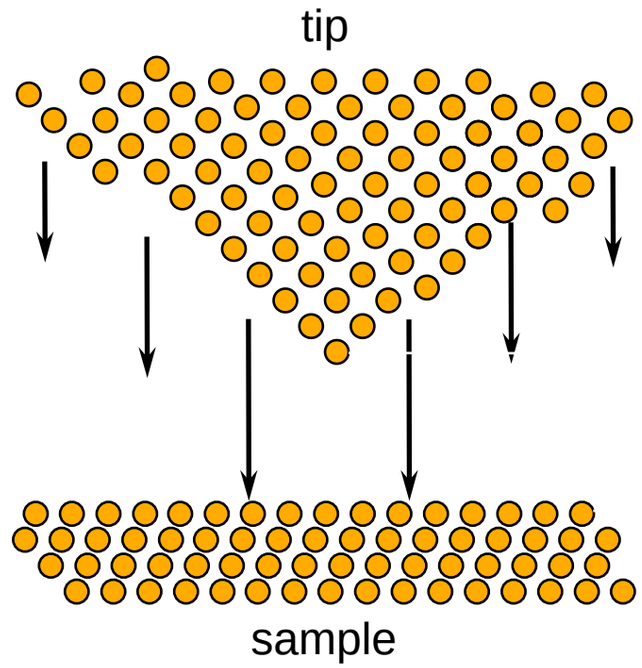

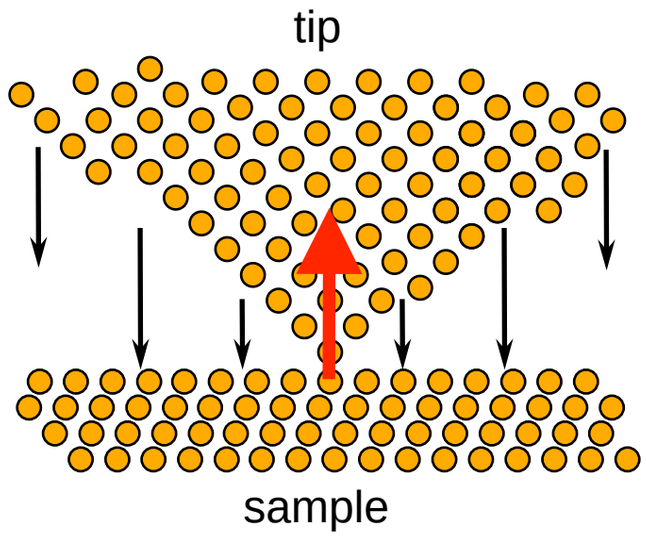

- **When the tip is in contact with the sample, a large, repulsive tip-sample force may occur to the tip apex due to the possibly large long-ranged attractice forces !!!**
- **So zero cantilever deflection does not mean that the tip apex force is zero !!!**

Refs.:

J. Israelachvili
Intermolecular and Surface Forces with Applications to Colloidal and Biological Systems, Academic Press (1985)
D. Tabor
Gases, liquids and solids, Cambridge University Press (1979)

How to measure Forces

tip-sample interaction

the deflection sensor determines:
- flexural or torsional deflection,
- sensitivity,
- measurement bandwidth,

note that
this is not
a *simple spring*
but
is (e.g.) determined by overlap of orbitals, i.e. chemical bonding (quantum mechanical exchange)

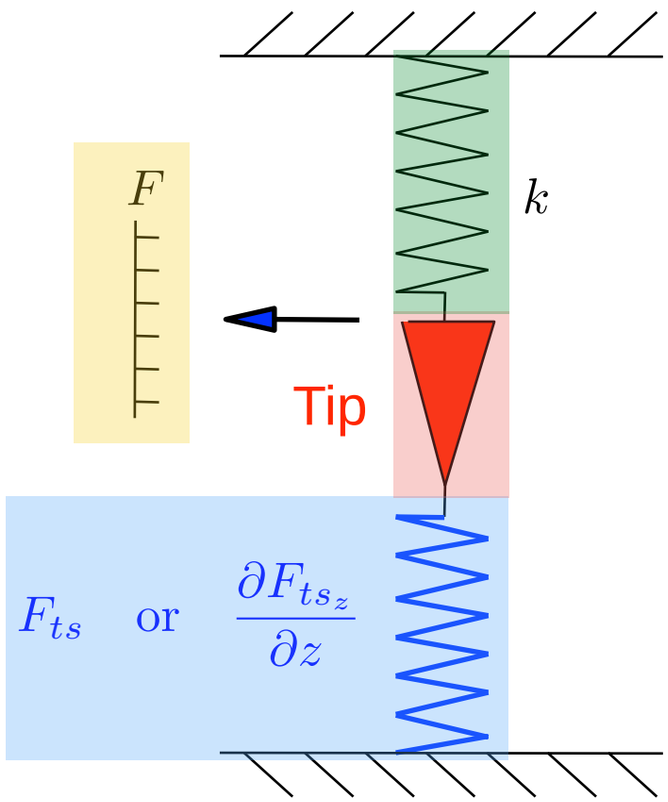

force sensor, cantilever determines:
- sensitivity,
- measurement bandwidth,
- instabilities, ...

tip determines:
- type of interaction force
- sensitivity,
- resolution, ...
- may depend on outside parameters

interaction determines:
- type of interaction force,
- decay length of force,
- sensitivity,
- resolution, ...
- may depend on outside parameters

- forces of various physical nature that act simultaneously
- physics of the cantilever (particularly in dynamic mode)
- the need to adjust the force sensor to the cantilever

➡ increased complexity of the **instrumentation** (hardware, electronics, software = measurement physics) and (real, sample) **physics** !

- more complex than STM, but more versatile and a much higher challenge, so more fun ... but STM can still be done!

Short-range Forces: inter-Atomic Forces

arise from overlap of electron wave functions of the tip and sample:

- short ranged, act for tip-sample distances < 1nm
- attractive, if overlap of wavefunctions reduces total energy, e.g. when (partial) chemical bonding occurs
- repulsive, e.g. arising from Pauli exclusion principle

Force can obtained from Morse Potential

$$V_{Morse}(r) = D_e \cdot \left(e^{-2a(r-r_e)} - 2e^{-a(r-r_e)} \right) \quad \text{with} \quad V_{Morse}(r_e) = -D_e \quad \text{and} \quad \lim_{r\to\infty} V_{Morse}(r) = 0$$

Lennard-Jones Potential

$$V_{LJ}(r) = 4\epsilon \left[\left(\frac{\sigma}{r}\right)^{12} - \left(\frac{\sigma}{r}\right)^{6} \right] = \epsilon \left[\left(\frac{r_m}{r}\right)^{12} - 2\left(\frac{r_m}{r}\right)^{6} \right]$$

with ϵ depth of potential,
$r_m = 2^{1/6}\sigma \approx 1.122\sigma$ distance of potential minimum

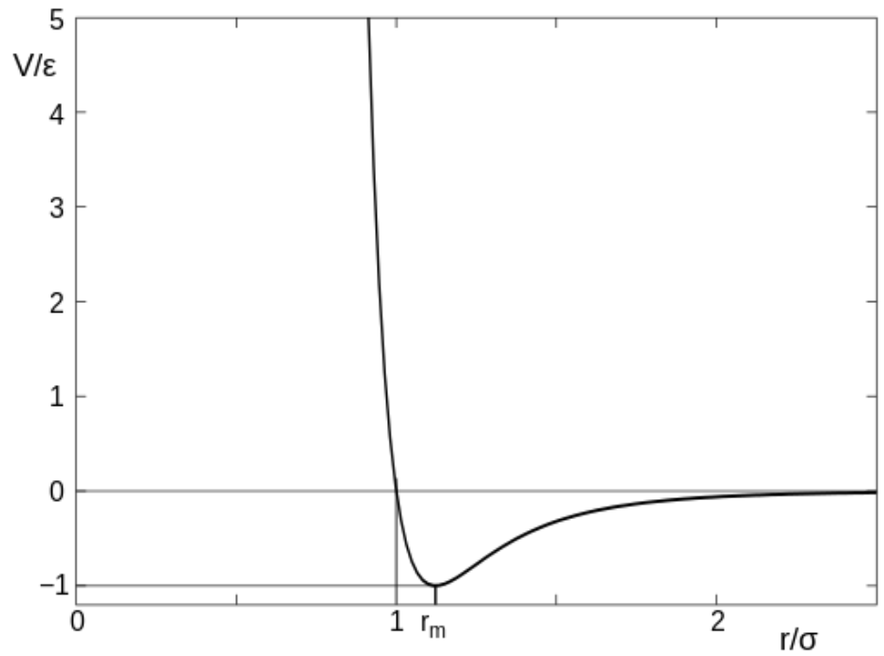

Stillinger-Weber Potential

$$V_{SW} = \frac{1}{2}\sum_{ij} \phi(r_{ij}) + \sum_{ijk} g(r_{ij}) g(r_{ik}) \left(\cos\theta_{jik} + \frac{1}{3} \right)^2$$

two-body potential — three-body potential

if $\cos\theta_{jik} = -\frac{1}{3}$ three-body potential vanishes

Long-range Forces: van der Waals

The term includes:
- force between two permanent dipoles (Keesom force)
- force between a permanent dipole and a corresponding induced dipole (Debye force)
- **force between two instantaneously induced dipoles (London dispersion force).**

force between a fluctuating dipole and a dipole induced by the electric field

$$F_{vdW}(r) = \propto \frac{1}{r^7}$$

force between a sphere and a flat surface $F_{vdW}(z) = \frac{HR}{6z^2}$

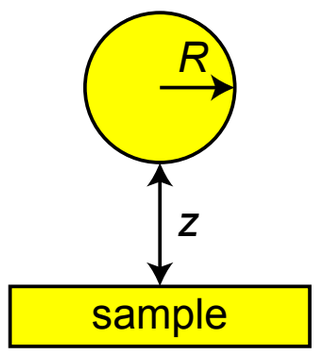

van der Waals forces in media:
- in vacuum and in most media vdW forces are attractive
- Lifshits theory predicts that the force is proportional to $(\varepsilon_1-\varepsilon_3)$ $(\varepsilon_2-\varepsilon_3)$ and $(n_{12}-n_{32})(n_{22}- n_{23})$, where ε and n are dielectric constant and refractive index of tip (1), sample (2), and medium (3) in between.
- medium with ε and n close to the respective values of tip and sample will greatly reduce van der Waals forces.
- immersing liquid can lead to a negative Hamaker constant and to repulsive van der Waals forces.
- repulsive van der Waals Forces in liquids are used to stabilize suspensions of (nano)particles
- repulsive van der Waals Forces have also been used for the first AFM experiments showing true atomic resolution [1]

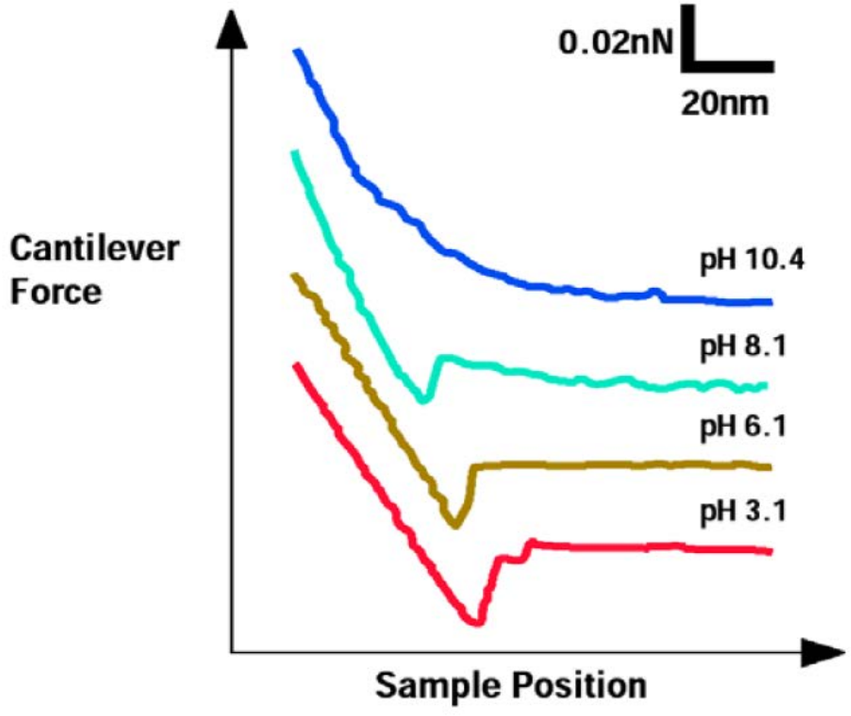

Si_3N_4 tip / mica surface

[1] F. Ohnesorge and G. Binnig, *Science* 260, 1451 (1993)

Long-range Forces: Electrostatic Forces

$$E_{el} = \frac{1}{2} C U_{tot}^2 \quad \Rightarrow \quad F_{el_z} = -\frac{1}{2} \frac{dC(z)}{dz} U_{tot}^2 \quad \text{with} \quad U_{tot} = U_{bias} - U_{cpd}$$

applied contact potential

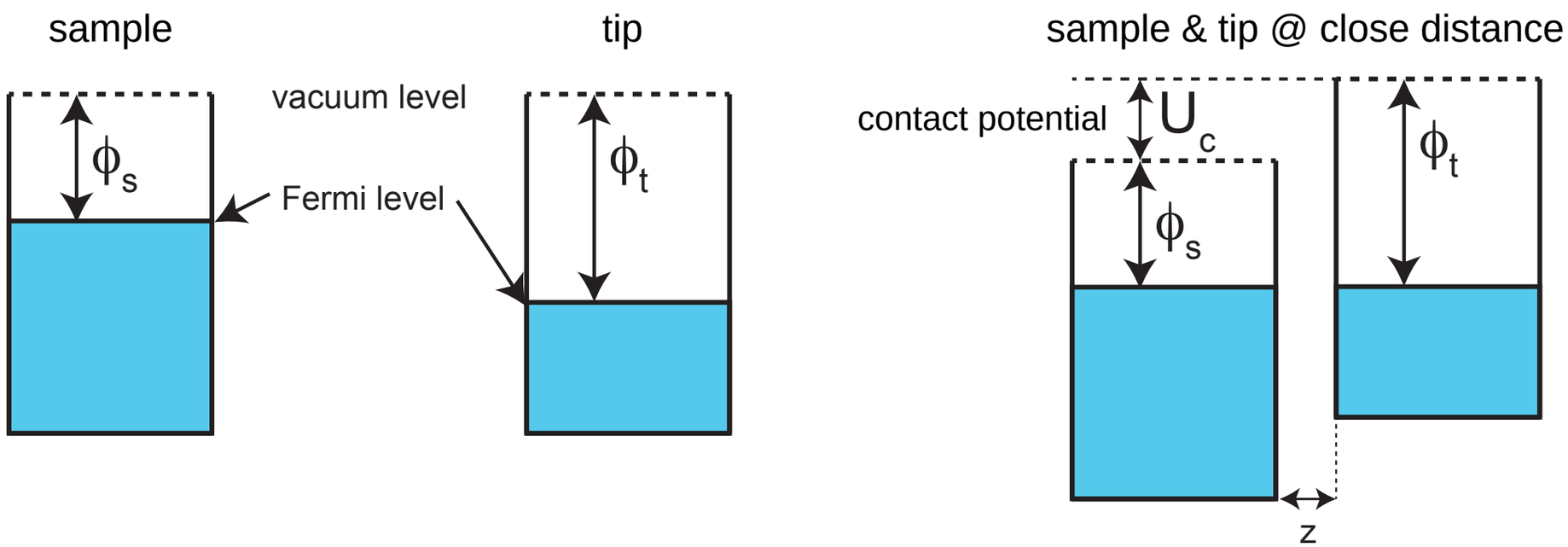

- the (average) contact potential can be compensated by an appropriate external bias that minimizes the total force
- electrostatic patch forces:

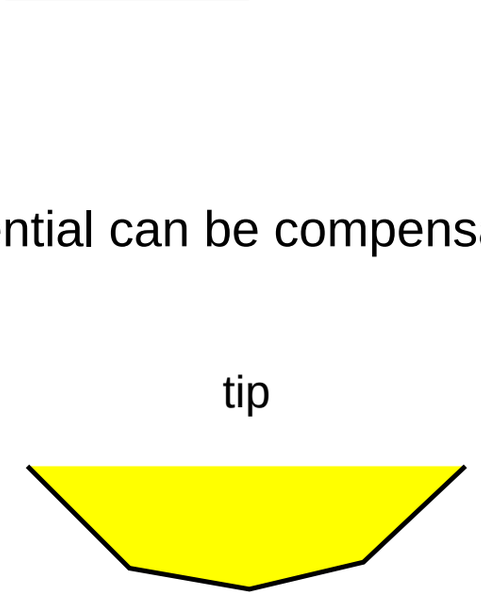

different surfaces at tip-apex have different contact potentials
➜ the total electrostatic force cannot be nulled by an applied bias.

Long-range Forces: Magnetostatic Forces

Empa
Materials Science and Technology

in direct space the force is:

$$\mathbf{F}(\mathbf{r}, z) = \mu_0 \int_{V'} (\nabla \mathbf{M}_{tip}(\mathbf{r}', z')) \, \mathbf{H}_{sample}(\mathbf{r} + \mathbf{r}', z + z') d\mathbf{r}' dz'$$

after some math in Fourier space

$$\mathbf{F}(\mathbf{k}, z) = \mu_0 \int_{V'} \underbrace{\nabla_k \mathbf{M}^*_{tip}(\mathbf{k}, z') e^{-\mathbf{k}z'}}_{=: \sigma^*_{tip}(\mathbf{k})} dz' \cdot \mathbf{H}_{sample}(\mathbf{k}, z)$$

➜ once this transfer function is known (tip calibration), the field can be obtained from the force

- Note that the the force on a magnetic dipole $\mathbf{m}$ in a field $\mathbf{B}$ is: $\mathbf{F}_{\mathrm{mag}} = \mathbf{m} \cdot \nabla \mathbf{B}$, but the tip is NOT a magnetic point dipole, but an extended dipole!

Hence:

- the magnetic force is rather proportional to the stray field (and NOT to the derivative of the stray field as documented in many manuals of SPMs and publications)

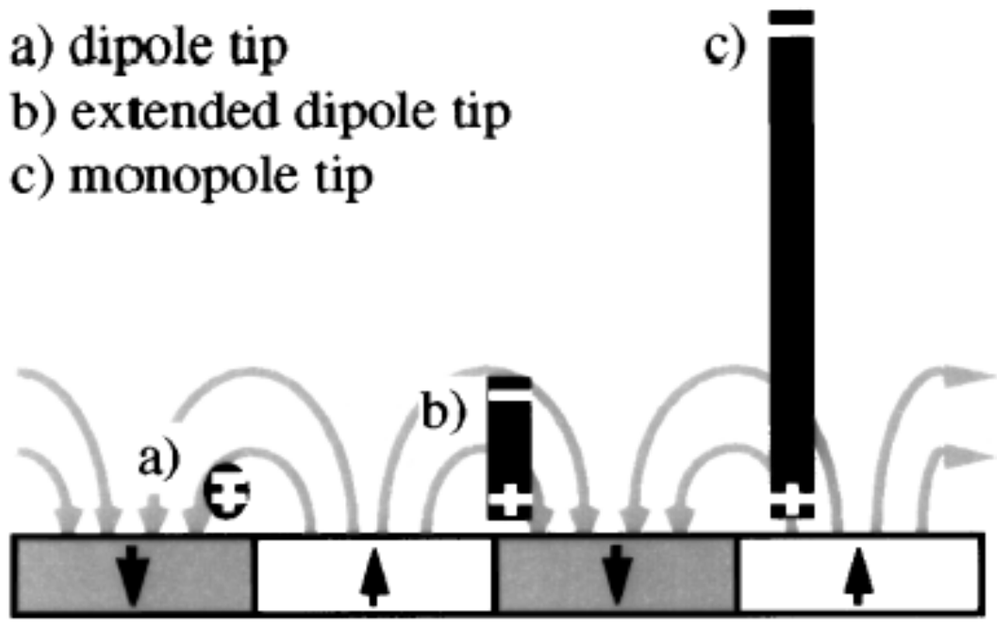

Capillary Forces

- microcontacts act as nuclei of condensation.
- In air, water vapor plays the dominant role.
- If the radius of curvature of the microcontact is below a certain critical radius (approximately equal to the Kelvin radius) a meniscus will be formed.
- The Kelvin radius is given by

$$r_K = \frac{\gamma V}{RT log(p/p_S)}$$

where γ is the surface tension, R the gas constant, T the temperature, V the molar volume and p_S the saturation vapor pressure.

- The surface tension of water is γ = 0.074 N/m at T = 20 C which gives the parameter $\gamma V/RT$ = 0.54 nm. Therefore we obtain for p/p_s = 0.9 a Kelvin radius of 100 nm.
- In Scanning Force Microscopy, typical tips having radii of less than 100 nm are possible nuclei of condensation. If a meniscus is formed an additional capillary force acts on the tip. A simple estimation is given by:

$$F = \frac{4\pi R\gamma \cos\Theta}{1 + D/(R(1 - \cos\phi))}$$

- where R is the radius of curvature, Θ the contact angle, D the distance between tip and sample and φ the angle of the meniscus. The maximum force is given by $F_{max} = 4\pi R\gamma \cos\Theta$.
- For a tip radius of 100 nm we obtain a force $F_{max}=9.3\cdot10^{-8}$N, which is significantly stronger than the corresponding van der Waals force.
- Typical force vs. distance curves in ambient conditions reveal forces of the order of 10^{-8}-10^{-7}N, which mainly originates from capillary forces.
- These adhesion forces limit the minimum force which acts on the outermost tip region, and have to be equilibrated by the repulsive force in this small contact region. Consequently, capillary forces can determine the size of the contact and play an essential role in force microscopy measurements in air.

Capillary Forces

$F_{max} = 4 \pi R \gamma \cos(\Theta)$

γ (H_2O) = 0.074N/m R=100nm

Contact angle foir hydrophilic surfaces $\Theta \approx 0°$

$\Rightarrow$ F_{max} = 90nN

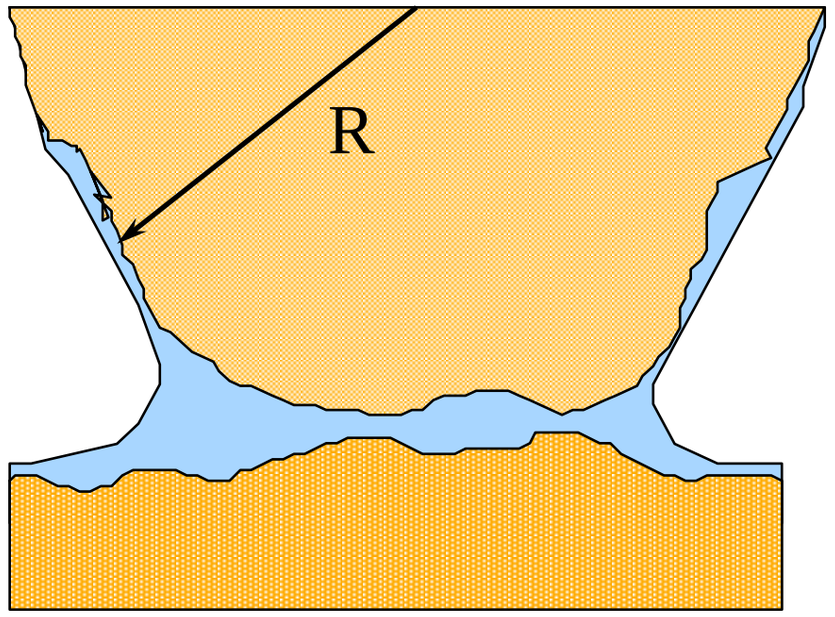

3.1.2. Force Sensors & their Properties

Force Sensors - Cantilevers

There are some simple criteria to be considered, when cantilevers are fabricated:

- resonance frequency f_R > 100Hz (building vibrations), > 10kHz (sound waves)
- high force sensitivity requires low spring constants (MFM:, 0.1 N/m, mRFM: 0.001 N/m)
- atomic resolution requires spring constant to be in range of atomic spring constants > 10N/m
- thermal vibrations of the cantilever < 0.1nm, i.e. k>0.4N/m @ 300K

It can be shown that only cantilevers of dimensions in the micrometer range fulfil these design criteria. Generally, higher resonance frequencies require smaller cantilevers.

single cristalline silicon cantilevers

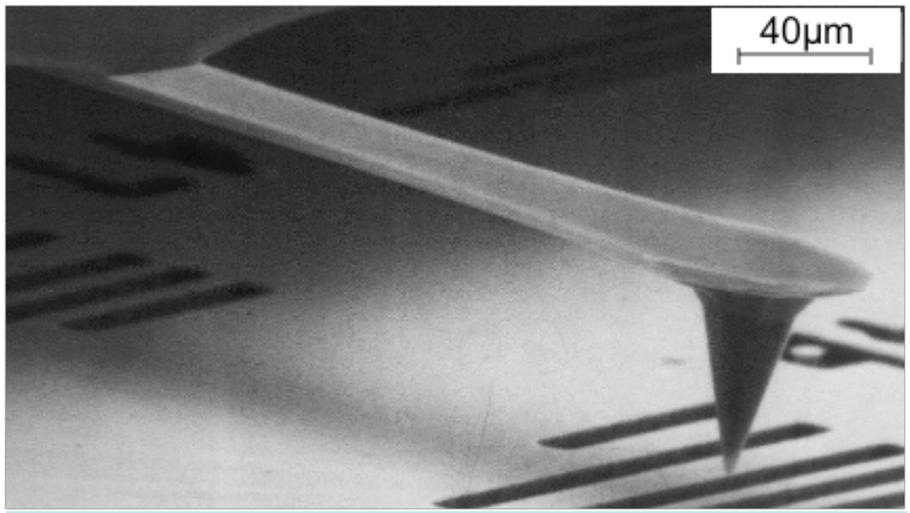

force constant: 0.01 – 100 N/m
resonance frequency: 5 – 500 kHz

high-aspect ratio tips

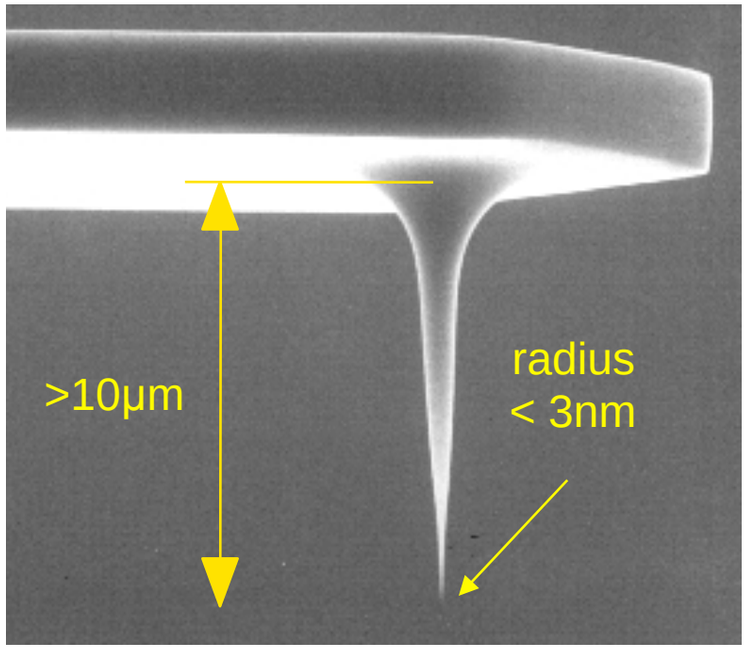

ultrasharp tip

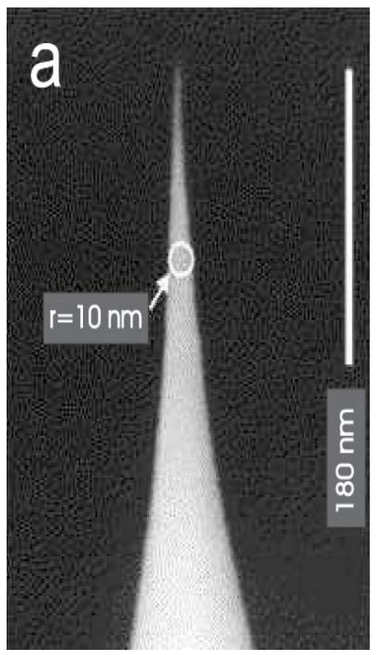

tuning fork sensor

Team Nanotec GmbH, www.team-nanotec.de

Spring Constants of Cantilevers

flexural spring constant

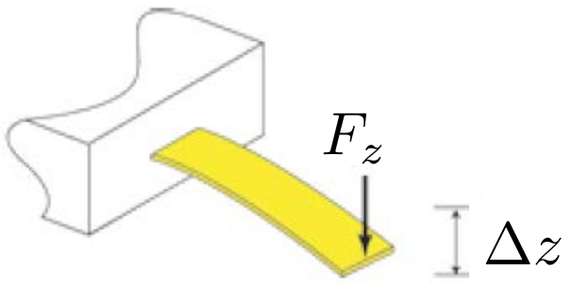

Fig. 1: Schematic illustration of the normal spring constant.

$$k_c = \frac{F_z}{\Delta z} \qquad k_c = \frac{E t^3 w}{4 L^3}$$ static, flexural spring constant

torsional spring constant

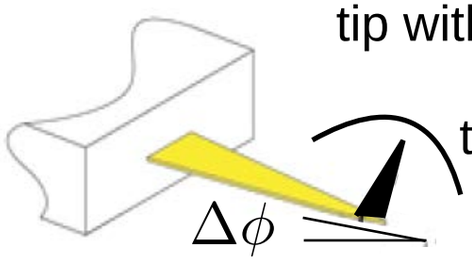

Fig. 2: Schematic illustration of the torsional spring constant.

$$k_\phi = \frac{T}{\Delta\phi} \qquad k_\phi = \frac{G t^3 w}{3 h^2 L}$$ torsional spring constant

cantilever dimensions & material properties

L, w, t length, width and thickness of cantilever. Note: particularly thickness is difficult to determine …

$$t = \frac{\omega_1}{\alpha_1^2} \cdot 2L^2 \cdot \sqrt{\frac{3\rho}{E}} \quad \text{with} \quad \alpha_1 = 1.875$$ thickness determined from resonance frequency

E: elasticity module for silicon: E_{Si} = 1.69x10^{11} N/m^2

G: torsional elasticity module for silicon: G_{Si} = 0.68x10^{11} N/m^2

Issues with Spring Constants of Cantilevers

spring constants have been calculated from cantilever dimensions and material properties, but:

- thickness is difficult to determine acurately
- the tip mass is neglected
- flexural theory becomes difficult, if shape of cantilever is not rectangular
- cantilever resonance is shifted in viscous fluids, i.e. in air or in water

1. calibration in air from resonance frequency:

[1] Sader et al., Rev. Sci. Instrum. 70, 3967 (1999)

[2] Sader, J. Appl. Phys. 84, 64 (1998)

Spring constant calibration of atomic force microscope cantilevers of arbitrary shape: Sader et al, Rev. Sci. Instrum. 83, 103705 (2012);

2. in vacuum from resonance frequency and known cantilever shape & materials properties

k from dimensions of cantilever

$$k_{dim} = \frac{3EI}{L^3} \quad \text{with} \quad I = \frac{1}{12}wt^3 \quad \text{and} \quad w = \frac{1}{2}(w_1 + w_2)$$

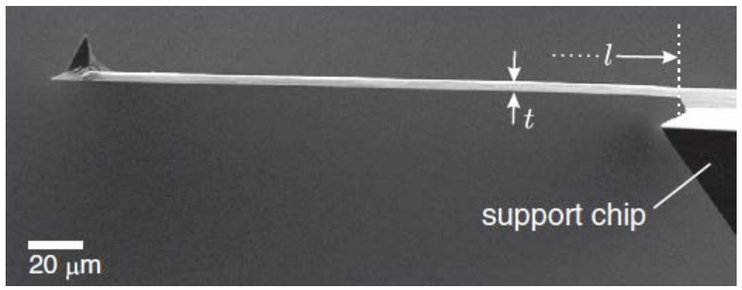

materials properties of silicon

$$\rho_{Si} = 2331\,\mathrm{kgm}^{-3} \qquad E_{Si(110)} = 169\,\mathrm{GPa}$$

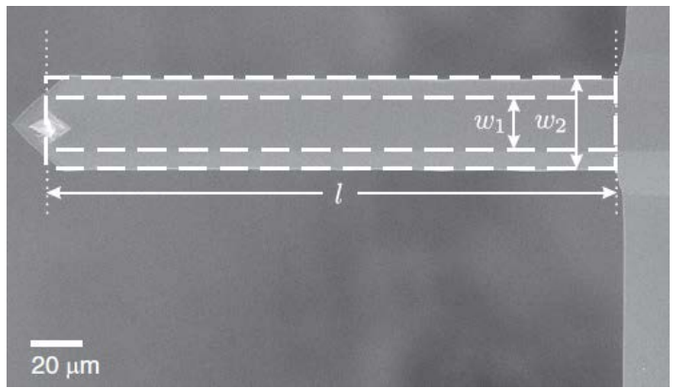

thickness from resonance frequency

$$f_n = \frac{\omega_n}{2\pi} = \frac{\alpha_n^2 t}{2\pi L^2}\sqrt{\frac{E}{12\rho}} \quad \text{with} \quad \cos\alpha_n \cosh\alpha_n + 1 = 0 \quad \text{resulting in} \quad \alpha_1 = 1.8751$$

n	α_n
1	1,8750
2	4,6941
3	7,8548
4	10,9955
5	14,1372
6	17,2788

from these equations, we obtain:

$$k_{dim,f_n} = \frac{2\pi^3 w L^3 f_n^3}{\alpha_n^6}\sqrt{\frac{12^3\rho^3}{E}}$$

Lübbe et al., Meas. Sci. Technol. 23 (2012) 045401 (9pp)

Cantilever, a mass-loaded beam - Flexural theory

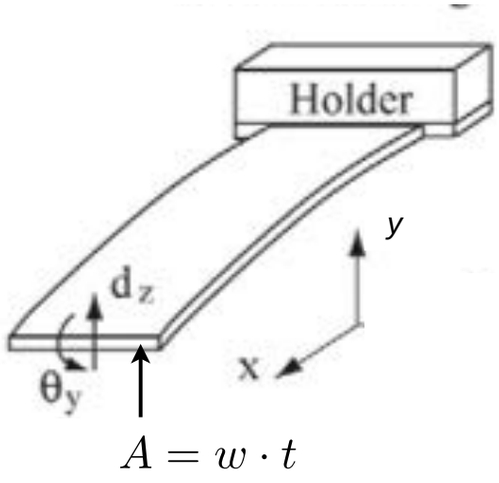

$A = w \cdot t$

equation of motion

$$EI\frac{\partial^4 y}{\partial x^4} + \rho A\frac{\partial^2 y}{\partial t^2}$$

note:
4th derivative, because wave equation of flexure of cantilever

E: elasticity module
E_{Si} = 169 GPa
I: area moment of inertia
ρ : density
ρ_{Si} = 2330 kg/m³
$I = w \cdot t^3/12$

general solution

$$y(x,t) = \left(a_1 e^{kx} + a_2 e^{-kx} + a_3 e^{ix} + a_4 e^{-ikx}\right) e^{-i\omega t}$$

inserting general solution in equation of motion results in dispersion relation

$$EIk^4 - \rho A \cdot \omega^2 = 0$$

with the boundary conditions (free cantilever end - no tip-sample interaction)

$$y = 0,\ \frac{\partial y}{\partial x} = 0 \quad \text{for } x = 0 \quad \text{and} \qquad \frac{\partial^2 y}{\partial x^2} = 0,\ \frac{\partial^3 y}{\partial x^3} = 0 \quad \text{for } x = L.$$

deflection, slope = 0 at cantilever support

moment, shear force = 0 at cantilever end

inserting general solution in boundary conditions. Resulting 4 equations can only be solved if characteristic equation is fulfilled:

$$\cos\alpha_n \cdot \cosh\alpha_n + 1 = 0 \qquad \text{with} \qquad \alpha_n = k_n L$$

Rabe, Rev. Sci. Instrum., 67 (1996) 3281 & Refs. therein

Cantilever, a mass-loaded beam - Flexural theory - Results

solutions of the characteristic equation:

n	α_n
1	1,8750
2	4,6941
3	7,8548
4	10,9955
5	14,1372
6	17,2788

n	α_n
7	20,4205
8	23,5619
9	26,7040
10	29,8450
11	32,9870
12	36,1280

with $\alpha_n := k_n L$

from the dispertion relation $EIk_n^4 - \rho \cdot \omega_n = 0$ then follow non-harmonic resonances

$$\omega_n = \frac{(\alpha_n)^2}{L^2} \cdot \sqrt{\frac{EI}{\rho A}} = \frac{\alpha_n^2}{\alpha_1^2} \cdot \omega_1$$ for example: $\omega_2 = 6.27 \cdot \omega_1$

$$I = \frac{1}{12} w t^3$$

Point-mass model of Cantilever

replacing the cantilever (a) by a point-mass at the end of a mass-less spring (b) that interacts with the sample

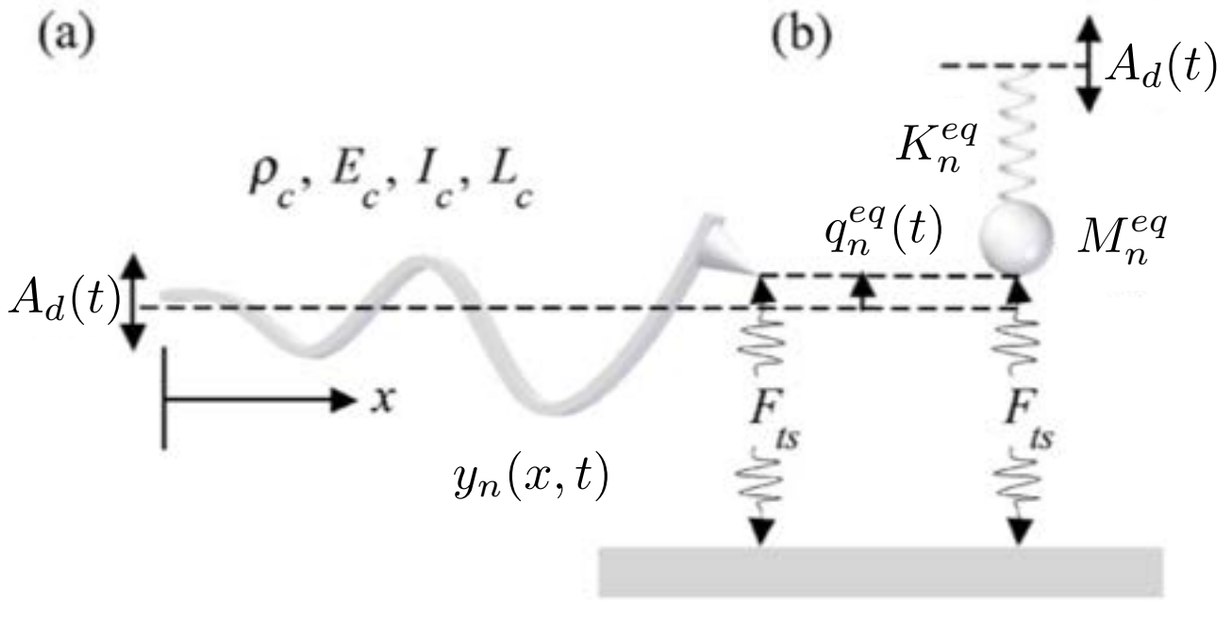

$y_n(x,t) = \phi_n(x) \cdot q_n^{eq}(t)$

$\phi_n(x)$ Eigenmode with scaling $\phi_n(x = L) = 1$

kinetic energy $T_n = \frac{1}{2}\int_0^L \rho \ddot{y}_n(x,t)^2\, dx$ ➜ $T_n = \frac{1}{2} M_n^{eq} \dot{q}(t)^2$ from this we obtain: $M_n^{eq} = \frac{m_c}{4}$ for the rectangular cantilever!

strain energy $V_n = \frac{1}{2}\int_0^L EI y_n''(x,t)^2\, dx$ ➜ $V_n = \frac{1}{2} K_n^{eq} q^2$ from this we obtain: $K_n^{eq} = \frac{k_c \alpha_n^4}{12}$ with $k_c = \frac{Ewt^3}{4L^3}$ for the rectangular cantilever!

Summary:

$$\omega_n = \frac{(\alpha_n)^2}{L^2} \cdot \sqrt{\frac{EI}{\rho A}} = \frac{\alpha_n^2}{\alpha_1^2} \cdot \omega_1$$

for example: $\omega_2 = 6.27 \cdot \omega_1$

$$K_n^{eq} = \frac{k_c \alpha_n^4}{12} \qquad I = \frac{1}{12} w t^3$$

for example: $K_2^{eq} = 39.28 \cdot K_1^{eq}$

and (!) $K_1^{eq} = 1.03 \cdot k_c$

n	α_n
1	1,8750
2	4,6941
3	7,8548
4	10,9955
5	14,1372
6	17,2788

Melcher et al. Appl. Phys. Lett. 91, (2007) 053101

Cantilevers and their Properties - Oscillation Modes

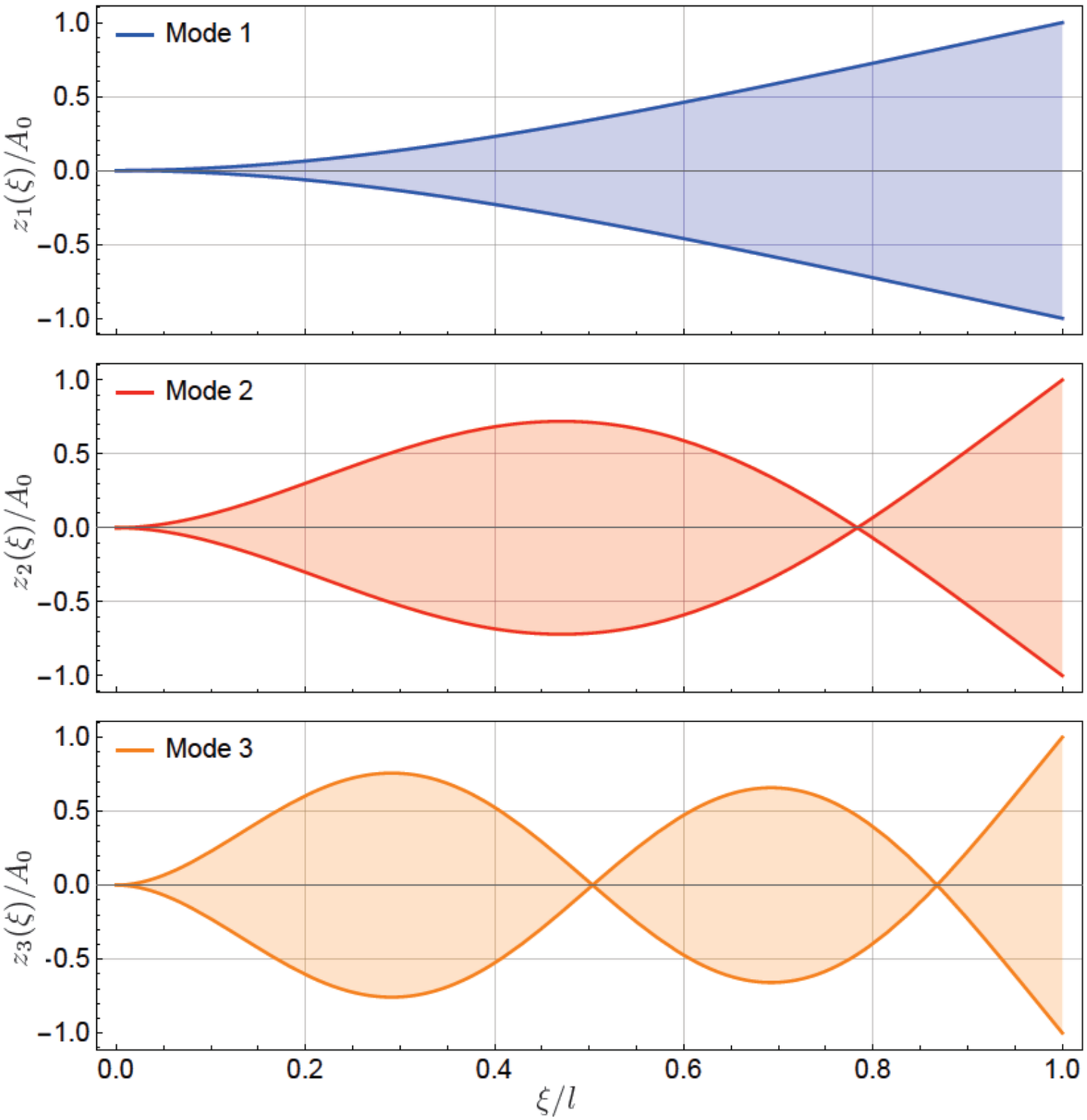

$$I = \frac{1}{12} w t^3$$

$$\omega_1 = \frac{\alpha_1^2}{L^2} \cdot \sqrt{\frac{EI}{\rho A}} \quad \text{with} \quad \alpha_1 = 1.875$$

$$K_1^{eq} = \frac{k_c \alpha_1^4}{12} \quad \text{with} \quad k_c = \frac{E t^3 w}{4 L^3}$$

$$\begin{aligned} \omega_2 &= \frac{\alpha_2^2}{L^2} \cdot \sqrt{\frac{EI}{\rho A}} \quad \text{with} \quad \alpha_2 = 4.6941 \\ &\approx 6.2676 \cdot \omega_1 \end{aligned}$$

$$\begin{aligned} K_2^{eq} &= \frac{k_c \alpha_2^4}{12} \\ &\approx 39.283 \cdot K_1^{eq} \end{aligned}$$

$$\begin{aligned} \omega_3 &= \frac{\alpha_3^2}{L^2} \cdot \sqrt{\frac{EI}{\rho A}} \quad \text{with} \quad \alpha_3 = 7.8548 \\ &\approx 17.5496 \cdot \omega_1 \end{aligned}$$

$$\begin{aligned} K_3^{eq} &= \frac{k_c \alpha_3^4}{12} \\ &\approx 307.99 \cdot K_1^{eq} \end{aligned}$$

➜ using different cantilever oscillation modes simultaneously is equivalent to using cantilevers of different stiffness and resonance frequency simultaneously.

Cantilever oscillation modes: Experiment versus Theory

results of Rabe et al.

	C
	2
Length (L_1)	233 μm
Width	51 μm
Thickness	1.5 μm
k_c	0.6 N/m
ω_0	36 kHz
Full length (L_2)	262 μm

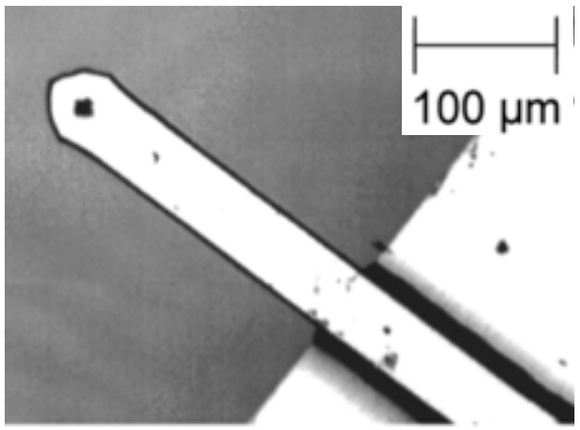

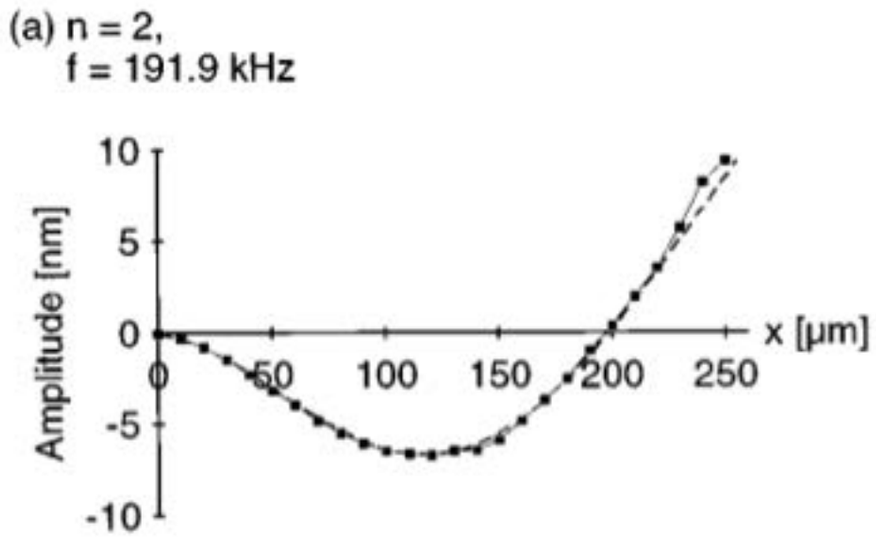

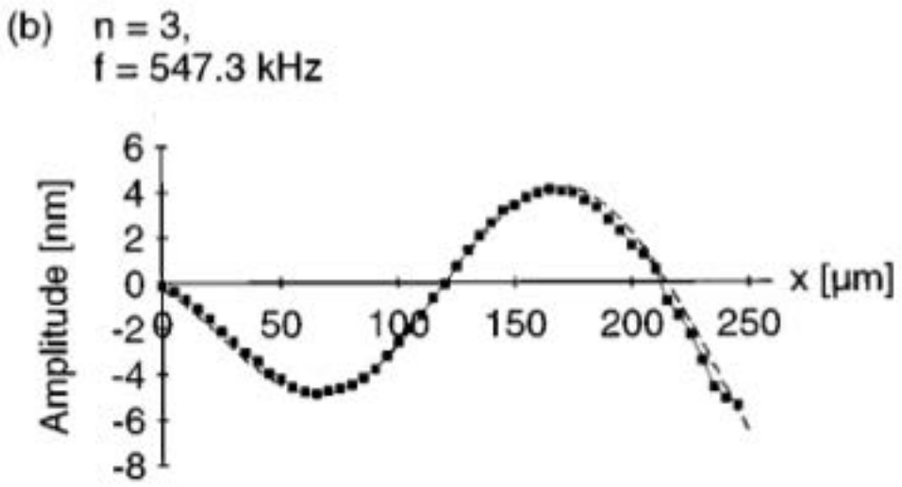

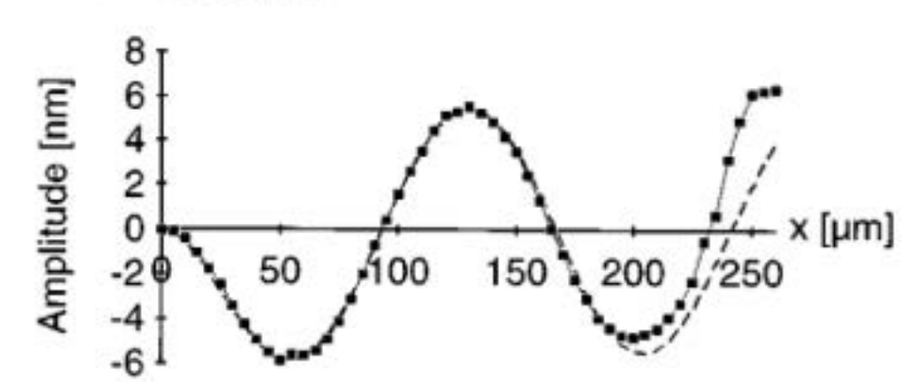

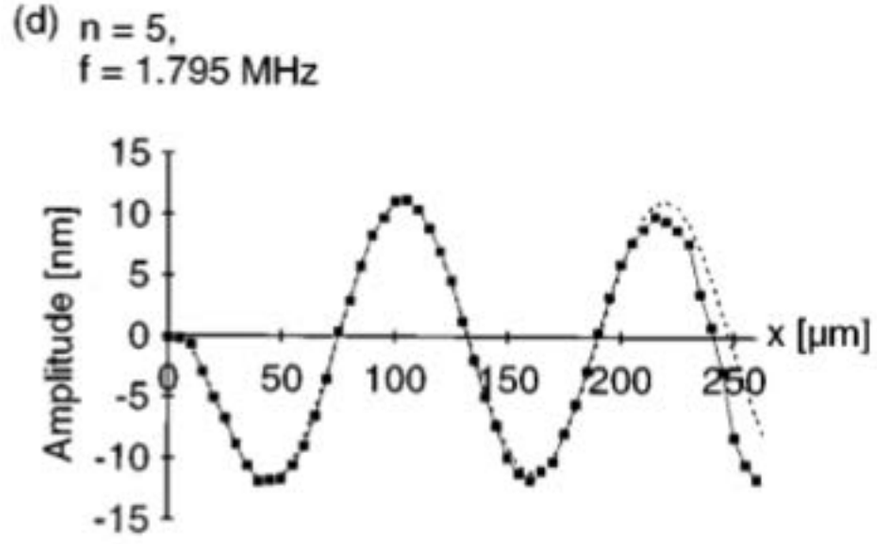

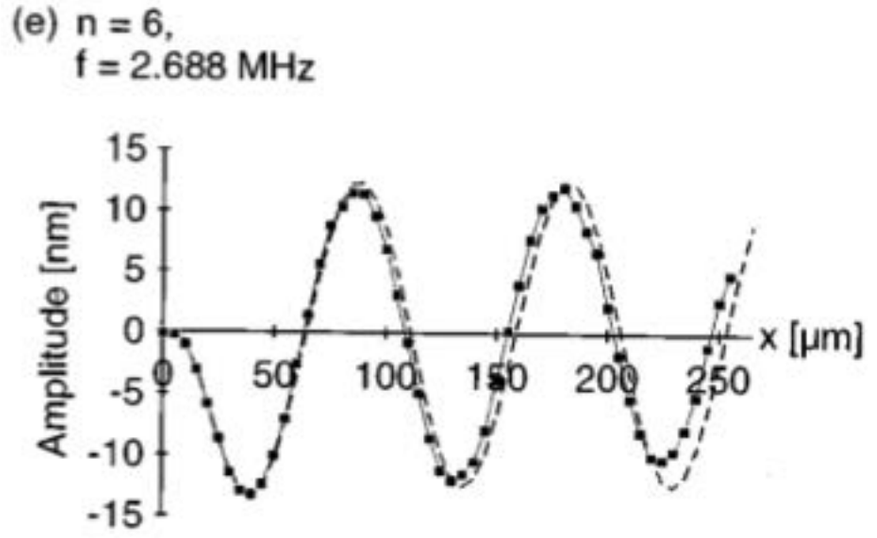

oscillation modes fitted at one point

Rabe, Rev. Sci. Instrum., 67 (1996) 3281 & Refs. therein

Thermal Noise of Cantilevers limiting Sensitivities

noise analysis based on harmonic oscillator model

$$M^{eq}\frac{d^2 z_n}{dt^2} + \Gamma_n \frac{dz_n}{dt} + K_n^{eq} z_n = F_{thermal}(t) \quad \text{with} \quad \omega_n^2 = \frac{K_n^{eq}}{M^{eq}} \quad \text{and} \quad \Gamma_n = \frac{K_n^{eq}}{\omega_n Q_n}$$ dissipation term [kg/s]

with flat thermal noise spectrum $S_F\,[\mathrm{N}^2/\mathrm{Hz}]$ the rms-deflection noise becomes

$$z_{n,rms}^2 = \int_0^\infty S_F \left|G(f)\right|^2 df \quad \text{with the harmonic oscillator transfer function} \quad G(f) = \frac{f_n^2/K_n^{eq}}{(f_n^2 - f^2) + i(f_n f/Q)}$$

from this we find $K_n^{eq} z_{n,rms}^2 = k_B T = \frac{S_F}{K_n^{eq}} \int_0^\infty \frac{f_n^4}{(f^2 - f_n^2)^2 + \frac{f^2 f_n^2}{Q_n^2}} \cdot df = \frac{S_F}{K_n^{eq}} \cdot \frac{\pi}{2} f_n Q_n$

where the integration is performed over each thermal noise peek separately, because the equipartition theorem applies to each mode.

The value of the flat thermal noise spectrum becomes: $S_F = \frac{2K_n^{eq} k_B T}{\pi f_n Q_n} = \frac{4K_n^{eq} k_B T}{\omega_n Q_n}$

and finally: $F_n|_{min,rms} = \sqrt{S_F B} = \sqrt{\frac{4K_n^{eq} k_B T B}{\omega_n Q_n}}$ where B is the measurement bandwidth. **minimally measurable force**

and: $\left.\frac{\partial}{\partial z} F_n\right|_{min,rms} = \frac{1}{A_n}\sqrt{\frac{4K_n^{eq} k_B T B}{\omega_n Q_n}}$ or: $\left.\frac{\Delta\omega_n}{\omega_n}\right|_{min,rms} = \frac{1}{A_n}\sqrt{\frac{k_B T B}{K_n^{eq}\omega_n Q_n}}$

minimally measurable force derivative or frequency shift

and: $\Delta\Gamma_n|_{min,rms} = \frac{F_n|_{min,rms}}{A\omega_n} = \frac{1}{A}\sqrt{\frac{4K_n^{eq} k_B T B}{\omega_n^3 Q_n}}$

minimally measurable dissipation change

Note: these are the thermodynamic limits, noise of the deflection detector, electronics etc. increases real values above these minimum values.
Q-control by external circuitry does not help, because it does not remove stochastic noise sources.

derived from D. Rugar et al., Appl. Phys. A **72** (2001) 3

Thermal noise of cantilevers

equipartition theorem valid for each oscillation mode

$$\frac{1}{2}k_BT = \frac{1}{2}K_n^{eq}\left\langle z_n^2\right\rangle = \frac{1}{2}K_n^{eq}z_{n,rms}^2 \Rightarrow \left\langle z_n^2\right\rangle = \frac{k_BT}{k_c}\cdot\frac{12}{\alpha_n^4}$$

using $K_n^{eq} = \frac{\alpha_n^4}{12}\cdot k_c$

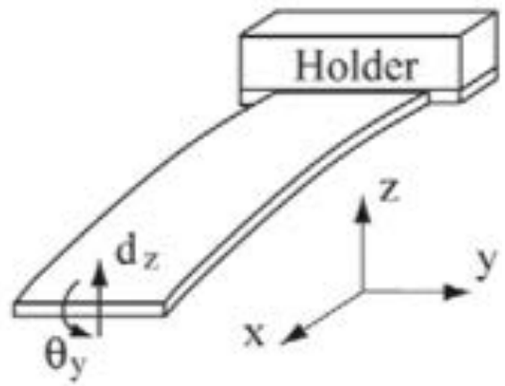

with this

$$\left\langle z_1^2\right\rangle = \frac{k_BT}{k_c}\cdot\frac{12}{\alpha_1^4} = 0.9707\cdot\frac{k_BT}{k_c}$$

the amplitude of the first mode is highest!

summed over all modes (with Boltzmann distributed excitation probability)

$$\left\langle z^2\right\rangle = \frac{12k_BT}{k_c}\cdot\sum_{n=1}^{\infty}\frac{1}{\alpha_n^4} \quad \text{with} \quad \sum_{n=1}^{\infty}\frac{1}{\alpha_n^4} = \frac{1}{12} \quad \Rightarrow \quad \left\langle z^2\right\rangle = \frac{k_BT}{k_c}$$

!

note: when going from the 1st to the 6th mode, the thermal noise amplitude drops about a factor of 100

Butt et al., Nanotechnology 6 (1995) 1

Quality factors of cantilevers

quality factor defined in terms of the energy loss per cycle

$$Q = \frac{2\pi W}{\Delta W}$$ loss factors: $$\frac{1}{Q_{\text{eff}}} = \frac{1}{Q_0} + \frac{1}{Q_{\text{mount}}} + \frac{1}{Q_{\text{air}}}$$ and $$\frac{1}{Q_0} = \frac{1}{Q_{\text{vol}}} + \frac{1}{Q_{\text{support}}} + \frac{1}{Q_{\text{TED}}} + \frac{1}{Q_{\text{surf}}}$$

- Q_{mount} : energy dissipated through the mounting of the cantilever in the force microscope
- Q_{air} : energy dissipated by viscous damping of oscillating cantilever
  use vacuum
- $Q_{support}$: energy dissipated from cantilever to support chip of cantilever
  do not use too hard and too short cantilevers or torsional oscillators, do not coat across support
- Q_{TED} : energy loss by thermoelastic damping
- $Q_{surface}$: energy dissipated by cantilever surface losses
  do not coat surface, be careful with reflective coatings
  bake cantilevers in UHV @ 150C to remove H_2O
  bake cantilevers in UHV @ 800C to remove oxide or perform HF etch
- Q_{vol} : energy dissipated in cantilever inside, can be neglected for single crystalline cantilevers

Support loss: analytical model
by Hao, Sensors Actuators A **109** (2003) 156

$$Q_{\text{support}} = 2.081 \times \left(\frac{l}{t}\right)^3$$ **long and thin is better**

Thermoelastic loss: Any bending of the cantilever is related to temperature changes, and an irreversible flow of heat driven by the generated temperature gradients gives rise to TED.
See Lifshitz Phys. Rev. B**61** (2000) 5600

$$Q_{\text{TED}} = \frac{\rho C_p}{E\alpha^2 T}\frac{1+(2\pi f_0\tau)^2}{2\pi f_0\tau} \quad \text{with} \quad \tau = \frac{\rho C_p t^2}{\pi^2 \kappa_{\text{th}}}$$ **very low T & thin is better**

or $$Q_{\text{TED}} = \frac{\rho C_p}{E\alpha^2 T}\left[\frac{6}{\xi^2} - \frac{6}{\xi^3}\times\frac{\sinh(\xi)+\sin(\xi)}{\cosh(\xi)+\cos(\xi)}\right]^{-1} \quad \text{with} \quad \xi = t\sqrt{\frac{2\pi f_0 \rho C_p}{2\kappa_{\text{th}}}}$$

Support loss: see Yasumura et al, J. Microelectromech. Syst. **9** (2000) 117

$$Q_{\text{surf}} = \frac{wt}{2\delta(3w+t)}\frac{E}{E_2^S}$$ **small w and no additional coating is better**

thickness of surface layer ↗ ↖ property of surface layer

Damping by molecular flow: see Bianco et al J. Vac. Sci. Technol. B **24** (2006) 1803

$$Q_{\text{molecular}} = \frac{\rho t \omega_0}{4}\sqrt{\frac{\pi}{2}}\sqrt{\frac{RT}{M}}\frac{1}{p}$$ $Q_{molecular}$ **> 10^{12} below 10^{-8} mbar**

Lübbe Meas. Sci. Technol. **21** (2010) 125501

Optimizing the Force Sensitivity of

$$\Gamma = \frac{K}{\omega Q} \quad \text{using} \quad \omega = \frac{(\alpha_1)^2}{L^2} \cdot \sqrt{\frac{EI}{\rho A}} \quad \text{and} \quad k_c = \frac{(\alpha_1)^4}{12} \cdot \frac{Ewt^3}{4L^3}$$

$$I = \frac{1}{12} wt^3$$

we find

$$\Gamma = \alpha_1^2 \cdot \frac{\sqrt{3}}{24} \cdot \frac{wt^2}{QL} \cdot \sqrt{E\rho} = 0.2536 \cdot \frac{wt^2}{QL} \cdot \sqrt{E\rho}$$

geometrical conditions for a sensitive cantilever:

- **high Q**
- **small w**
- **long L**
- **thin t**

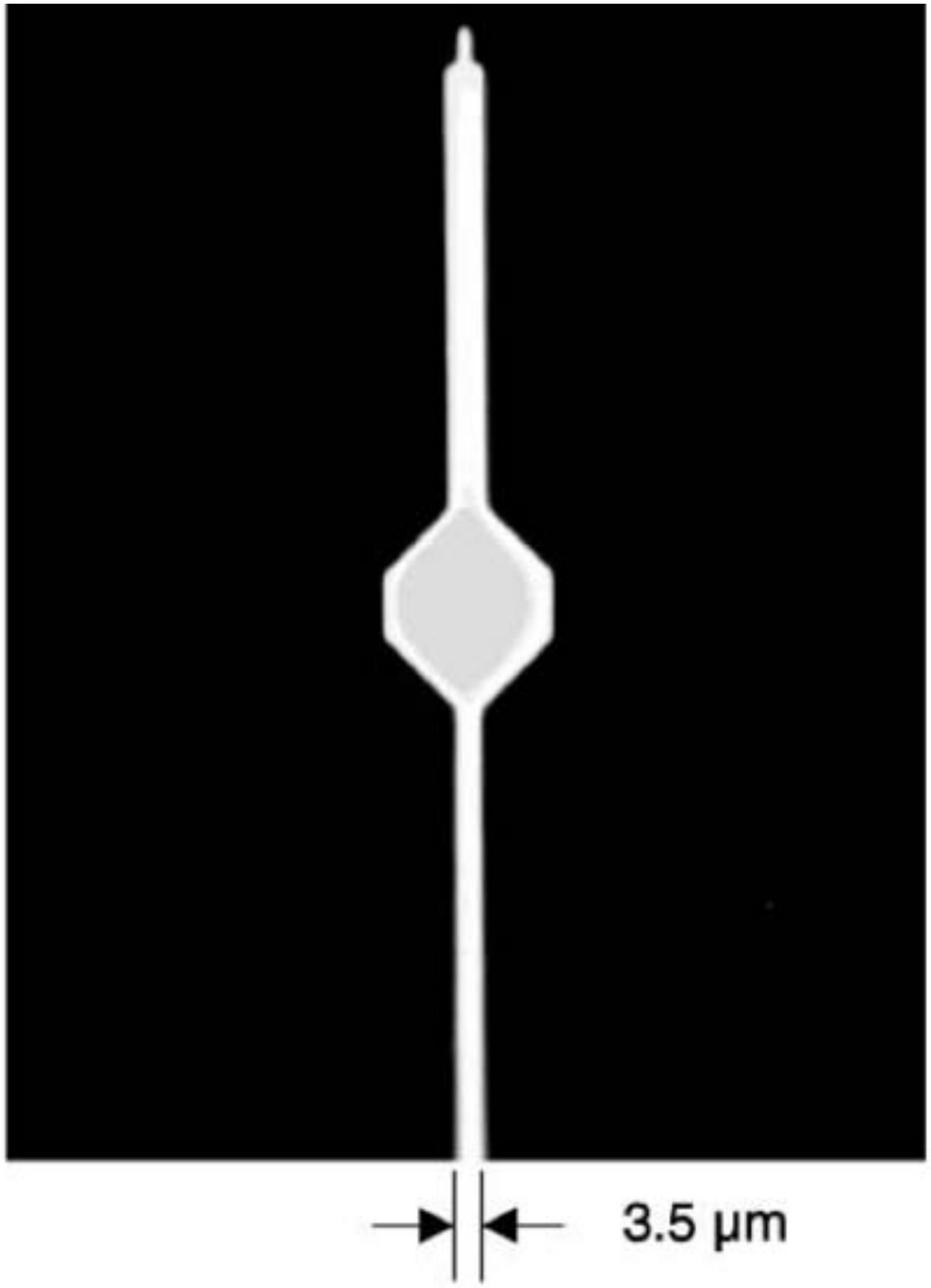

Fig. 1. Optical micrograph of a (111)-oriented silicon cantilever with a 3 µN/m spring constant. The cantilever, which is only 65 nm thick, was treated with ammonium fluoride to hydrogen-passivate the surface. A force resolution of 1.4 aN/Hz$^{1/2}$ was achieved at 2.6 K. The paddle near the middle of the cantilever serves as a reflector for a fiber-optic interferometer

D. Rugar et al., Appl. Phys. A 72 (2001) 3

3.1.3. Deflection Sensors

Deflection Sensors

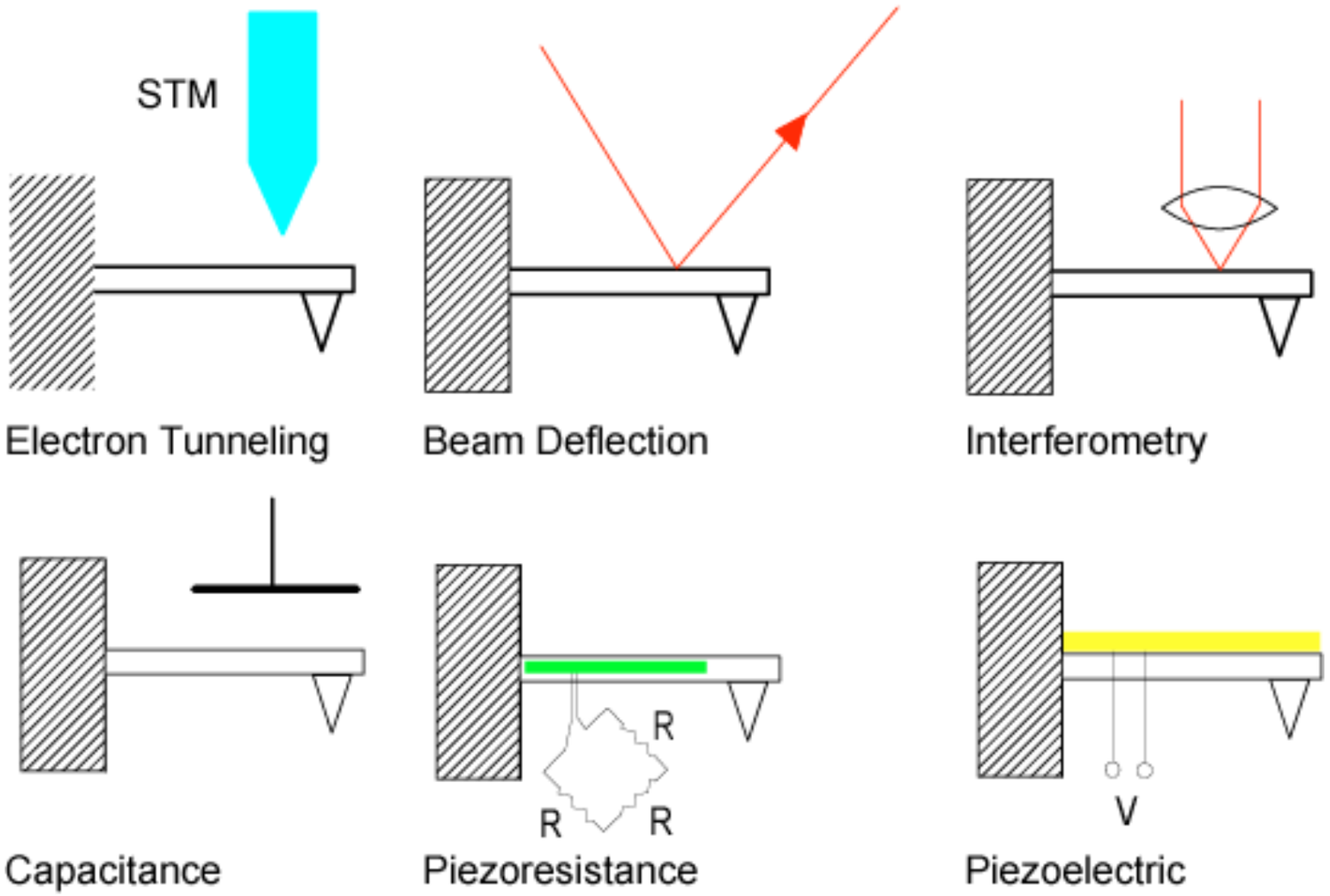

Electron Tunneling: original concept, potentially sensitive, practically problematic
Beam Deflection: most widely used, robust, high sensitivity, not directly quantitative, requires calibration
Interferometry: best sensitivity, quantitative, uses limited space, complicated
Capacitance: sensor can be microfabricated, strong force from sensor, limited sensitivity
Piezoresistance: ideal for microfabrication & integration, limited sensitivity, heating of cantilever
Piezoelectric: mostly quartz tuning forks, good for true atomic resolution, limited sensitivity

Beam Deflection Principle

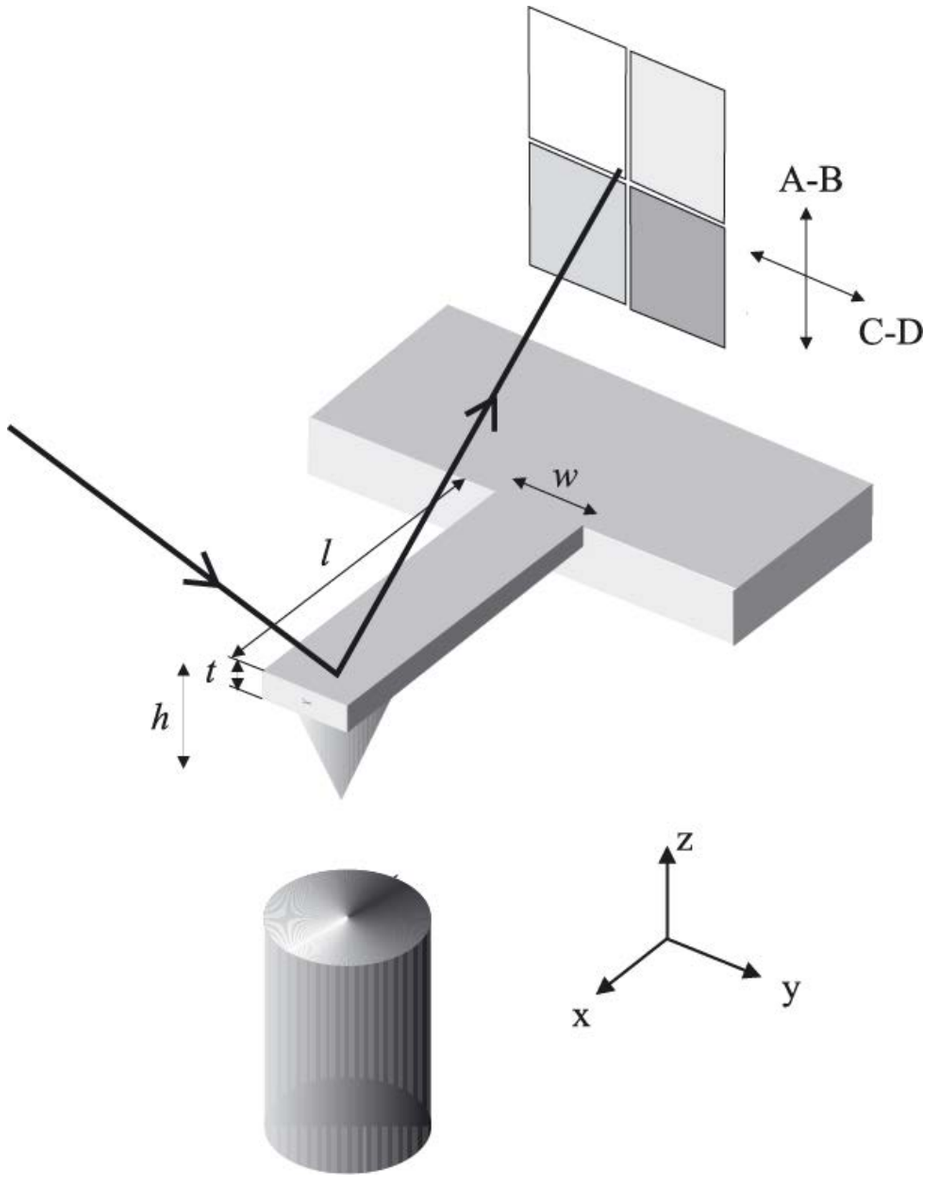

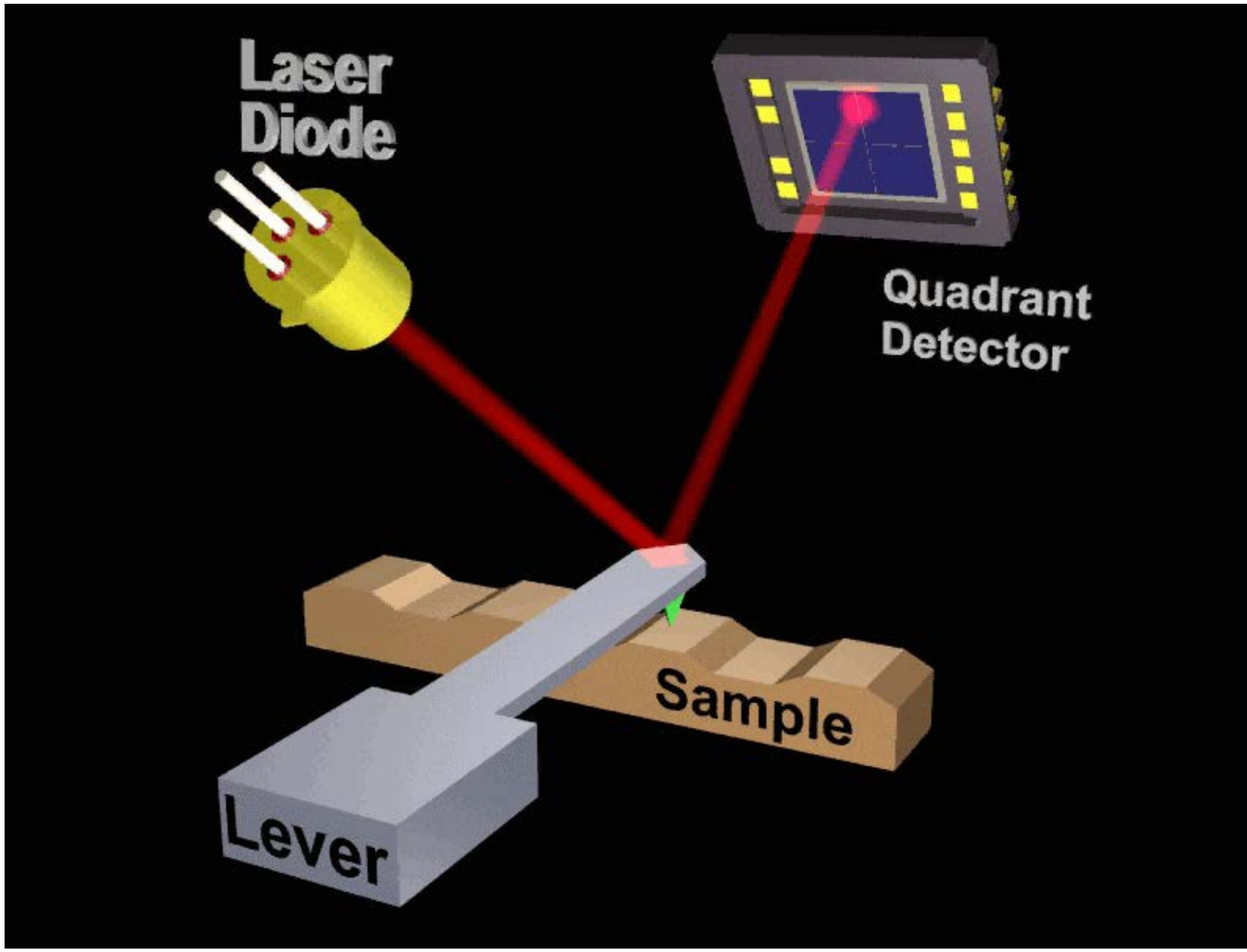

Animation: H.-R. Hidber, NCCR on Nanoscale Science University of Basel

A laser beam is reflected off the rear side of the cantilever. Angular deflections of the laser beam are measured with a position sensitive detector (4-quadrant photo diode). The A-B-signal is proportional to the normal force and the C-D-signal is proportional to the torsional force.

Beam Deflection Principle

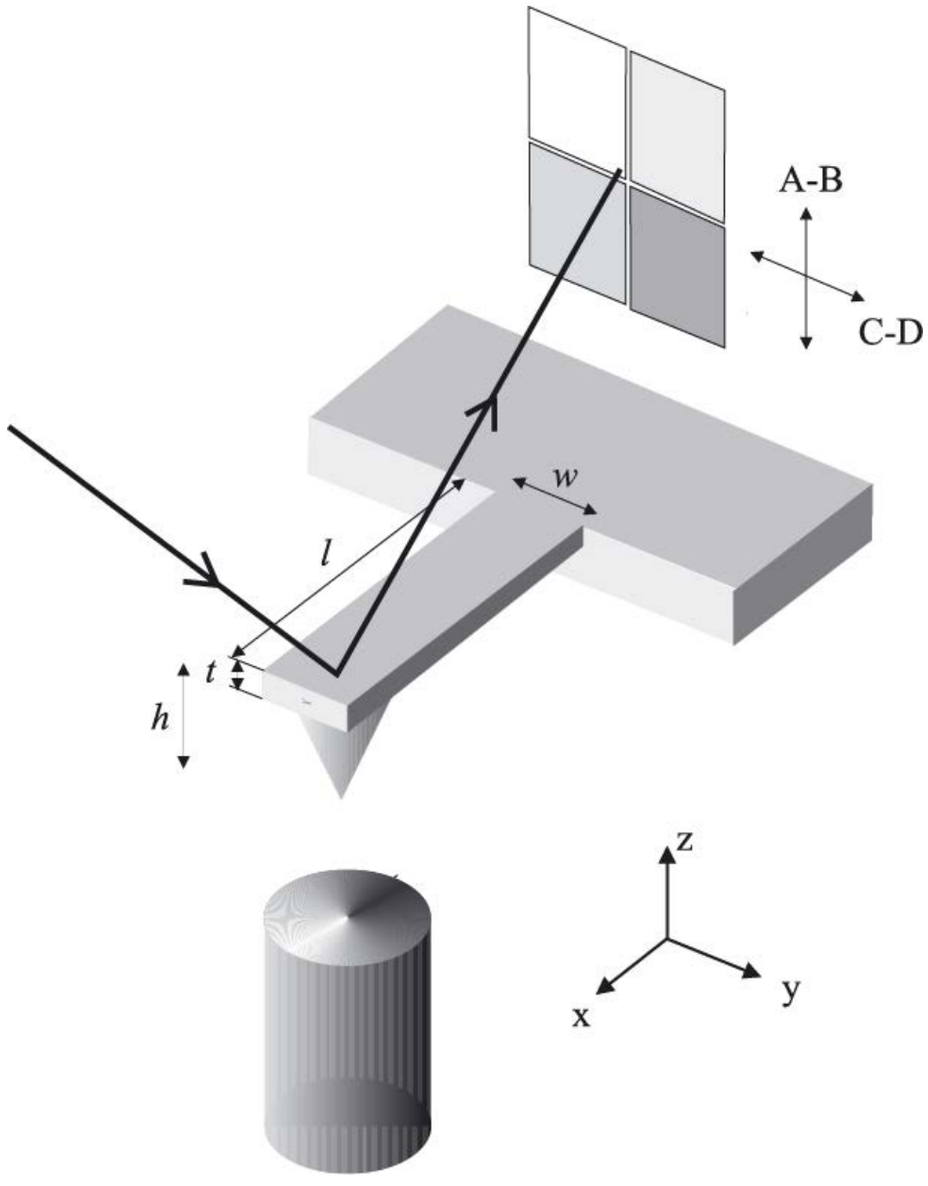

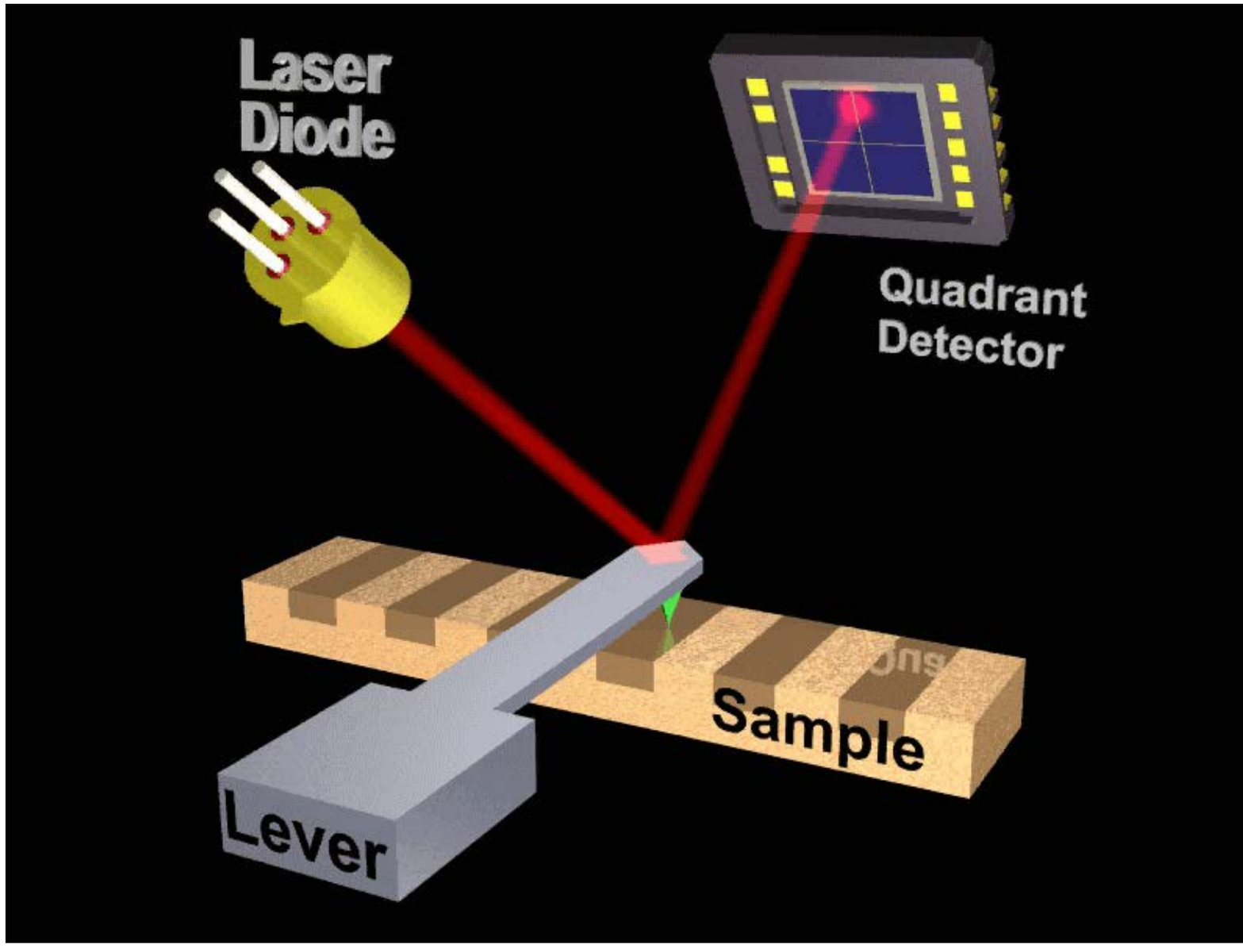

Animation: H.-R. Hidber, NCCR on Nanoscale Science University of Basel

A laser beam is reflected off the rear side of the cantilever. Angular deflections of the laser beam are measured with a position sensitive detector (4-quadrant photo diode). The A-B-signal is proportional to the normal force and the C-D-signal is proportional to the torsional force.

Determining Detector Sensitivity from Thermal Noise Peaks

need to know: invOLS (inverted optical lever sensitivity); [invOLS] = m/V

Procedure

measure a spectrum in $\mathrm{Volt}_{rms}/\sqrt{\mathrm{Hz}}$

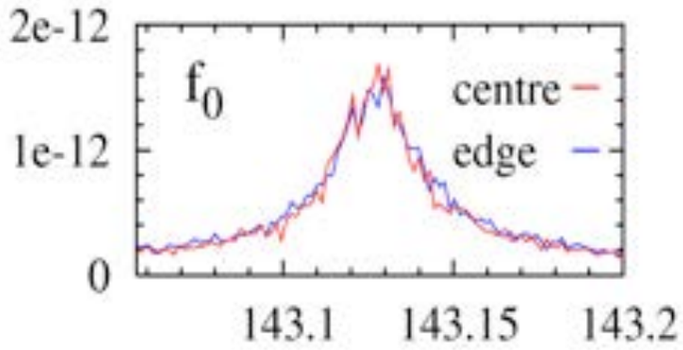

take the square of the spectrum to get $\mathrm{Volt}^2_{rms}/\mathrm{Hz}$

fit the peak(s) by the power response function of a harmonic oscillator

$$S(f) = P_{white} + \frac{P_{dc} f_n^4}{(f^2 - f_n^2)^2 + \frac{f^2 f_n^2}{Q^2}}$$

Then:

$$\mathrm{Volt}^2_{n,rms} = \int_0^\infty \frac{P_{dc} f_n^4}{(f^2 - f_n^2)^2 + \frac{f^2 f_n^2}{Q_n^2}} df = P_{dc} \cdot \frac{\pi}{2} f_n Q_n$$

with $\mathrm{z}^2_{n,rms} = \mathrm{invOLS}^2 \cdot \mathrm{Volt}^2_{n,rms}$ and $k_B T = K_n^{eq} z^2_{rms}$

we find: $$\mathrm{invOLS} = \sqrt{\frac{2 k_B T}{\pi K_n^{eq} f_n Q_n P_{dc}}}$$

derived from M.J. Higgins et al., Rev. Sci. Instrum. **77** (2006)

from measurement (in vacuum)

we can obtain ω_n and especially

with

- the cantilever length L
- the cantilever width w
- the elasticity module E_{Si} = 1.69e11 N/m²
- the density ρ_{Si} = 2330 kg/m³

$$t = \frac{\omega_1}{\alpha_n^2} \cdot 2L^2 \cdot \sqrt{\frac{3\rho}{E}}$$

and from this the *static* cantilever force constant

$$k_c = \frac{E t^3 w}{4 L^3}$$

and further the

$$K_n^{eq} = \frac{\alpha_n^4}{12} \cdot k_c \quad \text{and} \quad \langle z_n^2 \rangle = \frac{k_B T}{k_c} \cdot \frac{12}{\alpha_n^4} = \frac{k_B T}{K_n^{eq}}$$

3.2. Contact Mode Scanning Force Microscopy

3.2.1. Principles of SFM in Contact

Force-Distance Curves: Measuring Force vs z-Displacement

Coordinate System

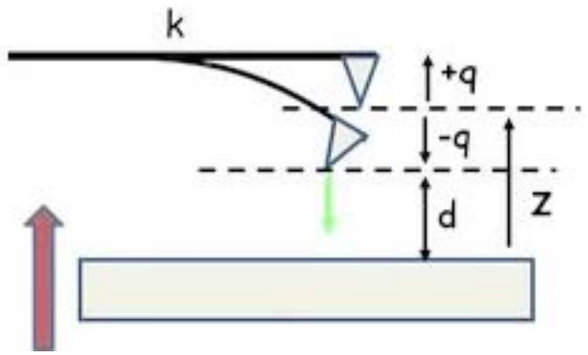

Note:

- cantilever is positioned at *z*
- tip deflects towards sample (for attractive force)
- tip-sample distance is *d* not *z* !
- force at position *z* is actually *F(d)* !

critical *z* when approaching ➜ snap-in

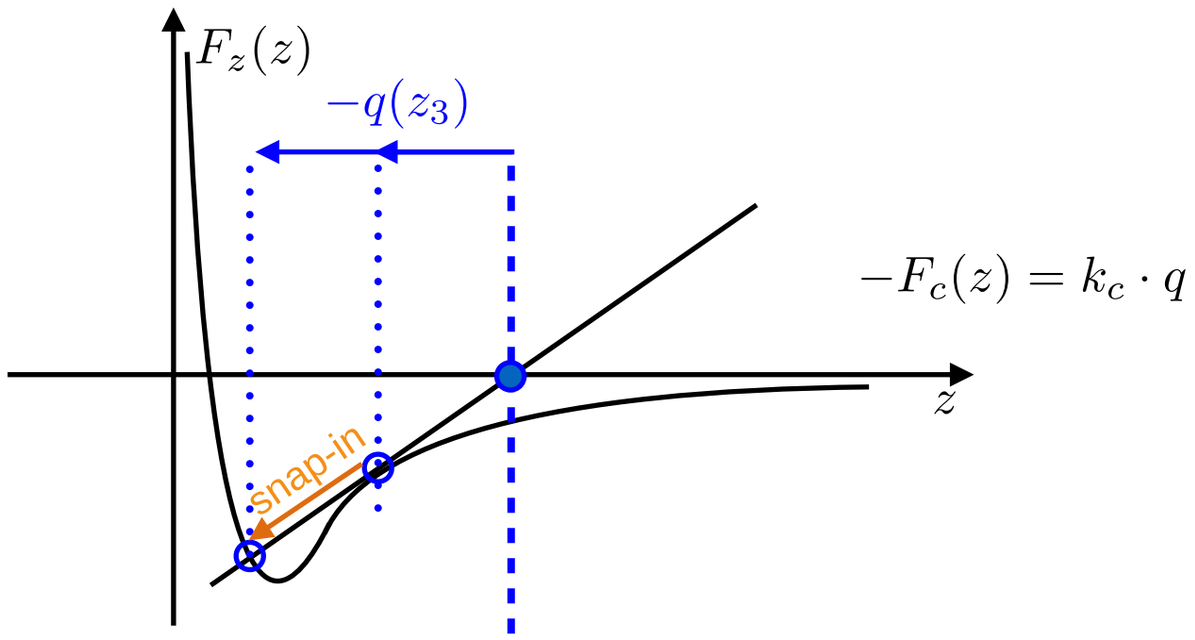

Force versus Distance Behavior

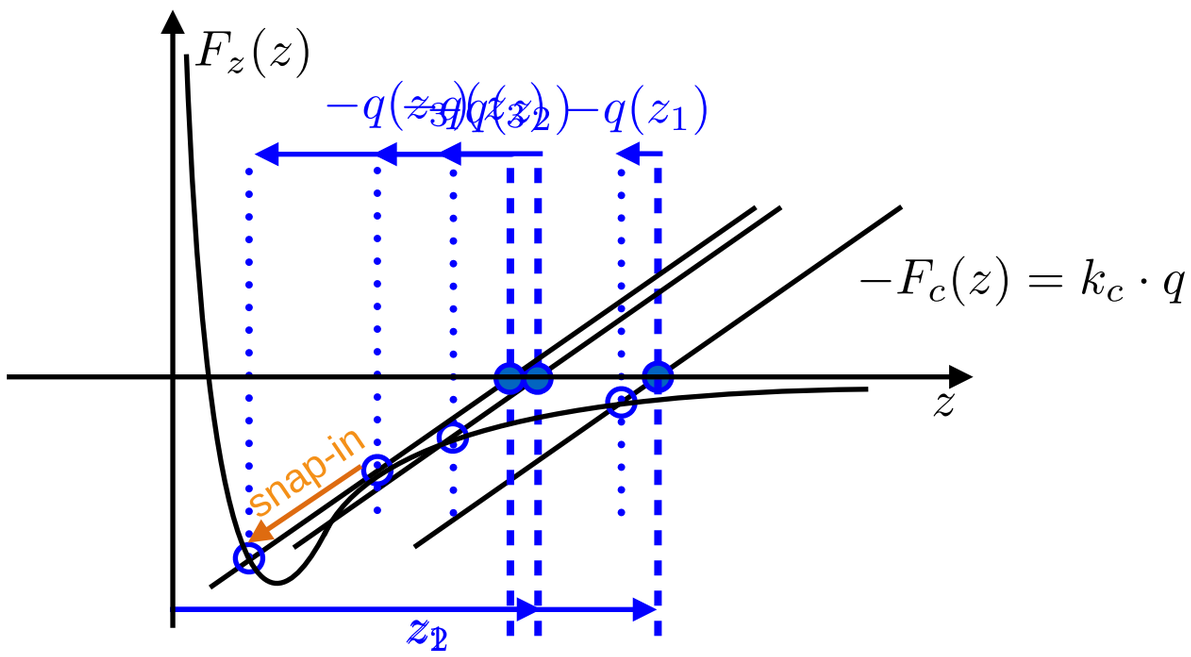

critical *z* when retracting ➜ snap-out

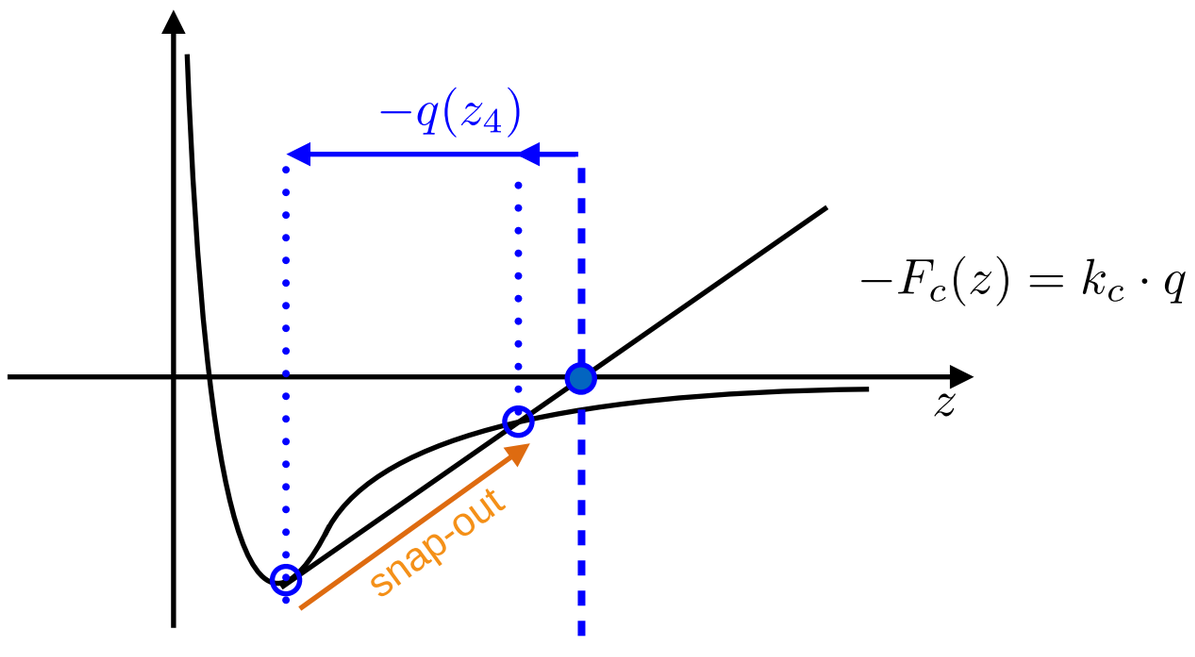

Force-Distance Curves: Measuring Force vs z-Displacement

Long-range contributions have force gradients like
dF/dz » 1-10 N/m.

Spring constants of
k ≈ 0.01-1 N/m provokes “jump-into-contact” when
k < dF/dz.

Adhesion causes hysteresis in force vs. distance curves.

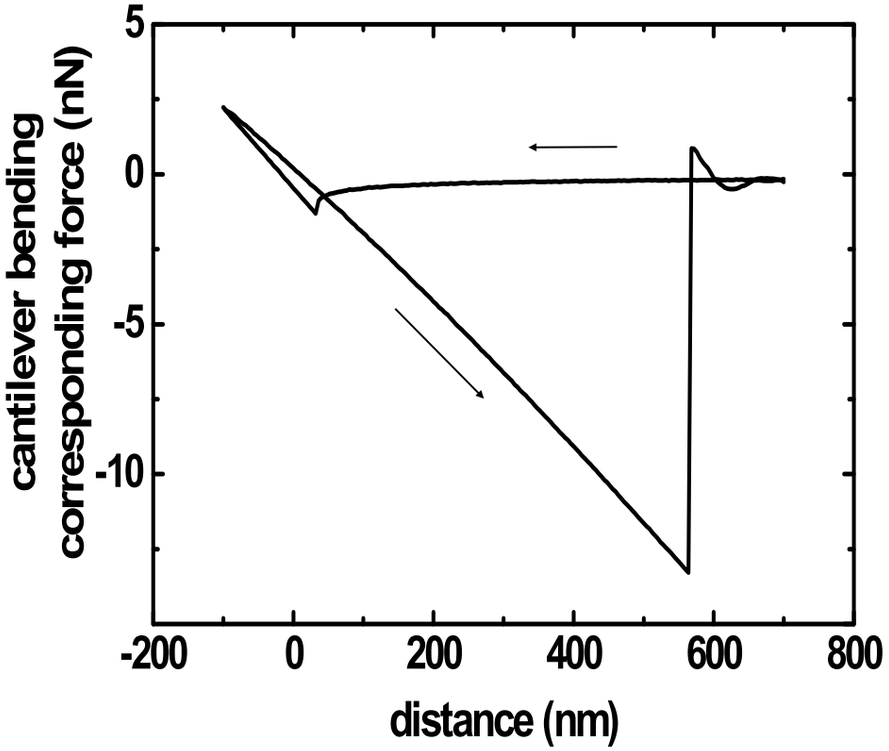

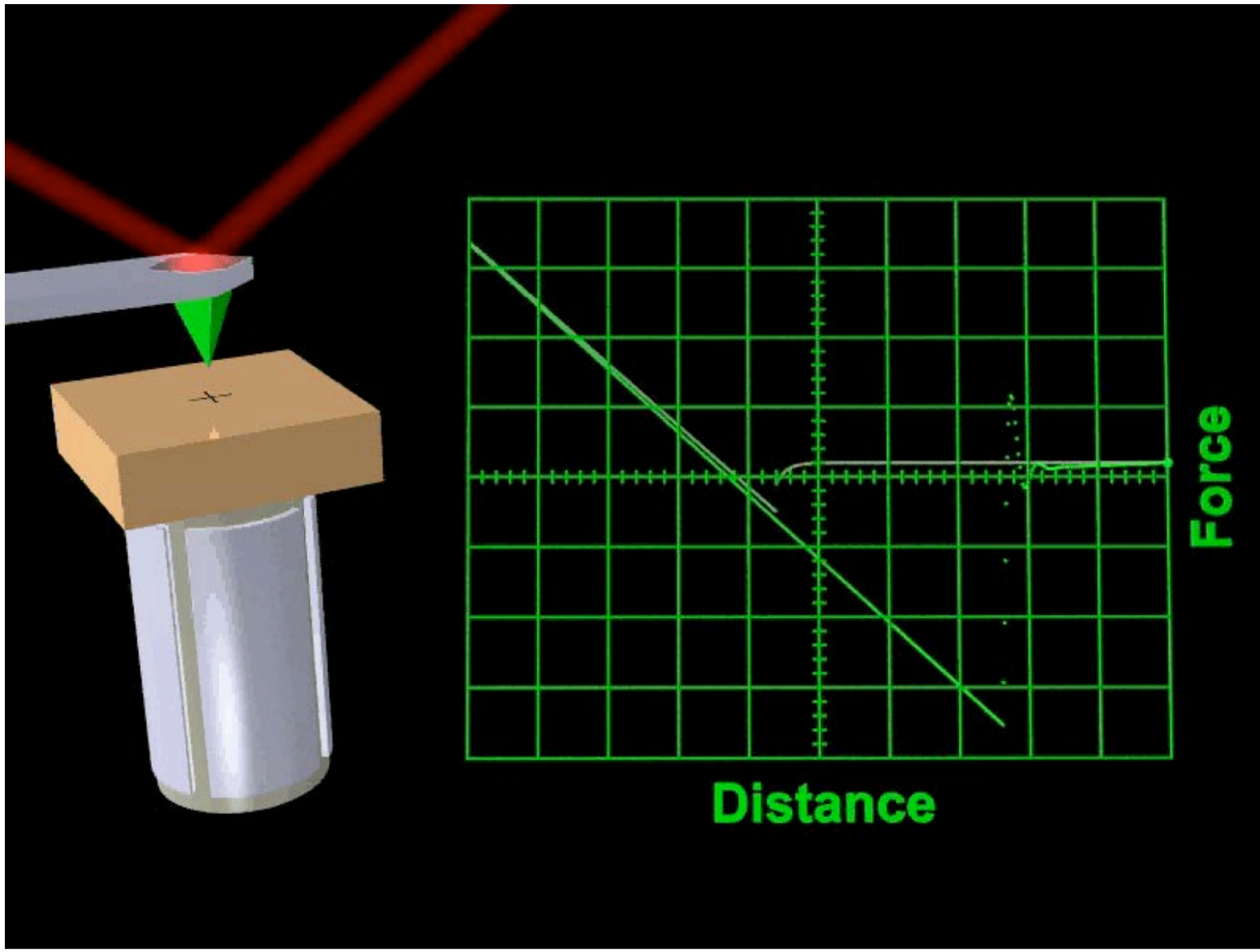

➜ sample stiffness & tip-sample adhesion can be measured; indentations can be made.

What Stiffness is required to avoid Snap-in?

$$F(d) = -\frac{HR}{6d^2}$$

$$slope(d) = effective\ spring\ constant = \frac{HR}{3d^3}$$

$$Use\ R = 6nm$$

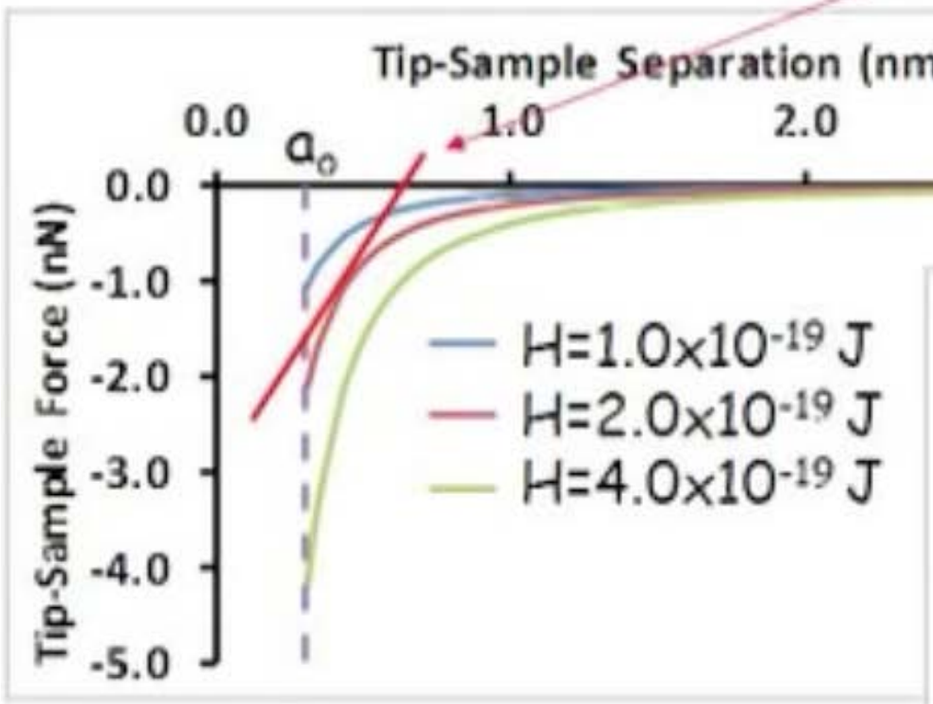

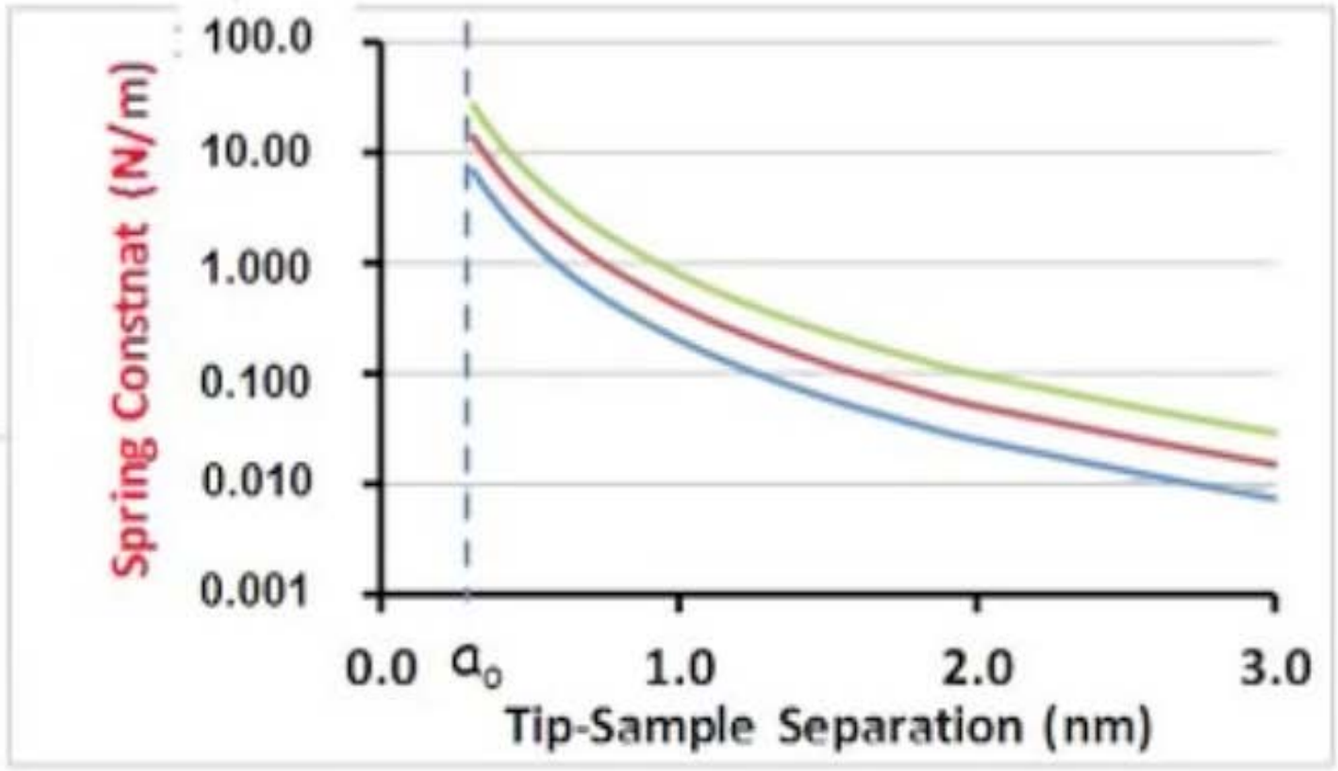

But:

- stiffer cantilevers provide smaller force sensitivity
- constant force mode feedback more critical, i.e. if cantilever-sensor position drifts ➜ tip-sample force will change (a lot!)
- and sample may deform (towards the tip); so for soft samples the total cantilever-sample stiffness matters!

Snap-to-Contact ➜ Tip Shape

Empa
Materials Science and Technology

critical tip-sample distance

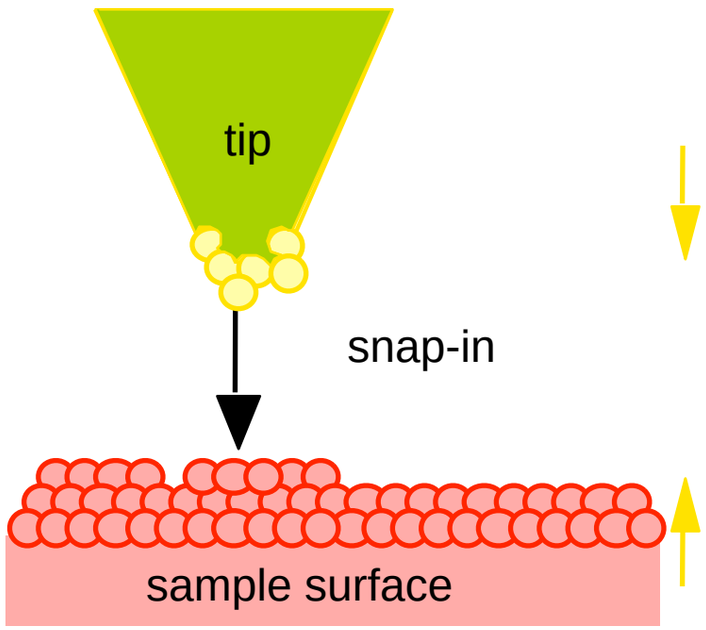

tip snaps to surface @ critical tip-sample distance due to attractive van der Waals force.

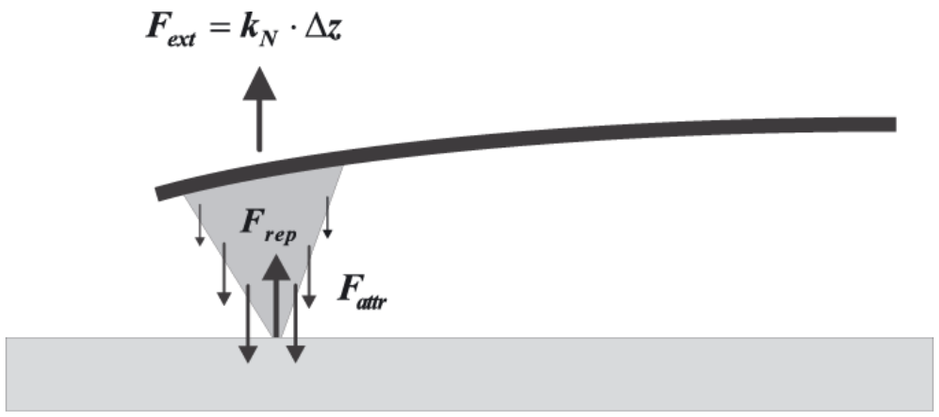

Contact Radius:

- in atmosphere: 2-10nm @ 1nN < F < 100nN
- in UHV: 1-4nm @ 0.1nN < F < 10nN

tip in contact with sample

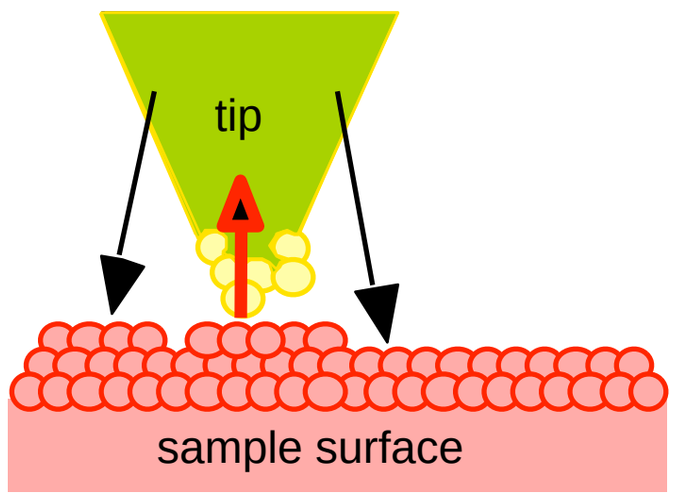

attractive van der Waals force acting on tip are compensated by local repulsive force at the tip apex.

multi-atom tip-sample contact

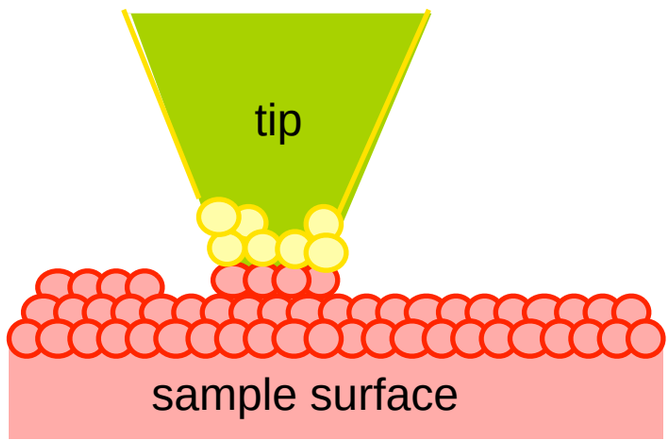

large repulsive force at tip apex leads to re-ordering of atoms at the tip apex. A multi-atom contact is formed. The imaging of single atoms and atomic defects is not possible under this condition.

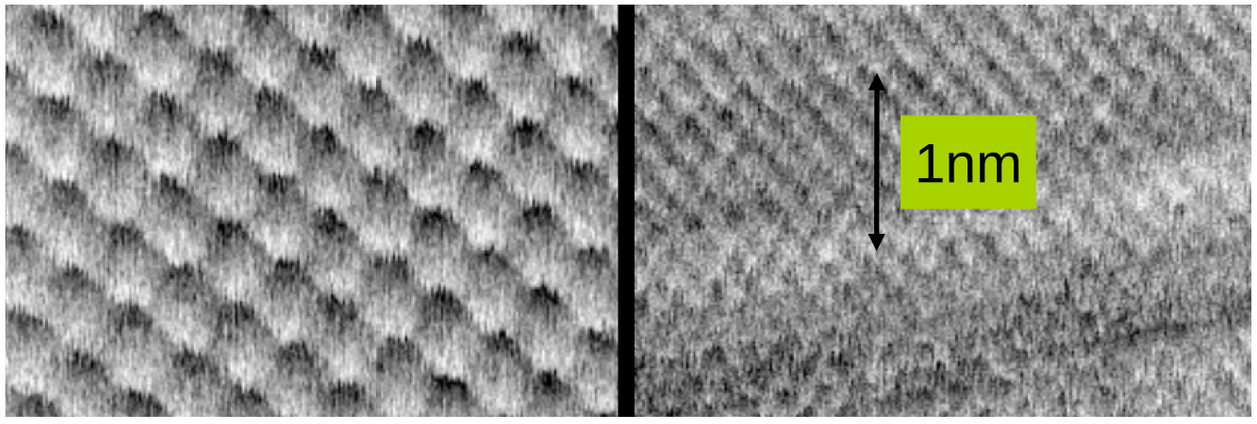

➜ „pseudo atomic resolution“, e.g. on NaF(001)
➜ atomic periodicity

Biologica Application: Unzipping Bacteriorhodopsin

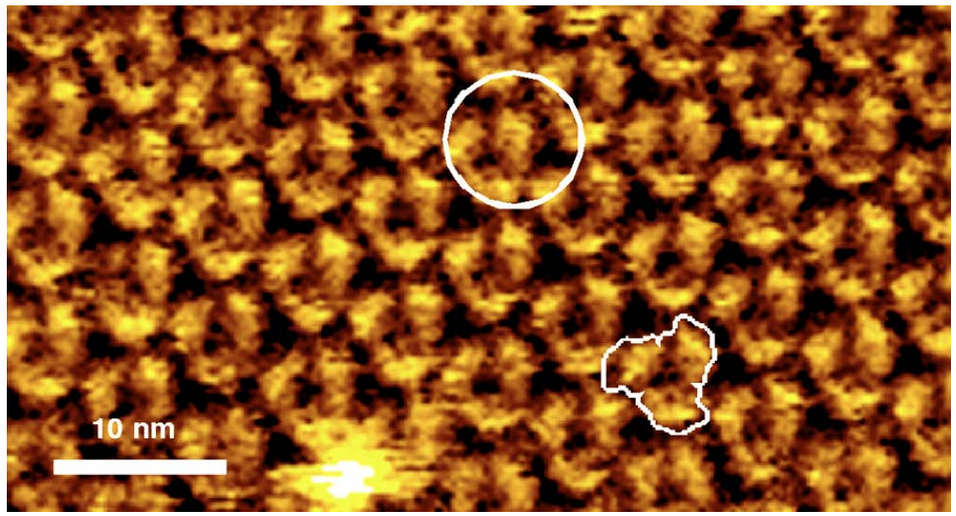

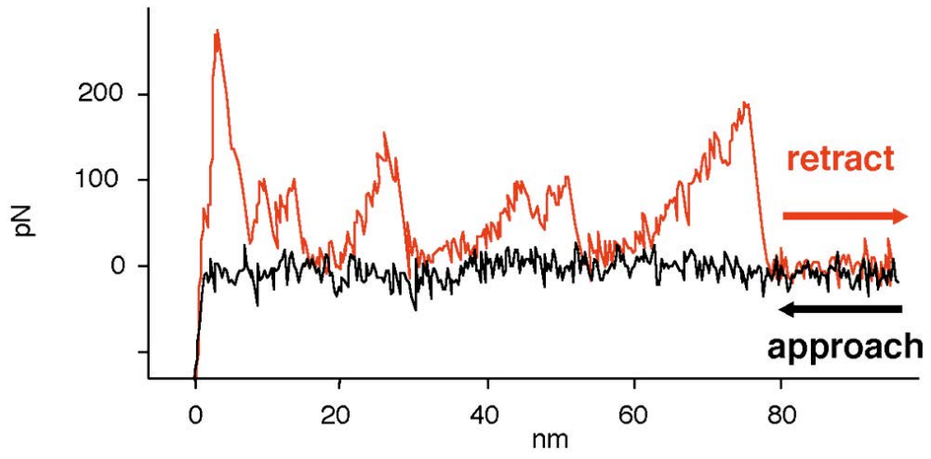

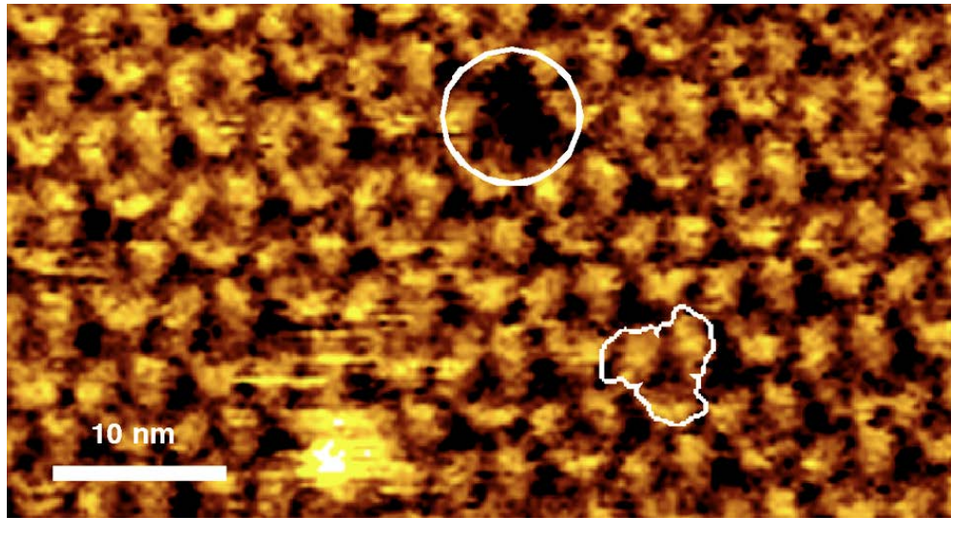

Oesterhelt et al. Science 2000

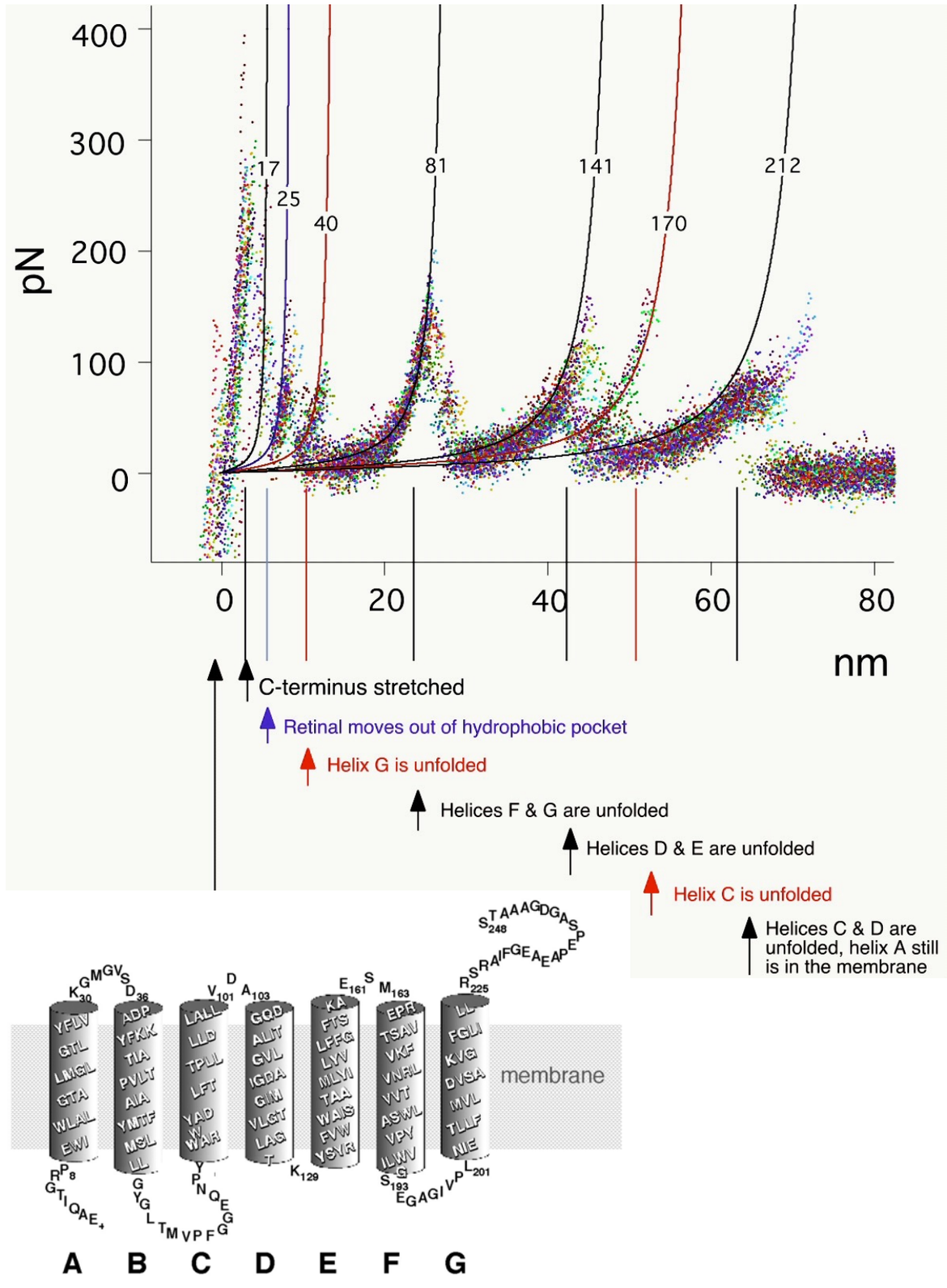

3.2.2. Examples of Dynamic Force Microscopy with Tip in Contact

Force Modulation Scanning Force Microscopy

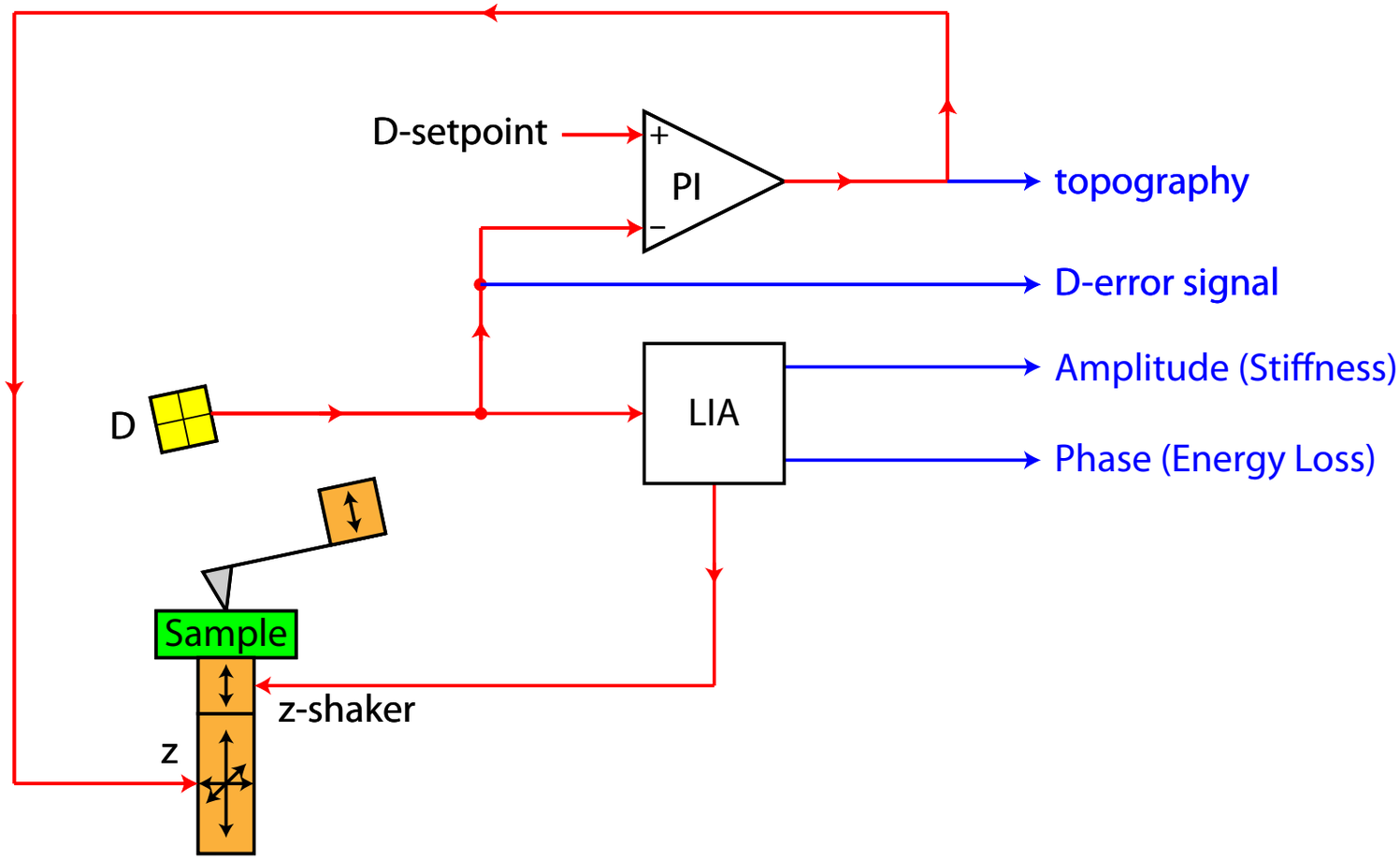

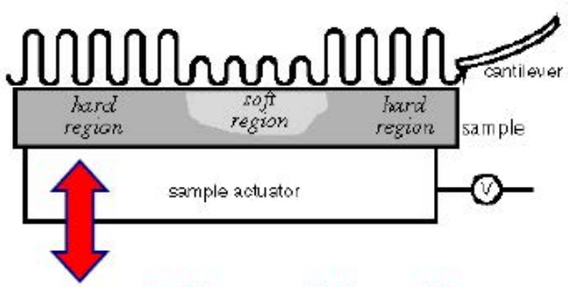

sample is modulated with constant amplitude

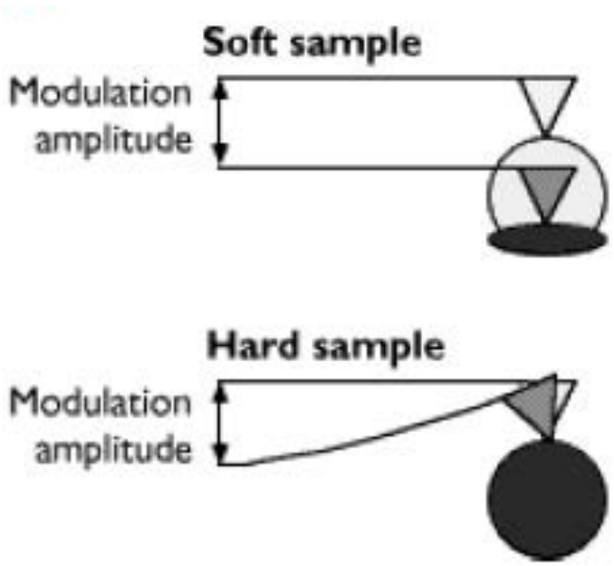

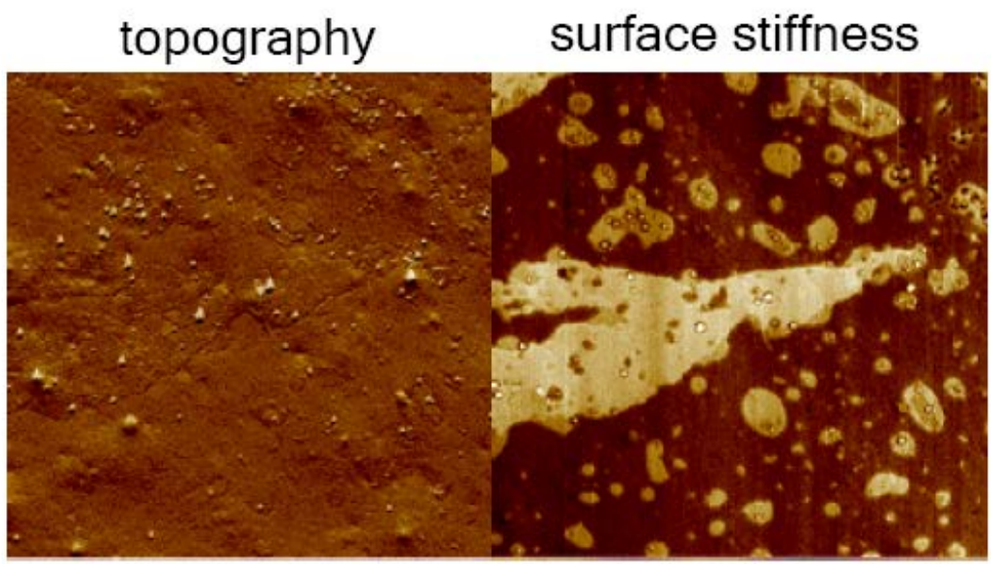

Piezo-response Force Microscopy (PFM)
(a dynamic mode with tip-sample contact)

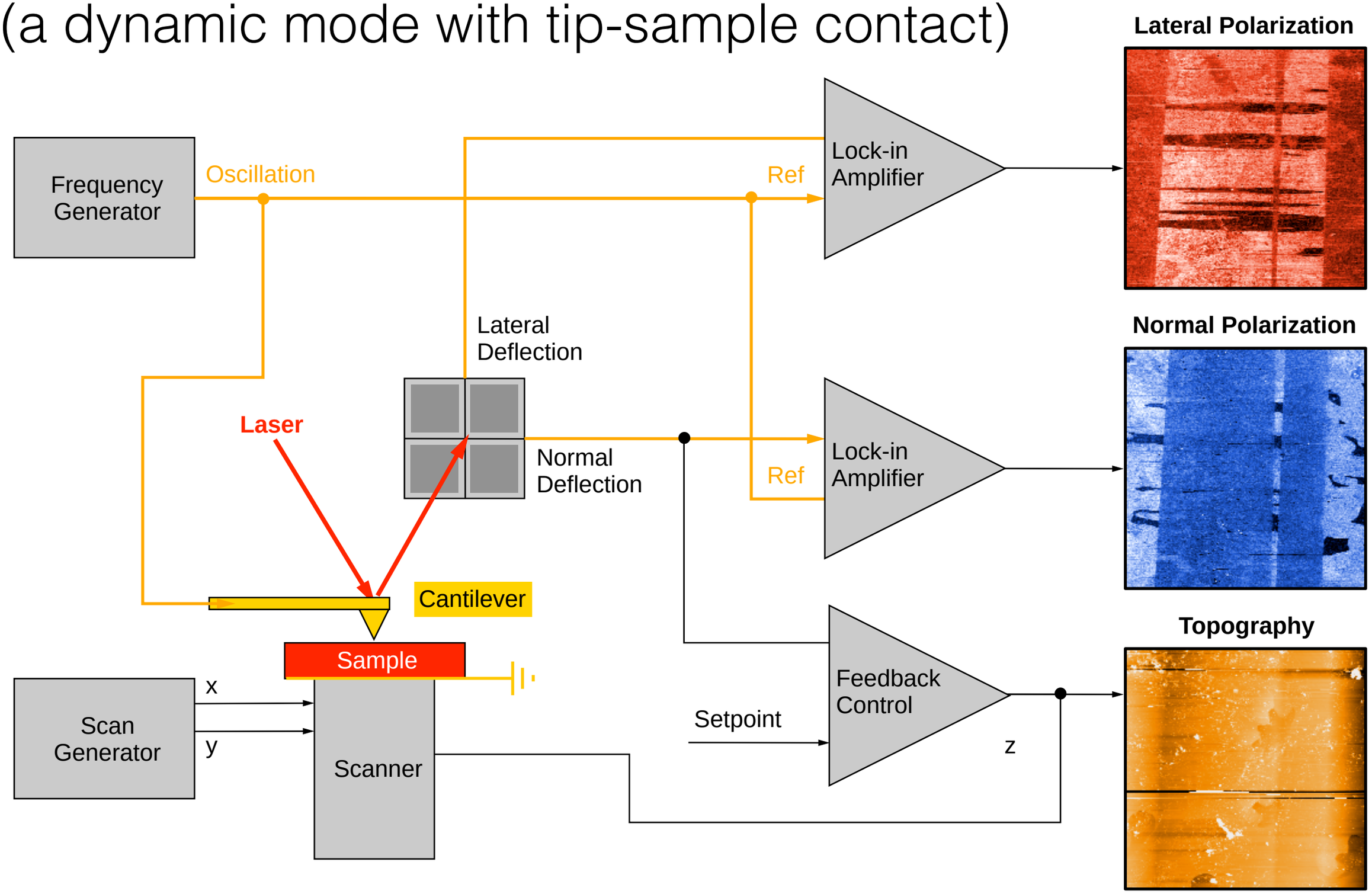

be aware: piezo-response signals can be very small

- use higher voltages
- use (contact) resonant modes

Piezo-response Force Microscopy (PFM) in contact resonance

be aware: piezo-response signals can be very small

- use electric field oscillation at contact resonance
  but be aware contact resonance changes with contact geometry, thus sample topography
  ➜ use resonance frequency tracking modes

➜ use double (or triple) resonance excitation

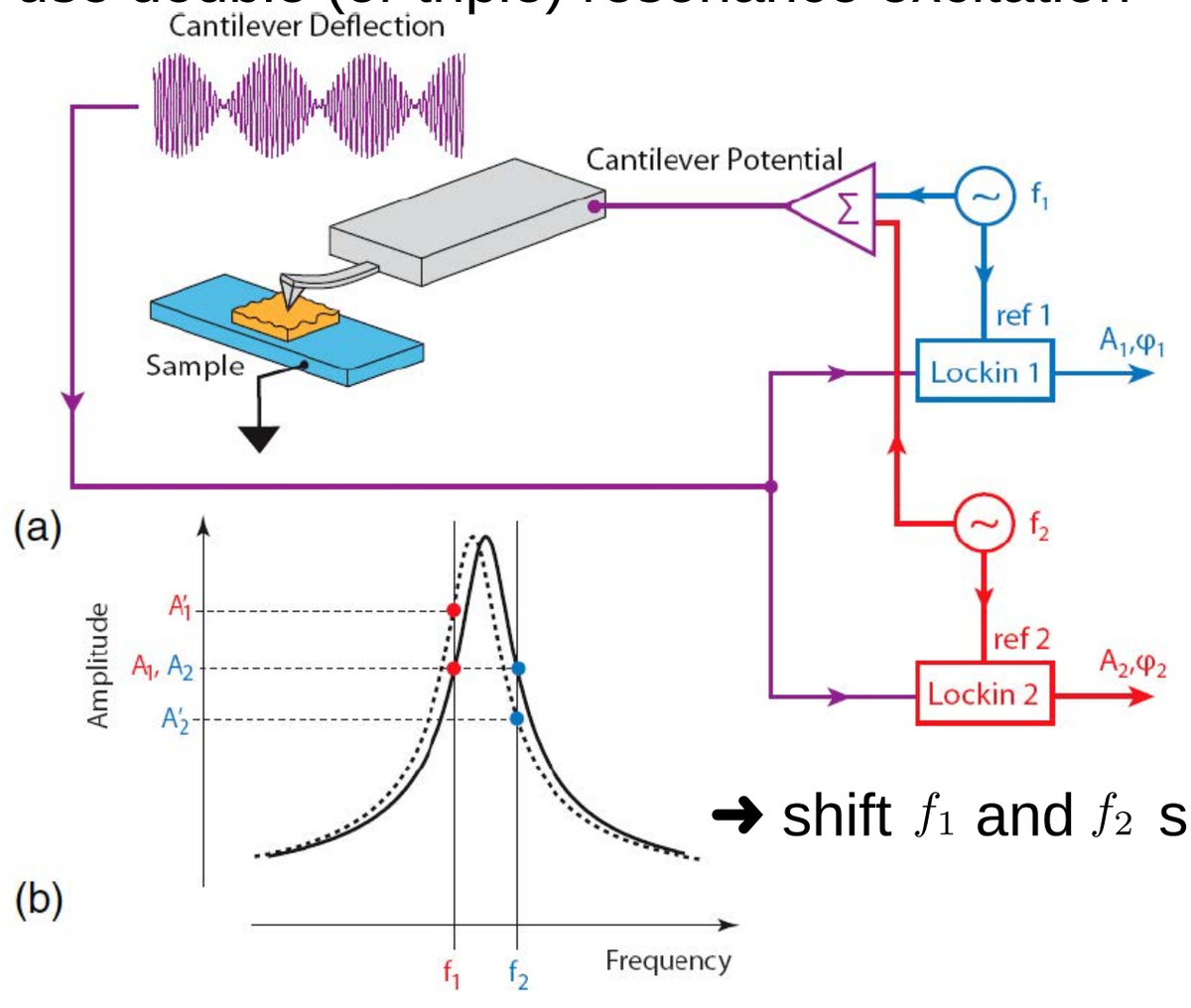

➜ shift f_1 and f_2 such that $\Delta A = A_{f_1} - A_{f_2} = 0$

B.J. Rodriguez, C. Callahan, S. Kalinin, R. Proksch, "Dual-frequency resonance-tracking atomic force microscopy." Nanotechnology 18, 475504 (2007).

Dopant Mapping with Spreading Resistance or Capacitance Mapping

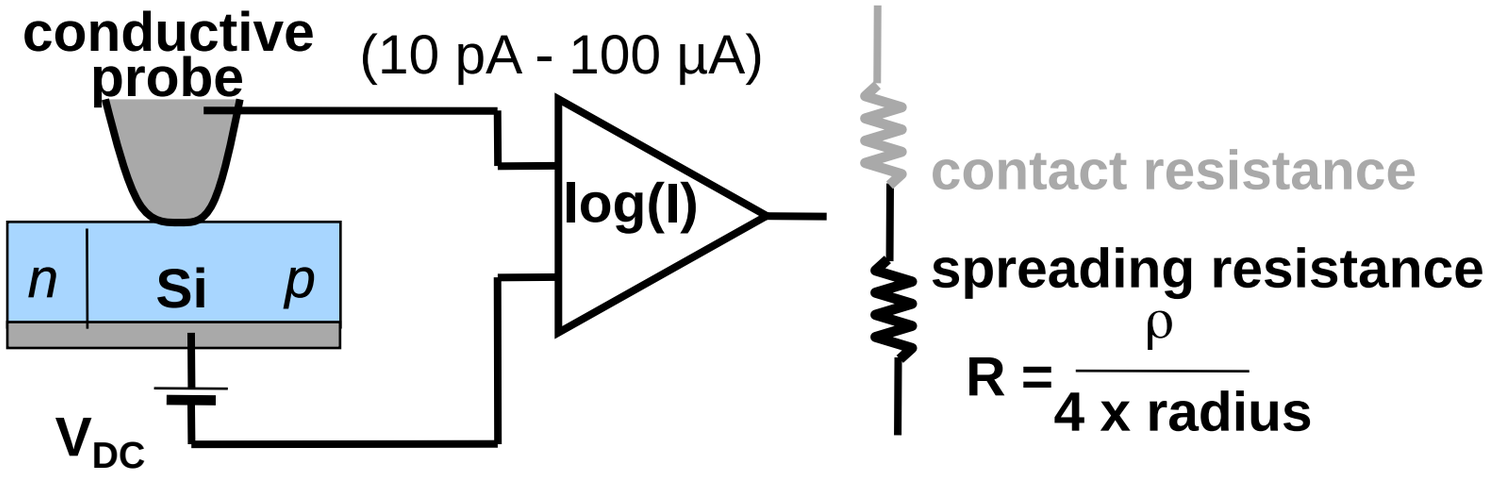

SSRM:

SPM-feedback, high force (up to µN)

Wide-range current measurement (logarithmic amplifier)

Dopant level (10^{15} – 10^{20} carriers/cm^3) via conductivity difference

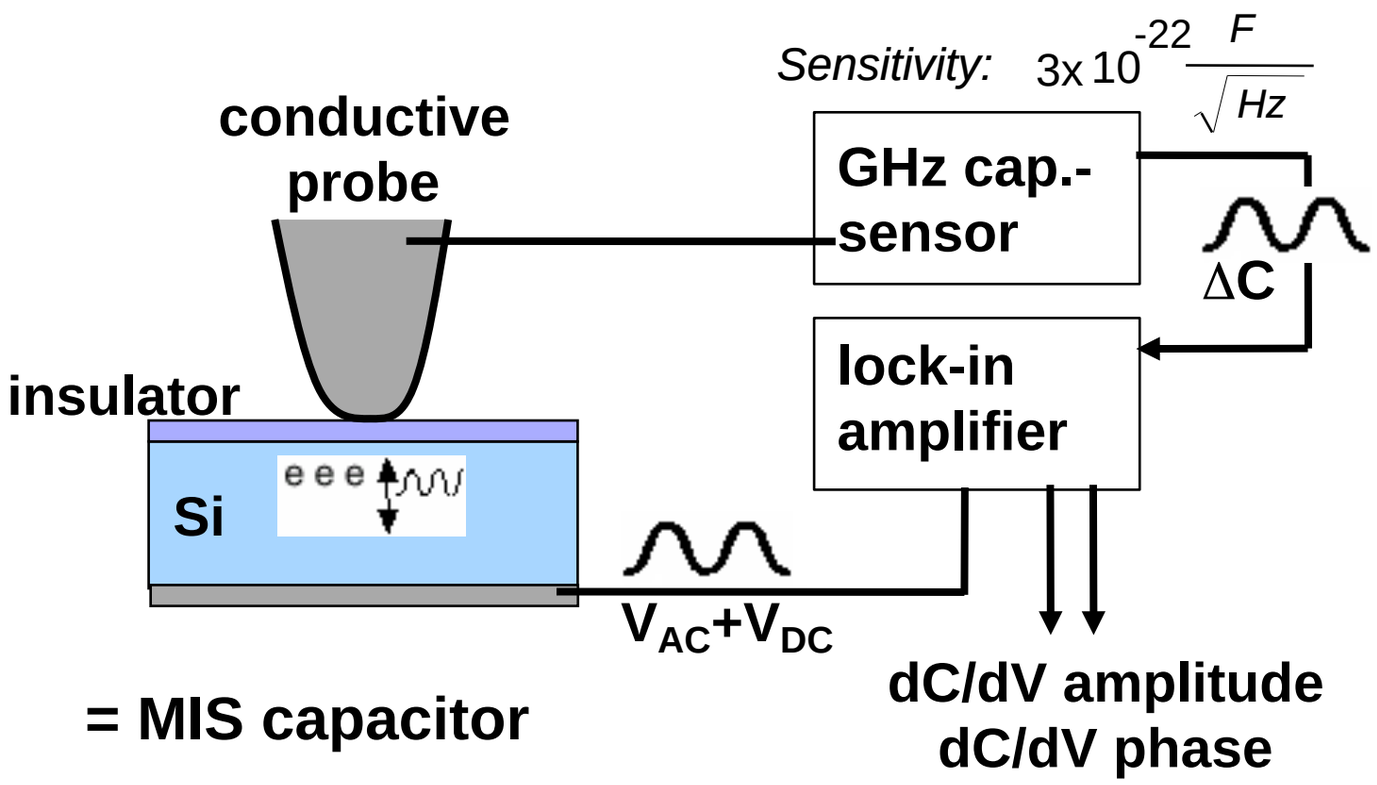

SCM:

SPM-feedback, low force

dC/dV measurement (GHz resonant circuit)

Dopant level (10^{15} – 10^{20} carriers/cm^3) and dopant type via depletion/ accumulation behavior

3.3. Intermittent Contact Mode and Peak Force Microscopy

Intermittent Contact Mode: Operation Principle

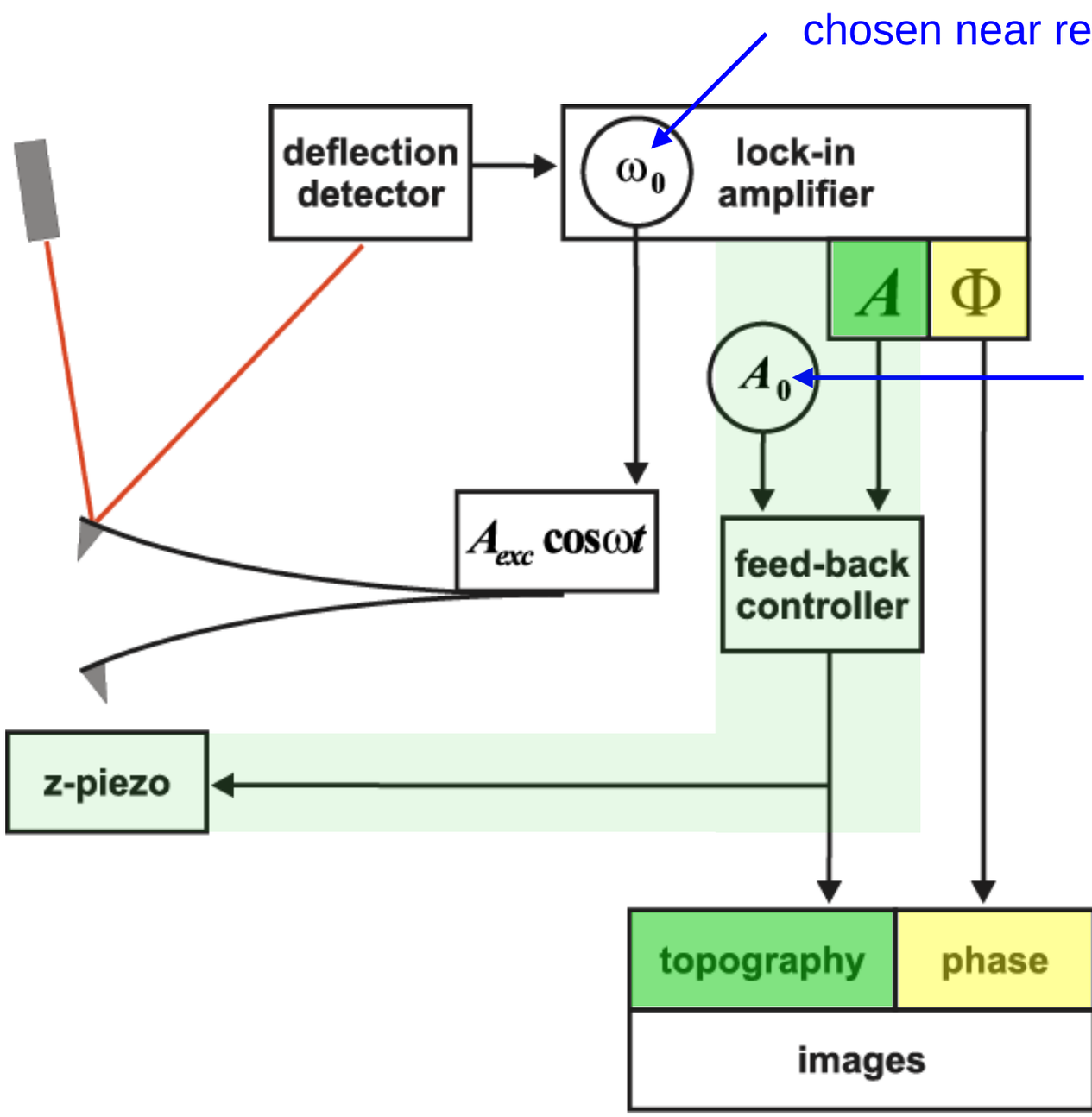

➜ be aware: use cantilevers with sufficient stiffness and drive at sufficiently larger amplitudes to keep energy loss from tip-surface contact << energy stored in cantilever

Intermittent Contact Mode ➜ Materials Contrast

Empa
Materials Science and Technology

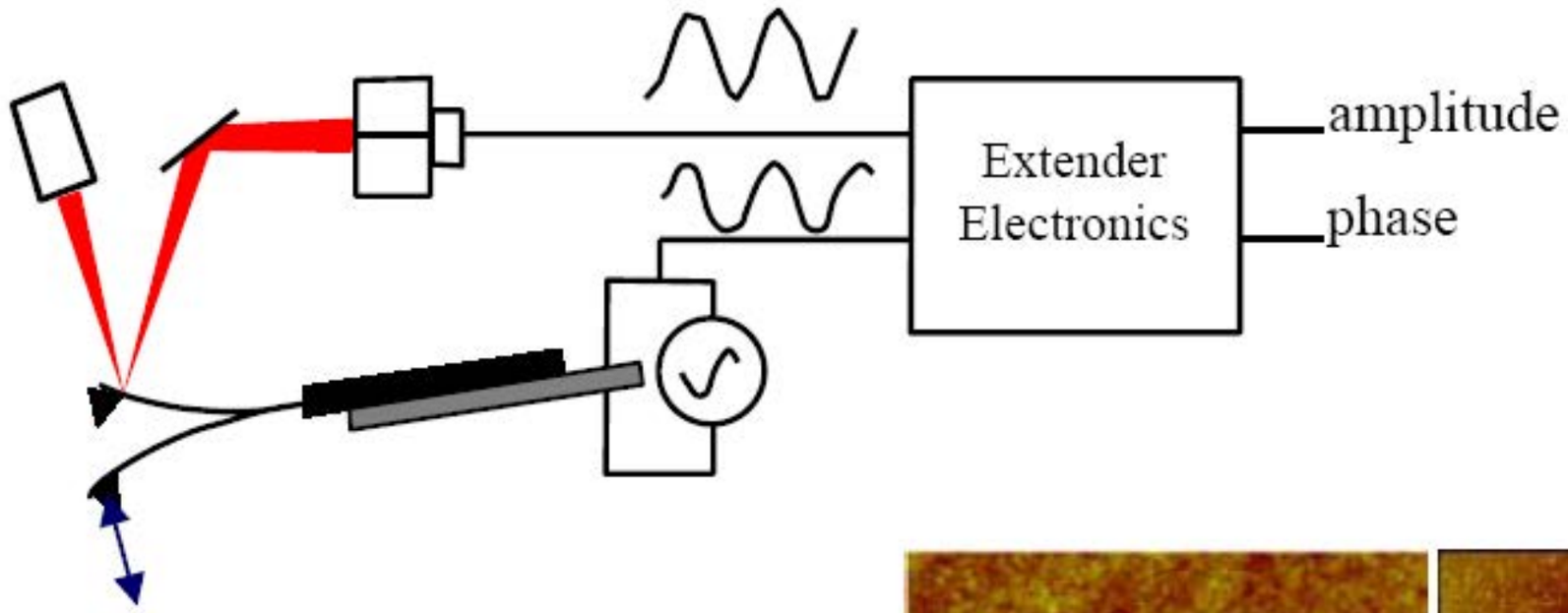

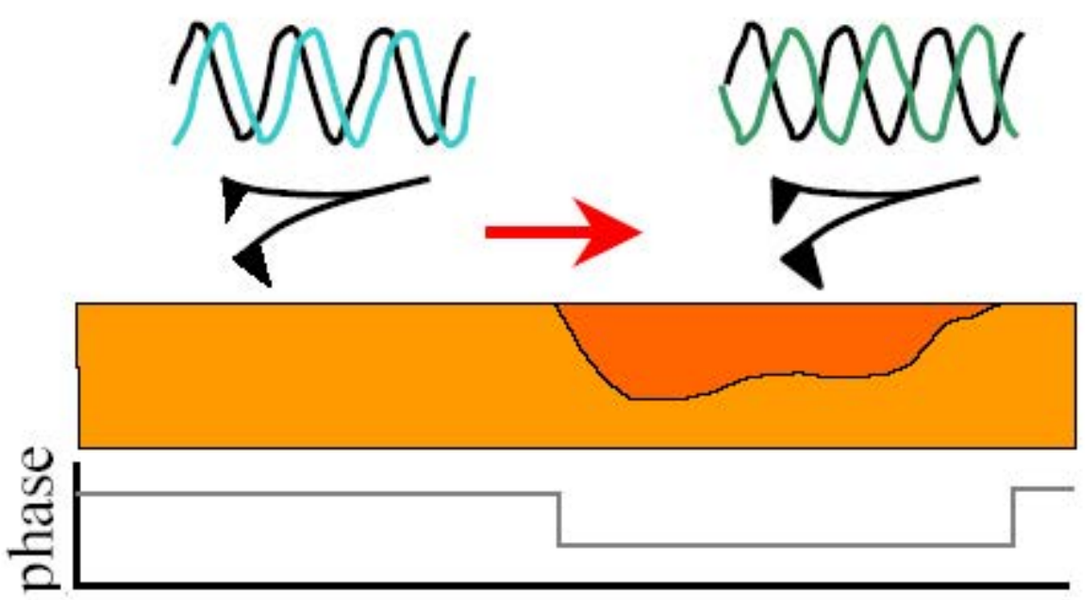

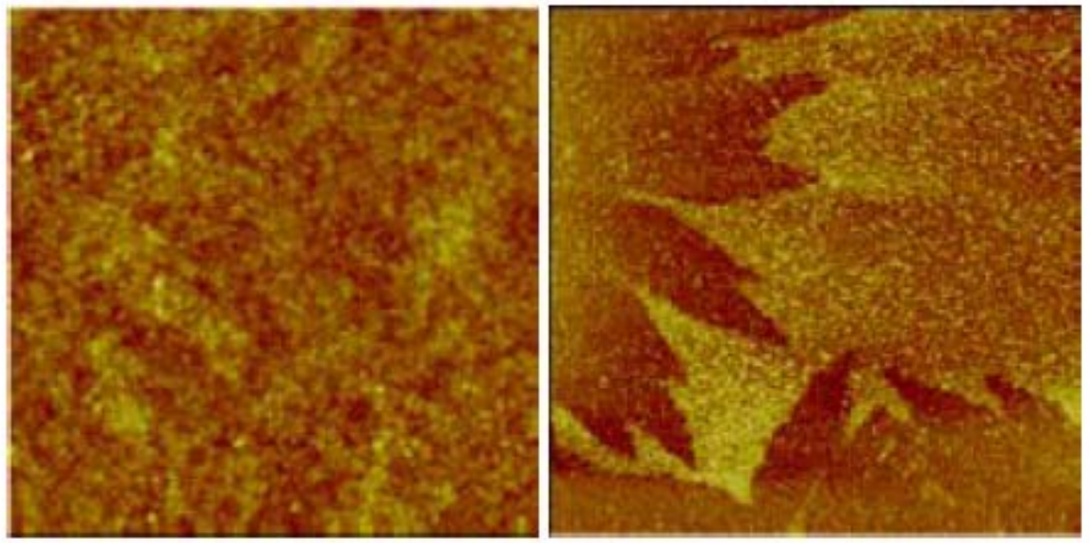

Two-phase structure of a semi-crystalline polymer

left: topography

right: phase image

Experiments:
Y. Martin et al, JAP 61, 4723 (1987)
Q. Zhong et al, SS 290, L688 (1993)

Theory:
R. Garcia and A.S. San Paulo, Phys. Rev. B 61, R13381 (2000)
A.S. San Paulo and R. Garcia, Phys. Rev. B 66, 041406R 2002

Intermittent Contact Mode Advantages

Empa
Materials Science and Technology

Intermittent contact mode is good for

- works best in air (not vacuum)
- measurement of topography on soft samples
- measurement of loose particles adsorbed on surfaces
- topography Measurement on samples with high friction
- topography on samples with vertical features
- is easy to use and robust !

but:

- the cantilever oscillation can be strongly non-harmonic, i.e. bent resonance curves with instabilities
- stable operation is obtained at high amplitudes and with hard cantilevers
- but the highest phase contrast is obtained close to the critical points

CSIC

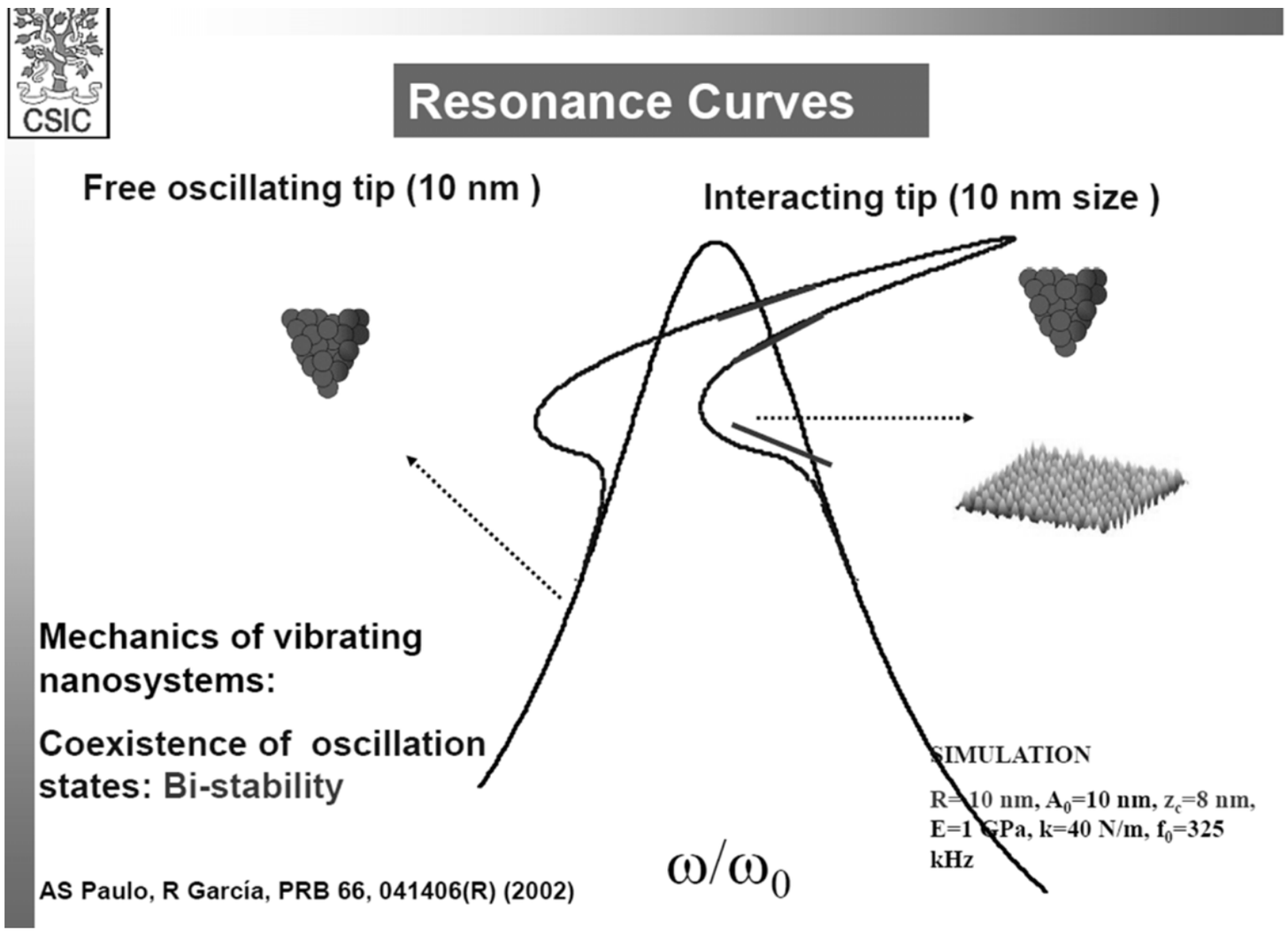

off-Resonance Intermittent Contact Modes

Empa
Materials Science and Technology

oscillation of sample
z-position at 2kHz

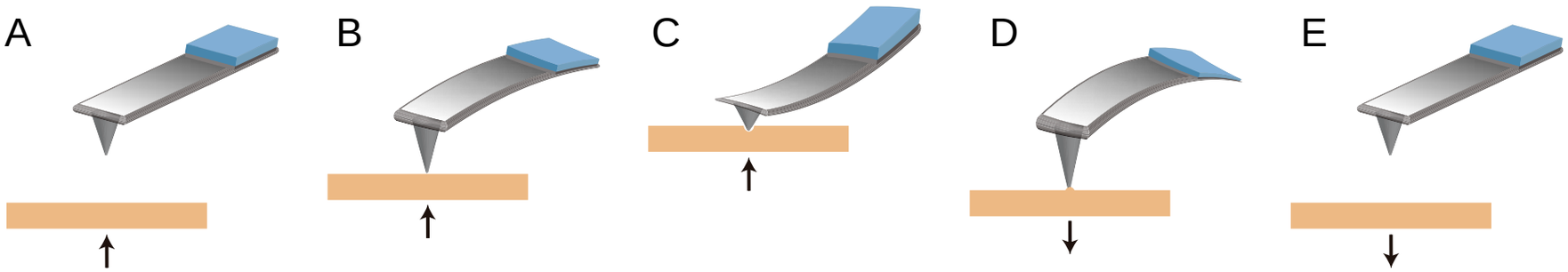

BRUKER

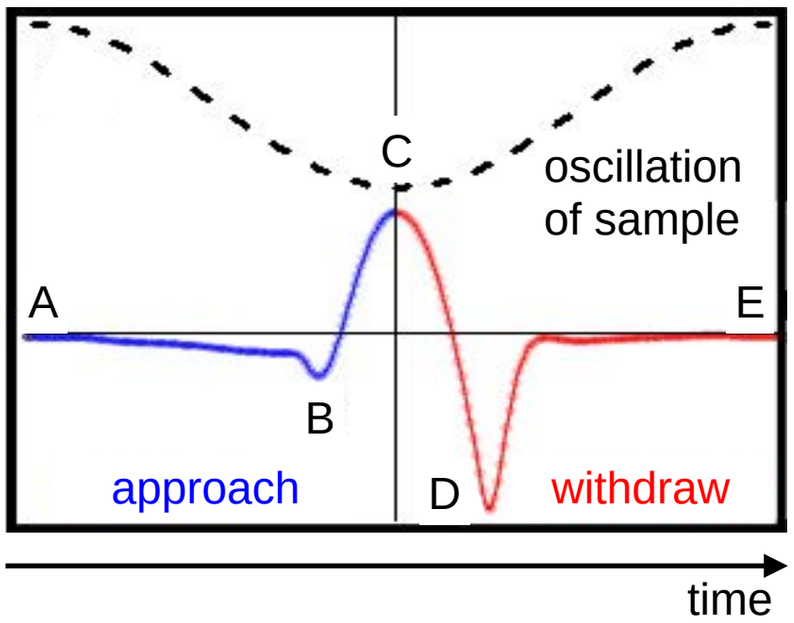

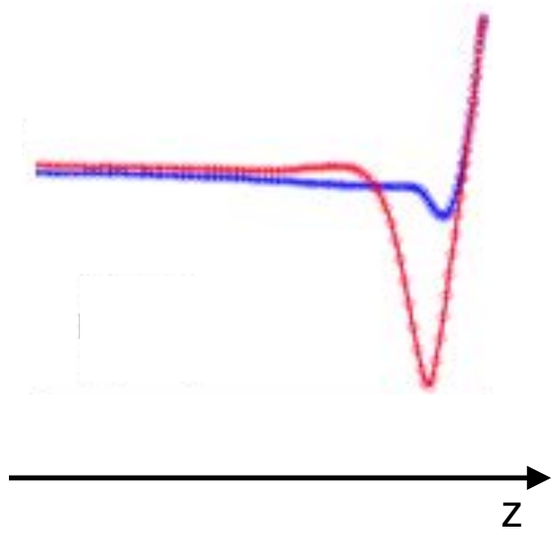

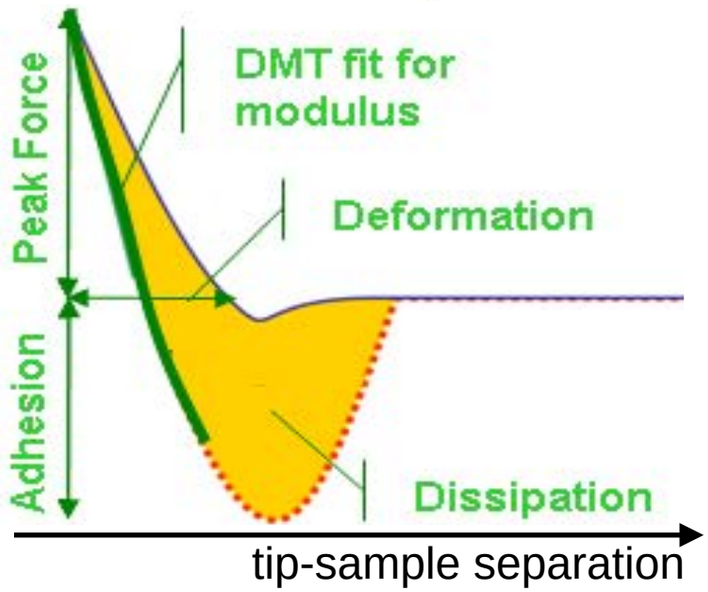

➜ sample or cantilever can be oscillated. Important: oscillation frequency different from cantilever resonance.
➜ recording multiple force-distance curves for each measured xy-point

Peak Force Method

➜ High Fidelity Topography on corrugated

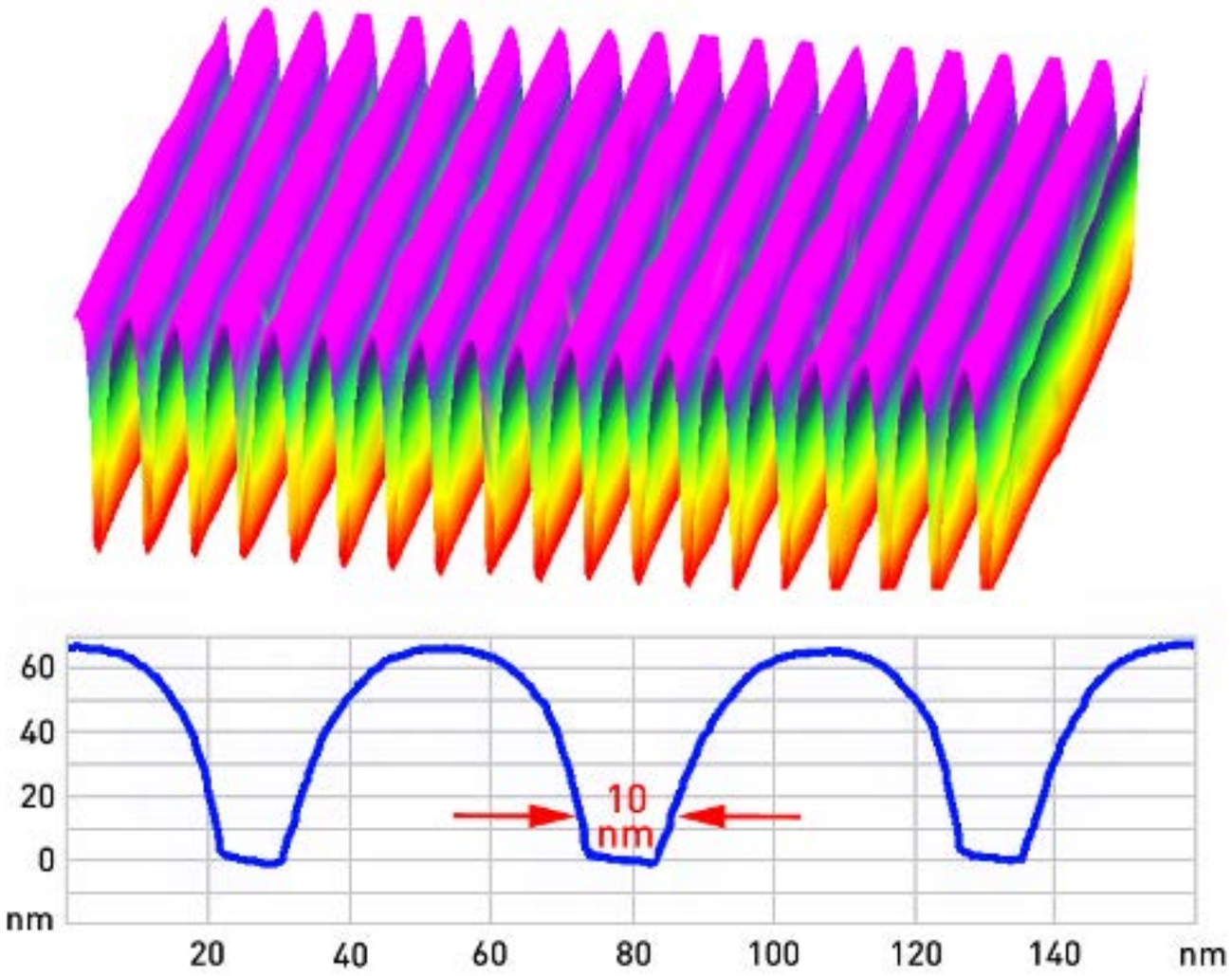

➜ Deep (~65 nm), narrow (~50 nm) trenches are difficult to image with intermittent contact mode, because of excessive damping of the probe oscillation.

➜ use Peak Force for z-feedback ➜ the tip easily reaches the bottom of the trenches.

Peak Force Method ➜ Young's Modulus

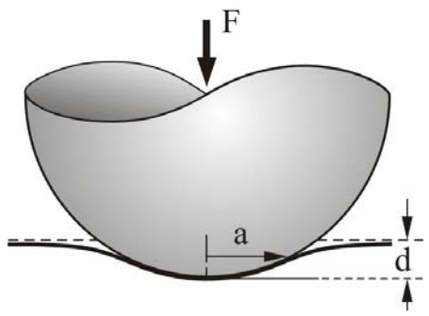

Derjaguin-Muller-Toporov (DMT) model

$$F_{\text{tip}} = \boxed{\frac{4}{3} E^* \sqrt{R}\, d^{3/2}} + F_{\text{adh}},$$

in contact:
Hertz Theory

$$\frac{1}{E^*} = \frac{1-\nu_1^2}{E_1} + \frac{1-\nu_2^2}{E_2}$$

and E_1,E_2 are the elastic moduli and ν_1,ν_2 the Poisson's ratios associated with each body.

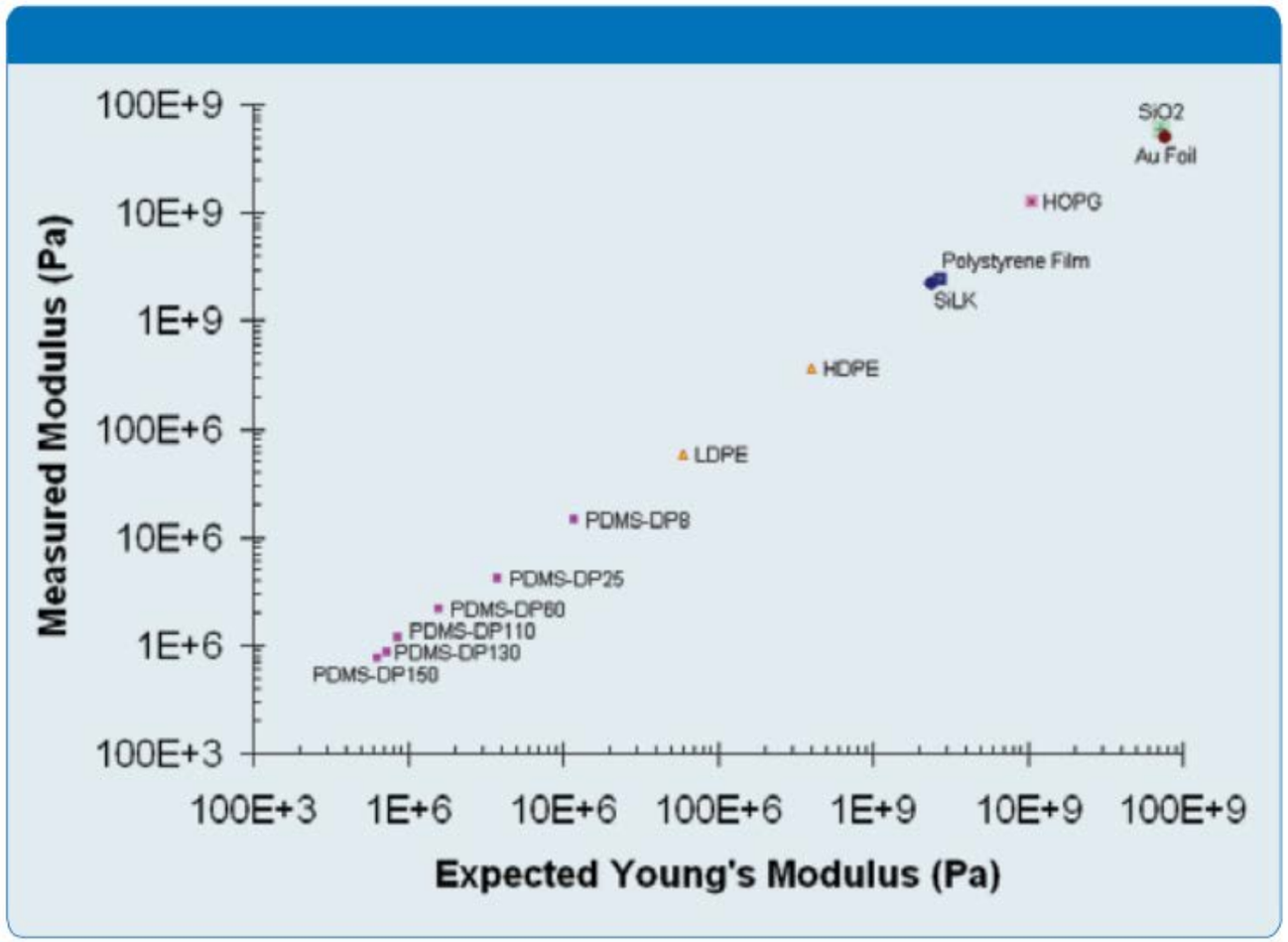

Figure 2. Plot of Measured Modulus vs. expected Young's Modulus (from the literature or from SPM Nanoindentation). Multiple probes were used with different spring constants to cover the entire range. Each probe was individually calibrated using the absolute method.

➜ local sample modulus can be measured simultaneously with topography and adhesion force

Peak Force Method ➜ Local mechanical Properties

Empa
Materials Science and Technology

PS-LDPE blend

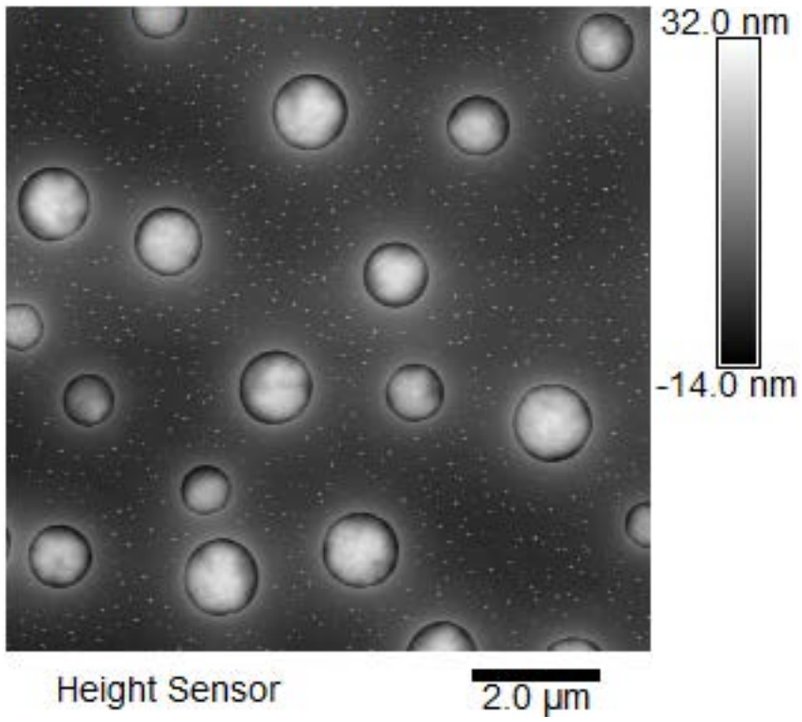

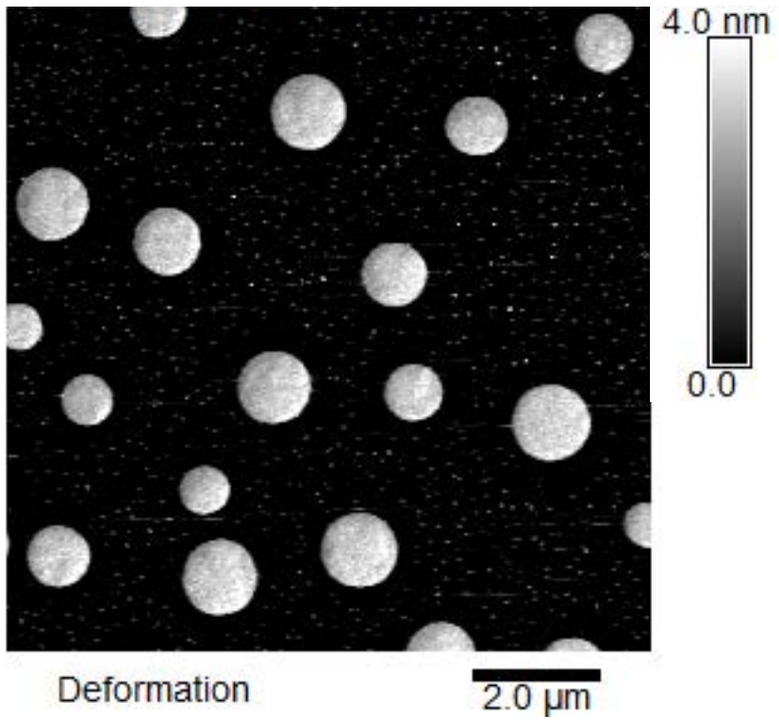

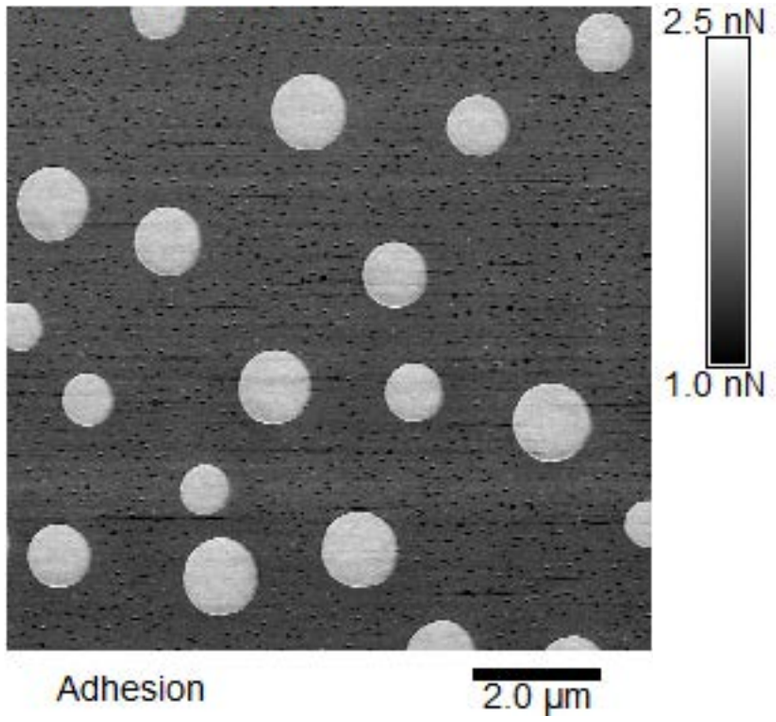

3d overlaid image
topography (height) & modulus (color)

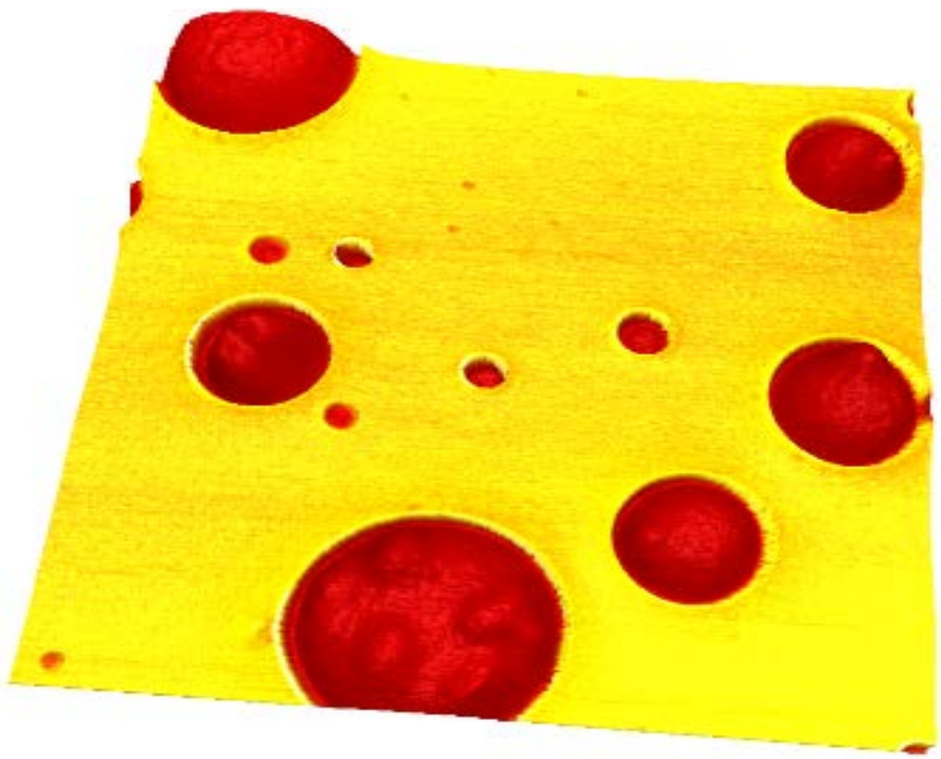

BRUKER

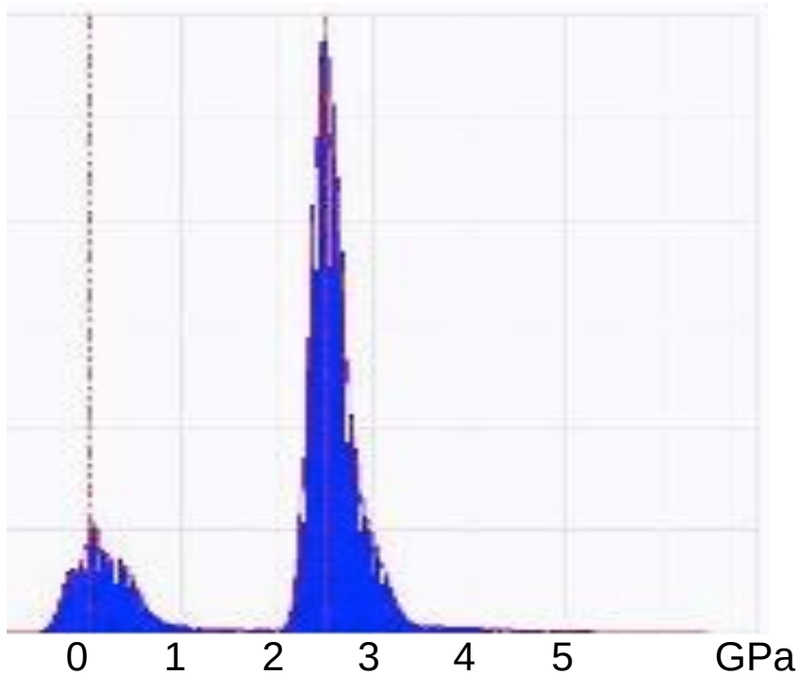

off-Resonance Intermittent Contact Modes

Empa
Materials Science and Technology

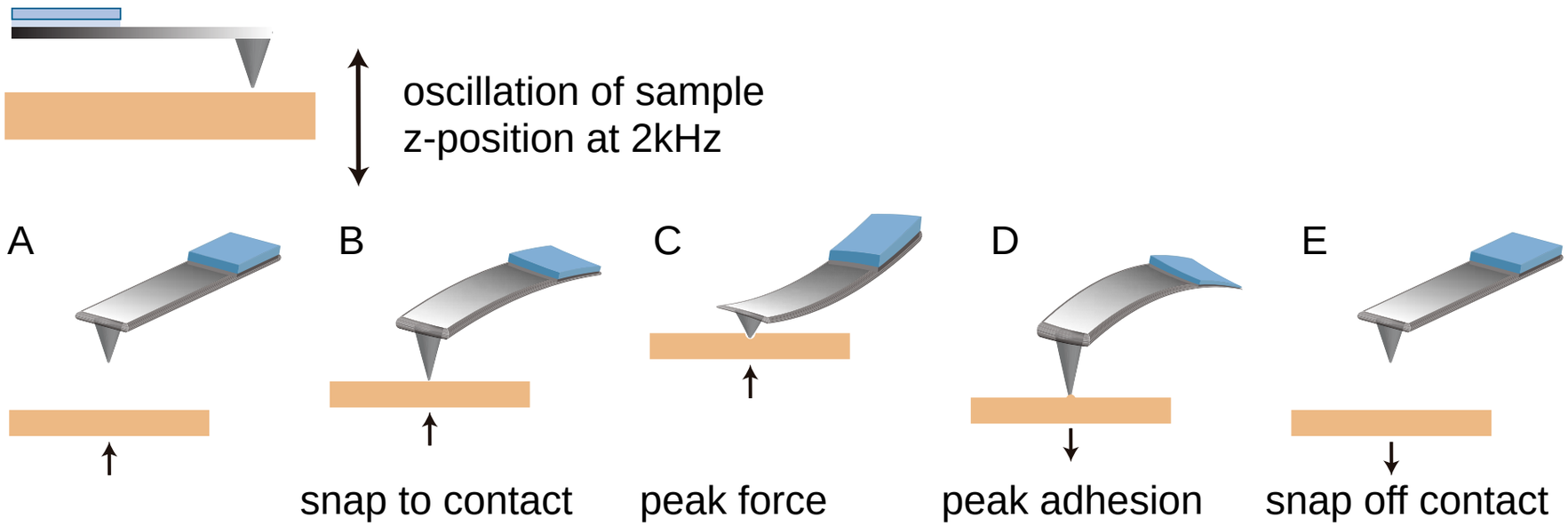

time trace of cantilever deflection signal

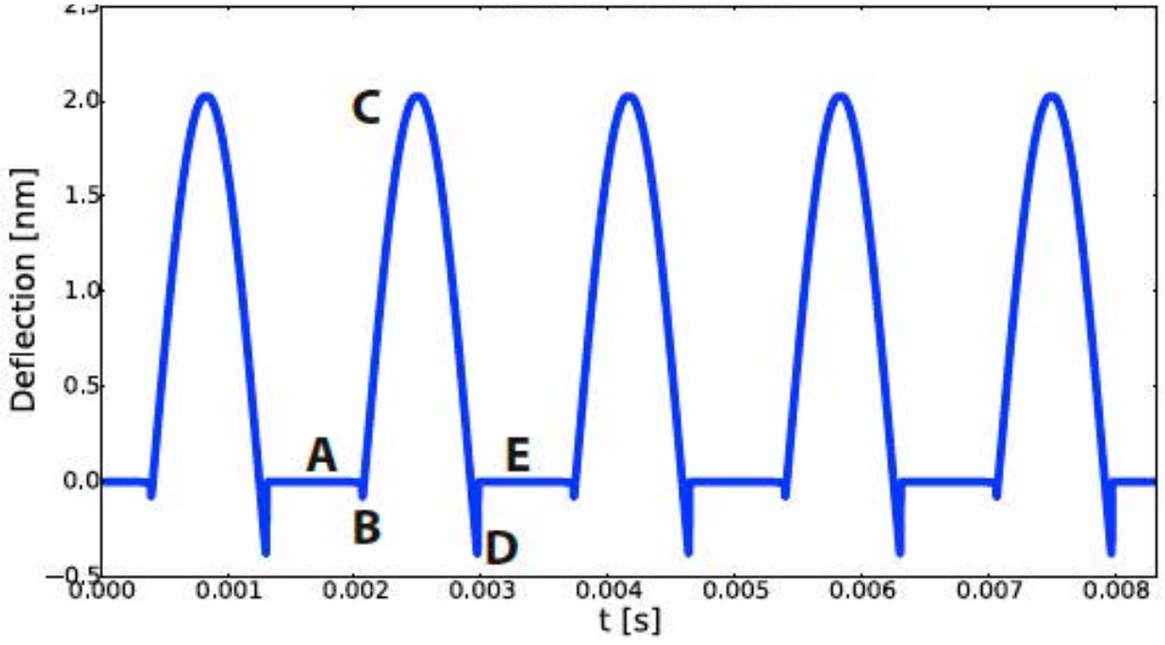

Fourier transform of time trace of cantilever deflection signal

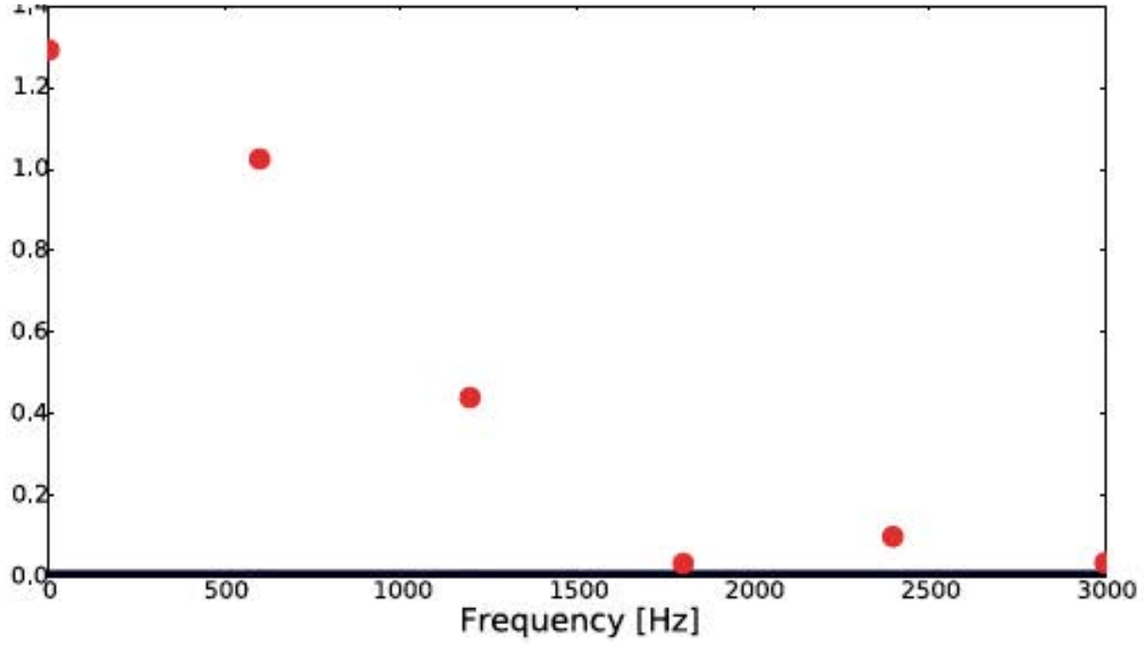

➜ measure multiple harmonics (instead of complete force curve)
➜ record higher harmonics images
➜ reconstruct force curves

M. Penedo and H.J. Hug, Appl. Phys. Lett. 113, 023103 (2018)

here: Amplitudes and Phases of 18 harmonics

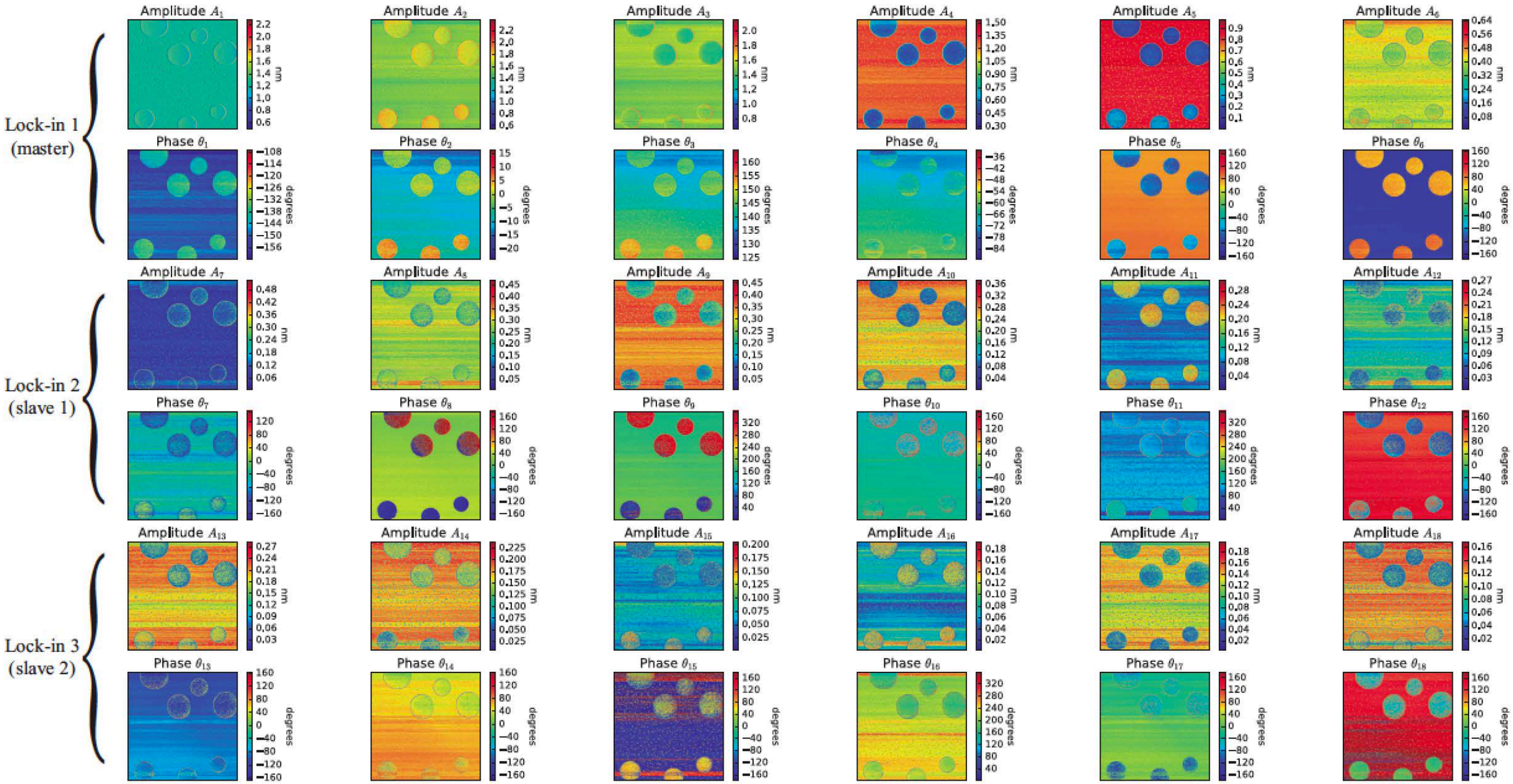

FIG. S 1: Magnitudes and phases of the first 18 harmonics on polystyrene (PS) and low density polyethylene (LDPE) polymer blend sample. The $1^{\text{st}} - 6^{\text{th}}$ harmonics were measured with the LIA-1 (master), the $7^{\text{st}} - 12^{\text{th}}$ harmonics with the LIA-2 (slave 2) and the $13^{\text{st}} - 18^{\text{th}}$ harmonics with the LIA-3 (slave 3).

M. Penedo and H.J. Hug, Appl. Phys. Lett. 113, 023103 (2018)

here: Amplitudes and Phases of 18 harmonics

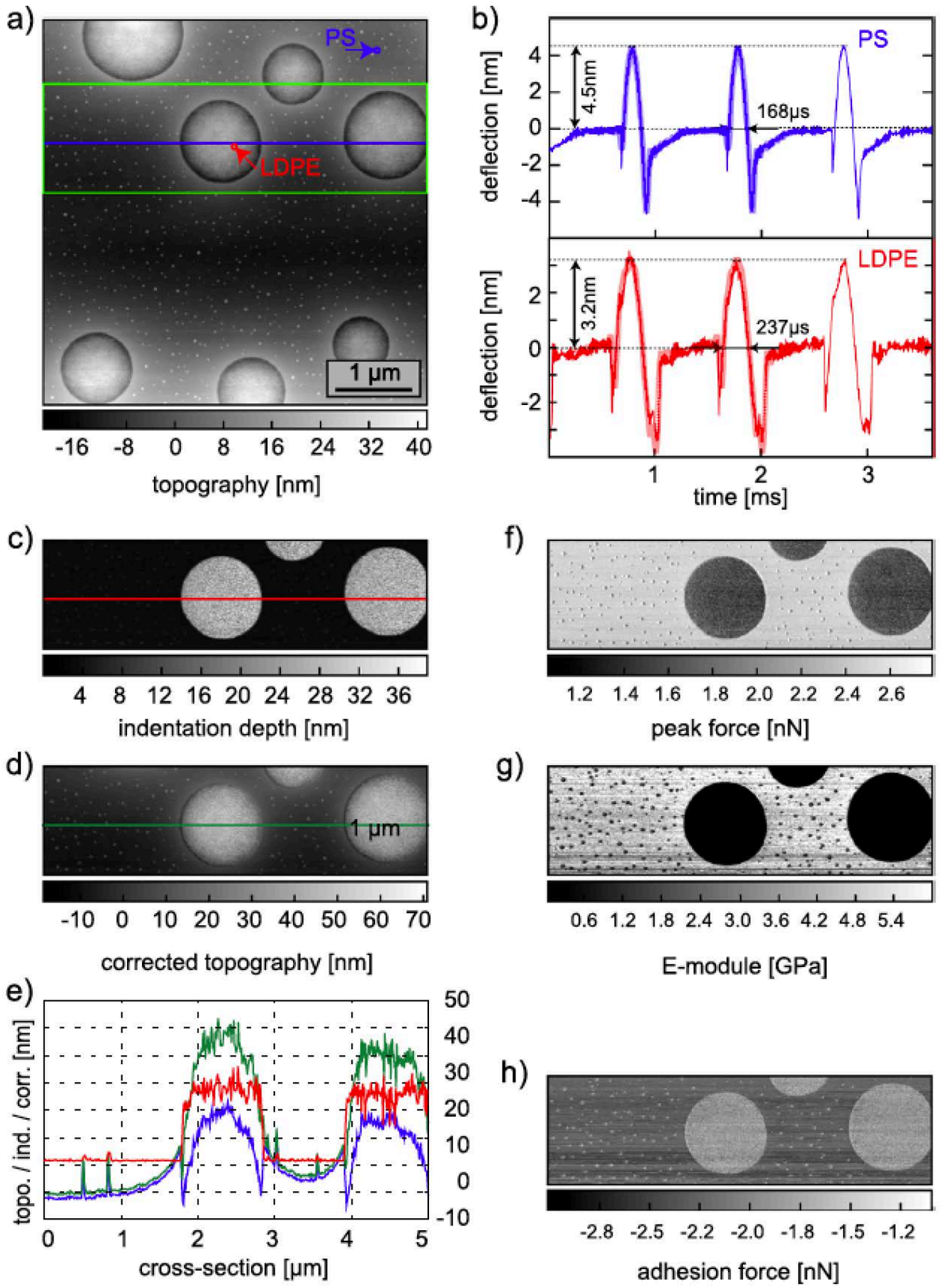

FIG. 4. (a) As-recorded topography. (b) Typical cantilever-deflection time trace signals reconstructed from the 18 harmonic magnitude and phase values at the PS (red wide line) and LDPE (blue wide line) displayed together with time trace signals recorded directly with a digital oscilloscope (fine blue and red lines). (c) Spatial map of the indentation depth. (d) Corrected topography image. (e) Comparison of cross-sections of the as-measured topography (blue line), indentation depth (red line), and corrected topography (green line). The locations of the cross sections are indicated by the blue, red, and green lines in panels (a), (c), and (d), respectively. (f) Map of the peak force. (g) Image of the local Young's moduli. (h) Image of the local adhesion force.

M. Penedo and H.J. Hug, Appl. Phys. Lett. 113, 023103 (2018)

Multi-modal intermittent contact
➜ materials contrast

Graphene layers on silicon dioxide.

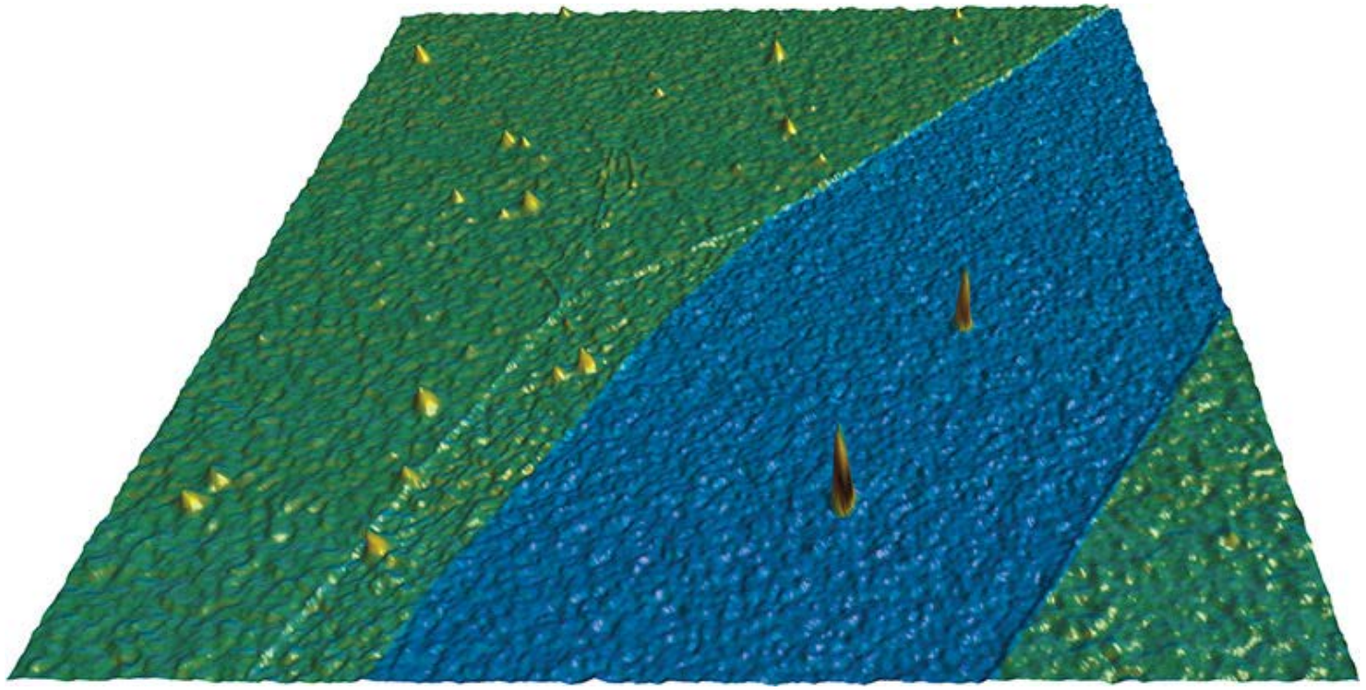

- topography measured in intermittent contact mode using 1st cantilever oscillation mode

- resonance frequency shift of second mode is proportional to local sample stiffness

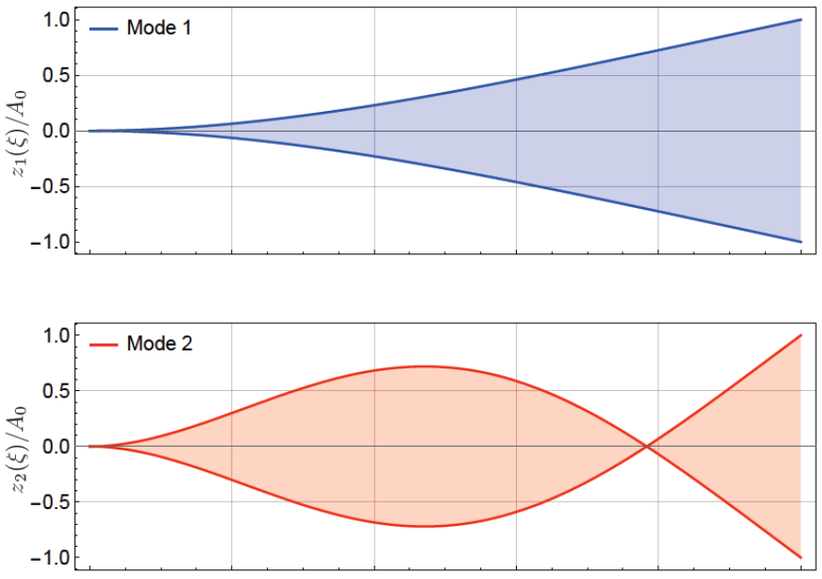

➜ using different cantilever oscillation modes simultaneously is equivalent to using cantilevers of different stiffness and resonance frequency simultaneously.

3.4. non-contact AFM (ncAFM) or Dynamic Force Microscopy (DFM)

3.4.1. Principles and Instrumentation

Damped harmonic Oscillator

Amplitude of Cantilever

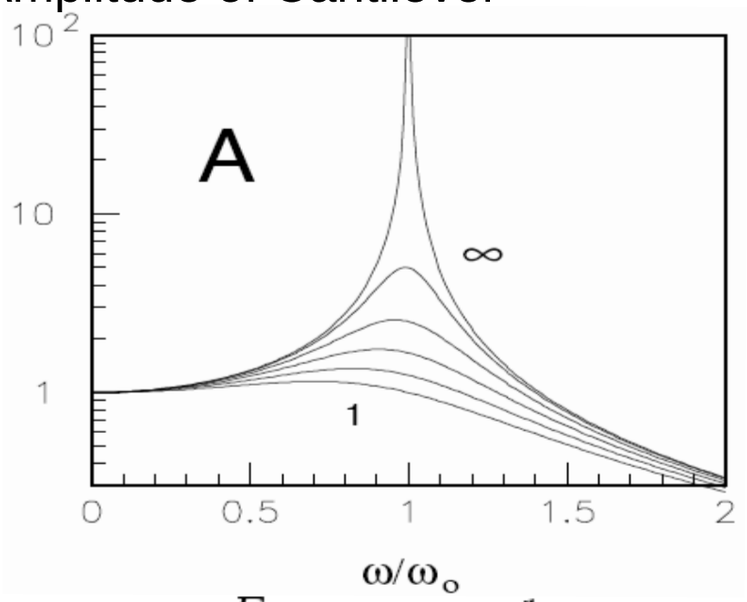

$$A(\omega) = \frac{F_0}{k} \frac{1}{\sqrt{\left(1 - \frac{\omega^2}{\omega_o^2}\right)^2 + \frac{\omega^2}{Q^2\omega_o^2}}}$$

Phase Loss of Cantilever relative to Excitation

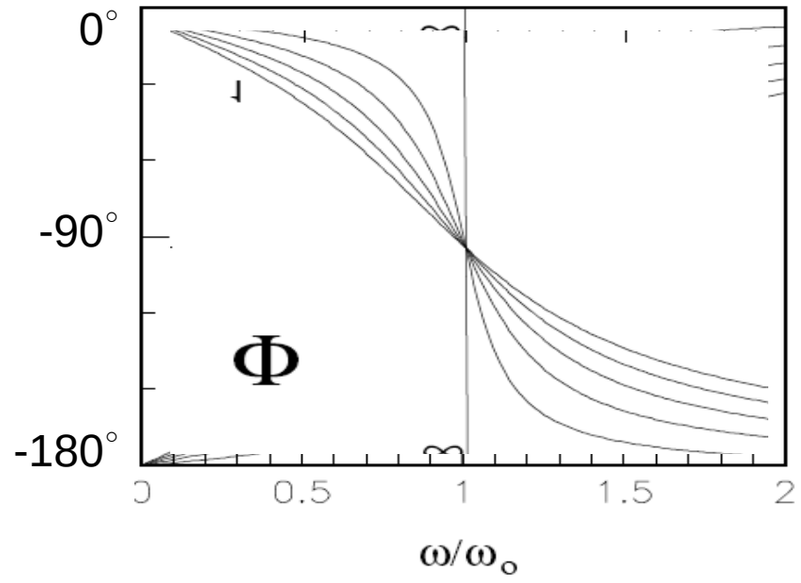

$$\Phi(\omega) = -\arctan\left(\frac{\omega_0\omega}{Q(\omega_0^2 - \omega^2)}\right)$$

on resonance the cantilever lags 90° behind the excitation

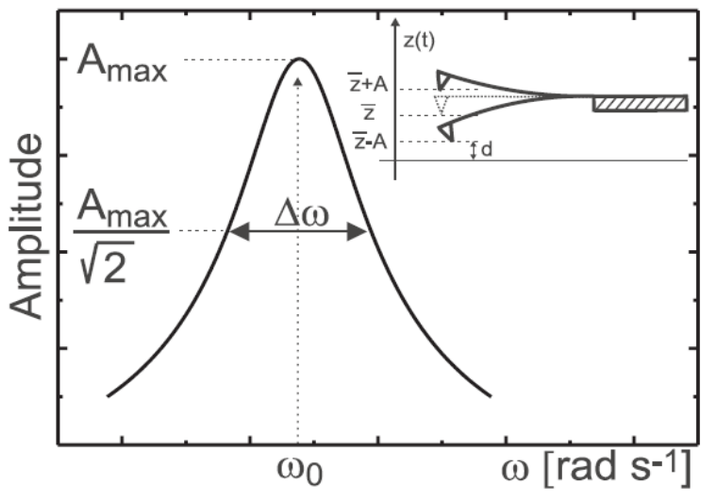

$$Q = A_{max}/A_{exc} = \omega_0/\Delta\omega$$

be aware: these equations hold only after the transient phase !
this can take a long time for high-Q cantilevers

Dynamic Operation with low & high Quality Factor

cantilever resonance

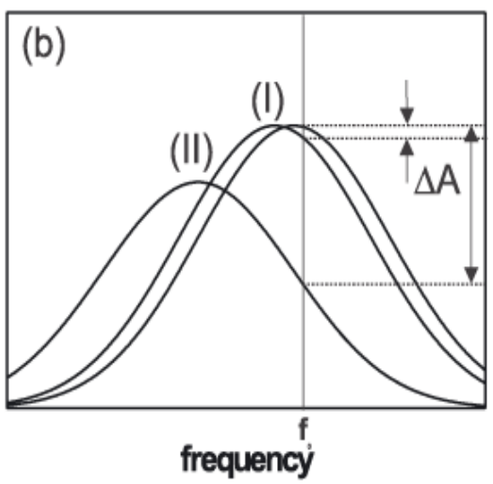

in air
-> low quality factor of cantilever
-> excitation with fixed frequency
-> lock-in amplifier

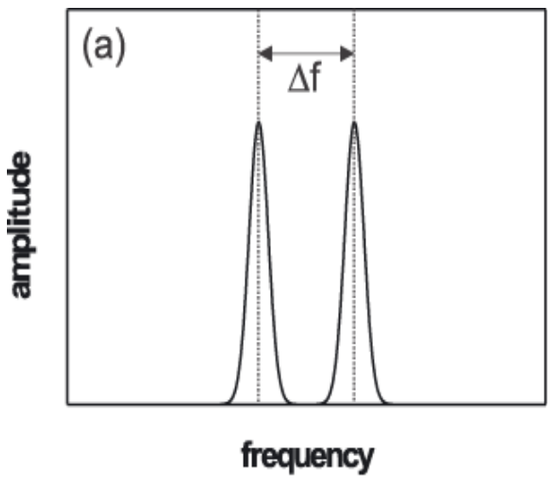

in vacuum
-> high quality factor
-> excitation on resonance
-> requires phase locked loop

low Q: use fixed frequency

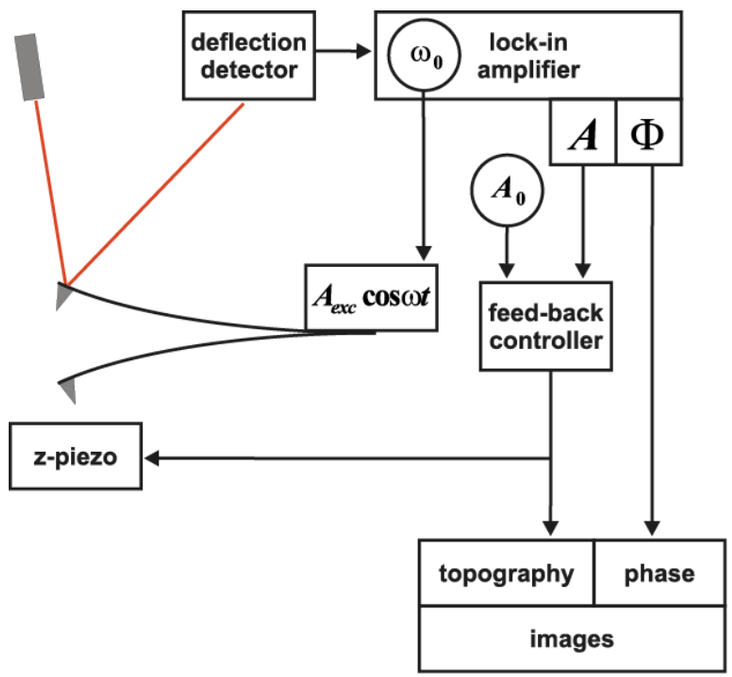

high Q: use excitation frequency must track resonance

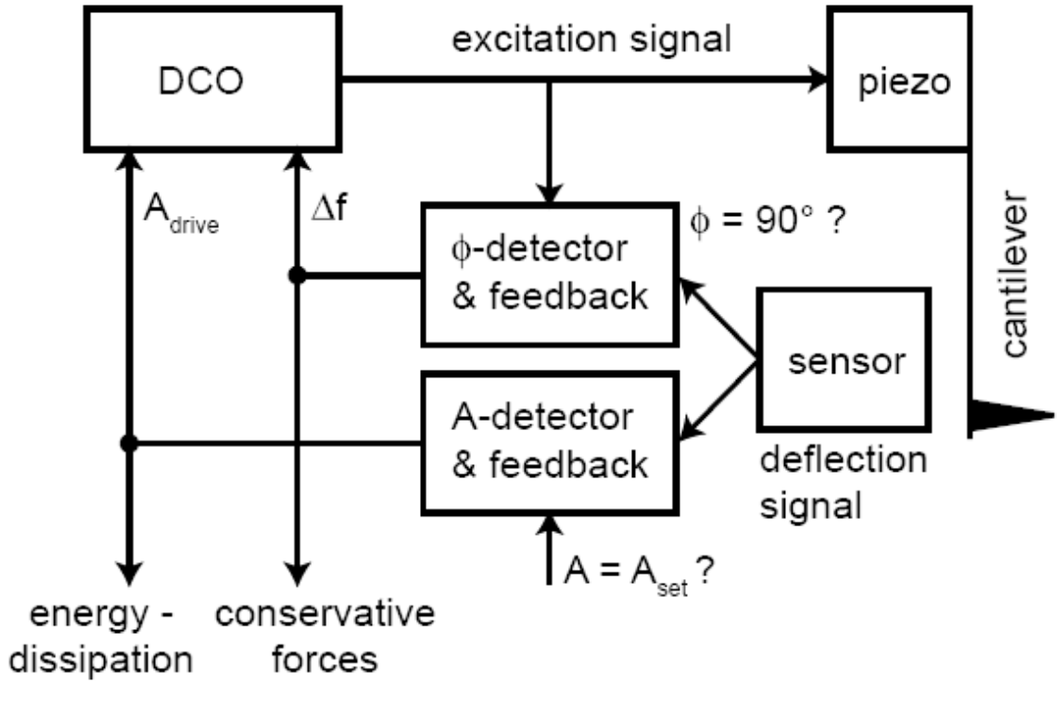

Frequency Shift from harmonic Tip-Sample Potential

Conventional Spring

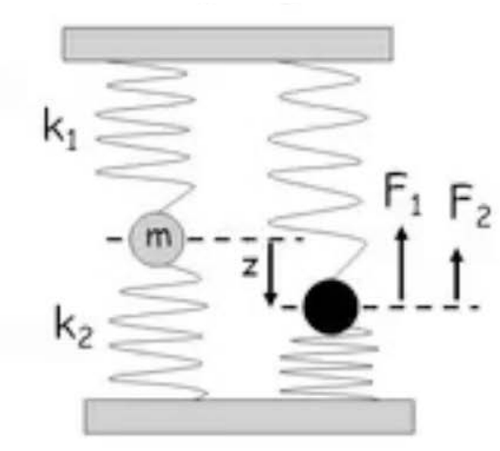

$$m\ddot{z} = -k_1 z - k_2 z$$

$$\omega = \sqrt{\frac{k_1 + k_2}{m}}$$

Harmonic Tip-Sample Potential

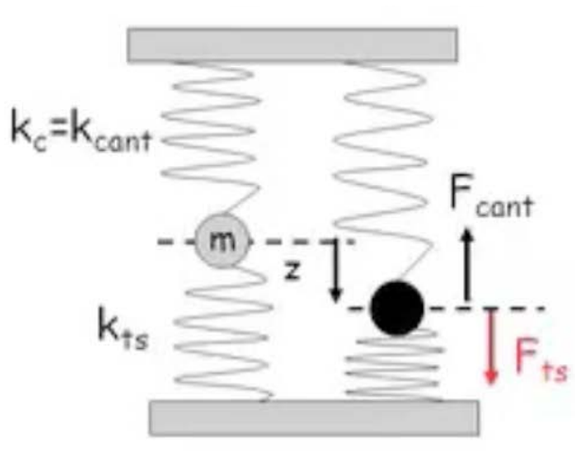

$$m\ddot{x} = -k_c z + k_{ts} z$$

$$m\ddot{x} = -(k_c z - k_{ts}) z$$

$$\omega = \sqrt{\frac{k_c - k_{ts}}{m}} = \sqrt{\frac{k_c}{m} \cdot \left(1 - \frac{k_{ts}}{k_c}\right)}$$

$$\approx \omega_0 \cdot \left(1 - \frac{1}{2}\frac{k_{ts}}{k_c} + \ldots\right)$$

with $\omega_0 = \sqrt{\frac{k_c}{m}}$

Frequency Shift from a realistic Potential (small Amplitude Approximation)

small oscillation amplitude

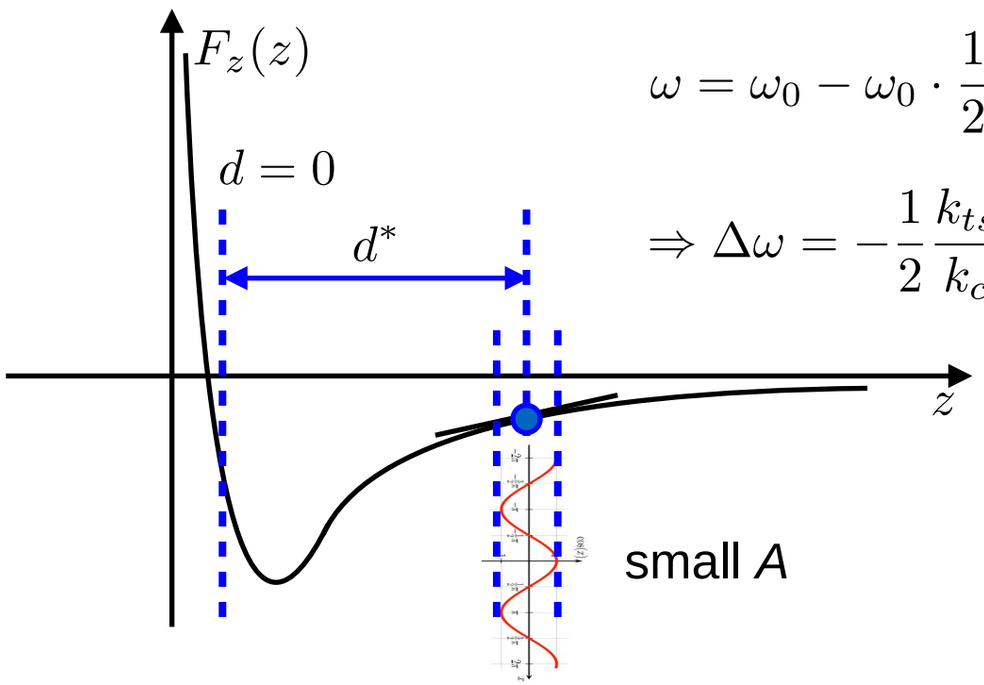

$$\omega = \omega_0 - \omega_0 \cdot \frac{1}{2}\frac{k_{ts}}{k_c}$$

$$\Rightarrow \Delta\omega = -\frac{1}{2}\frac{k_{ts}}{k_c}$$

measure $\Delta\omega(z) \Rightarrow F_{ts}(d^*) = -2k_c \cdot \int_{\infty}^{d^*} \frac{\Delta\omega(z)}{\omega_0}\, dz$

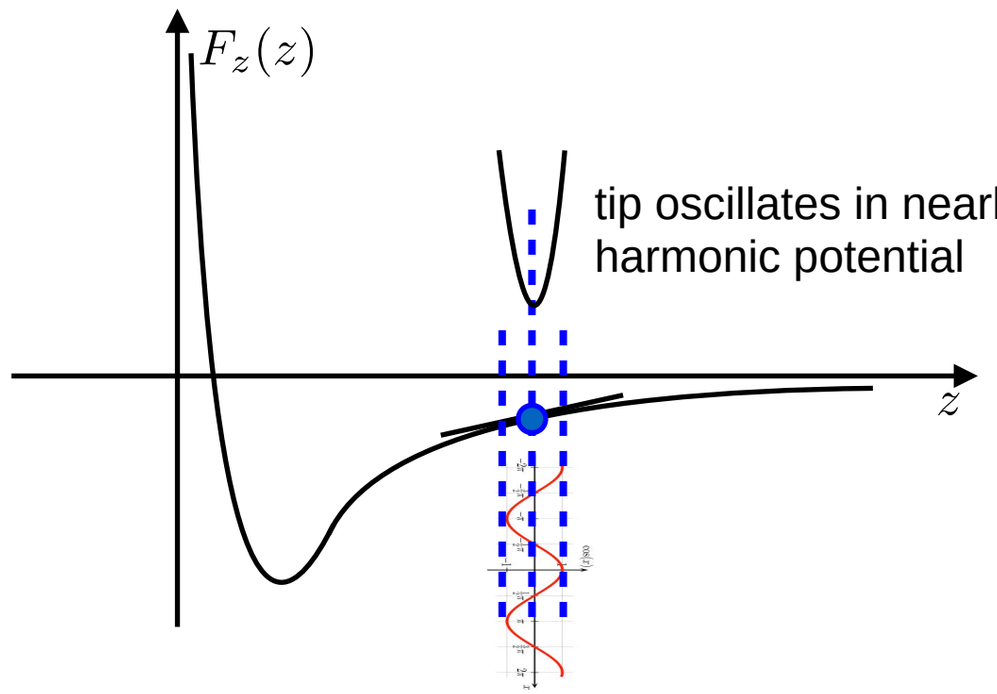

Frequency Shift from harmonic Tip-Sample Potential

Conventional Spring

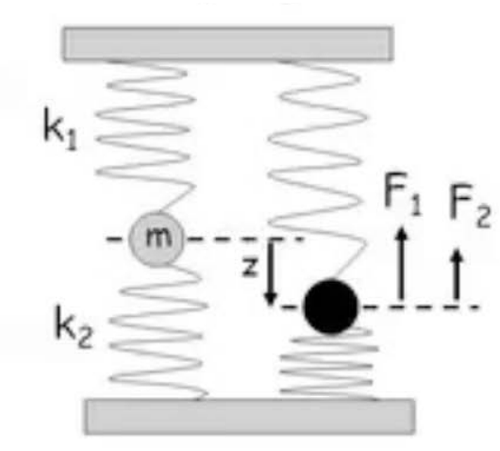

$$m\ddot{z} = -k_1 z - k_2 z$$

$$\omega = \sqrt{\frac{k_1 + k_2}{m}}$$

Harmonic Tip-Sample Potential

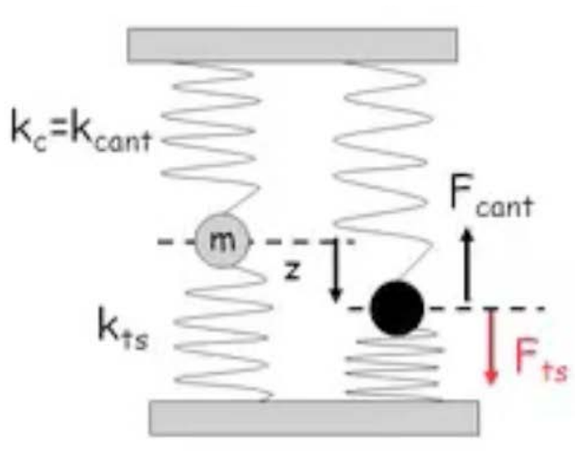

$$m\ddot{x} = -k_c z + k_{ts} z$$

$$m\ddot{x} = -(k_c z - k_{ts}) z$$

$$\omega = \sqrt{\frac{k_c - k_{ts}}{m}} = \sqrt{\frac{k_c}{m} \cdot \left(1 - \frac{k_{ts}}{k_c}\right)}$$

$$\approx \omega_0 \cdot \left(1 - \frac{1}{2}\frac{k_{ts}}{k_c} + \ldots\right)$$

with $\omega_0 = \sqrt{\frac{k_c}{m}}$

Frequency Shift from a realistic Potential (small Amplitude Approximation)

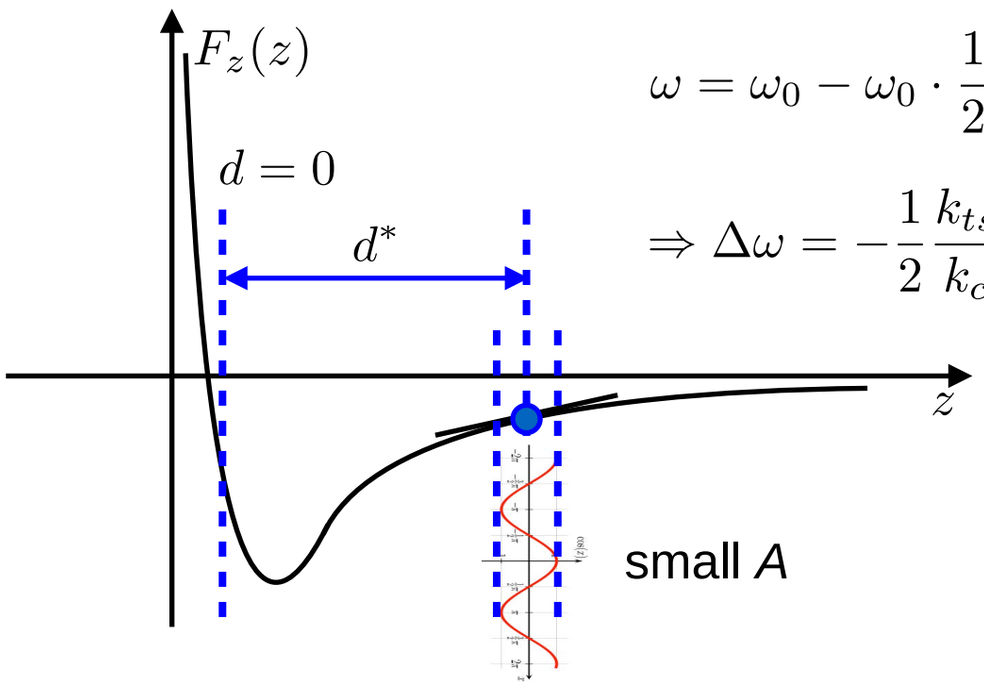

$$\omega = \omega_0 - \omega_0 \cdot \frac{1}{2}\frac{k_{ts}}{k_c}$$

$$\Rightarrow \Delta\omega = -\frac{1}{2}\frac{k_{ts}}{k_c}$$

measure $\Delta\omega(z) \Rightarrow F_{ts}(d^*) = -2k_c \cdot \int_{\infty}^{d^*} \frac{\Delta\omega(z)}{\omega_0}\, dz$

large oscillation amplitude

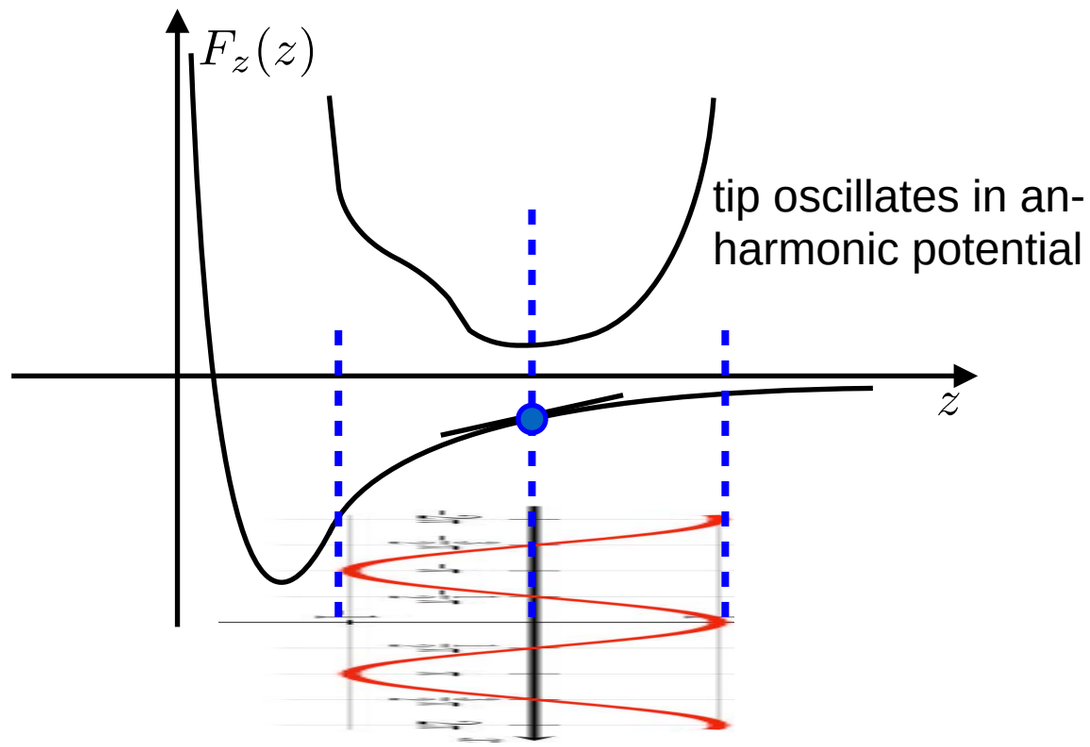

Modeling dynamic AFM

small amplitude approximation:

$$\omega = \sqrt{\frac{c_L - k_{ts}(z)}{m_{eff}}} = \omega_0 \sqrt{1 - \frac{k_{ts}(z)}{c_L}} \qquad \text{with} \quad \omega_0 = \sqrt{\frac{c_L}{m_{eff}}} \qquad \text{free oscillation frequency}$$

and $k_{ts}(z) = \dfrac{\partial F_{ts}}{\partial z}$ and $c_L = K_n^{eq}$ for selected mode n

using Taylor expansion we obtain $\Delta f(z) = \dfrac{f_0}{2c_L} k_{ts}(z)$

otherwise:

$$\begin{aligned}
\Delta f &= -\frac{f_0}{kA^2} \langle F_{ts} q(t) \rangle \quad \text{with: } q(t) = A\cos(2\pi f_0 t) \\
&= -\frac{f_0^2}{kA^2} \int_0^T F_{ts}(z_{lpt} + A - q(t)) \cdot q(t) dt \\
&= -\frac{2f_0^2}{kA^2} \int_0^{T/2} F_{ts}(z_{lpt} + A - q(t)) \cdot q(t) dt
\end{aligned}$$

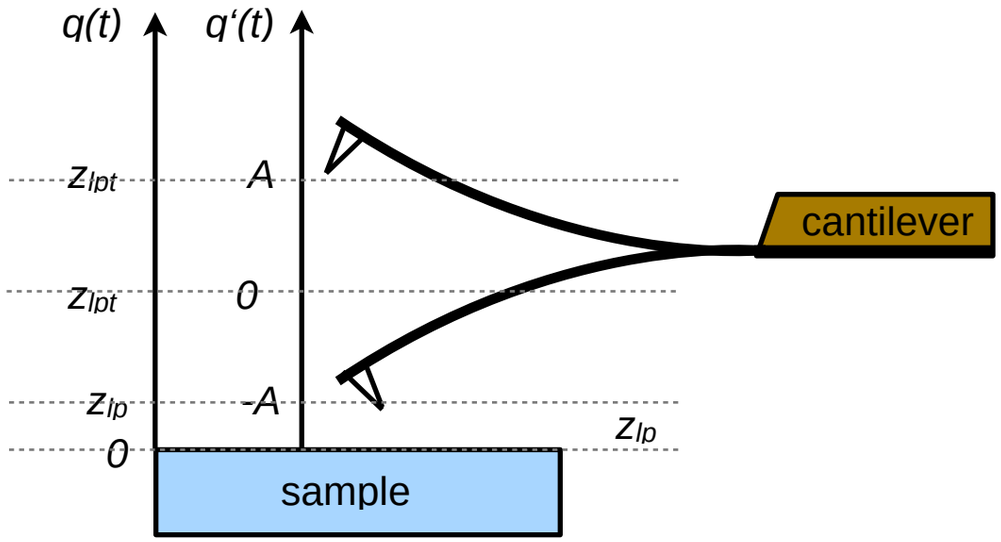

$$\begin{aligned}
dq &= -2\pi f_0 A \sin(2\pi f_0 t) dt \\
\Rightarrow dt &= -\frac{1}{2\pi f_0} \frac{dq}{\sqrt{A^2 - q^2}} \quad \text{with: } A\sin(2\pi f_0 t) = \sqrt{A^2 - A^2\cos(2\pi f_0 t)}
\end{aligned}$$

$$\begin{aligned}
\Delta f &= +\frac{2f_0}{2\pi k A^2} \int_{+A}^{-A} F_{ts}(z_{lpt} + A - q) \cdot \frac{q}{\sqrt{A^2 - q^2}} dq = -\frac{2f_0}{2\pi k A^2} \int_{-A}^{+A} F_{ts}(z_{lpt} + A - q) \cdot \frac{q}{\sqrt{A^2 - q^2}} dq \\
&= -\frac{f_0}{2k} \int_{-A}^{+A} k_{ts}(z_{lpt} + A - q) \cdot \frac{\sqrt{A^2 - q}}{2A^2/\pi} \qquad \Delta f(z_{ltp}) = \frac{f_0}{2k} \frac{2}{\pi A^2} \int_{-A}^{A} k_{ts}(z_{ltp} + A - q') \sqrt{A^2 - q'^2}\, \mathrm{d}q' \\
\uparrow &\quad \text{integration by parts}
\end{aligned}$$

derived from Giessibl, Rev. Mod. Phys. **75** (2003) 949 and Welker et al., Beilstein J. of Nanotechnology **3** (2012) 238

Modeling dynamic AFM

$$\Delta f(z) = f_0 \frac{\langle k_{ts}(z) \rangle}{2k} \quad \text{with} \quad \langle k_{ts}(z) \rangle = \frac{1}{\frac{\pi}{2} A^2} \int_{-A}^{A} k_{ts}(z - q') \sqrt{A^2 - q'^2}\, dq'$$

for $A \to 0 \Rightarrow k_{ts} = \text{const.} \Rightarrow \frac{1}{\frac{\pi}{2}A^2} \cdot \int_{-A}^{A} k_{ts}(z-q')\sqrt{A^2-q'^2}\, dq' = \frac{1}{\frac{\pi}{2}A^2} k_{ts} \cdot \int_{-A}^{A} \sqrt{A^2-q'^2}\, dq'$

area of semi-circle: $\frac{\pi}{2}A^2$

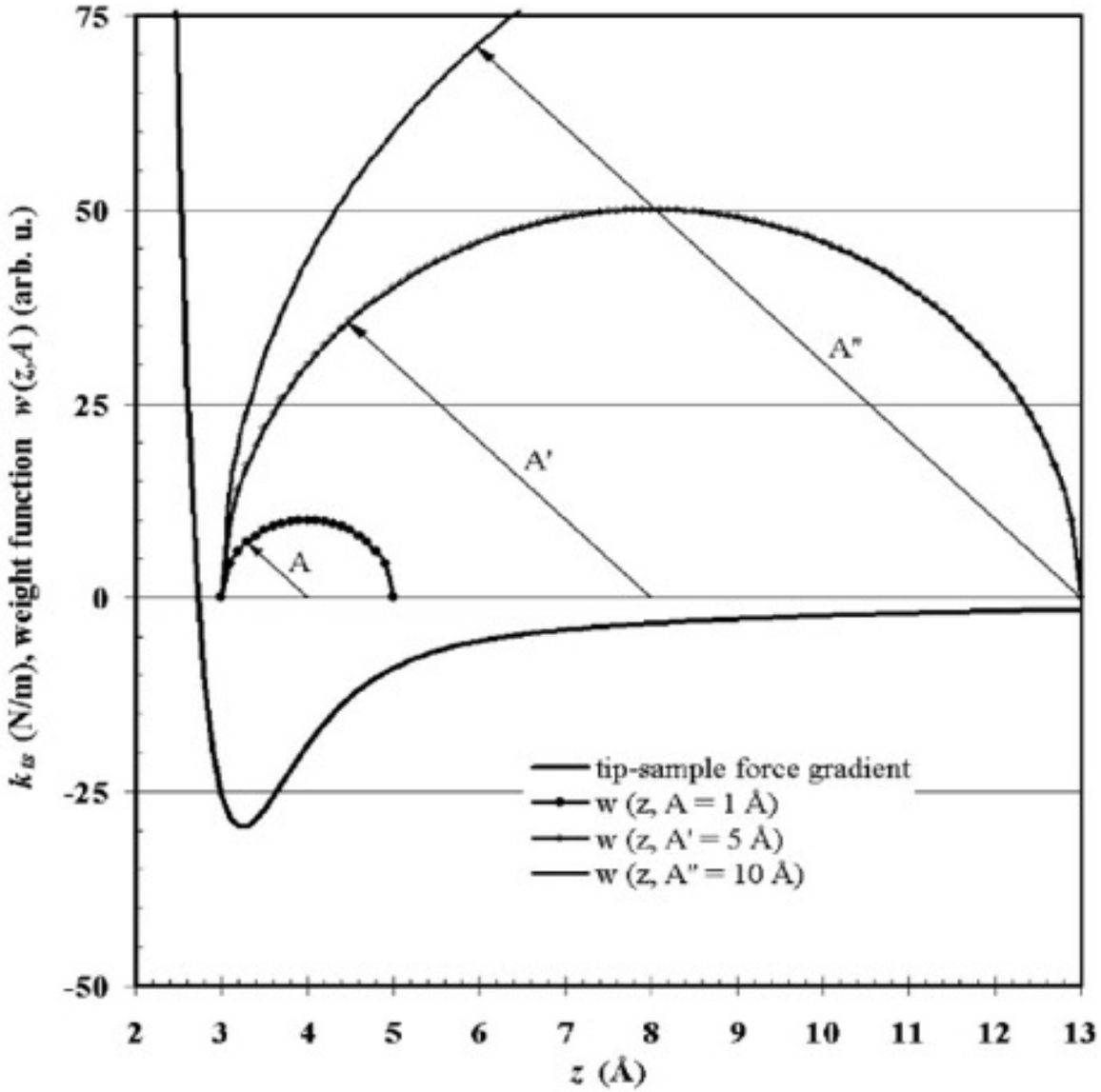

relevant issues

- large amplitudes reduce <k_{ts}>; cantilever does not snap
- large amplitudes reduce signal, but improve noise
- large amplitudes suppresses non-harmonic terms and higher harmonics
- large A: $\Delta f \propto A^{-1.5}$
- large A allows renormalization $\gamma(z, A) := \frac{kA^{3/2}}{f_0} \cdot \delta f(z, A)$
- large amplitudes increase contribution of long-range force compared to short-range force
- ideal amplitude corresponds to interaction length of force
- ideal amplitude maximizes higher harmonics generation
- small amplitude: frequency shift no longer depends on *A*, but becomes proportional to k_{ts}

Giessibl, Rev. Mod. Phys. 75 (2003) 949

3.4.2. Imaging with True Atomic Resolution

Avoid Snap to Contact & Multi-atom Tip-Sample Contact

critical tip-sample distance

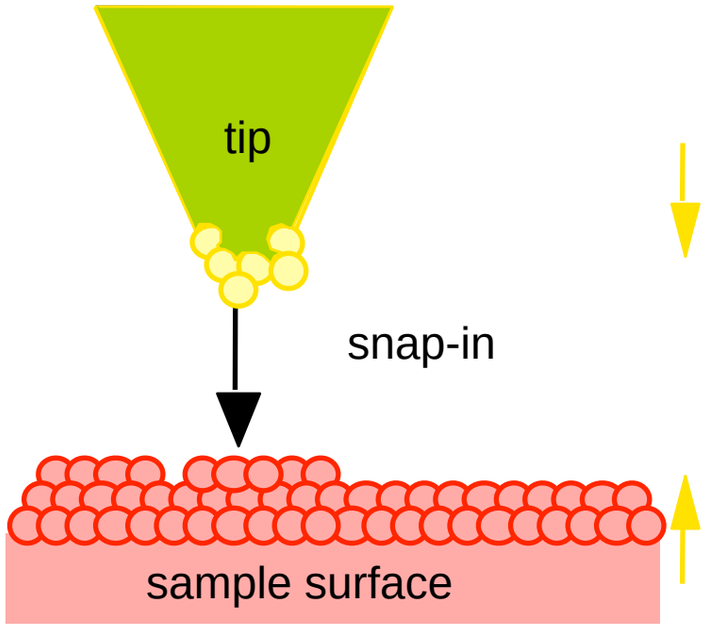

tip snaps to surface @ critical tip-sample distance due to attractive van der Waals force.

tip in contact with sample

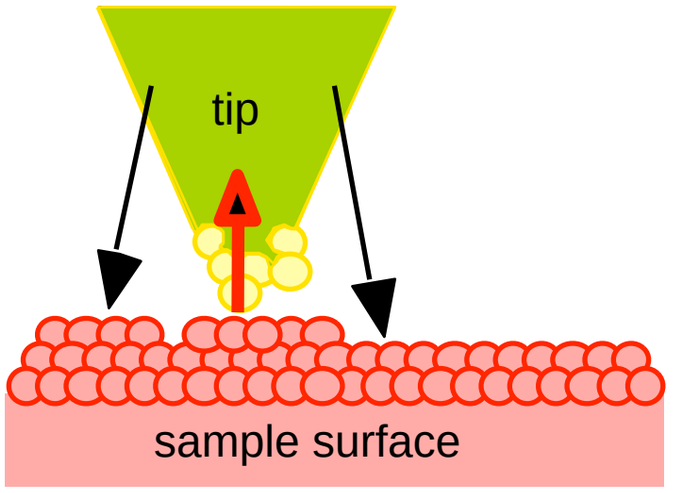

attractive van der Waals force acting on tip are compensated by local repulsive force at the tip apex.

multi-atom tip-sample contact

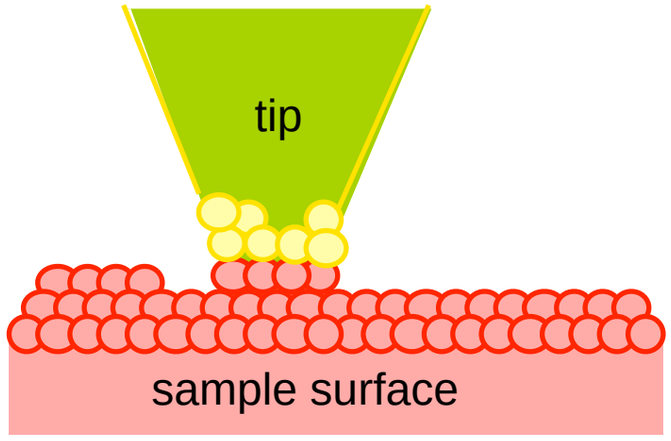

large repulsive force at tip apex leads to re-ordering of atoms at the tip apex. A multi-atom contact is formed. The imaging of single atoms and atomic defects is not possible under this condition.

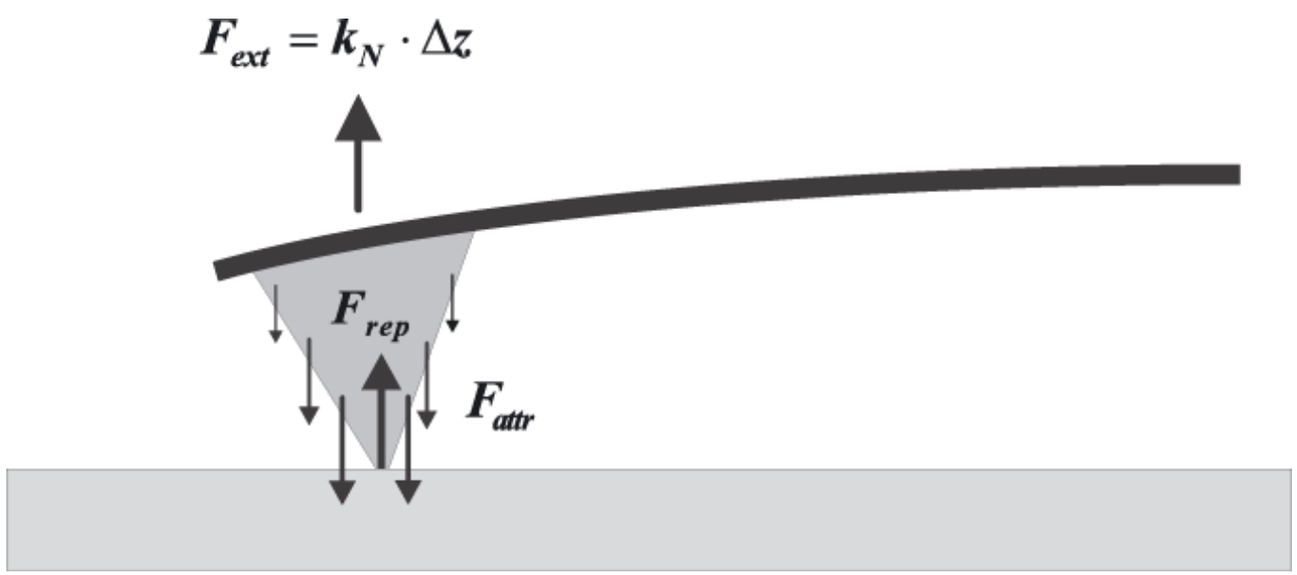

Contact Radius:

- in atmosphere: 2-10nm @ 1nN < F < 100nN
- in UHV: 1-4nm @ 0.1nN < F < 10nN

Pseudo Atomic Resolution

- contact AFM on NaF(001)
- observation of atomic lattice (Moirée-effect)
- step width approximately 1nm
  indication of tip radius
- single atoms or atomic defects not visible

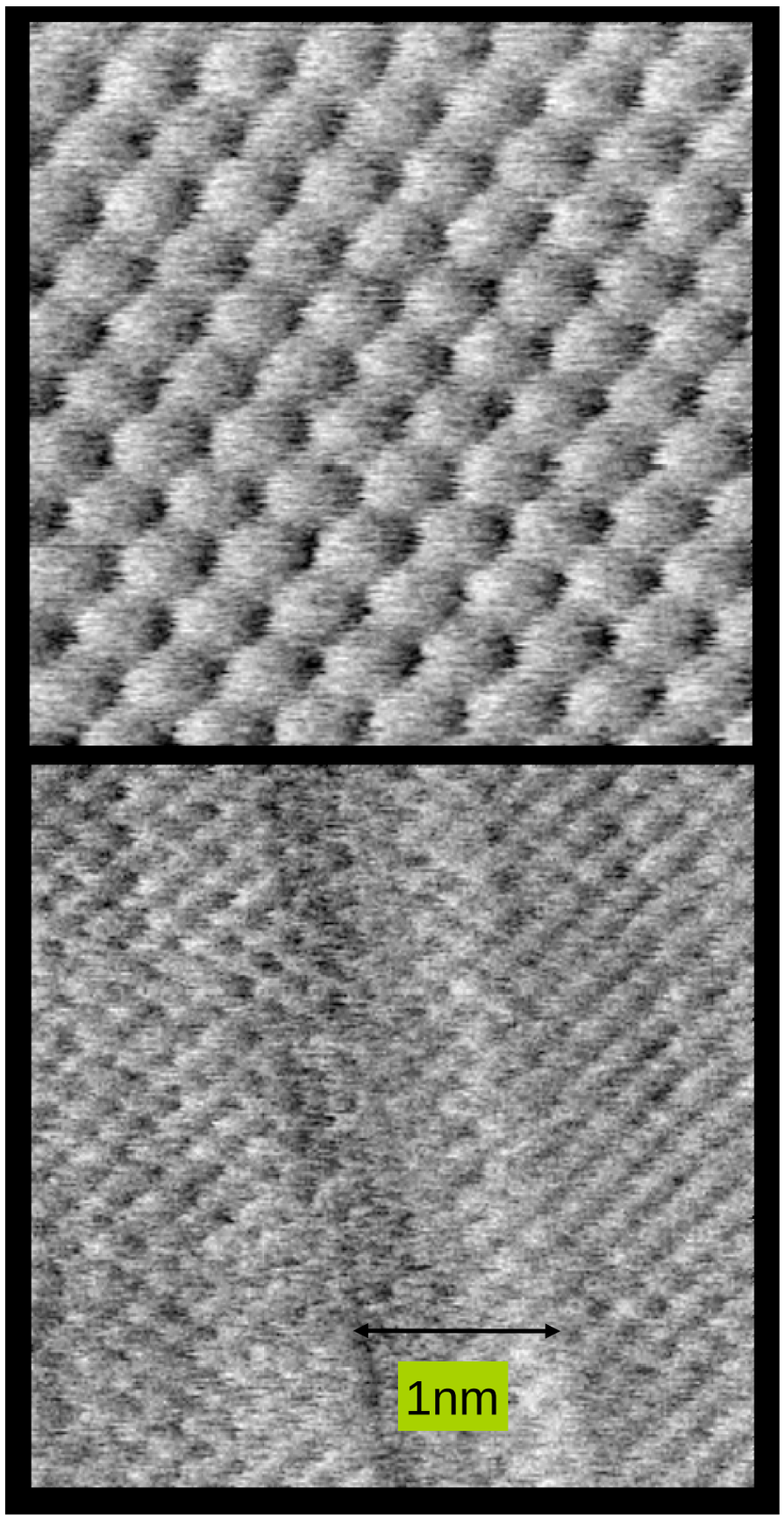

How to obtain Atomic Resolution in AFM:

1st stability criterion

Avoid snap-to contact of soft levers

$$\frac{\partial F_{TS}^{\max}}{\partial z} = k_{TS}^{\max}(Si) = -10N/m$$

Stability criterion 1 (avoiding jump to contact, JTC)

$$k > \frac{\partial F_{TS}}{\partial z} \quad \text{or} \quad k \times A > -F_{TS}$$

2nd stability criterion

Energy stored in cantilever: $E_{CL} = \frac{1}{2} kA^2$

Intrinsic energy loss per cycle: $E_0 = 2\pi \frac{E_{CL}}{Q} = \frac{\pi k A^2}{Q}$ sustained by the drive amplitude: $A_{drive} = \frac{A}{Q}$

When damping ΔE_{TS} occurs, the following condition must hold:

$\Delta E_{ts} << Q$ Energy lost per oscillation cycle

Assume k_c = 20N/m and A = 1nm ➜ E_0 = 62eV >> typical tip-sample induced energy losses (1eV)

Assume k_c = 2000N/m and A = 0.1nm ➜ E_0 = 62eV >> typical tip-sample induced energy losses (1eV)

➜ ***Use ultrasmall Amplitudes ONLY with hard cantilevers or softer cantilevers operated in higher modes!***

Beginning of Noncontact AFM with true atomic resolution

1995 **Si(111)-(7x7)** by noncontact AFM, **F.J.Giessibl**
Science 267 (1995) pp.68-71 [**30 Aug.1994**; accepted 31 Oct.1994]

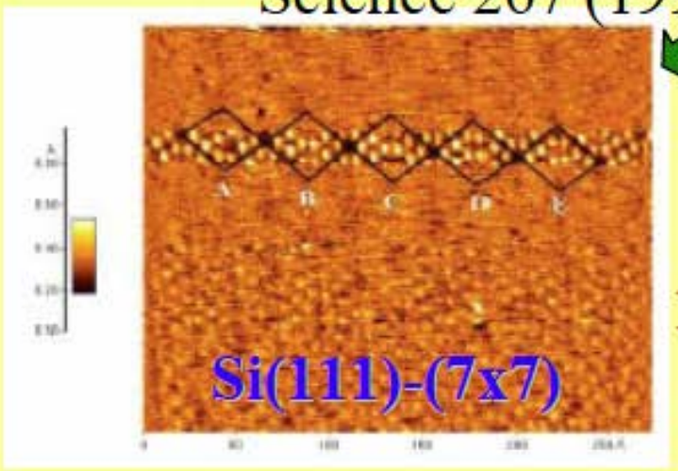

In 1995, Achievement of True Atomic Resolution

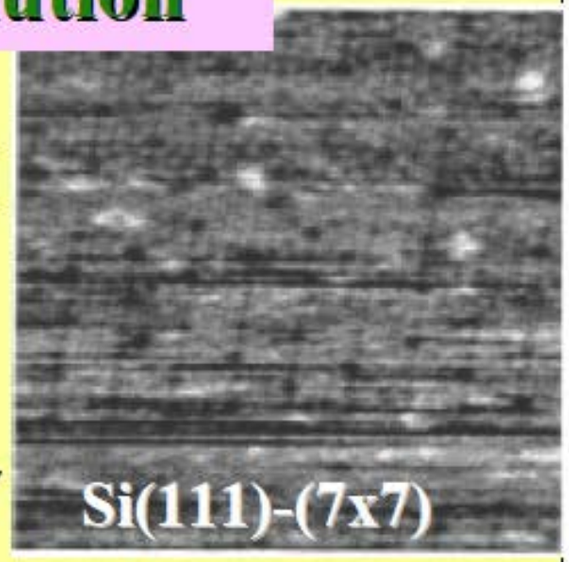

1995 **Si(111)-(7x7)** by noncontact AFM,
S.Kitamura and M.Iwatsuki,
Jpn.J.Appl.Phys. 34 (1995) pp.L145-L148
[**Nov.14, 1994**; Accepted Dec.6, 1994]

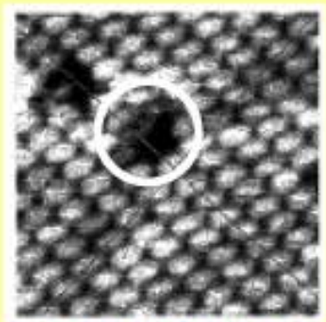

1995 **Atomic point defects** of **InP(110)** **cleaved surface** by noncontact AFM,
H.Ueyamam, M.Ohta, Y.Sugawara and S.Morita,
JpanJ.Appl.Phys. 34 (1995) pp.L1086-L1088 [**May 31, 1995**; accepted July 13, 1995]

1995 **Defect Motion** of **Atomic point defects** of **InP(110)**,
Y.Sugawara, M.Ohta, H.Ueyamam and S.Morita,
Science 270 (1995) pp.1647-1648 [**27 July, 1995**; accepted 11 Oct, 1995]

1997 **Dissipation image** of **NaCl(001)** and by noncontact AFM, M.Bammerlin, R.Luthi, E.Meyer, A.Baratoff, J.Lu, M.Guggisberg, Ch.Gerber, L.Howald and H.-J.Guntherodt, Probe Microscopy, 1 (1997) pp.3-9.

1997 **TiO_2(110)** by noncontact AFM,
K.Fukui, H.Onishi and Y.Iwasawa, Phys.Rev.Lett, 79 (1997) pp.4202-4205.

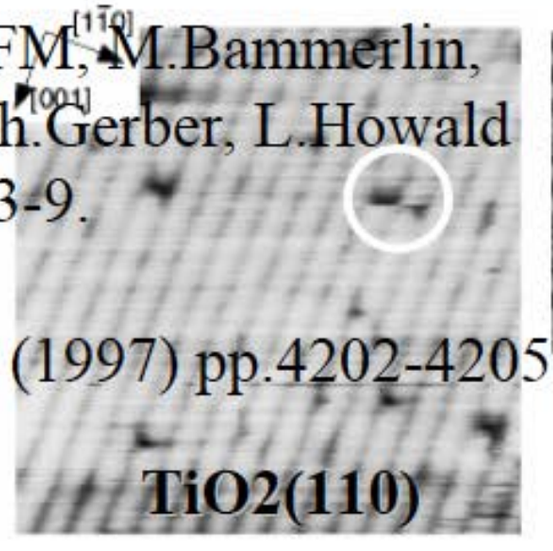

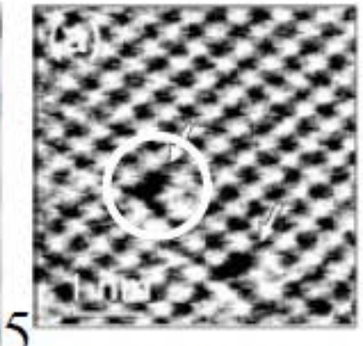

slide from S. Morita

ncAFM with True Atomic Resolution

Dynamic Operation

distance of cantilever to surface and oscillation amplitude adjusted to obtain less than 1nm minimal tip-sample distance at lower turning point

View from the oscillating tip

during a large fraction of the oscillation period only the long-ranged van der Waals force is acting on the tip. Only at the lower turning point a chemical interaction between the tip apex atom and a surface atom may occur.

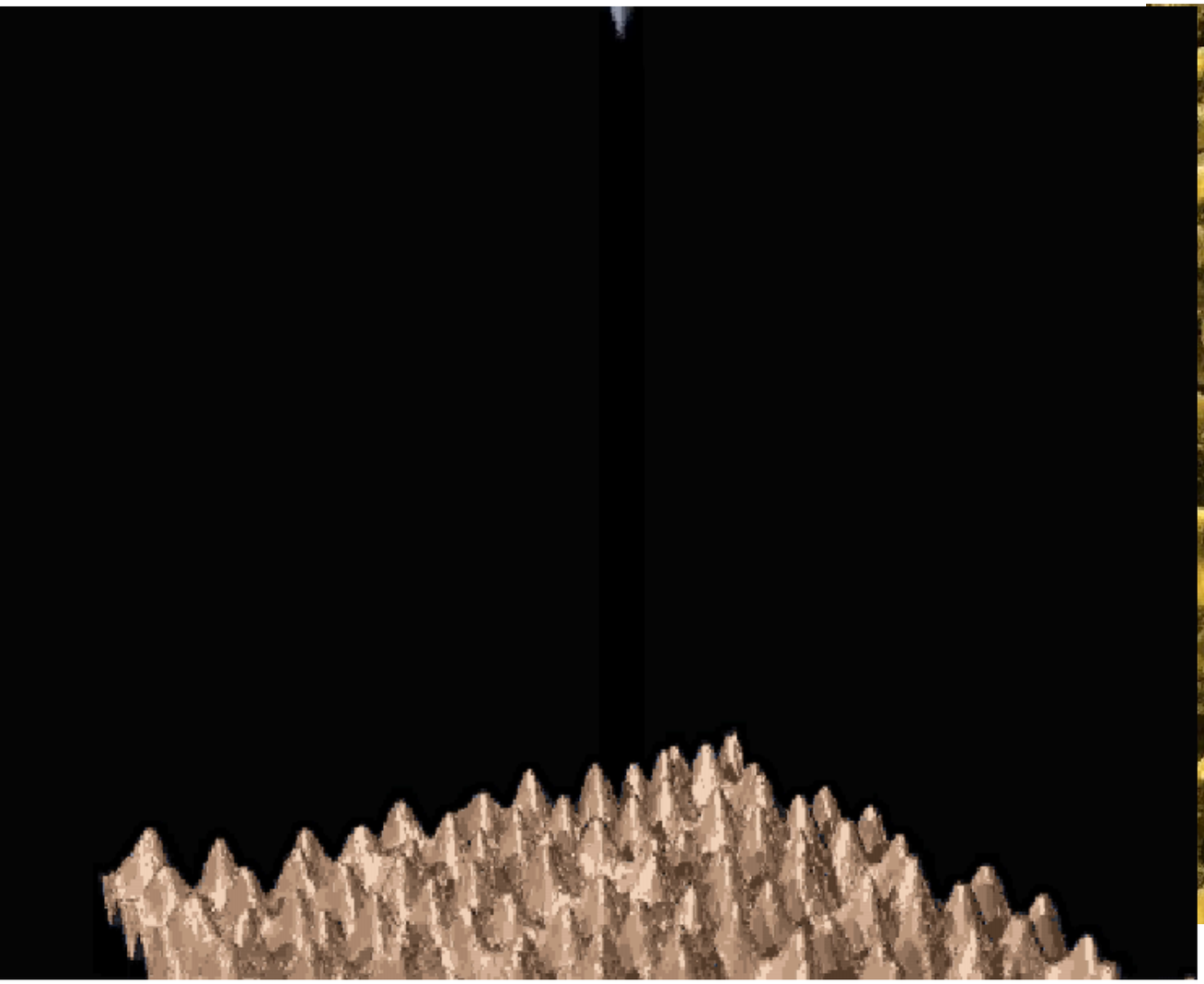

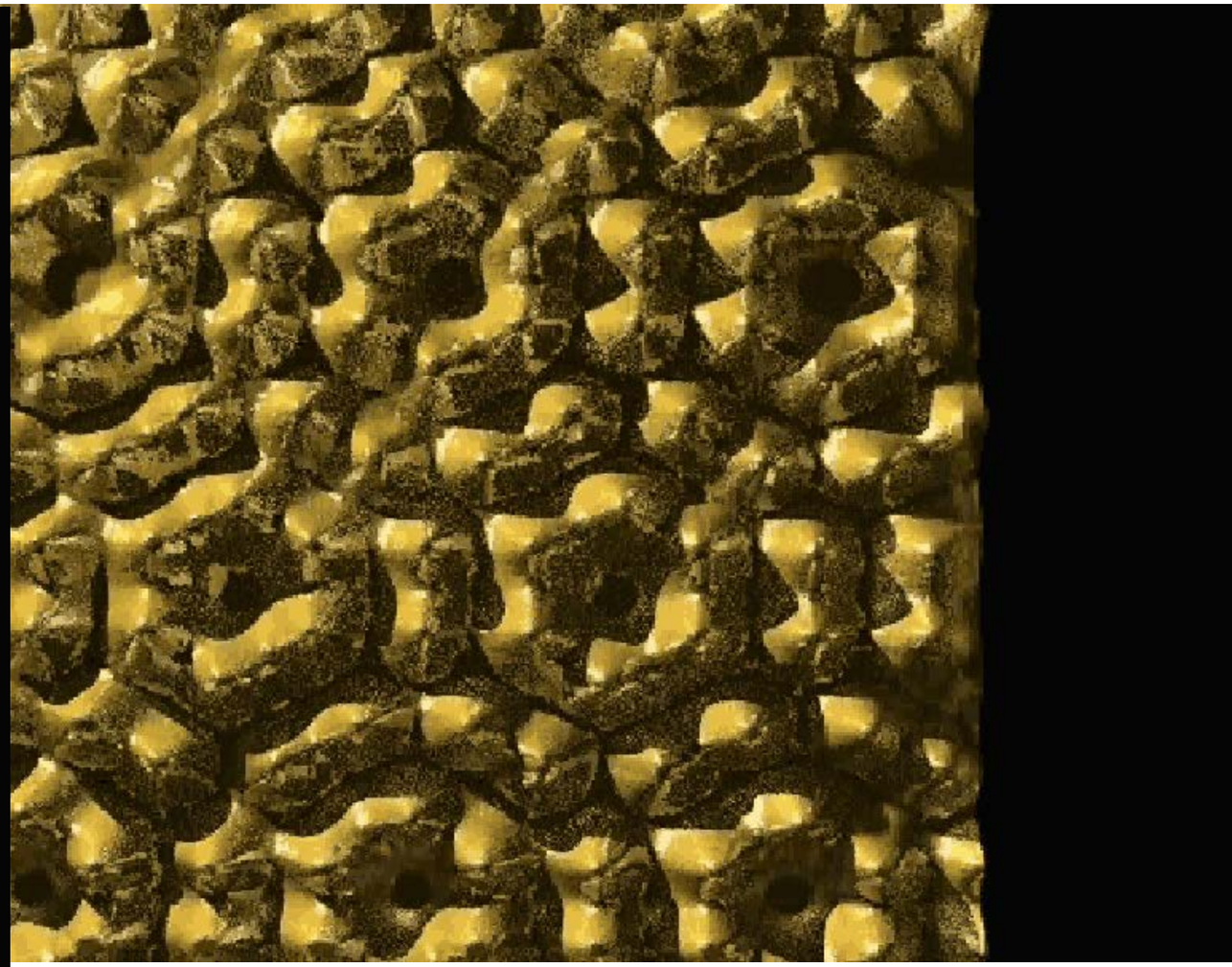

Animation: H.-R. Hidber,
NCCR on Nanoscale Science
University of Basel

Atomic Resolution on Si(111)-7x7

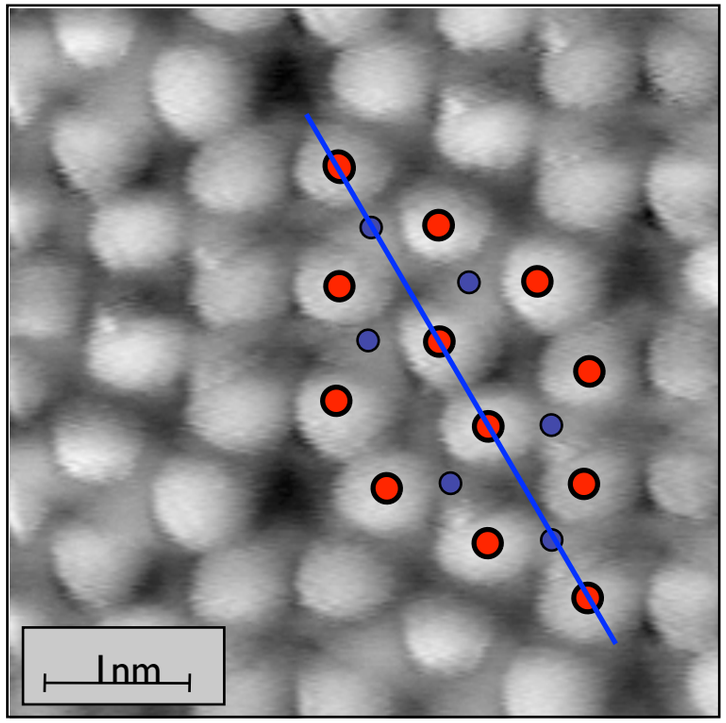

measurement parameters
Δf = -31Hz, scan speed 0.6nm/s
Cantilever: c_L = 28.6 N/m,
f_0 = 155 719.3 Hz, Q = 370‘000
temperature: 7.2K

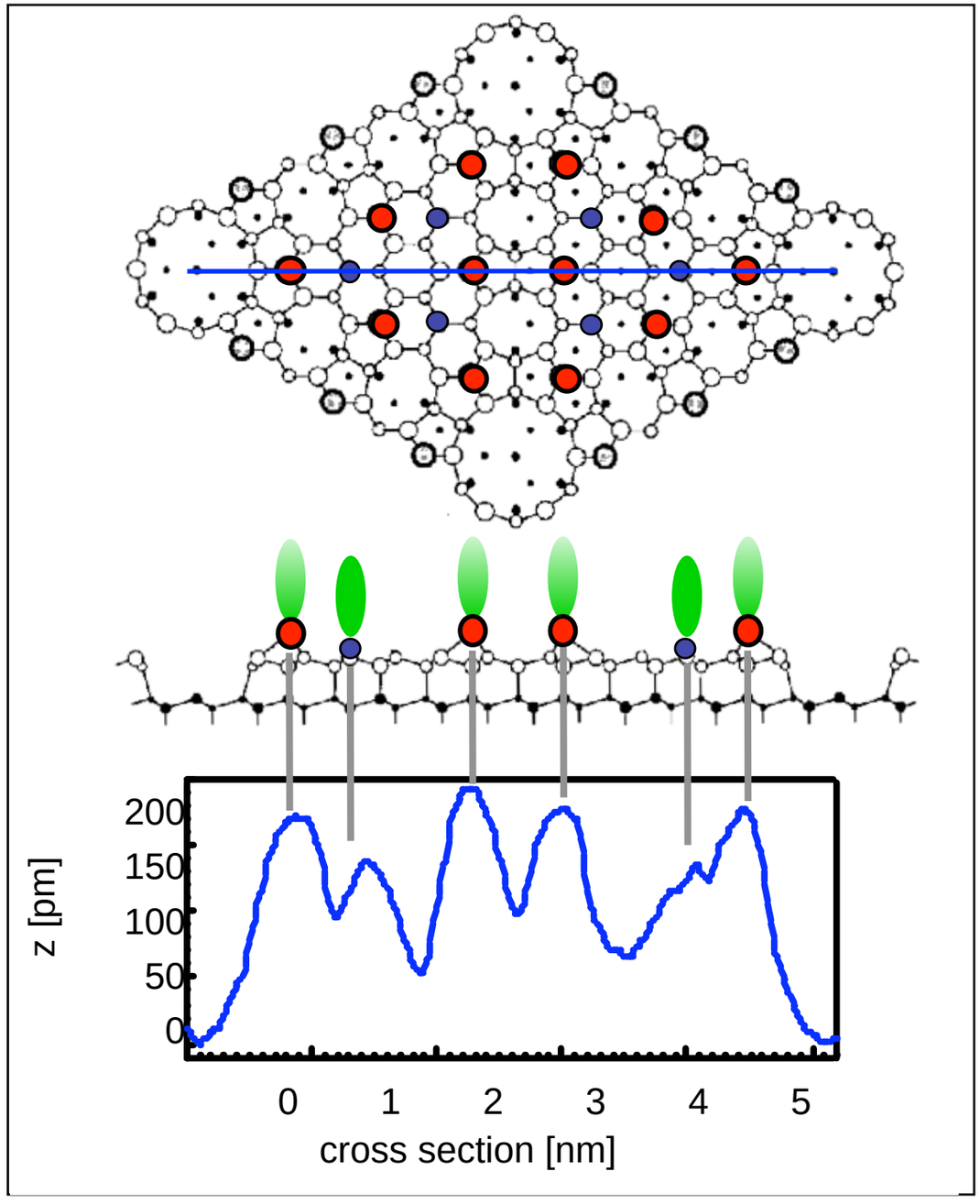

- height difference between inequivalent adatoms due to small differences in reactivity

M. A. Lantz and H.J. Hug et al., Phys. Rev. Lett. 84, 2642 (2000)
K. D. Brommer, et al., Phys. Rev. Lett. 68, 1355 (1992) &
I. Stich, et al., Phys. Rev. Lett. 68, 1351 (1992).

Site Specific Forces

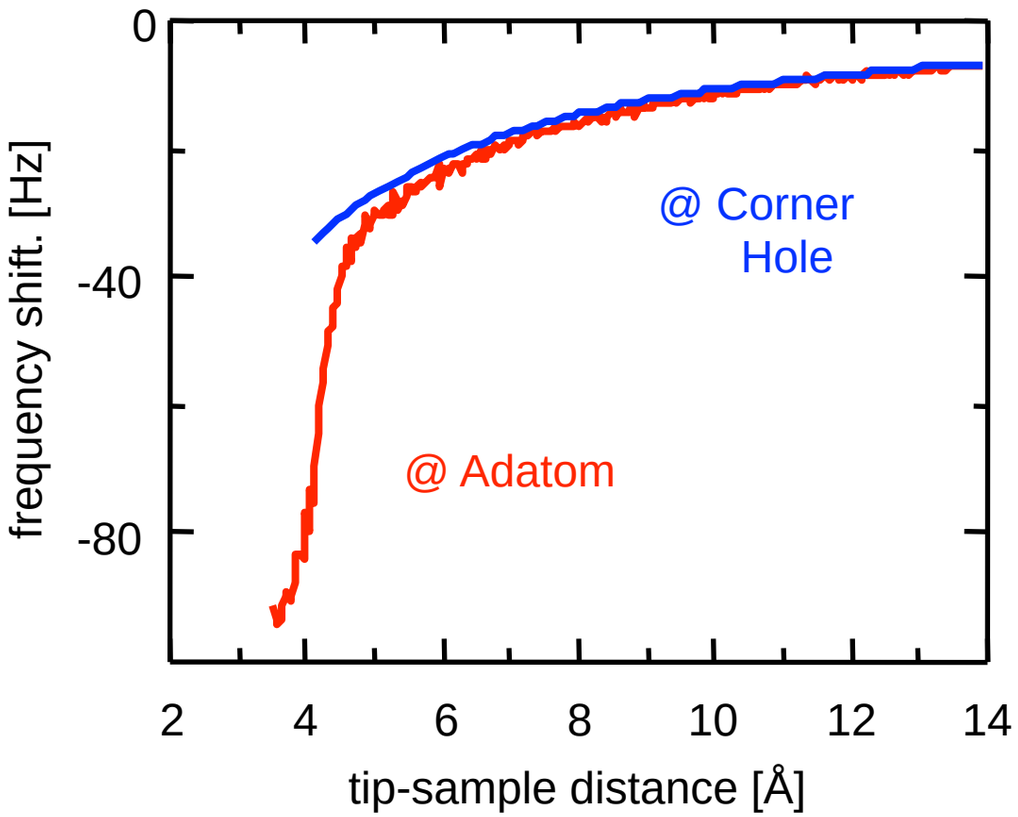

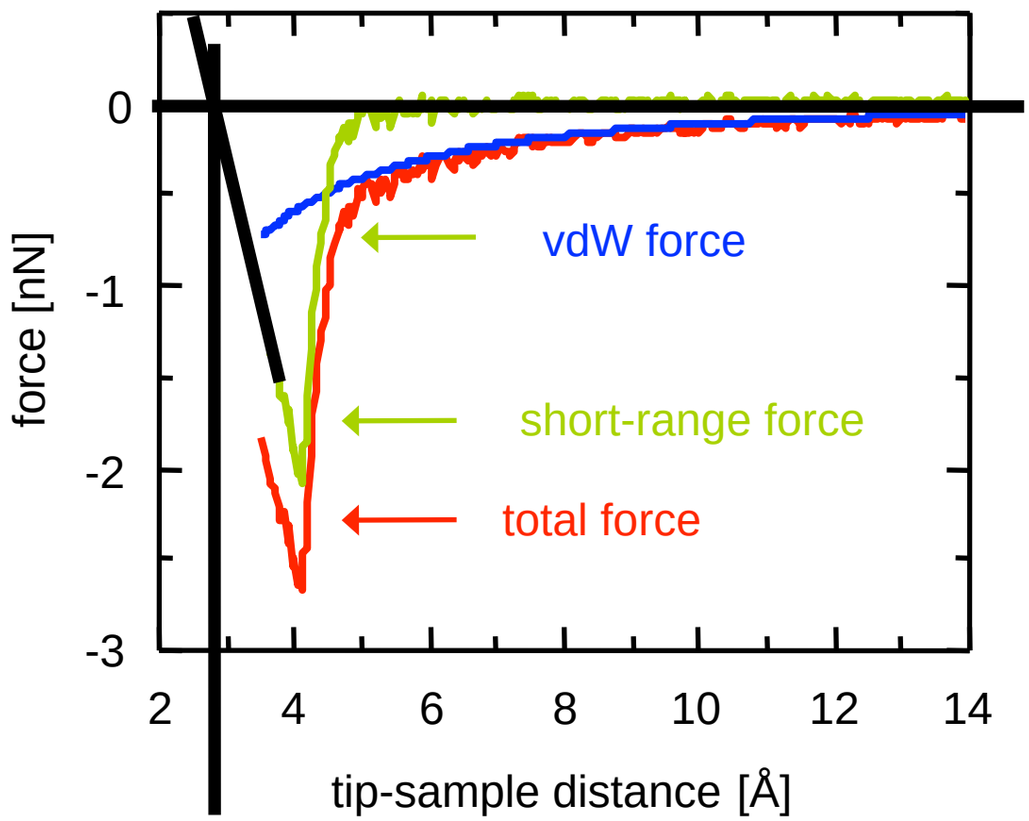

conversion from df(z) to F(z) [1]

$$\frac{\Delta f}{f_0} = \frac{f_0}{kA_0^2} \cdot \int_0^{1/f_0} F_{ts}[d + A_0 + z(t)]z(t)dt$$

$$\text{with } z(t) = A_0 \cos(2\pi f_0 t)$$

235pm

absolute distance to sample from Si-Si bond-length: 235pm !

atomic resolution imaging @ F= -0.4nN and 4.5A tip-sample distance !

[1] U. Dürig, APL. 75, 433 (1999) and APL 76, 1203 (2000) **and other inversion methods ...**
[2] Lantz and Hug et al., Science 291, 2580 (2001)

Imaging Molecules

Figure 1. Model of a CO-modified tip (C gray, O red) above a pentacene molecule (C gray; the colored surface represents experimental data.

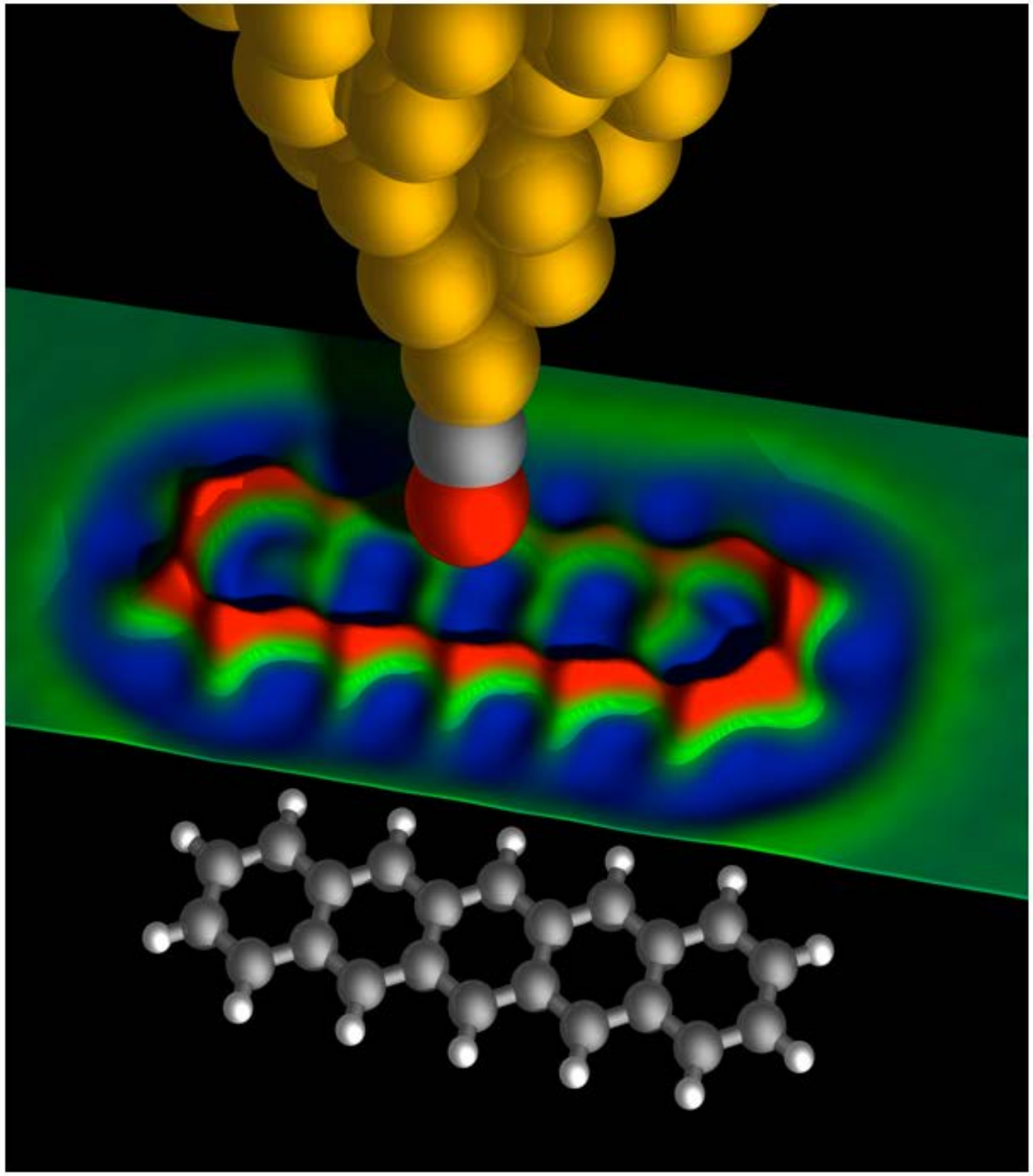

Imaging the chemical structure of molecules with atomic resolution was achieved by probing the short-range chemical forces via noncontact atomic force microscopy (NC-AFM). Our low-temperature STM/AFM is based on a qPlus sensor design [1] and is operated in an ultrahigh vacuum at a temperature of 5 K.

The key step to achieving atomic resolution on molecules is the functionalization of the microscope's tip apex with suitable, atomically well-defined terminations, such as CO molecules (see schematic image). In this case, atomic manipulation techniques are essential for the controlled buildup of the tip used for AFM imaging.

Density functional theory (DFT) calculations are performed to elucidate the physical origin of the observed atomic contrast. The calculations reveal that the Pauli repulsion is the source of the atomic resolution, whereas van der Waals and electrostatic forces only add a diffuse attractive background [2].

References
[1] F. J. Giessibl, Appl. Phys. Lett. 76, 1470 (2000).
[2] L. Gross, F. Mohn, N. Moll, P. Liljeroth, G. Meyer, Science 325, 1110 (2009).

Identifying Atoms - atomic scale chemical Analysis ?

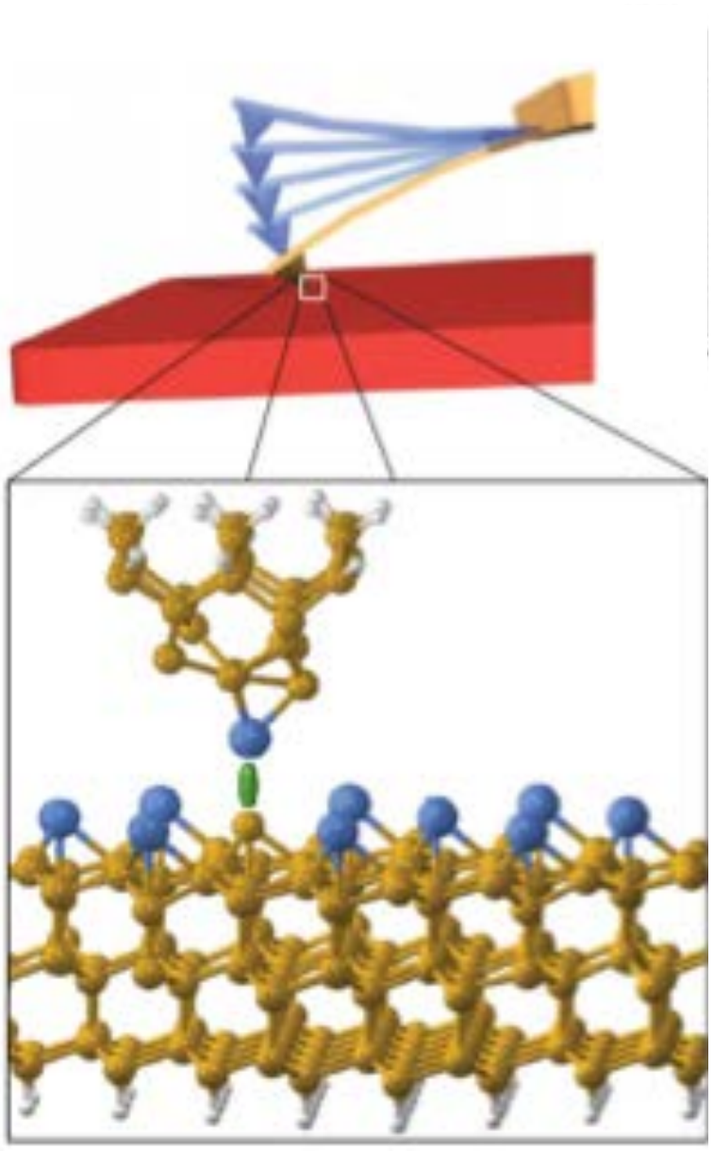

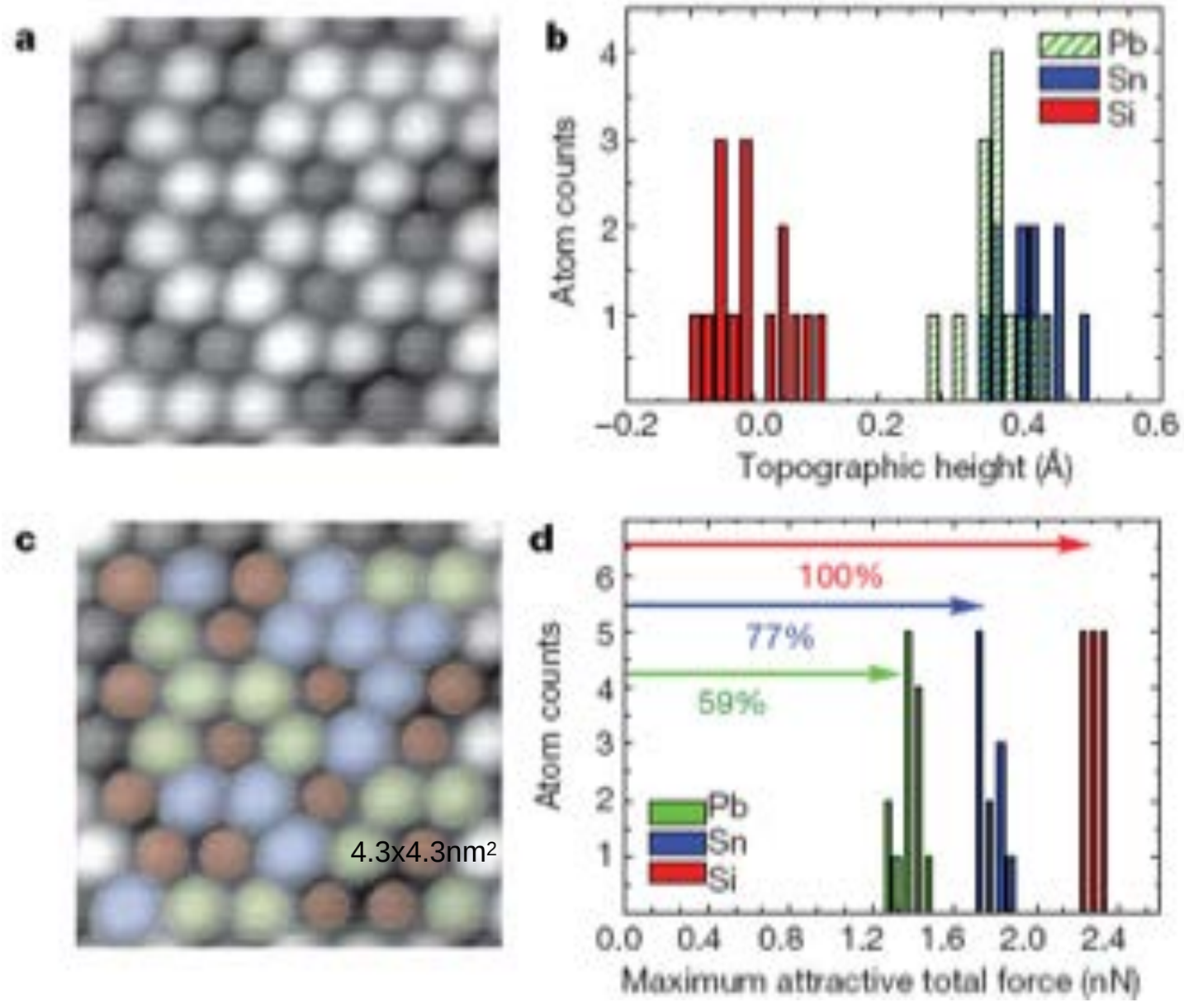

Sugimoto et al, Nature 446 (2007) 64

- Identification of 3 atomic species on flat single crystalline surface possible
- **But: SFM is NOT a true chemical analytical tool**

Atomic Resolution in Water

Galleries | Cypher AFM Gallery

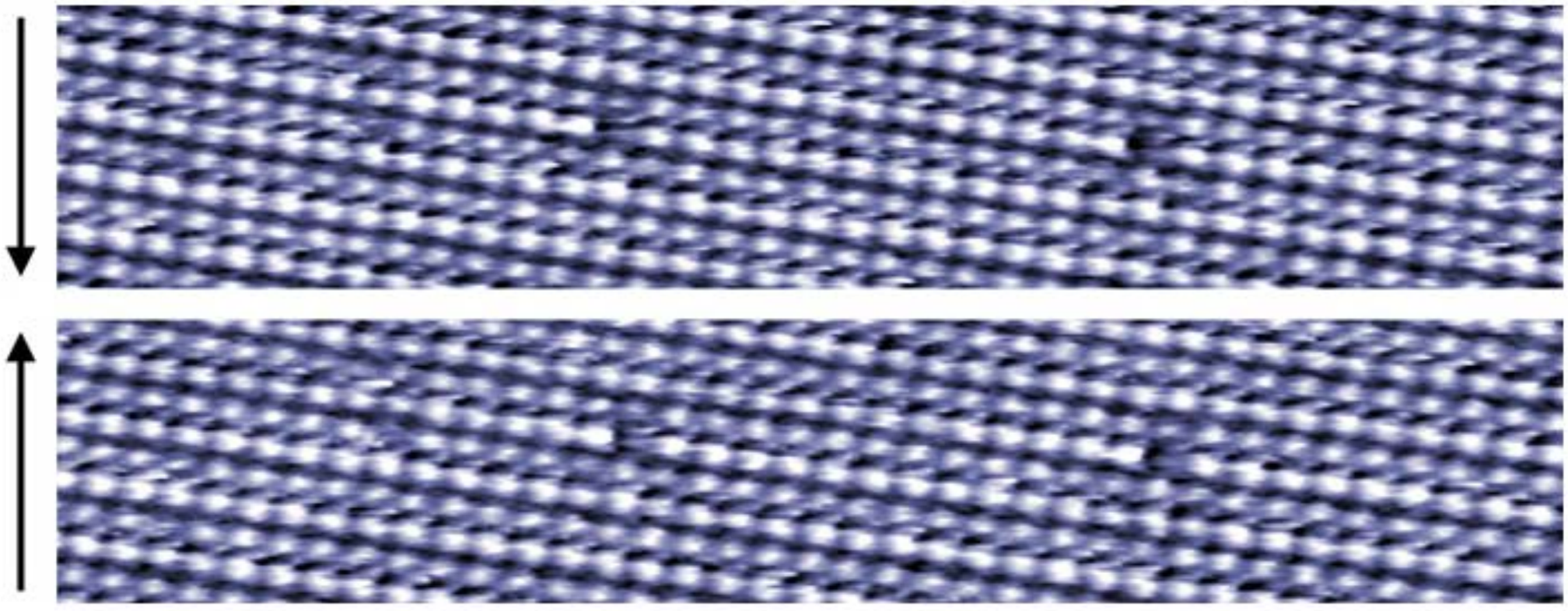

Repeated Point Defects

Successive AC mode topography images of the cleavage plane of a calcite crystal in water. The repeated point defects demonstrate the true atomic resolution capabilities of the Cypher AFM. Arrows indicate scan direction. Scan size 20nm; Z scale 3.2Å; Cantilever Amplitude 4Å; Cantilever Frequency 454 kHz.

Issues with controlling dynamic AFM

distance feedback issues:

1. measured signal(z) must be monotonous; note that this is NOT the case for small *A*
2. further note that (attractive) short-range force may not exist at all sample locations
3. slope of signal(z) changes
4. at closer distances, the overall z-feedback speed increases. The z-feedback may start to oscillate.
5. PLL instabilities at small *A*

how to overcome these issues:

1. make measured signal(z) remains monotonuous
   - check feedback direction (does frequency decrease when going closer? note the opposite is true for tunnel current)
   - note that this is NOT the case for small *A,* so use larger A to average differently such that long range attractive part of potential dominates
   - use blunter tip, this is to generate sufficient van der Waals background force for feedback operation
2. further note that (attractive) short-range force may not exist at all sample locations
   - use larger A to average differently such that long range attractive part of potential dominates
   - use blunter tip, this is to generate sufficient van der Waals background force for feedback operation
3. slope of signal(z) changes
   - make sure this does not happen using frequency-versus-distance curves
   - use correct feedback sign
4. at closer distances, the overall z-feedback speed increases. The z-feedback may start to oscillate.
   - watch for signs of feedback oscillations: - avoid them
   - carefully reduce P,I of z-feedback when approaching to keep overall z-feedback speed constant
   - smarter feedback (local log ... needs to be implemented in software)
5. PLL instabilities
   - do not use silicon tips at small *A*, to avoid stochastic energy dissipation events; use metal tips
   - use sufficiently high dynamic reserve
   - work @ larger tip-sample distances or use bimodal operation
6. hands-on-practice

3.4.3. Kelvin Probe Force Microscopy

AM Kelvin Potential Measurement in Air, Intermittent Contact Mode: 1st passage

Empa
Materials Science and Technology

Contact Potential Formation

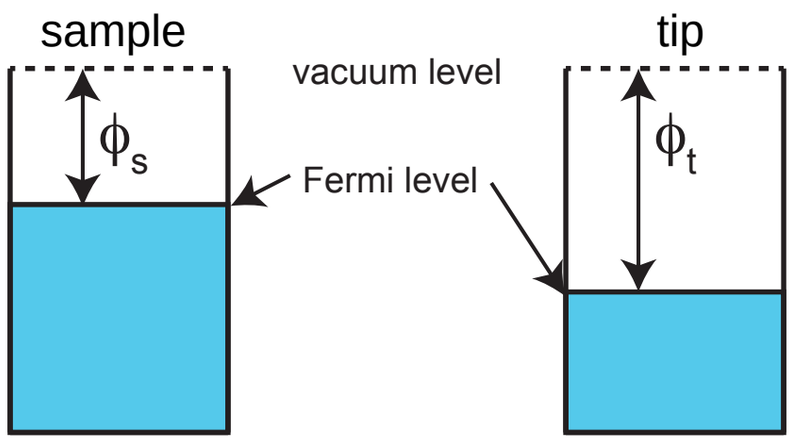

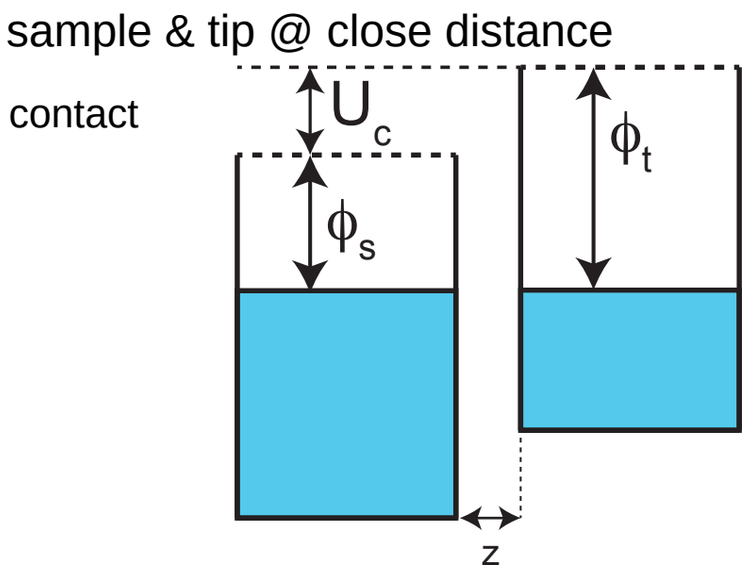

block diagram of Kelvin Potential measurement (AM method)

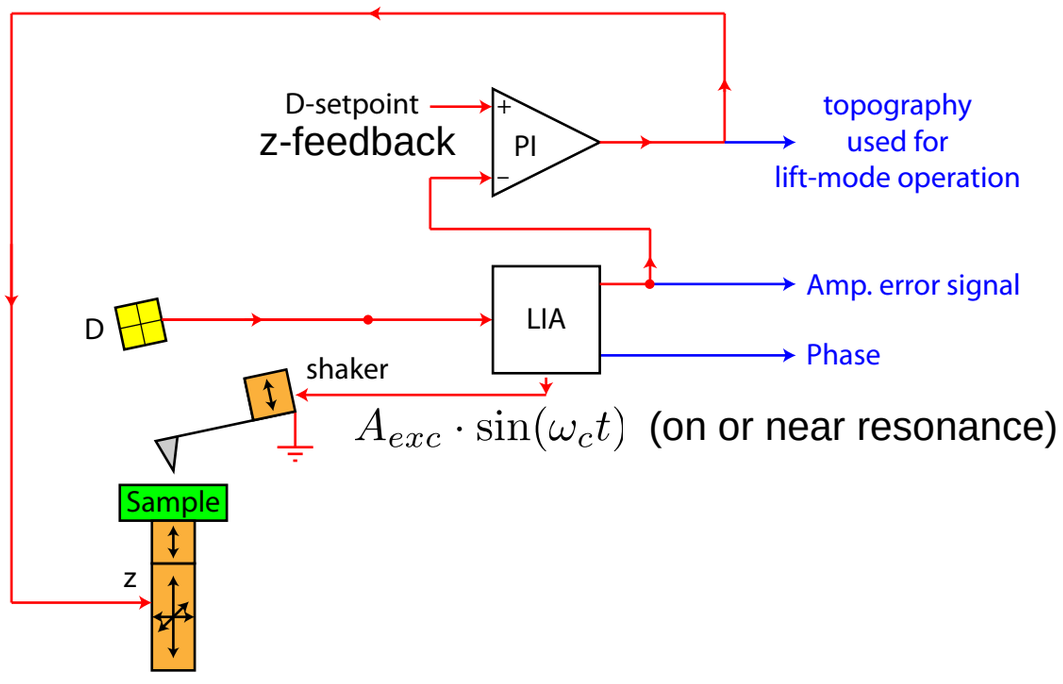

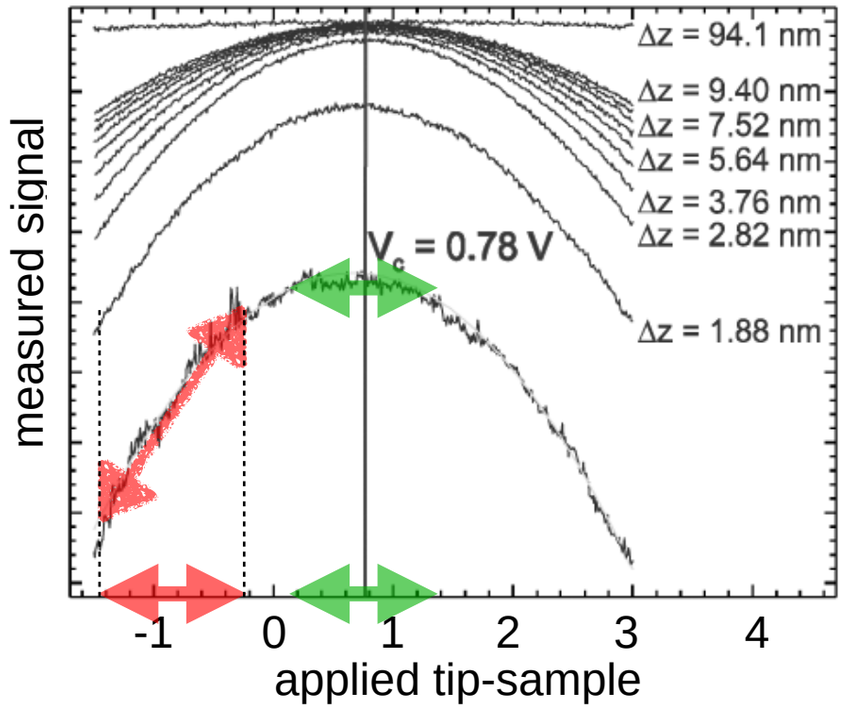

1st passage: mapping the topography in intermittent contact mode

1ω-signal ≠ 0 1ω-signal = 0

AM Kelvin Potential Measurement in Air, Intermittent Contact Mode: 1st passage

Empa
Materials Science and Technology

Contact Potential Formation

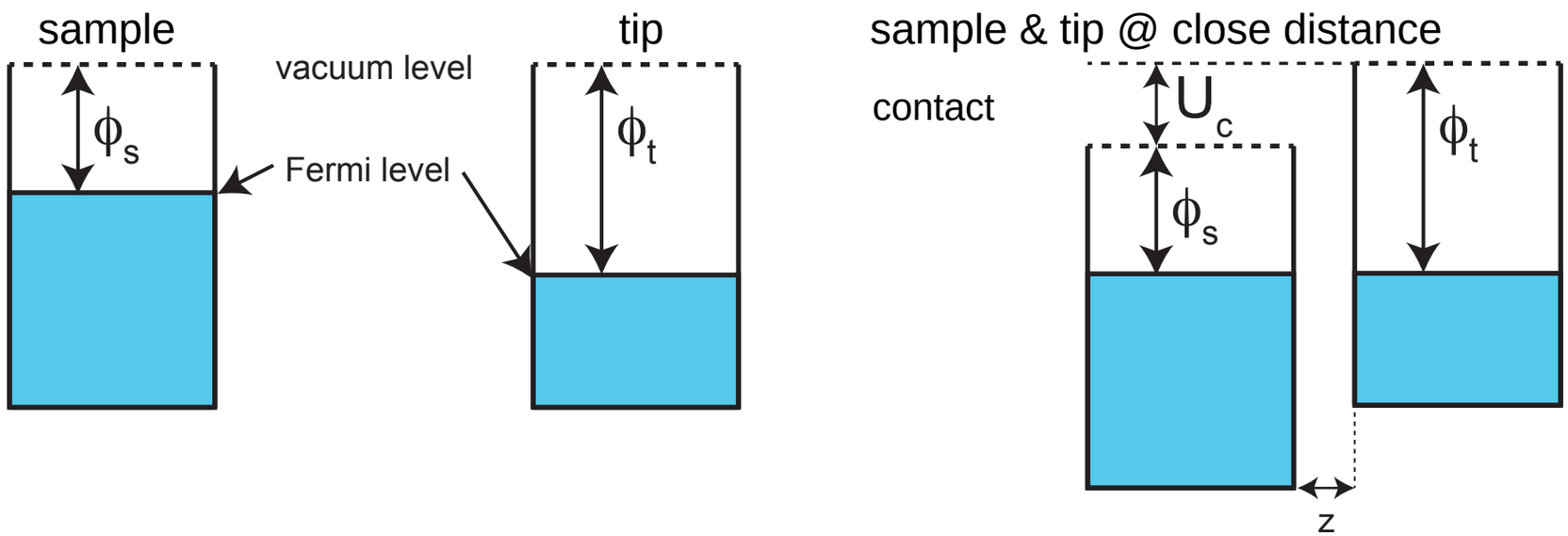

(on or nea

block diagram of Kelvin Potential measurement (AM method)

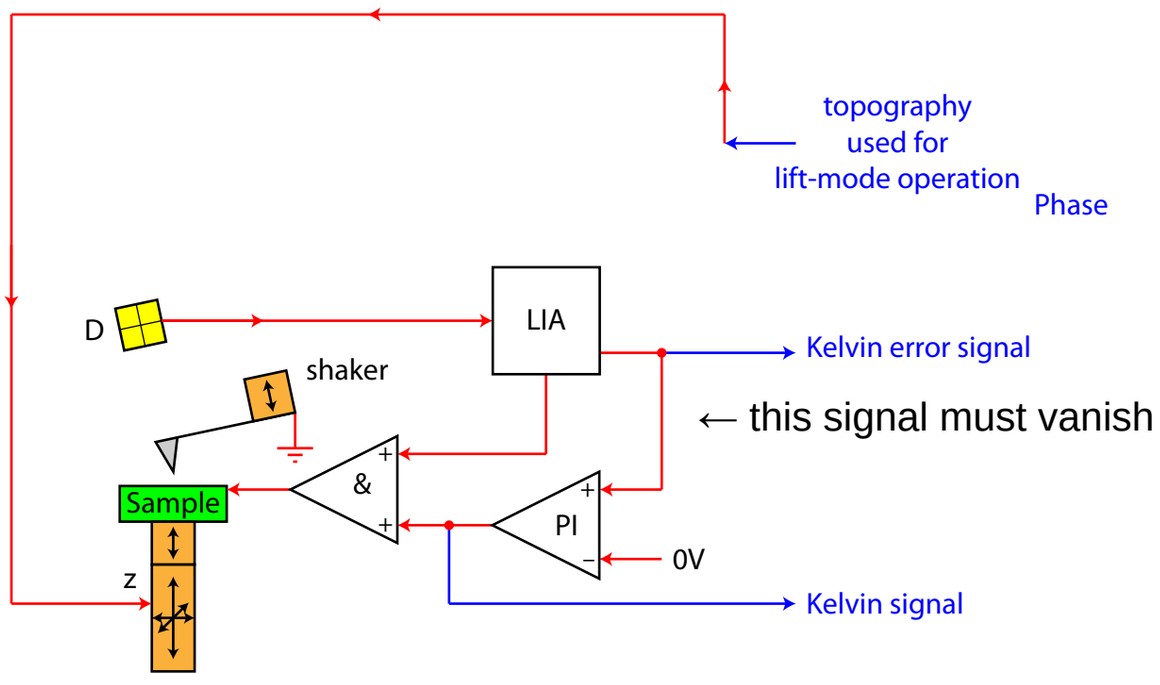

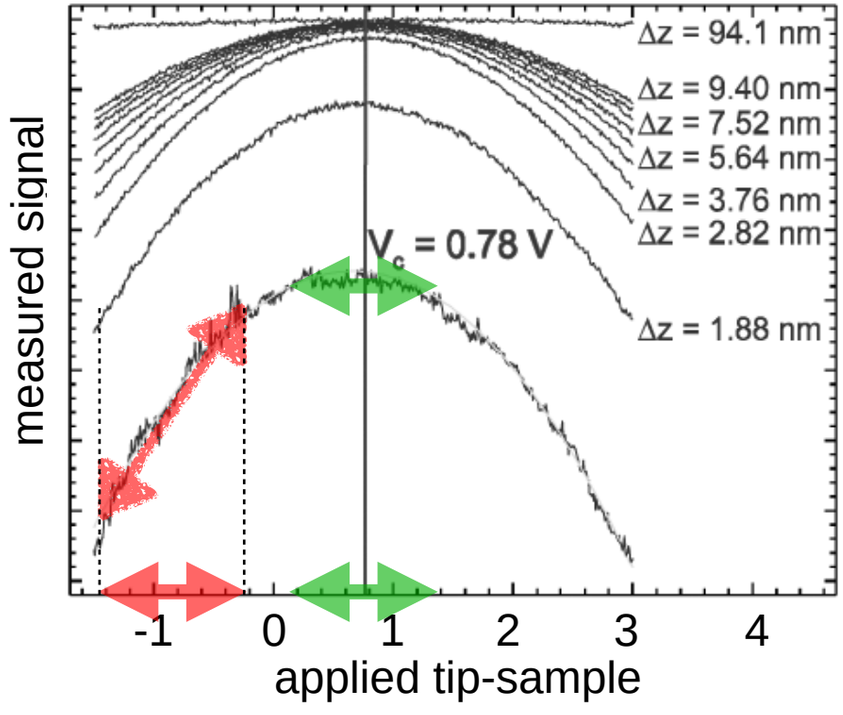

2nd passage: mapping the Kelvin signal following previous topography 1ω-signal ≠ 0 1ω-signal = 0

AM vs FM Kelvin Potential Measurement in Air,

Empa
Materials Science and Technology

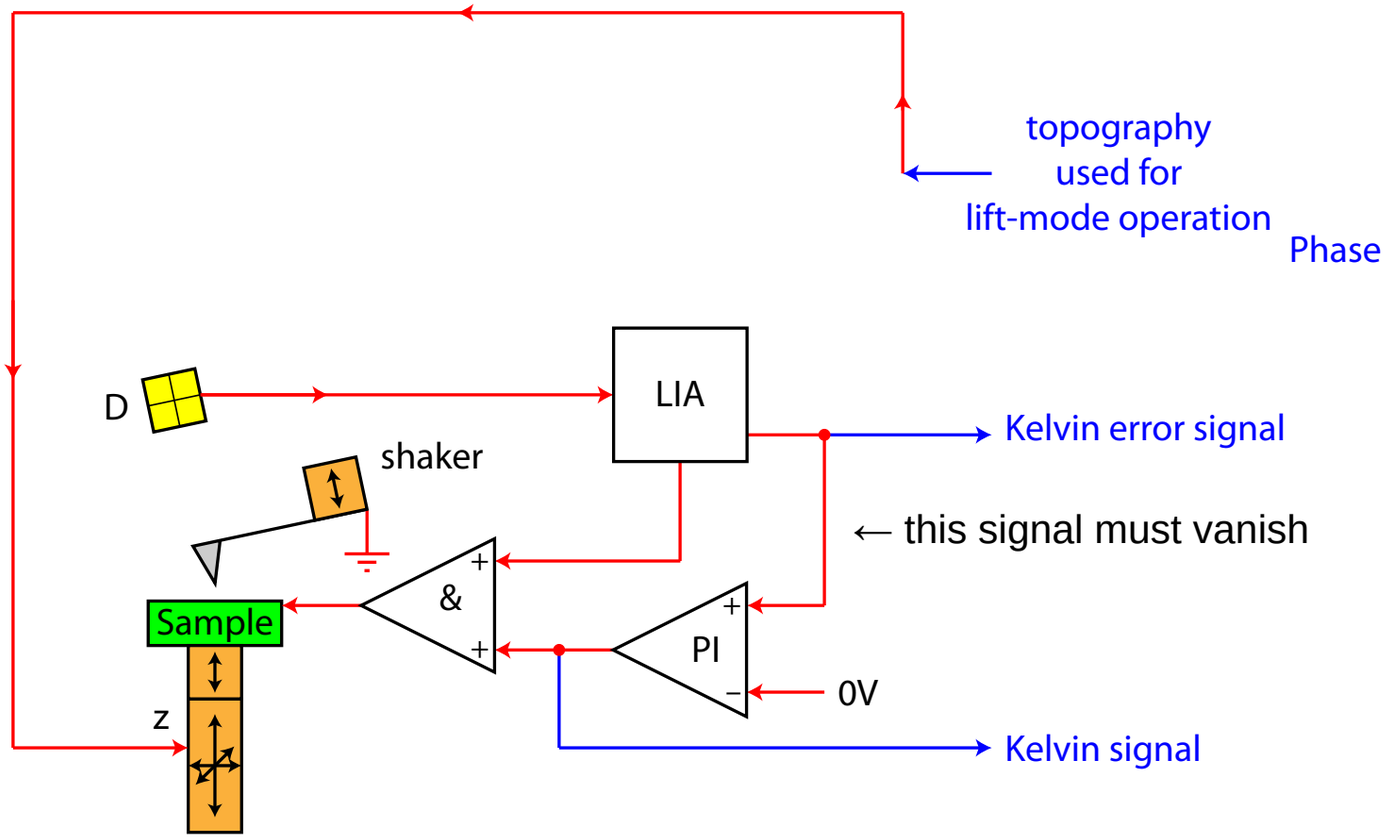

AM-method:

electrostatic force driven cantilever oscillation amplitude is nulled.

+ resonance amplification
  ➜ good sensitivity

– lateral resolution limited, because electrostatic force averages over larger areas of tip apex

– slow

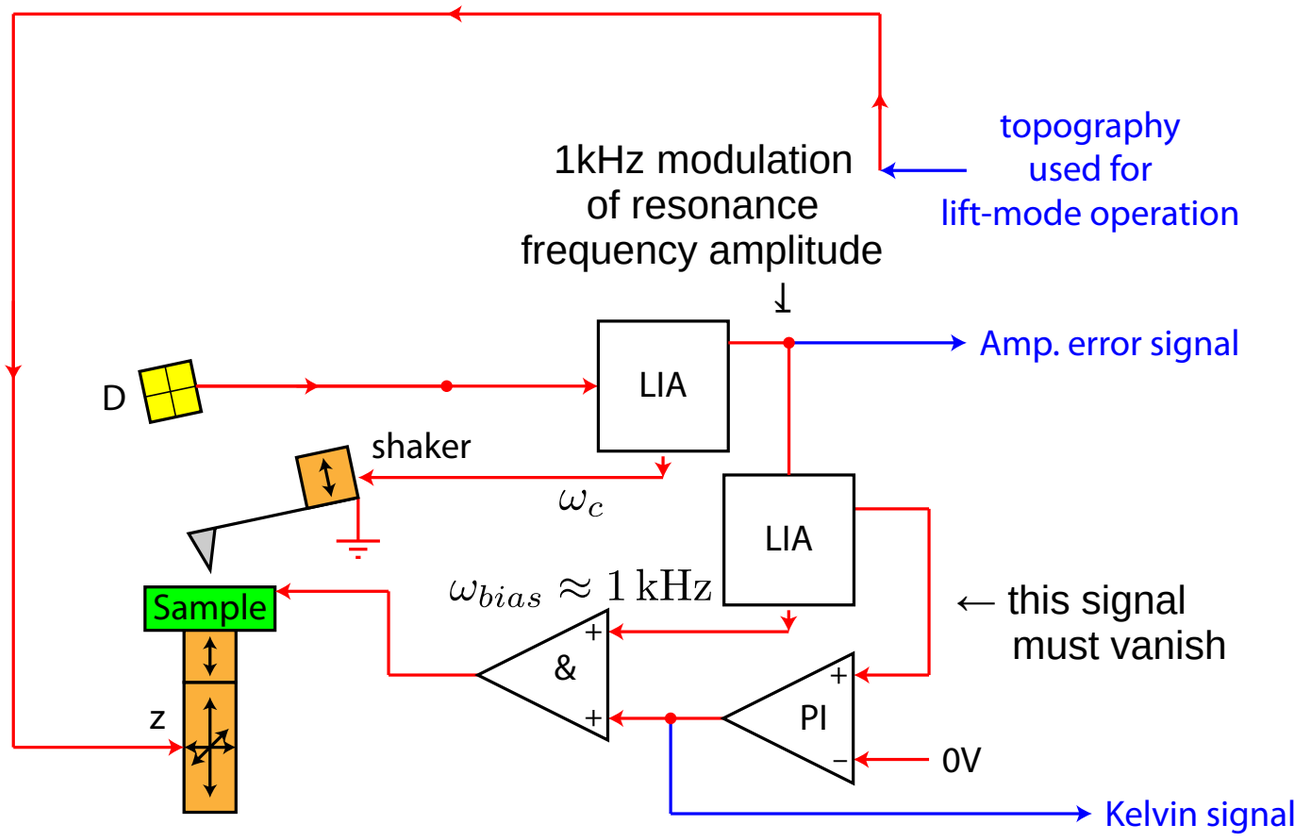

FM-method:

electrostatic force derivative driven change of cantilever resonance is nulled.

+ electrostatic force derivative is measured ➜ spatial resolution

+ fast

– poorer sensitivity

FM-method: potential-induced change of resonance frequency is nulled

5. Kelvin Potential Measurement
Comparison results obtained in air & under vacuum

Empa
Materials Science and Technology

measurement performed in air

topography obtained in peak force mode

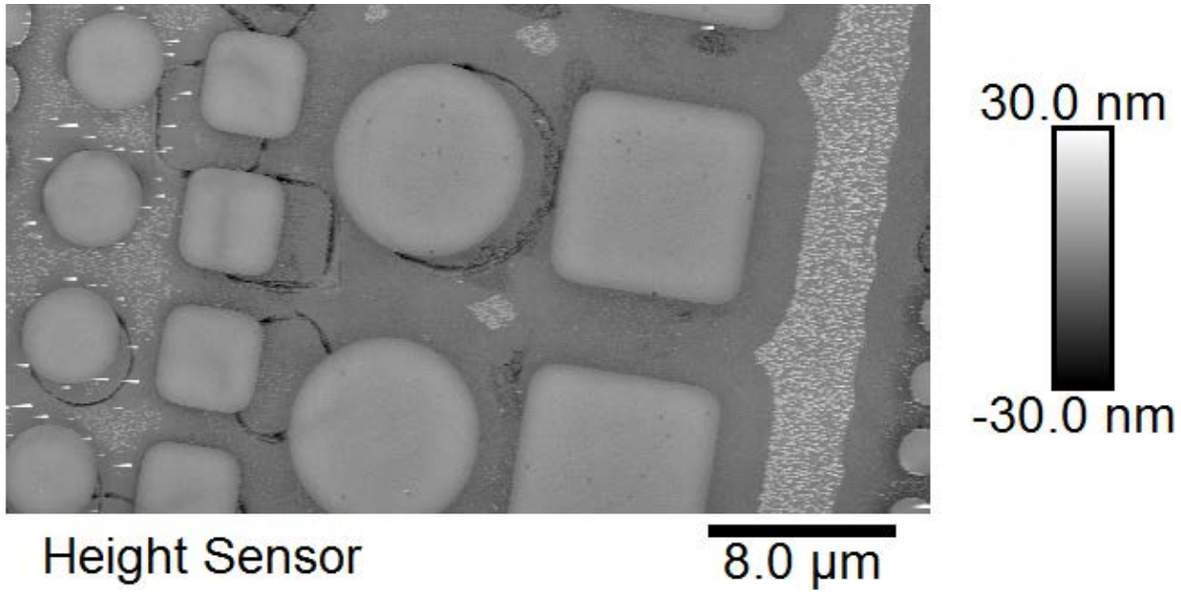

Kelvin potential obtained in FM mode (5V osc.)

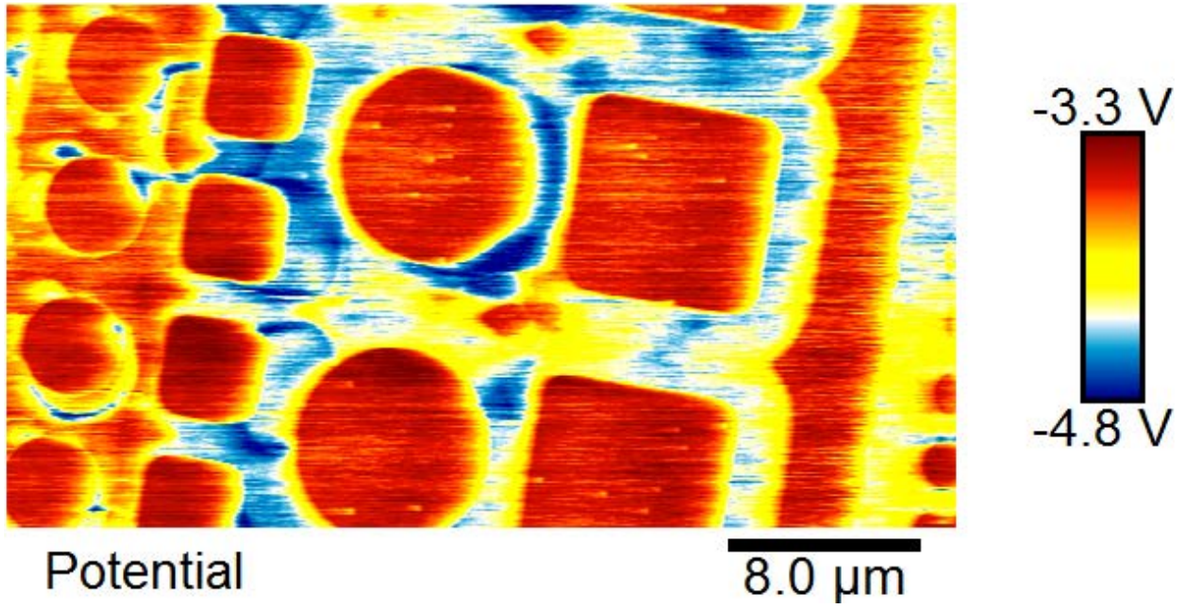

measurement performed in vacuum

topography measured constant @ Δf_1

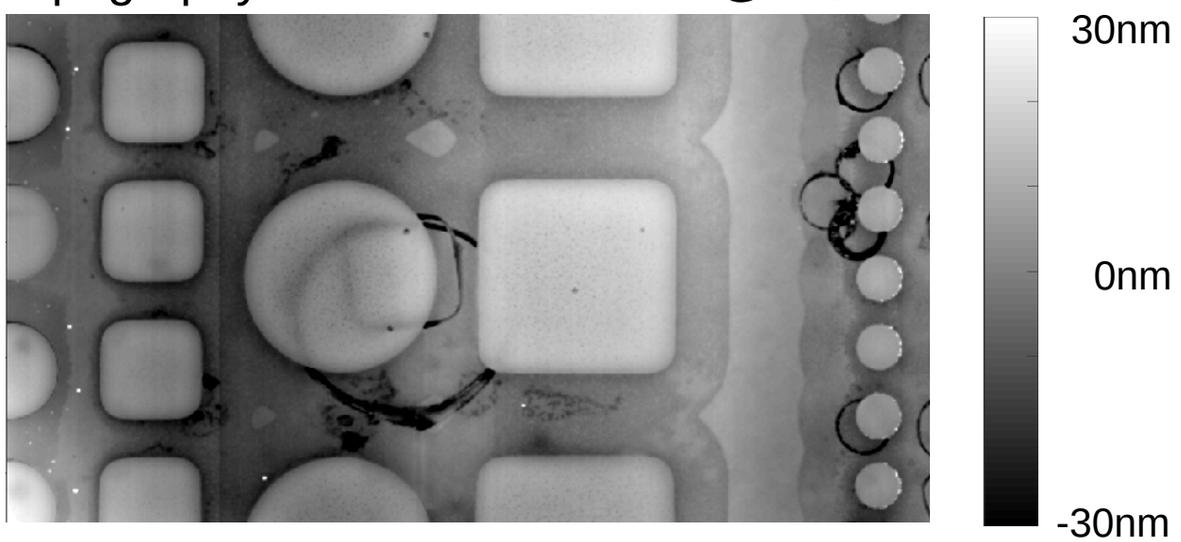

Kelvin potential obtained in FM mode (0.55V osc.)

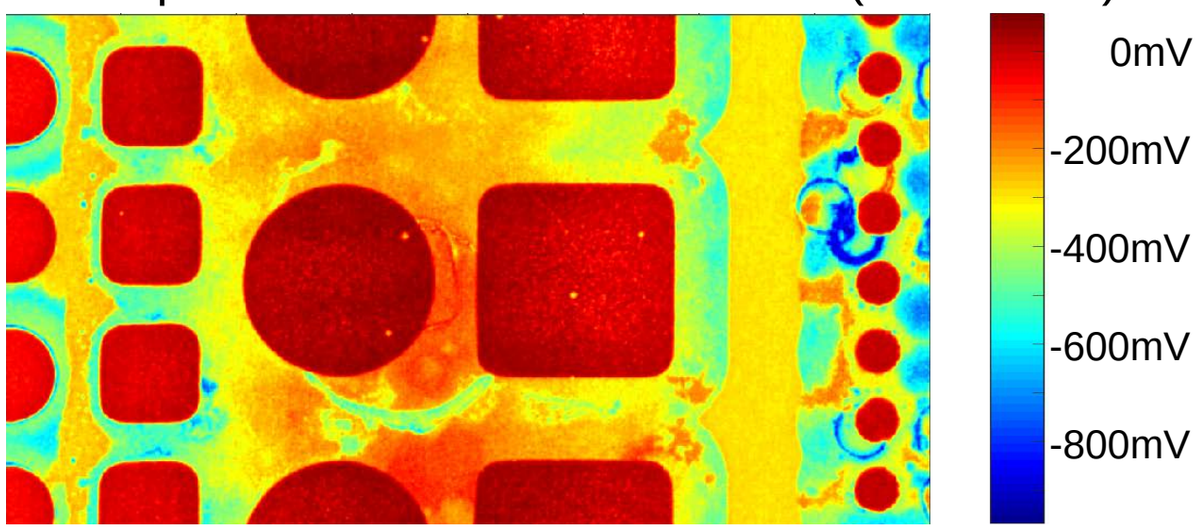

➜ measurement in vacuum with 0.5V instead of 5V oscillating bias

➜ measurement in vacuum much better SNR

5. Kelvin Potential Measurement
Comparison results obtained in air & under vacuum

Empa
Materials Science and Technology

measurement performed in air

topography obtained in peak force mode

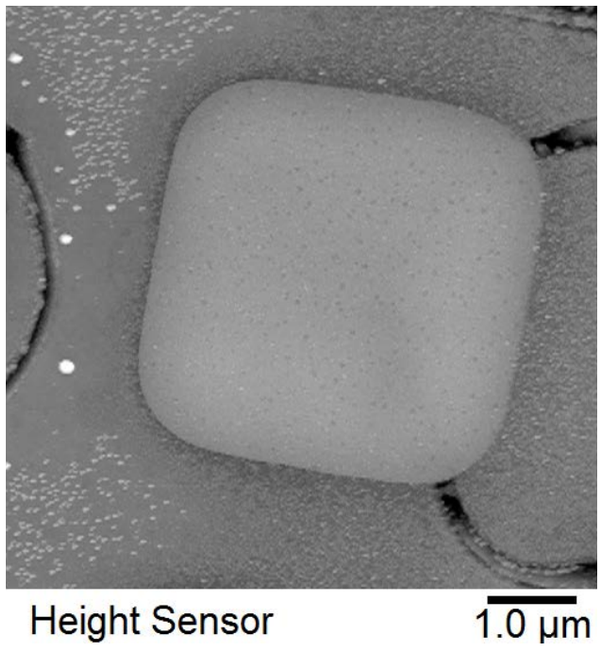

Kelvin potential obtained in FM mode (5V osc.)

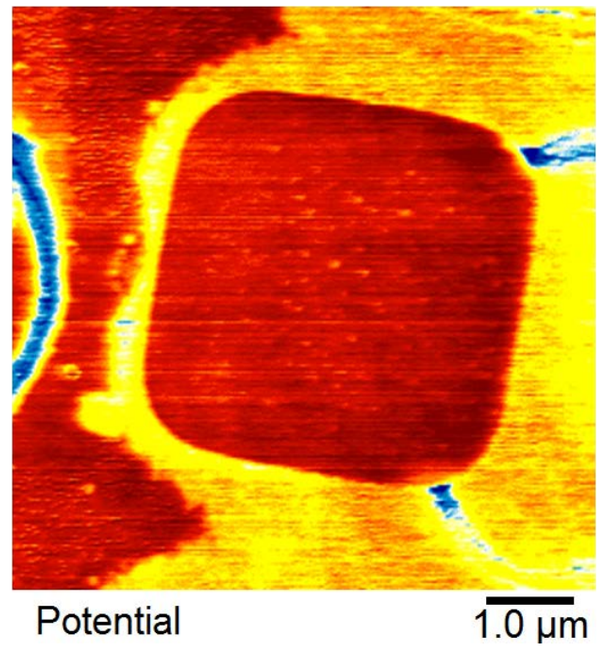

measurement performed in vacuum

topography measured constant @ Δf_1

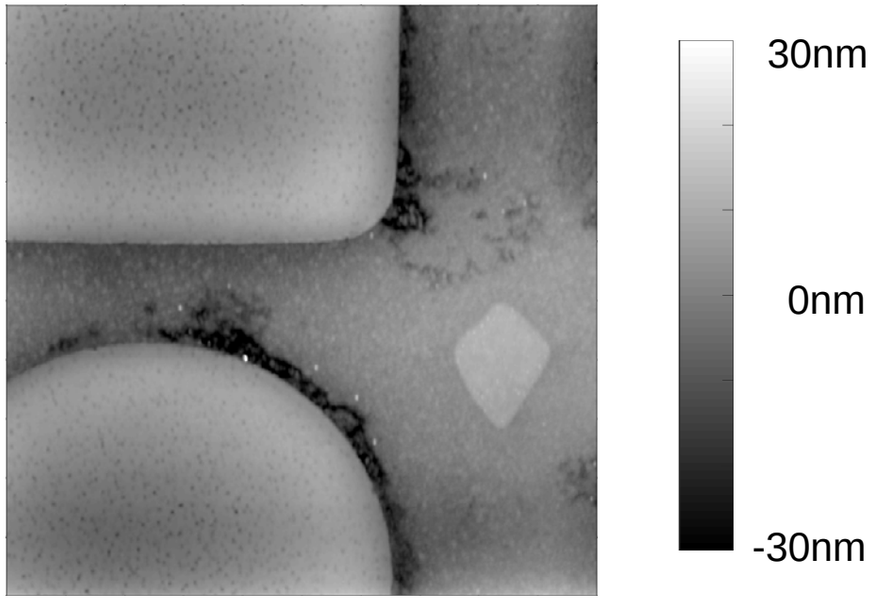

Kelvin potential obtained in FM mode (0.55V osc.)

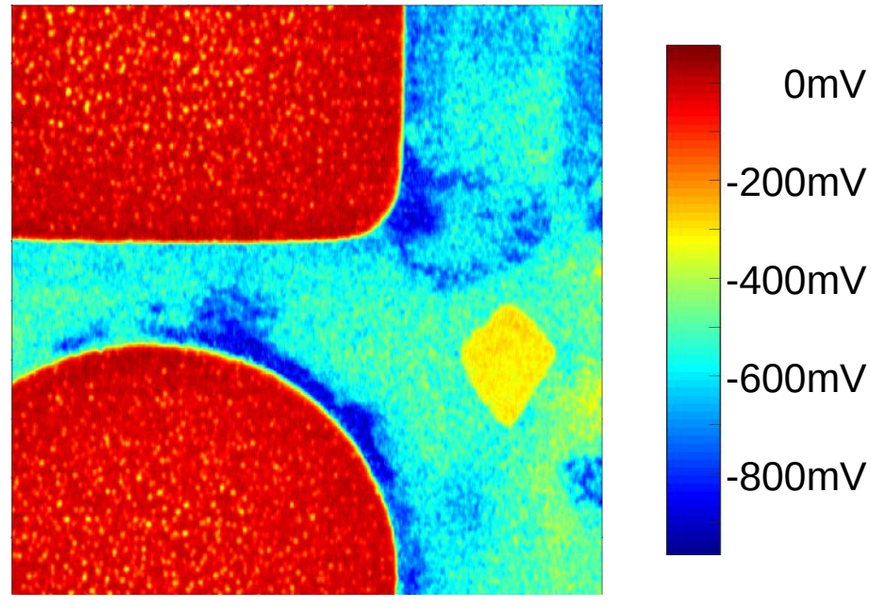

3.4.4. Magnetic Force Microscopy

Magnetic Stray Fields

$$\mathbf{H}(\mathbf{r}) = -\int_V \nabla\mathbf{M}(\mathbf{r_s})\frac{\mathbf{r}-\mathbf{r_s}}{|\mathbf{r}-\mathbf{r_s}|^3}dV_s + \int_A \mathbf{n}\cdot\mathbf{M}(\mathbf{r_s})\frac{\mathbf{r}-\mathbf{r_s}}{|\mathbf{r}-\mathbf{r_s}|^3}dA_s$$

magnetic volume charge $\rho_m = \nabla\mathbf{M}$

magnetic surface charge $\sigma_m = \mathbf{n}\cdot\mathbf{M}$

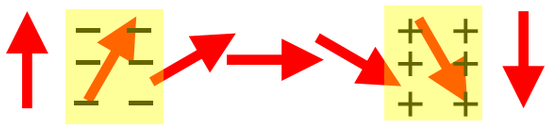

divergence inside film

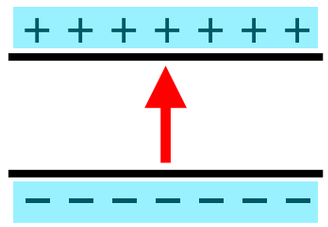

note:

$$\mathbf{M} = \mathbf{M}_{rot} + \mathbf{M}_{div}$$

$$\nabla\cdot\mathbf{M}_{rot} = 0 \qquad \nabla\times\mathbf{M}_{div} = 0$$

source free part of vector field does not generate a stray field, i.e. can not be measured in an MFM

- the source free part of the magnetization does not generate a stray field
- different magnetization patterns can generate the same stray field

➜ the stray field NOT the magnetization pattern can be obtained from a quantiative analysis of MFM data

➜ the magnetization pattern can be inferred from the stray field with addtional knowledge in many situations

Magnetic Stray Fields outside a magnetic Sample

Empa
Materials Science and Technology

outside the sample: $\Delta\phi_m = 0$

$\nabla \times \mathbf{H}_{ext} = \mathbf{j} = 0 \Rightarrow \mathbf{H}_{ext} = -\nabla\phi$

inside the sample: $\triangle\phi_m = -\rho_m$

magnetic volume charge $\rho_m = \nabla \mathbf{M}$

boundary condition: $\left.\frac{\partial\phi_m}{\partial n}\right|_{z\to 0^-} - \left.\frac{\partial\phi_m}{\partial n}\right|_{z\to 0^+} = -\sigma_m$

magnetic surface charge $\sigma_m = \mathbf{n}\cdot\mathbf{M}$

solution: $\phi(x,y,z) = \frac{1}{4\pi^2}\int \phi(k_x,k_y,0)e^{i\mathbf{k}\cdot\mathbf{r}}e^{-\sqrt{k_x^2+k_y^2}\,z}d\mathbf{k}$ with: $\mathbf{H}(\mathbf{k},z) - \nabla\phi_m(\mathbf{k},z)$

gradient operator in Fourier space: $\nabla_k = (ik_x, ik_y, -k)$ ➜ $H_z(k_x,k_x,z) = k\phi_m(k_x,k_x,z)$

can be obtained
from MFM Δf-data

$$\left.\begin{aligned}\phi_m(\mathbf{k},z) &= \frac{1}{k}\mathbf{H}_z(\mathbf{k},z)\\ \mathbf{H}(\mathbf{k},z) &= -\nabla_k\phi_m(\mathbf{k},z)\end{aligned}\right\} \Longrightarrow \mathbf{H}(\mathbf{k},z) = -\frac{1}{k}\nabla_k\mathbf{H}_z(\mathbf{k},z)$$

➜ it is sufficient to measure the z-component image of the stray field !

➜ all other components can then be calculated from the z-component !

Sensitivity - the Key to high Resolution

Empa
Materials Science and Technology

$$H_z(\mathbf{k}, z) = \frac{M}{2} \cdot \exp(kz) \cdot (1 - \exp(kt))$$

distance loss

thickness loss

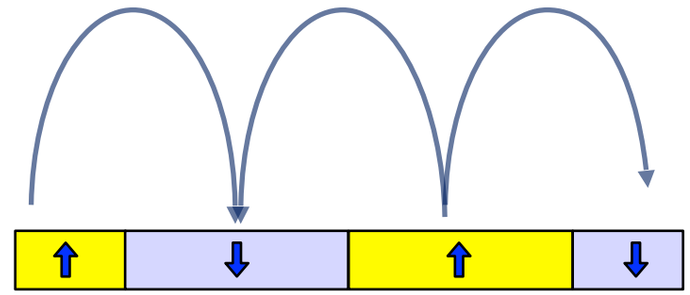

- measure at small tip-sample distances
- maximize force (derivative) sensitivity of cantilever
- use sharp, high aspect ratio tip coated on one side with a thin ferromagnetic layer

MFM tip

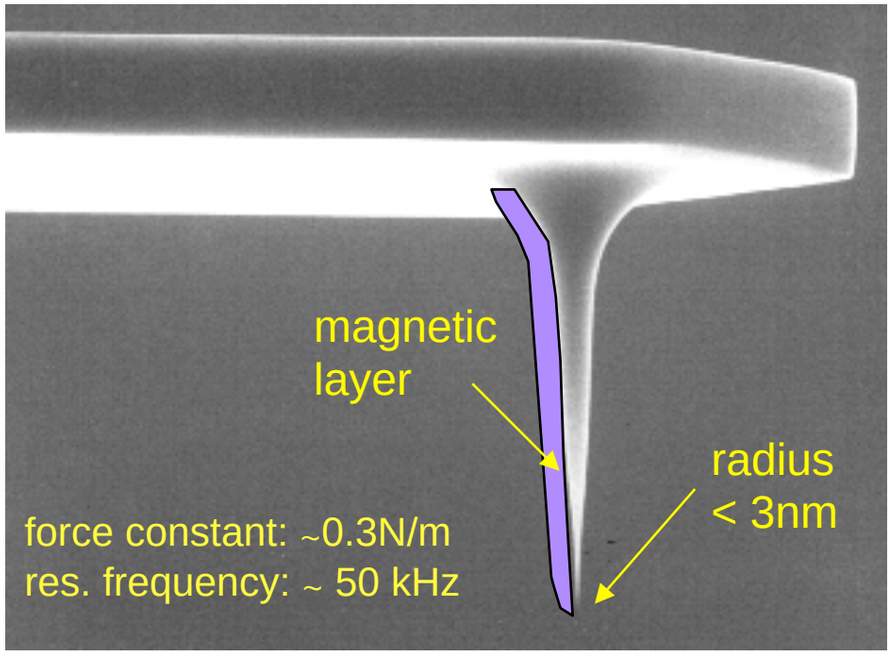

minimal measurable force derivative

$$\left.\frac{\partial}{\partial z} F_n\right|_{min,rms} = \frac{1}{A_n}\sqrt{\frac{4K_n^{eq} k_B T B}{\omega_n Q_n}}$$

k: force constant, ω_0: free resonance
Q: quality factor, *T*: temperature, *A*: amplitude

$$Q_{vac} > 40'000 \quad Q_{air} \approx 100$$

sensitivity > 20 times higher in vacuum

➜ measure in vacuum, avoid thick coating on cantilever

10nm wide domain

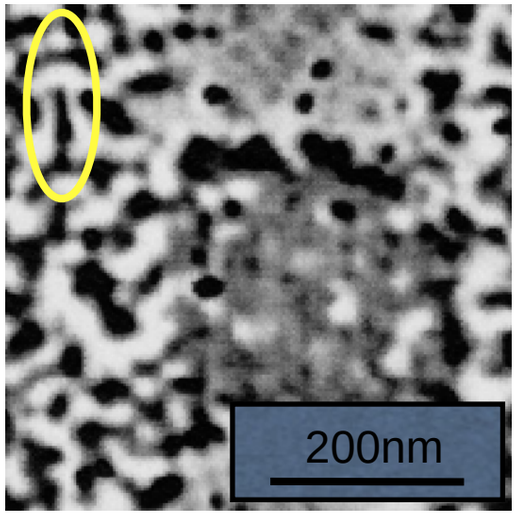

MFM with Q = 1’000’000 versus Q = 100

Empa
Materials Science and Technology

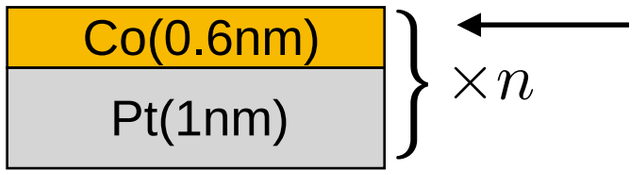

← ~ 3 atomic monolayers of Co

$$\left.\frac{\partial}{\partial z}F_n\right|_{min,rms} = \frac{1}{A_n}\sqrt{\frac{4K_n^{eq}k_BTB}{\omega_n Q_n}}$$

measured
$Q = 10^6$

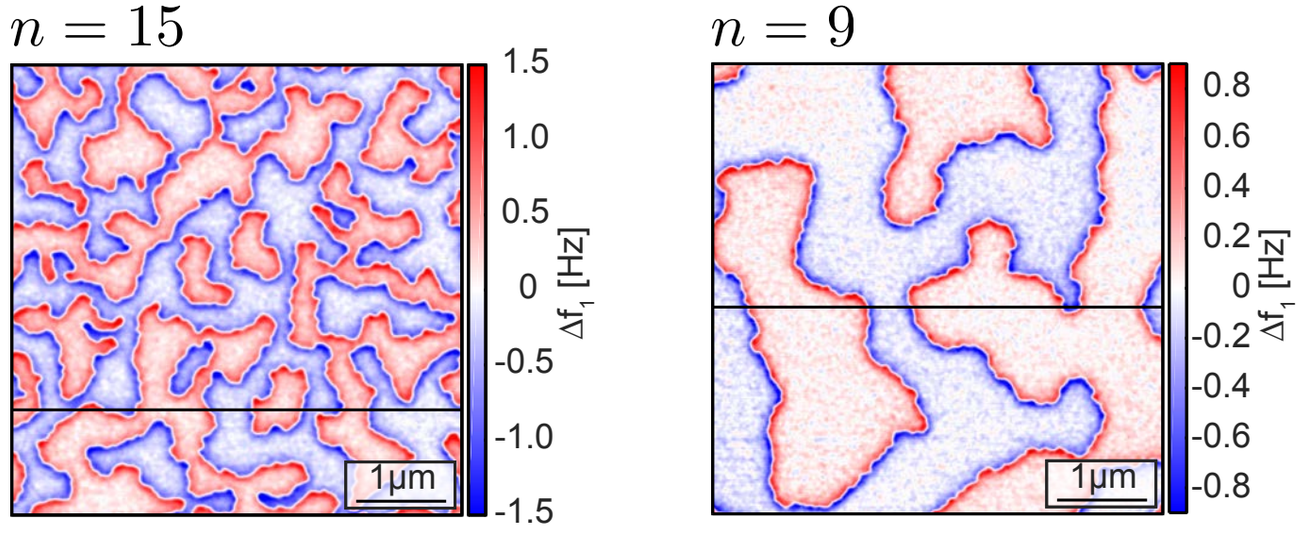

simulated
$Q = 10^2$

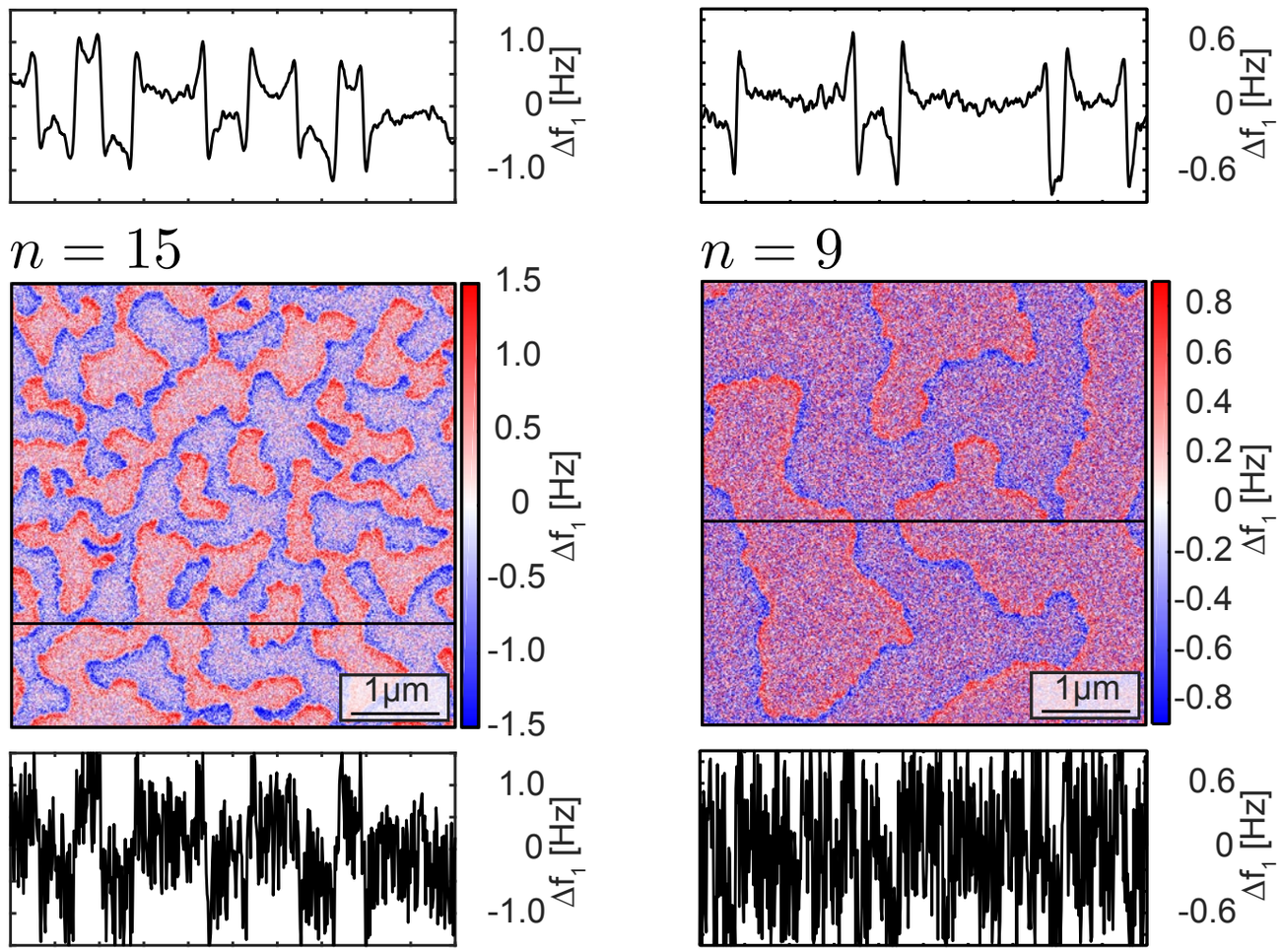

M. Penedo & H.J. Hug et al., (2018)

MFM with Q = 1’000’000 versus Q = 100

Empa
Materials Science and Technology

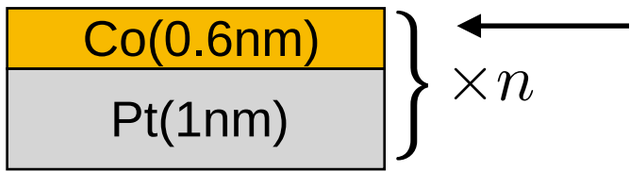

← ~ 3 atomic monolayers of Co

$$\left.\frac{\partial}{\partial z}F_n\right|_{min,rms} = \frac{1}{A_n}\sqrt{\frac{4K_n^{eq}k_BTB}{\omega_n Q_n}}$$

measured
$Q = 10^6$

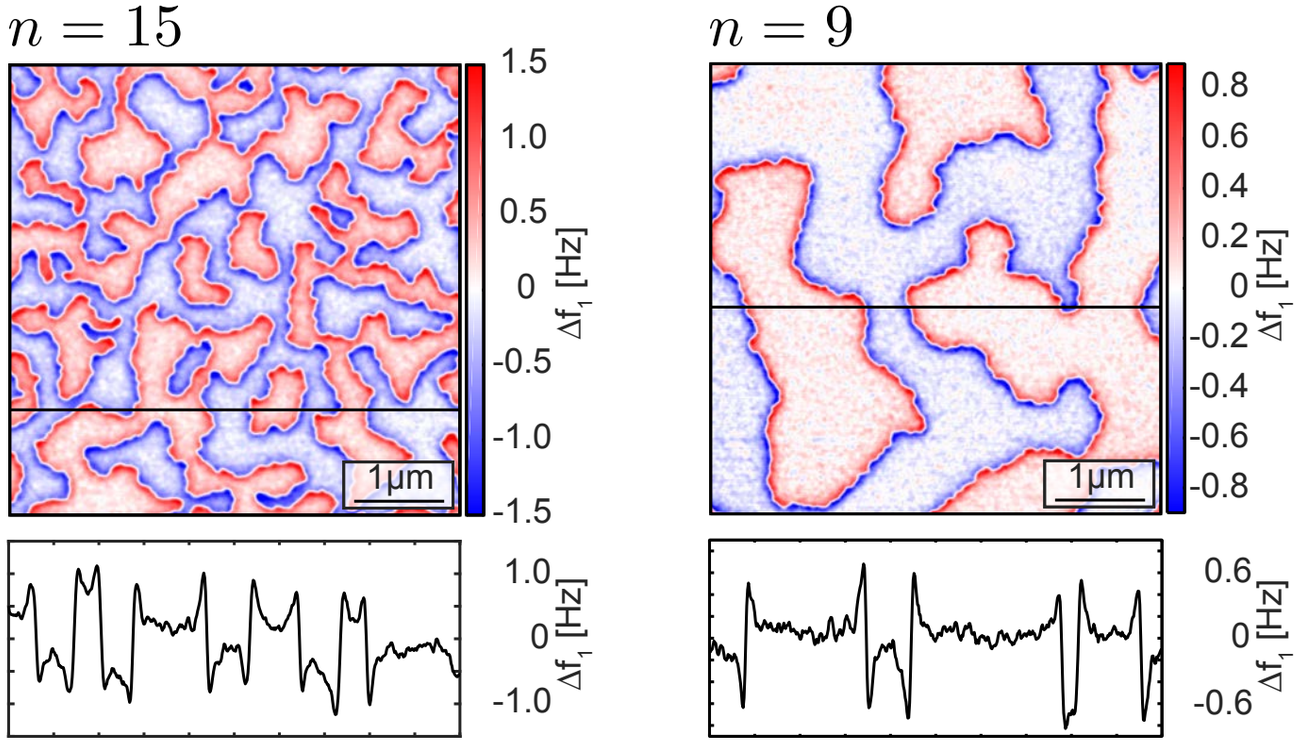

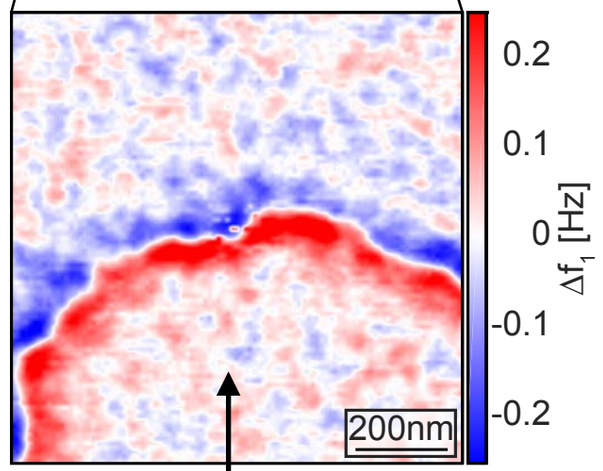

not noise !

M. Penedo & H.J. Hug et al., (2018)

Is MFM a competitive Technique?

Domains (low res.) Skyrmions (high

STXM
From : Moreau-Luchaire et al.
Additive interfacial chiral interaction in multilayers for stabilization of small individual skyrmions [...]
Nat. Nanotech. 2016.
http://doi.org/10.1038/nnano.2015.313

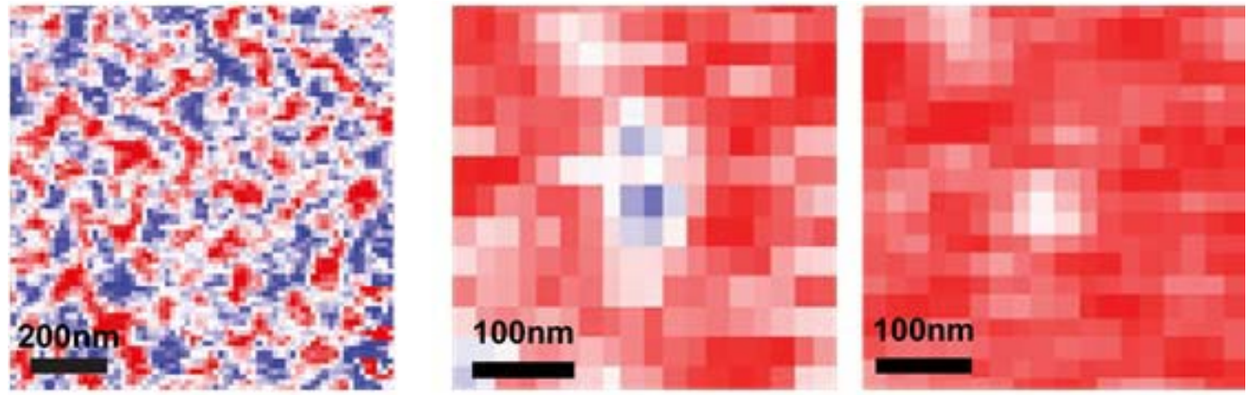

Imaging the Spin Texture of a Skyrmion Under Ambient Conditions Using an Atomic-Sized Sensor.
arXiv:1611.00673 [cond-mat.str-el] (subm. 2016)

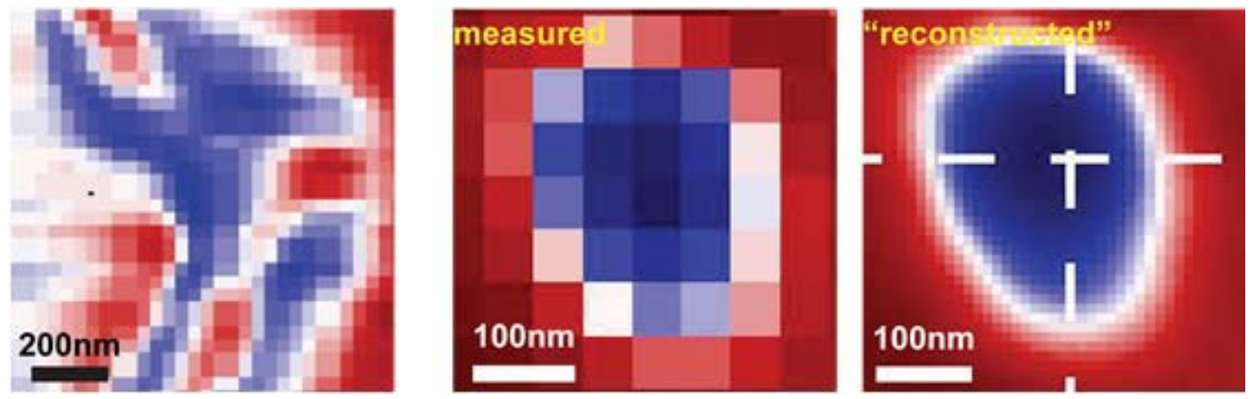

MFM
This work

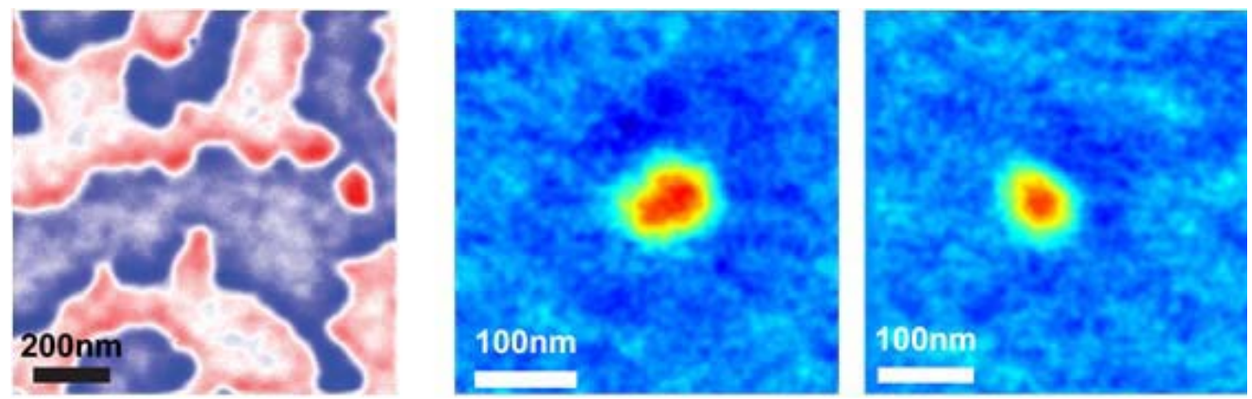

➜ The signal-to-noise ratio & the resolution of the MFM data allows the extraction of local properties from the skyrmion image

Force on Tip - Quantitative Field Measurement

Empa
Materials Science and Technology

in direct space the force is:

$$\mathbf{F}(\mathbf{r}, z) = \mu_0 \int_{V'} (\nabla \mathbf{M}_{tip}(\mathbf{r}', z')) \, \mathbf{H}_{sample}(\mathbf{r} + \mathbf{r}', z + z') d\mathbf{r}' dz'$$

after some math in Fourier space

$$\mathbf{F}(\mathbf{k}, z) = \mu_0 \int_{V'} \underbrace{\nabla_k \mathbf{M}^*_{tip}(\mathbf{k}, z') e^{-\mathbf{k}z'}}_{=: \sigma^*_{tip}(\mathbf{k})} dz' \cdot \mathbf{H}_{sample}(\mathbf{k}, z)$$

➜ once this transfer function is known (tip calibration), the field can be obtained from the force

MFM tip response:

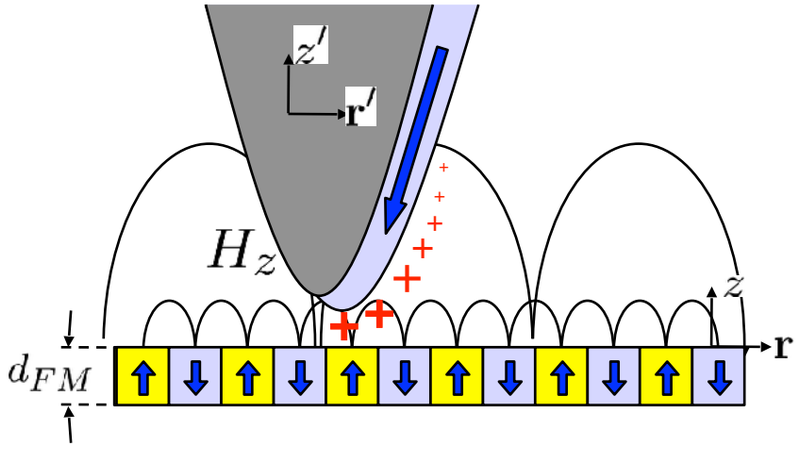

➜ calibration of the tip on Si/Pt_{10nm} [Pt_{1nm}/$Co_{0.6nm}$/Pt_{1nm}]$_{x5}$/Pt_{3nm}

… and further transfer functions for the measured frequency shift (including cantilever tilt & finite oscillation amplitude)

$$\Delta f_{mag}(\mathbf{k}, z) = \underbrace{\frac{\mu_0 f_0}{2k_l} \sigma^*_{tip}(\mathbf{k}) \cdot \frac{2}{kA_{osc}} \cdot \mathrm{LCF}(\mathbf{k}, \vartheta) \cdot \mathrm{I}_1(\tilde{z})}_{\text{transfer function}} \cdot \frac{\partial H_z(\mathbf{k}, z)}{\partial z}$$

qMFM: van Schendel & Hug, et. al. JAP **88,** 435 (2000).
Simulations (Matlab): *https://qmfm.empa.ch/qmfm/*

MFM Tip Calibration

Empa
Materials Science and Technology

MFM tip response

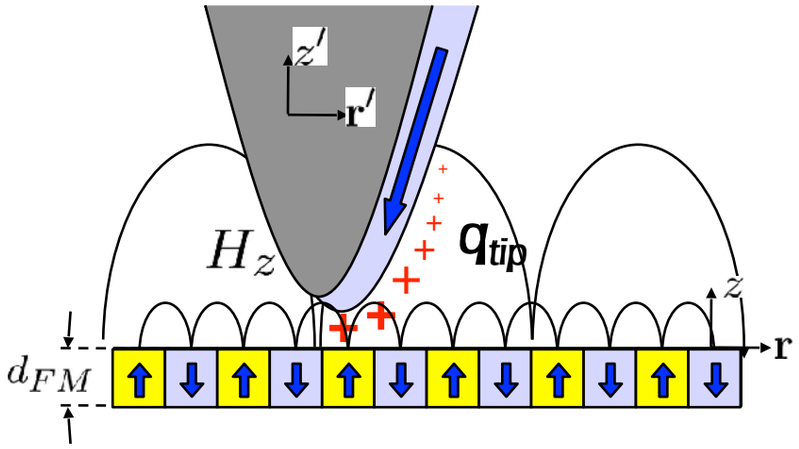

➜ magnetic charge of tip depends on wavelength

calibration sample

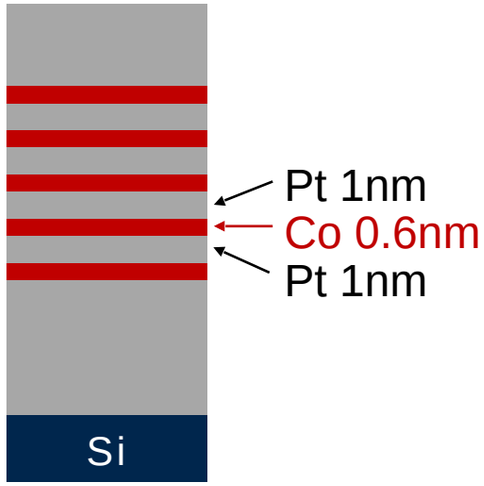

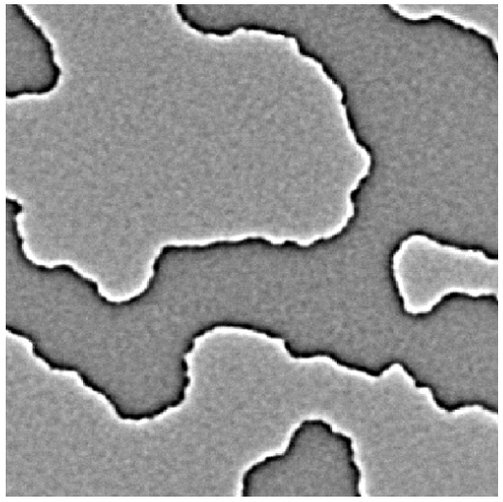

M_{avg} = 347kA/m
$\mu_0 H_c$ = 900.4mT
K_{eff} = 0.469 MJ/m³
K_{ms} = 0.681MJ/m³
K_u = 1.150 MJ/m³

MFM data

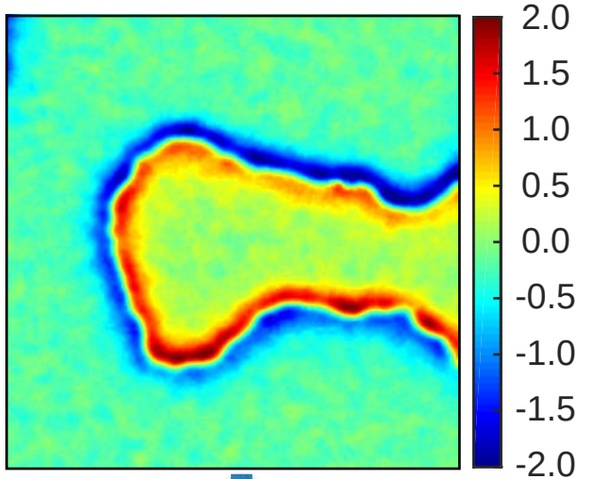

calibrated MFM tip

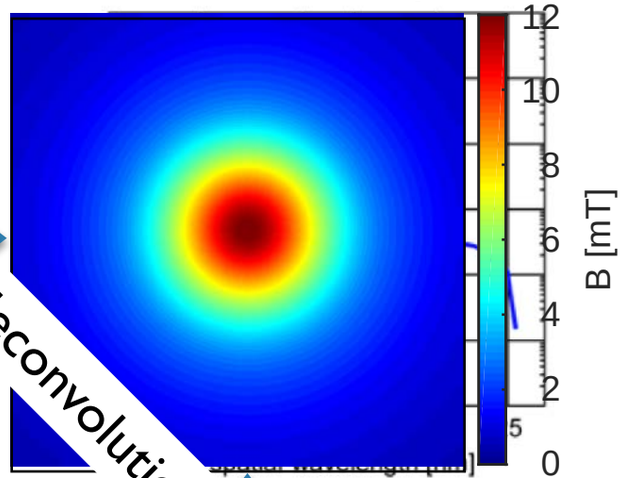

magnetization pattern

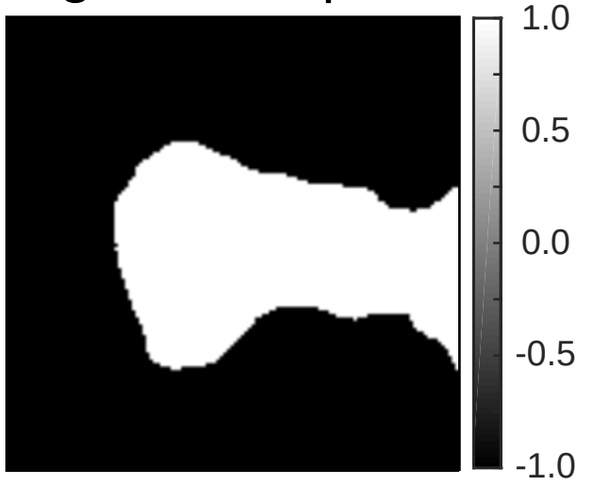

stray field pattern

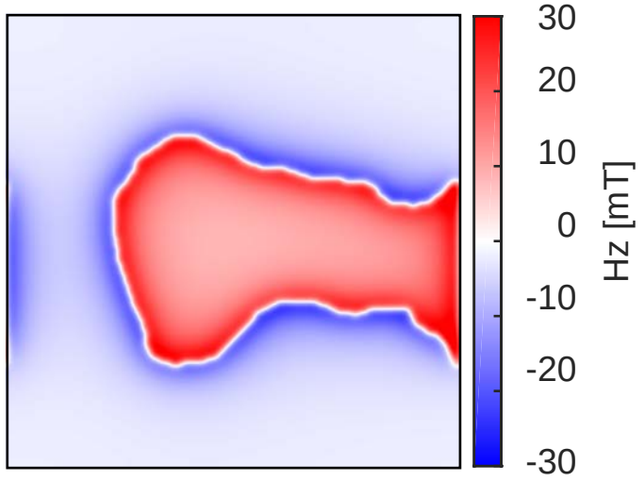

& repeat this process for many images
to obtain
an averaged tip transfer function

MFM simulation

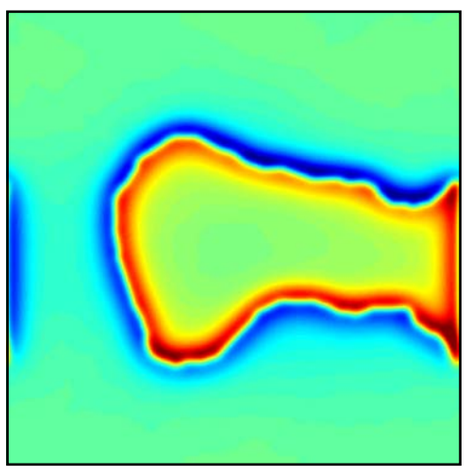

difference

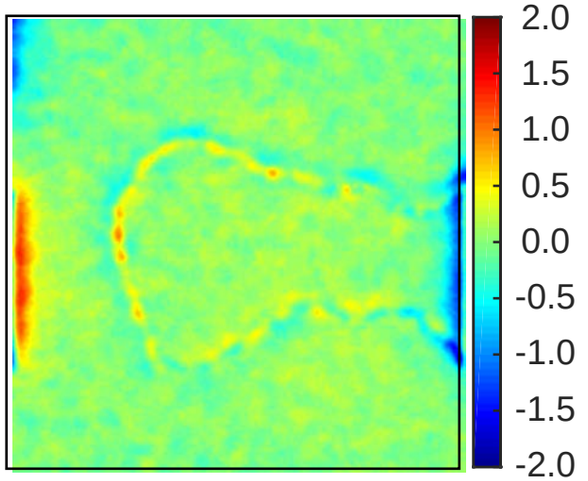

qMFM: van Schendel & Hug, et. al. JAP **88,** 435 (2000).
Simulations (Matlab): *https://qmfm.empa.ch/qmfm/*

Frequency modulated Distance Control

Empa
Materials Science and Technology

modulate U_{ts} @ low frequency ➜ side bands of f_c!

$$U_{\mathrm{ts}}(t) = U_{dc} + U_{ac}\cos(2\pi f_{ac} t) \;\rightarrow\; F_E(z,t) = \frac{1}{2}\frac{\partial C(z)}{\partial z}\cdot\left[\, U_{dc}^2 + \boxed{2U_{dc}U_{ac}\cos(2\pi f_{ac} t)} \right] \;\rightarrow\; \text{Kelvin signal}$$

$$+ \;\boxed{U_{ac}^2\cos^2(2\pi f_{ac} t)\,]} \;\rightarrow\; \text{capacitive signal}$$

$$\rightarrow\; F_{E,2f_{ac}}(z) = \frac{1}{4}\frac{\partial C(z)}{\partial z}\cdot\boxed{U_{ac}^2} \;\rightarrow\; \text{capacitive signal is frequency doubled}$$

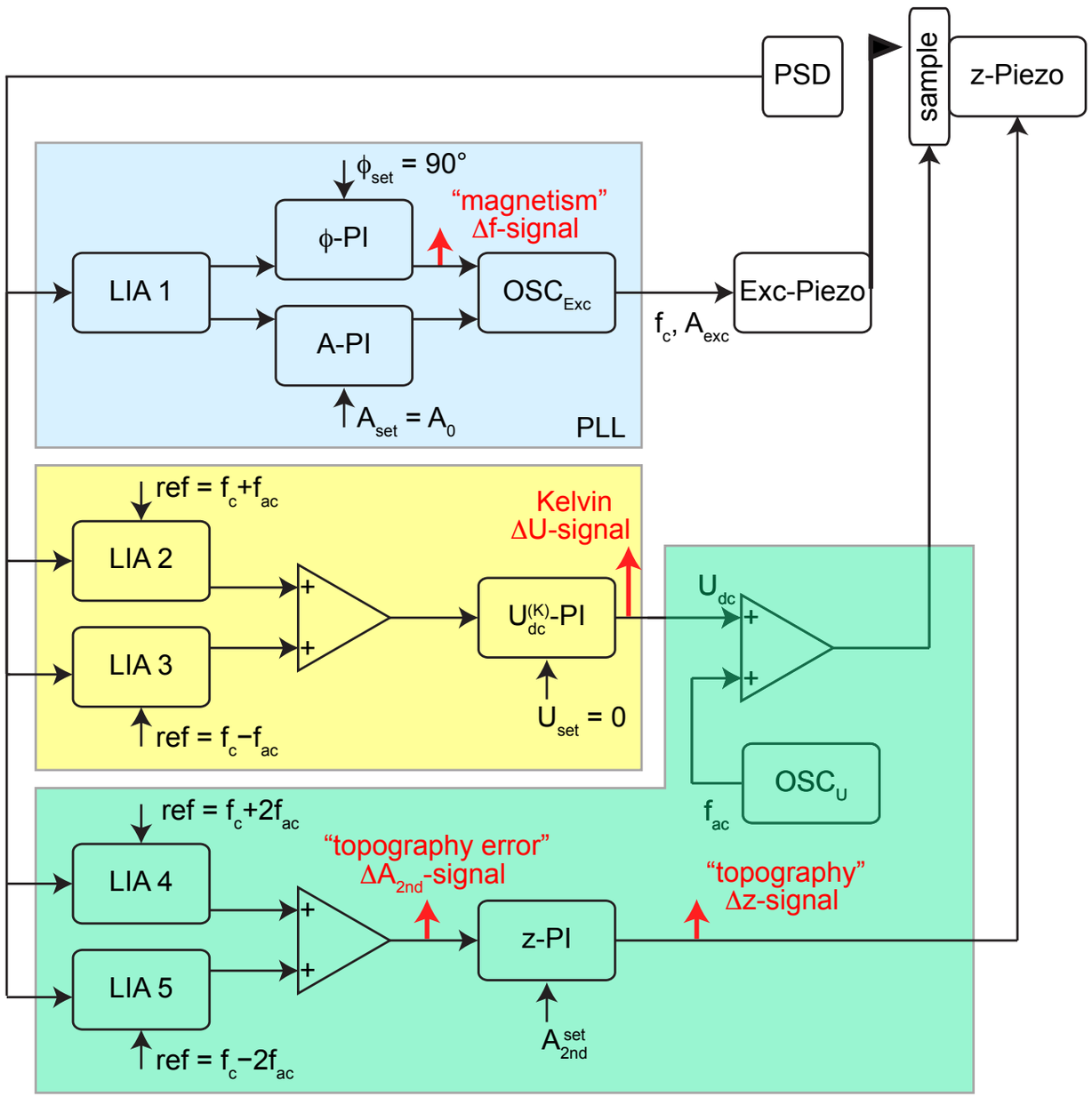

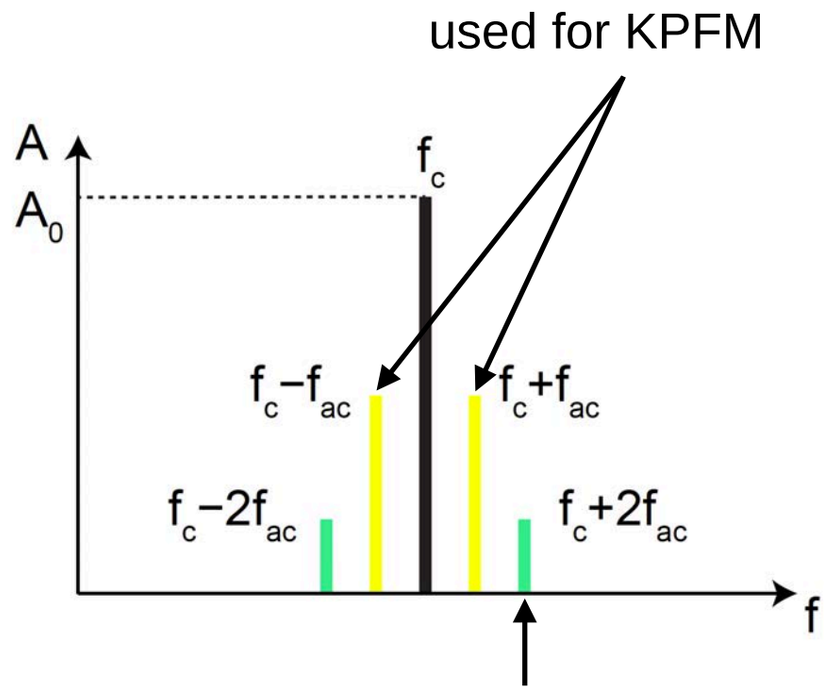

X. Zhao, & H. J. Hug et al., New J. Phys. **20** (2018) 013018

Be careful with Data Interpretation

Problem: Interpretation of resulting image:

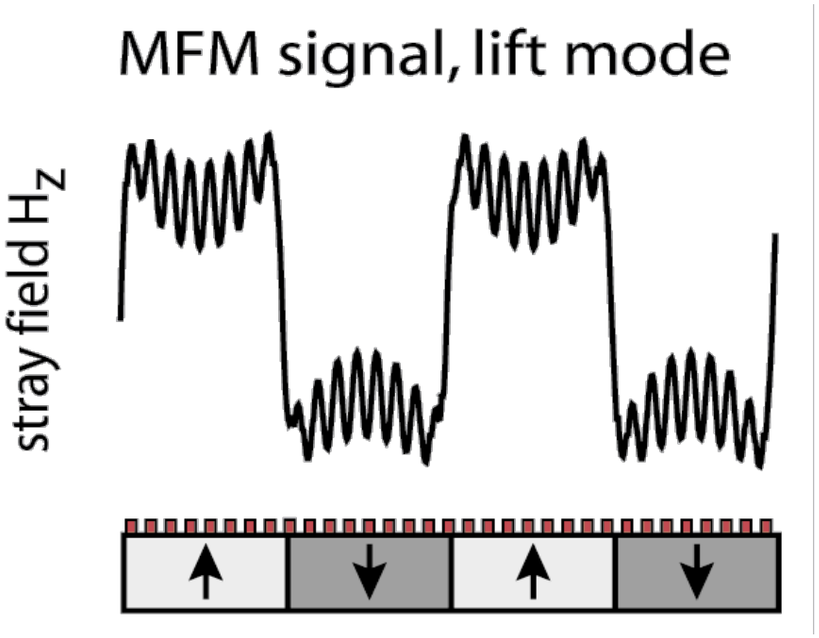

local tip-sample is kept constant, but tip-sample averaged over the „sample“ area contributing to the measured magnetic field then is ***NOT*** constant.

➜ topographical features appear in the „magnetic image“

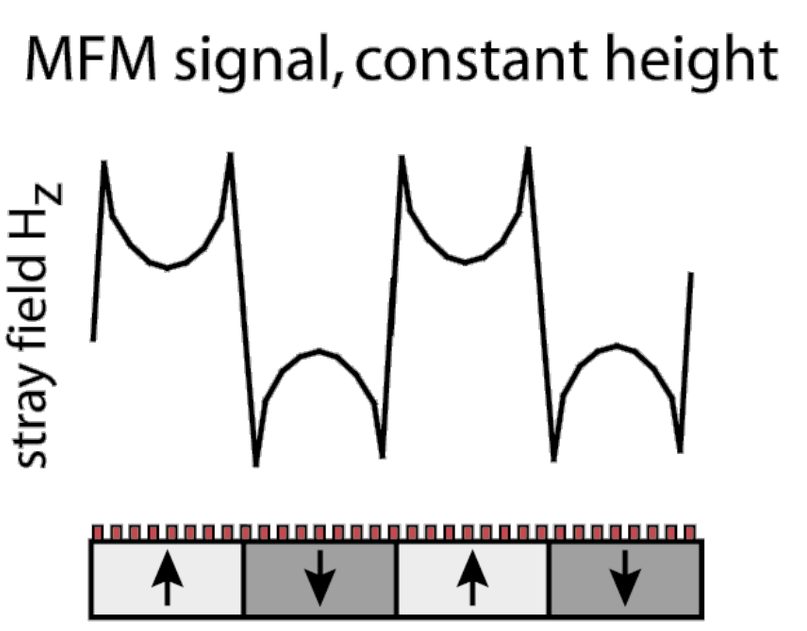

local tip-sample is ***NOT*** constant.

➜ local tip-sample distance not constant

➜ variation of local van der Waals force

➜ topographical features appear weakly in the „magnetic image“

Van der Waals Forces and their Contribution to the MFM Signal (in constant-average-height imaging)

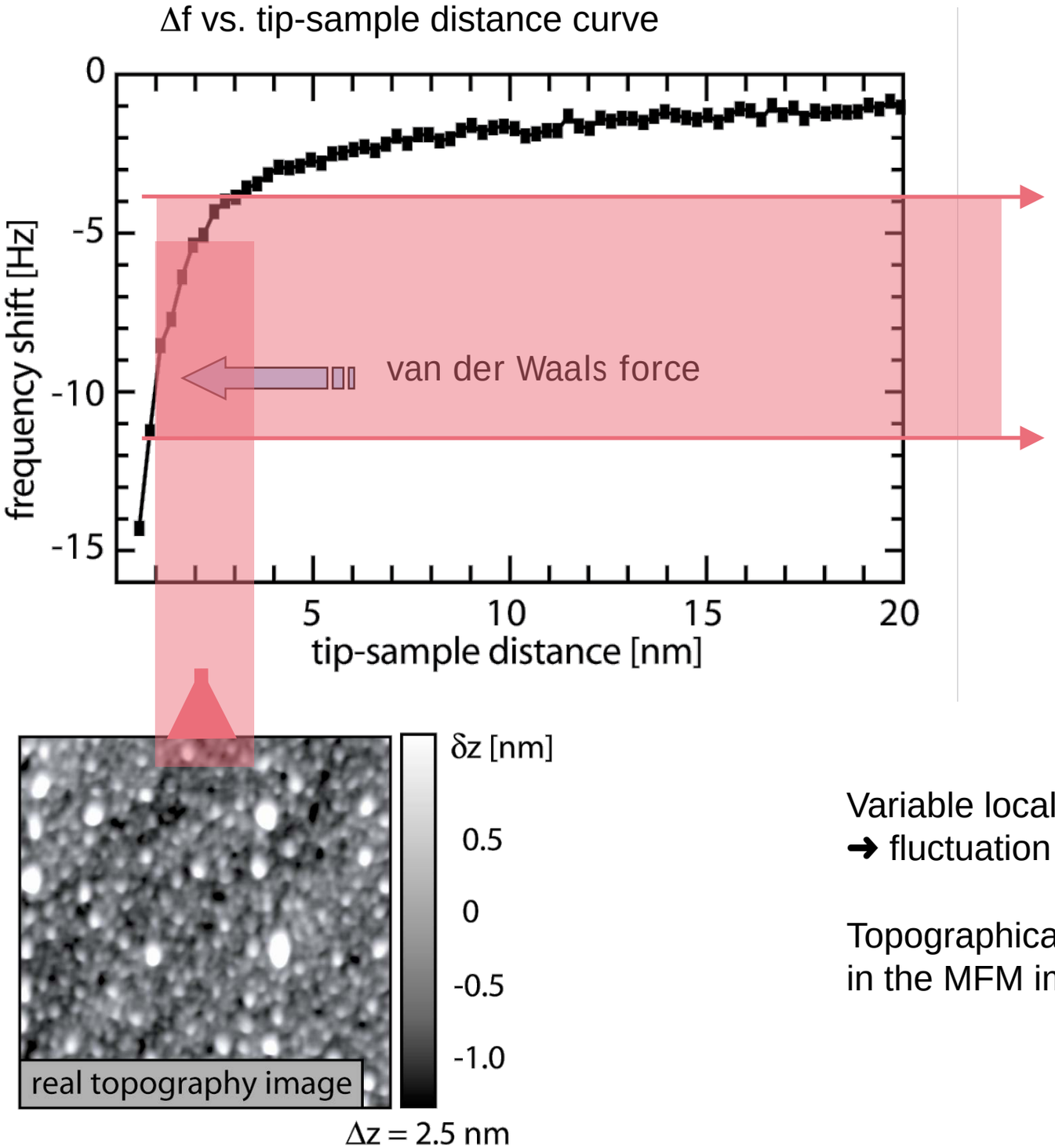

Real topography image

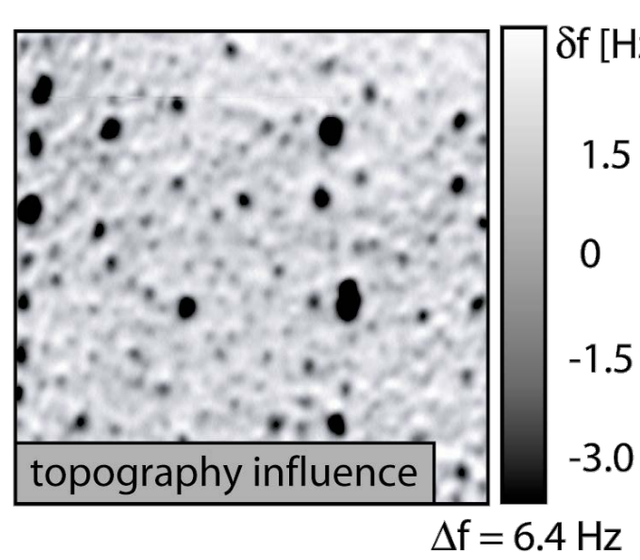

Variable local tip-sample distance:
➜ fluctuation of local vdW force.

Topographical features become visible in the MFM image.

Separation of Topography and Magnetism

Measure with opposite magnetization states of tip

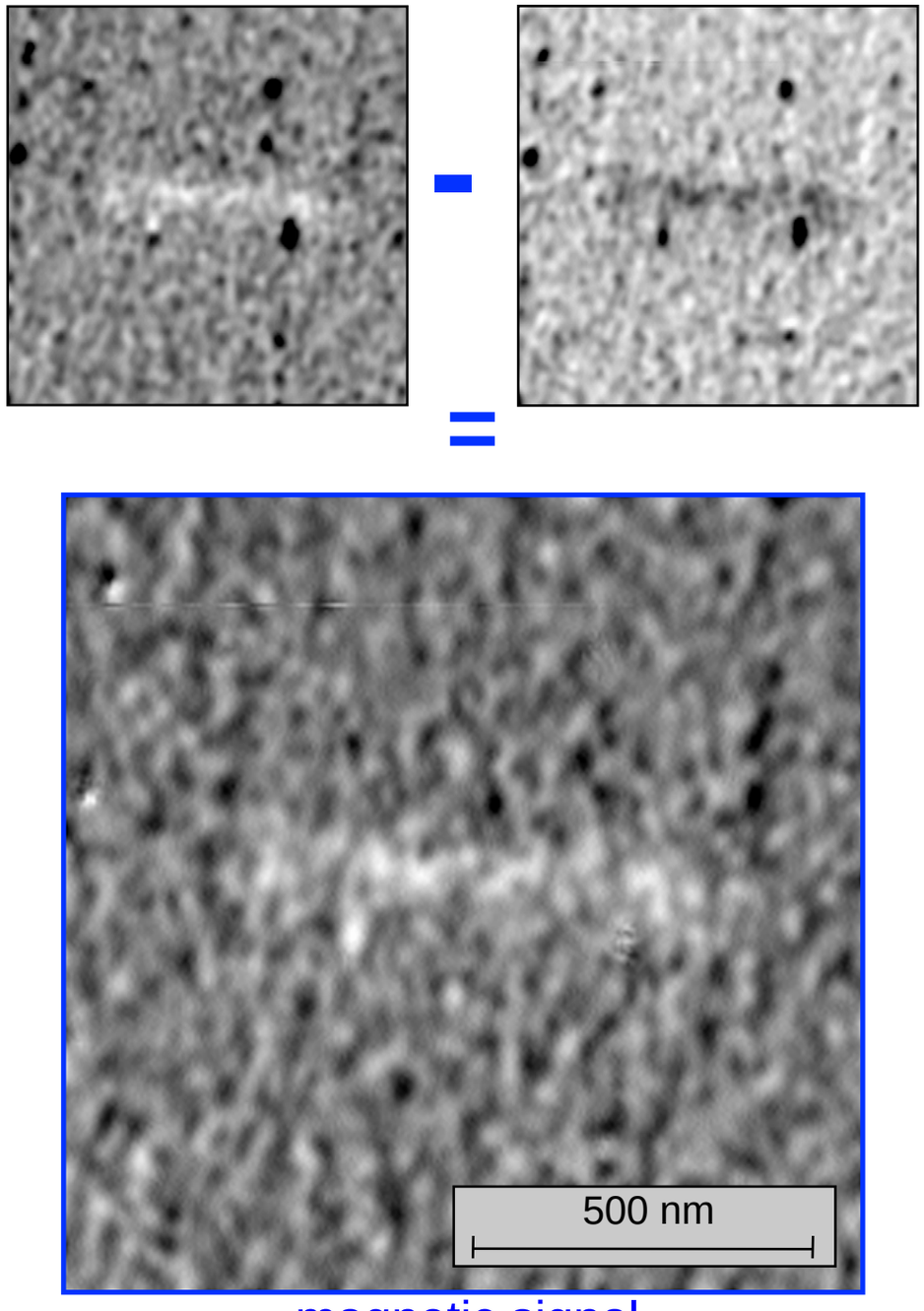

magnetic signal

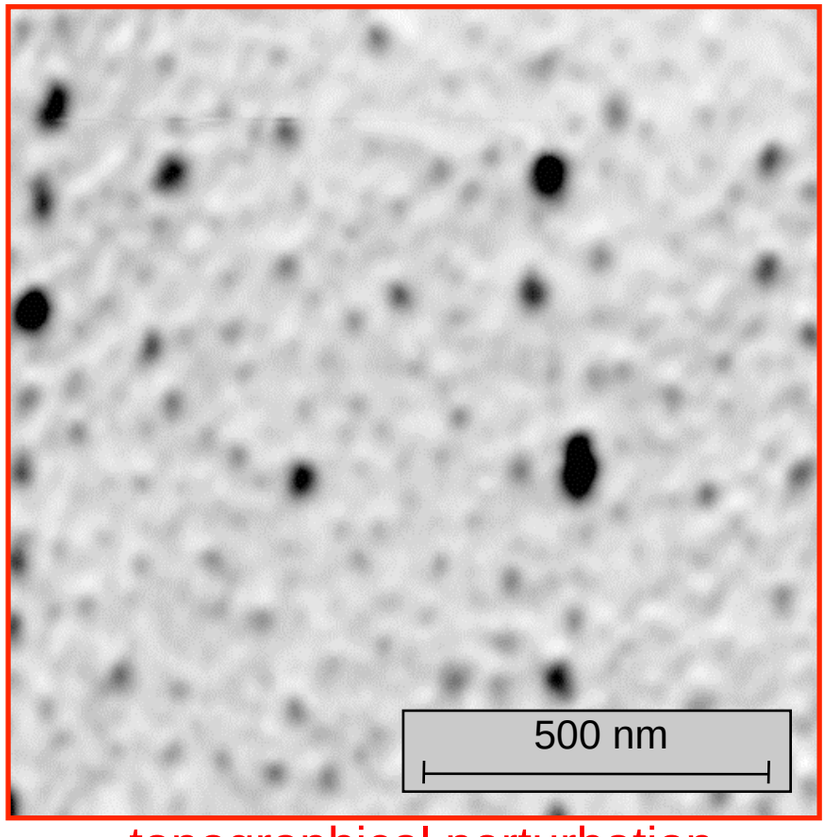

topographical perturbation

Topography generated Magnetic Fields

topography

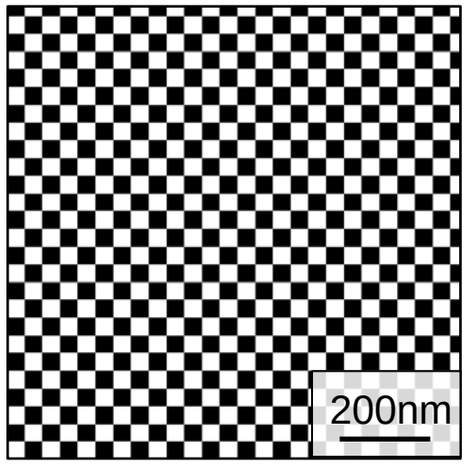

magnetic domains

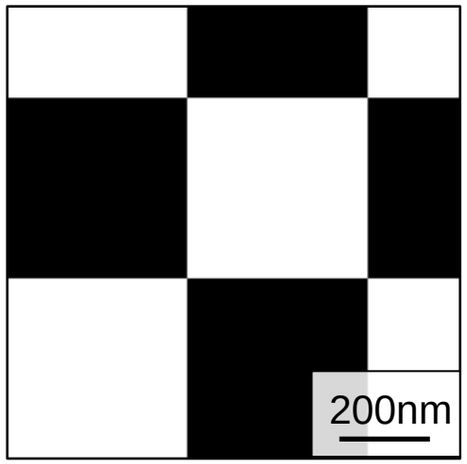

saturated M

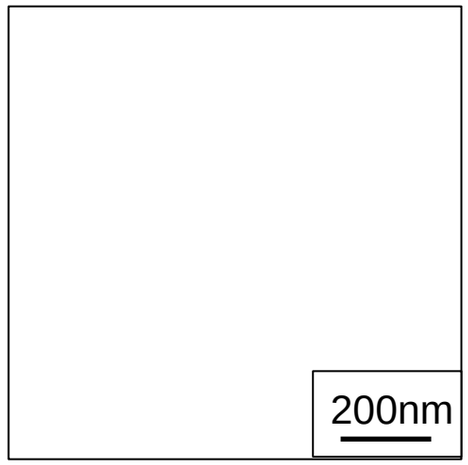

topography side view

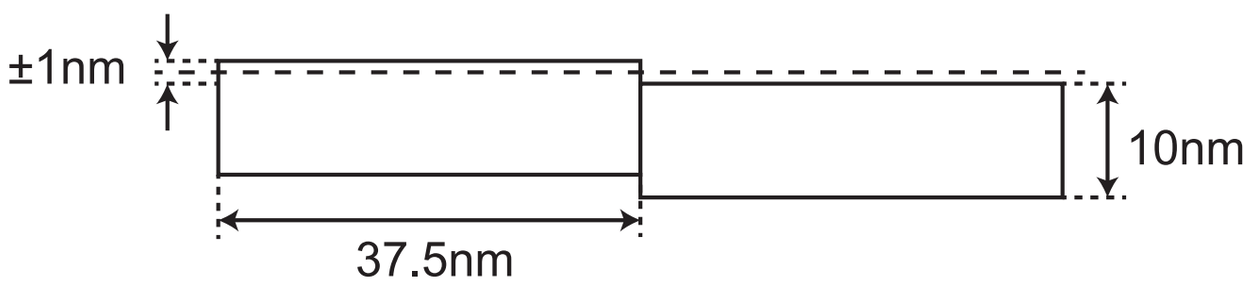

Constant avg. height
$H_z(z = 10\text{nm})$

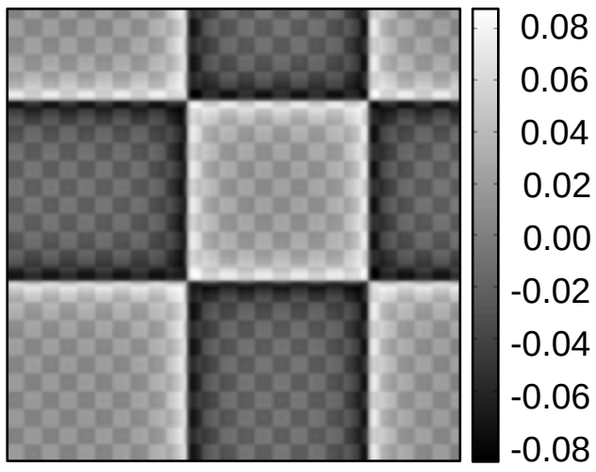

Constant avg. height
$H_z(z = 10\text{nm})$, M_{sat}

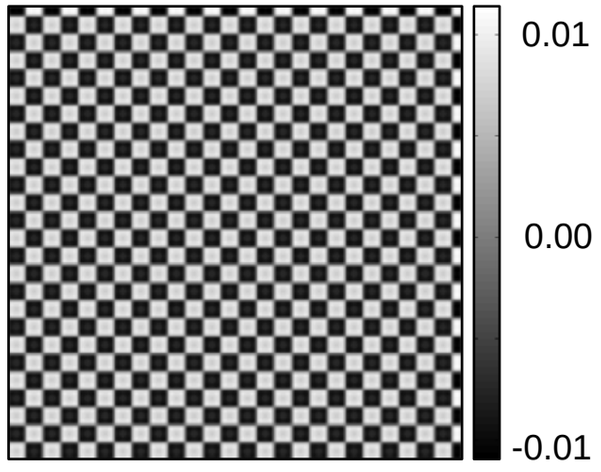

Difference Image

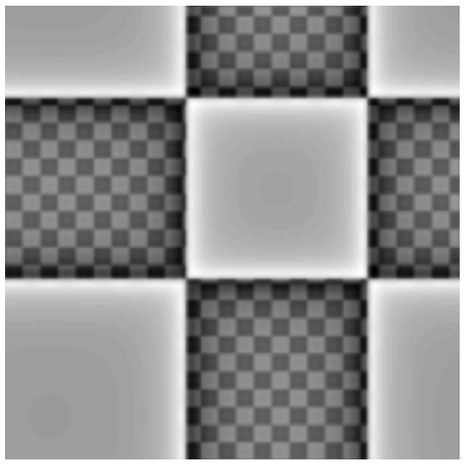

difference image: ➜ topography induced fields double in down domain

Note: these are real magnetic fields; in addition topography induced artifacts may exist

Our System studied by MFM & Magnetometry

Empa
Materials Science and Technology

Fabrication: DC magnetron sputtering
Room T, 2.2 µbar
Si substrate (nat. oxide)

Measurement: Room T vacuum MFM
Team Nanotec SS ISC tips, 4nm Co sputter coated
Tip-sample distance z = 12nm

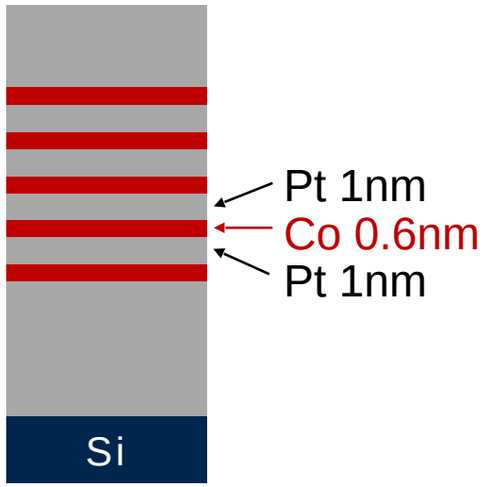

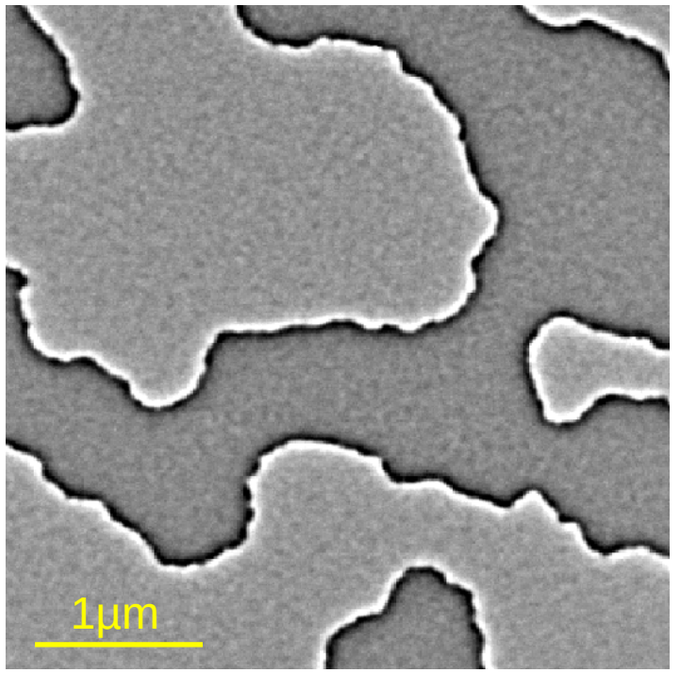

M_{Co} = 1041kA/m
$\mu_0 H_c$ = 900.4mT
K_{eff} = 0.469 MJ/m^3
K_{ms} = 0.681MJ/m^3
K_u = 1.150 MJ/m^3

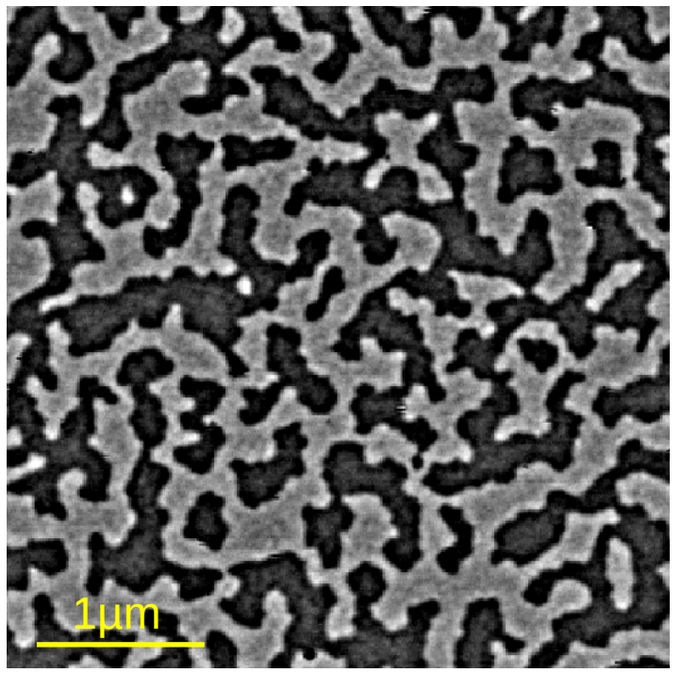

M_{Co} = 653.6kA/m
$\mu_0 H_c$ = 446.1 mT
K_{eff} = 0.146 MJ/m^3
K_{ms} = 0.268 MJ/m^3
K_u = 0.414 MJ/m^3

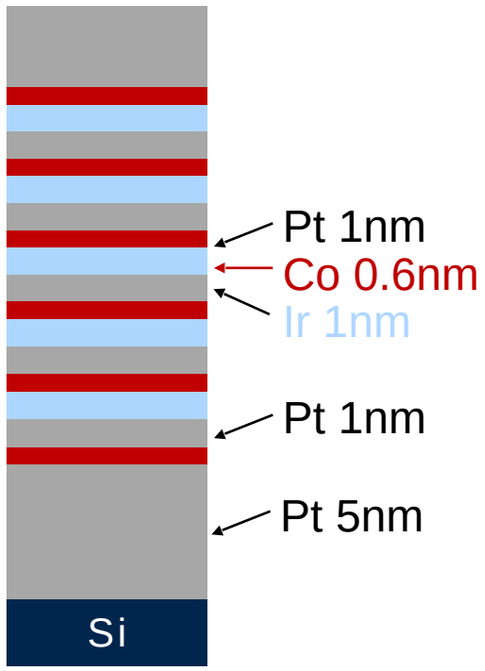

M. Bacani, M.A. Marioni, and H.J. Hug et al., arXiv:1609.01615 [cond-mat]

Magnetization of Sample with Ir/Co/Pt Interfaces ➜ Skyrmions

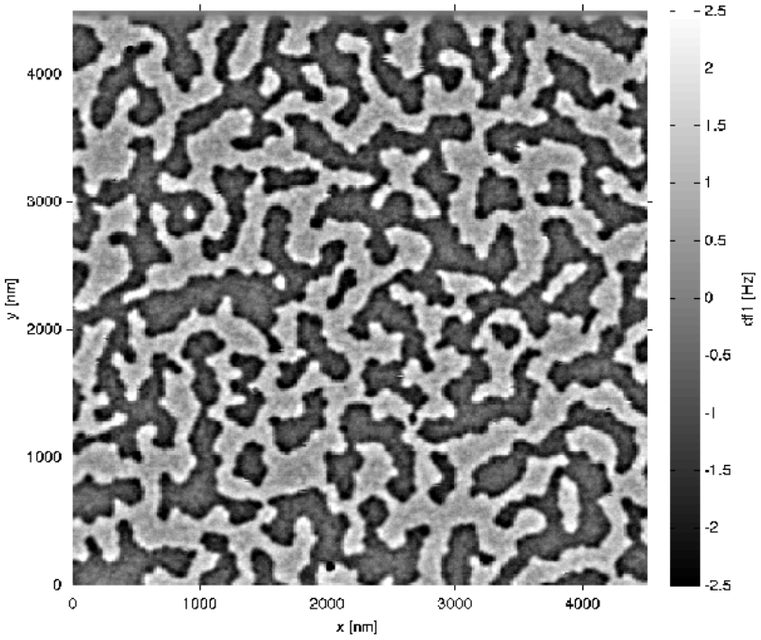

0mT, after perp. demag

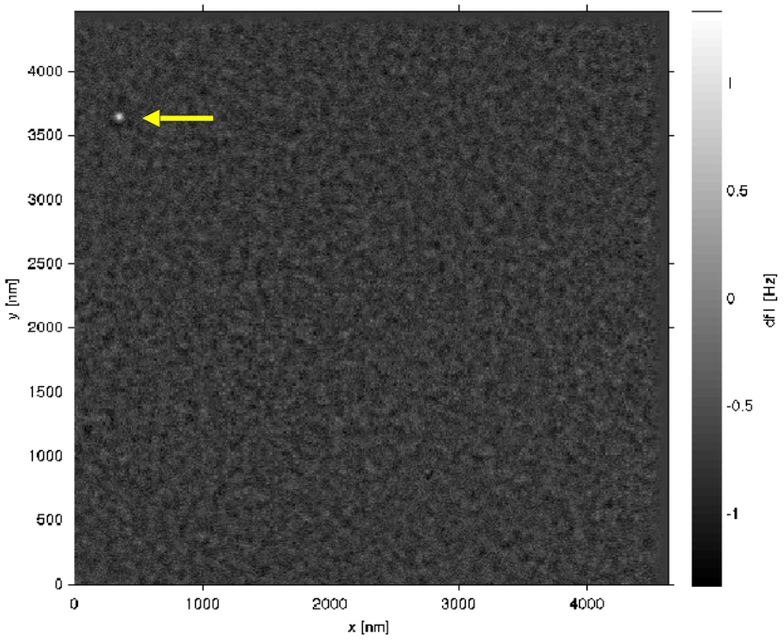

128.34mT
➜ 1 skyrmion visible

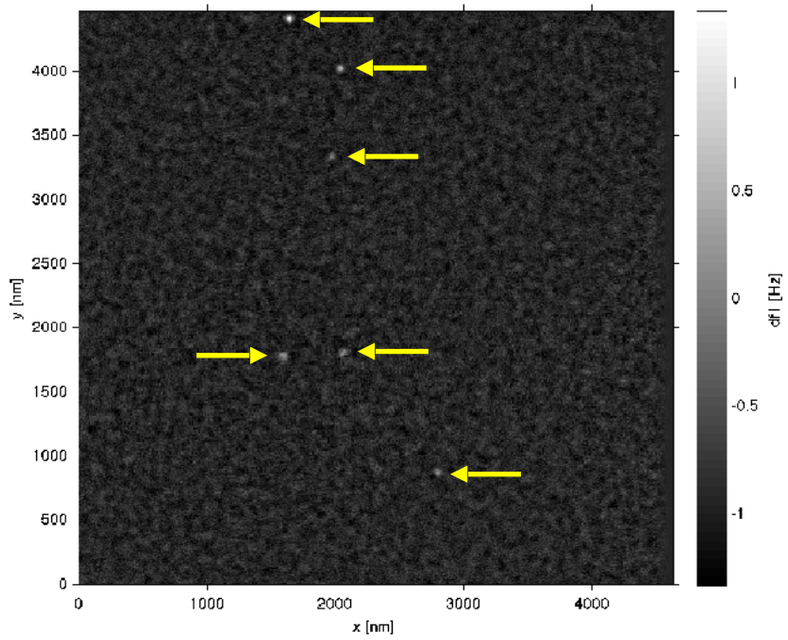

1mT after saturation at 273mT
➜ several skyrmions

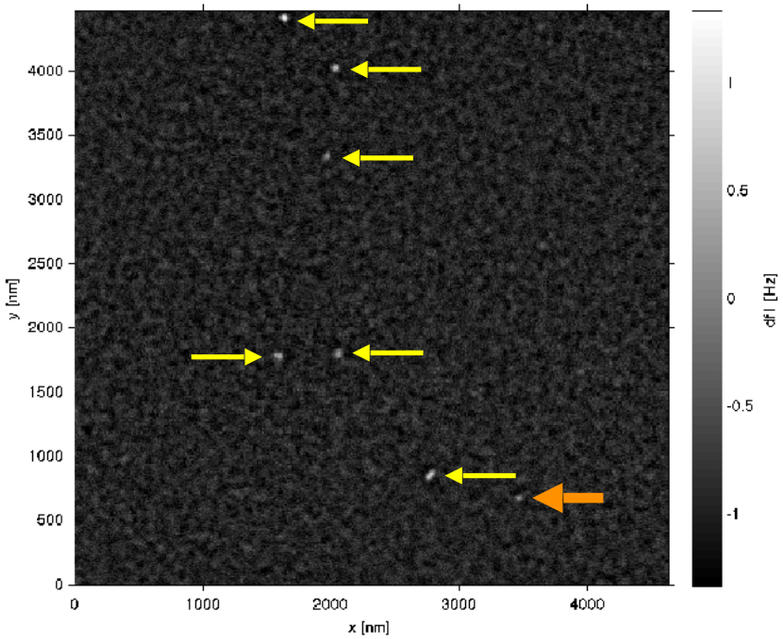

1.19mT after „some time“:
new skyrmion

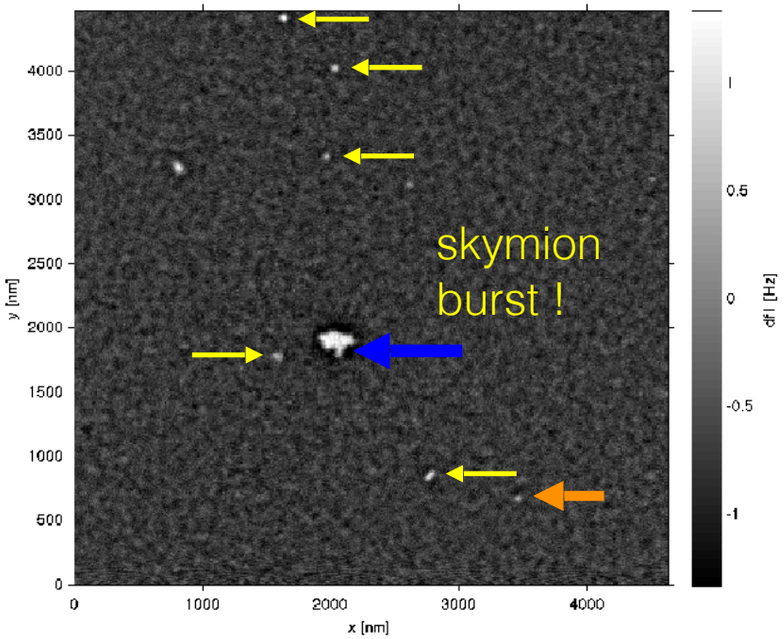

-4.04mT: new skyrmions
skyrmion burst

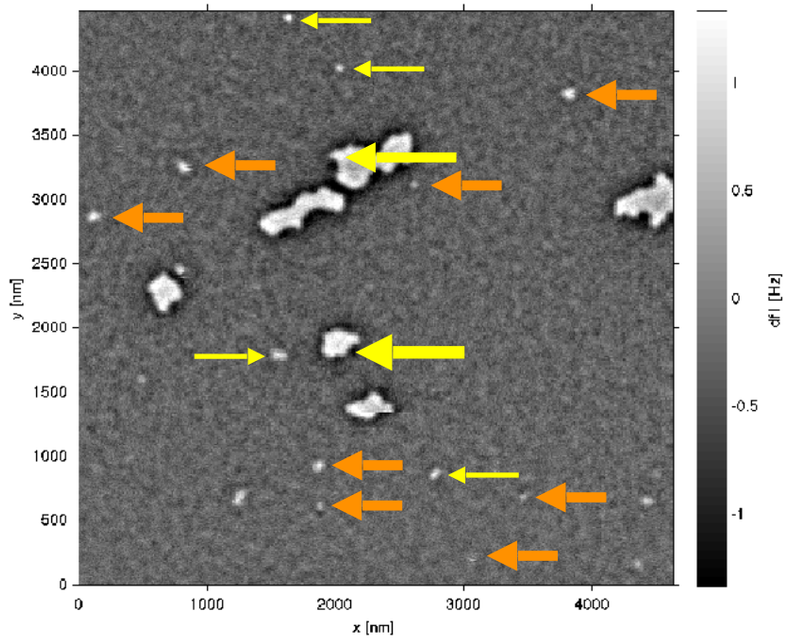

-8.45mT: new skyrmions and skymions expanded into domains

➜ few skyrmions with core magnetization opposite to applied saturation field appear @ low fields
➜ skyrmions burst into larger domains @ small negative fields

M. Bacani, M.A. Marioni, and H.J. Hug et al., arXiv:1609.01615 [cond-mat]

Modelling & Comparing with Measurement

Empa
Materials Science and Technology

experimental and modelled cross section

D=3.470 mJ/m²

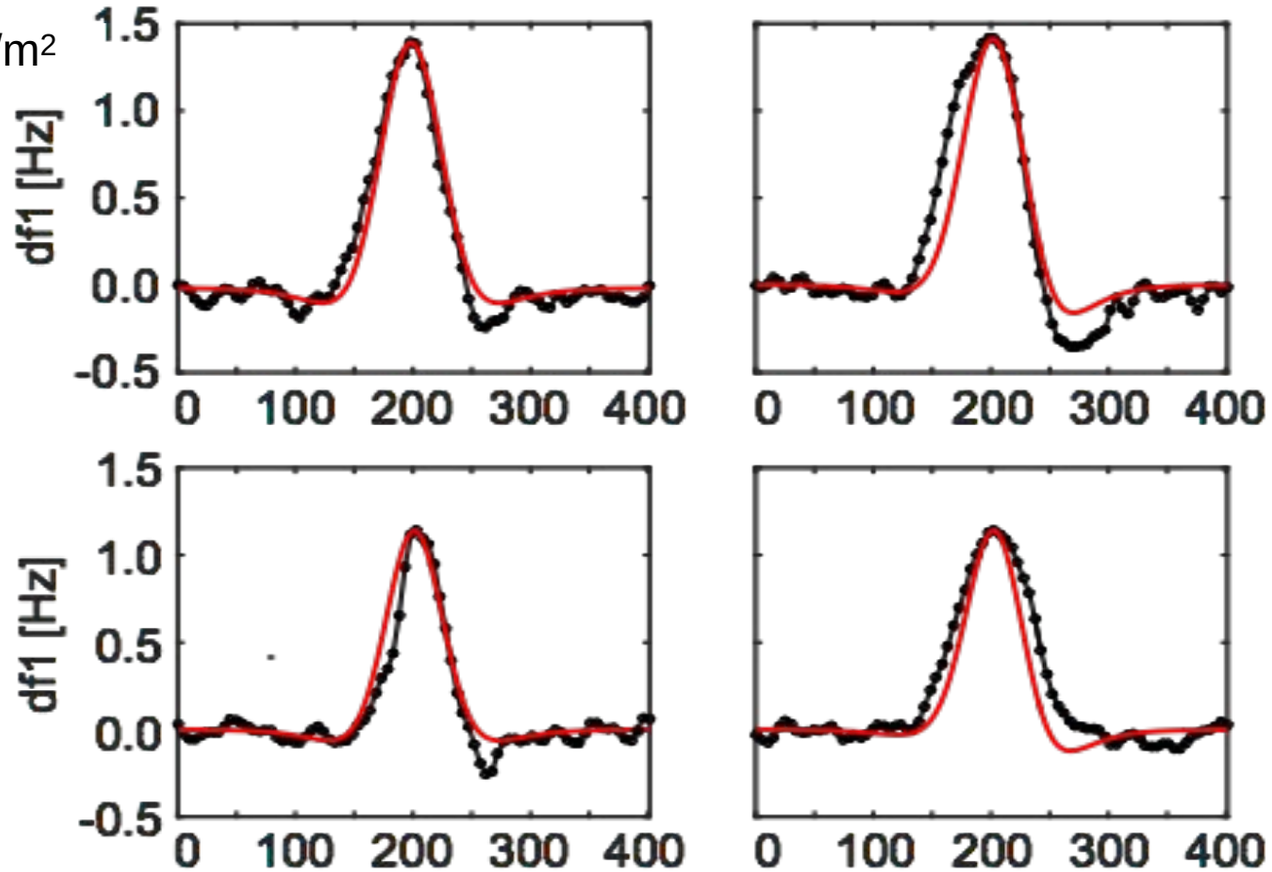

D=3.427 mJ/m²

skyrmion profile

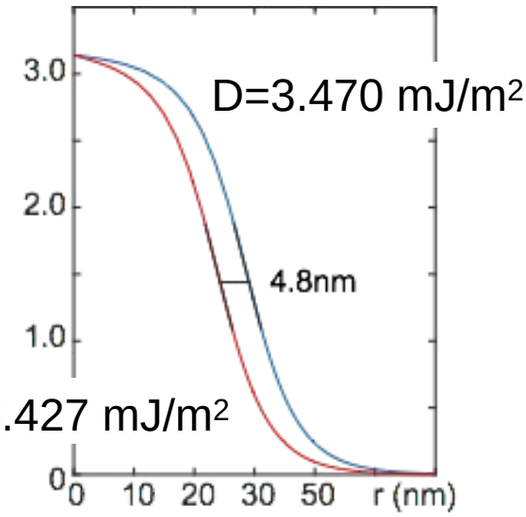

MFM data

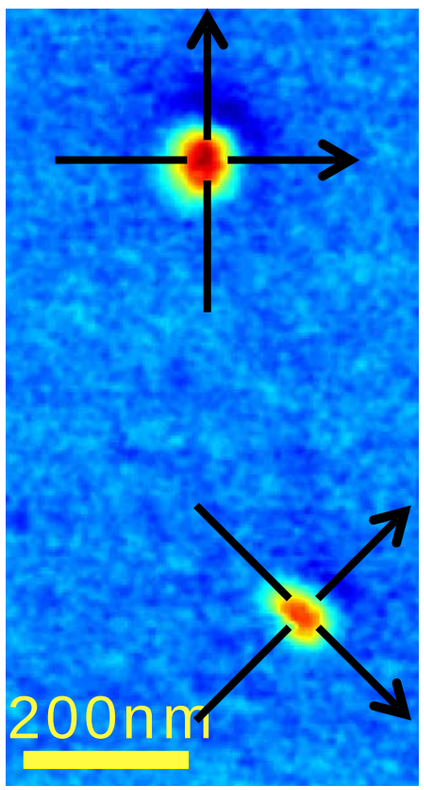

modelled MFM data

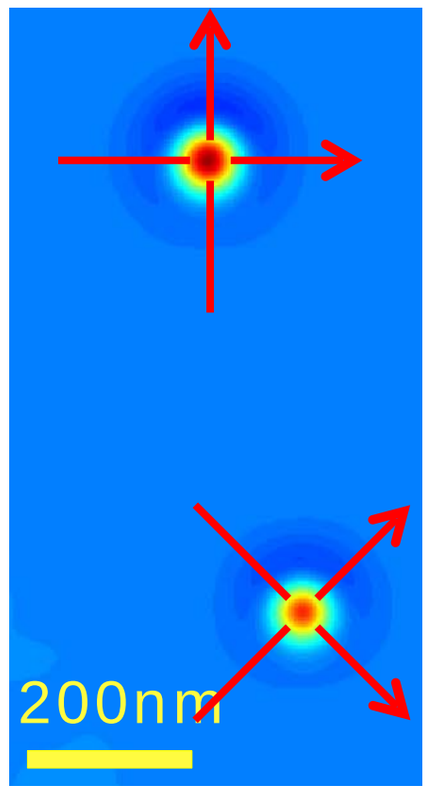

➜ excellent agreement between model and measurement with A = 16pJ/m & K_u = 414kJ/m³

➜ $D_{Sk} \approx 3.5 mJ/m^2 \gg D_{avg} = 1.97 mJ/m^2$

➜ pinning of Skyrmions & Deviations from circular shape

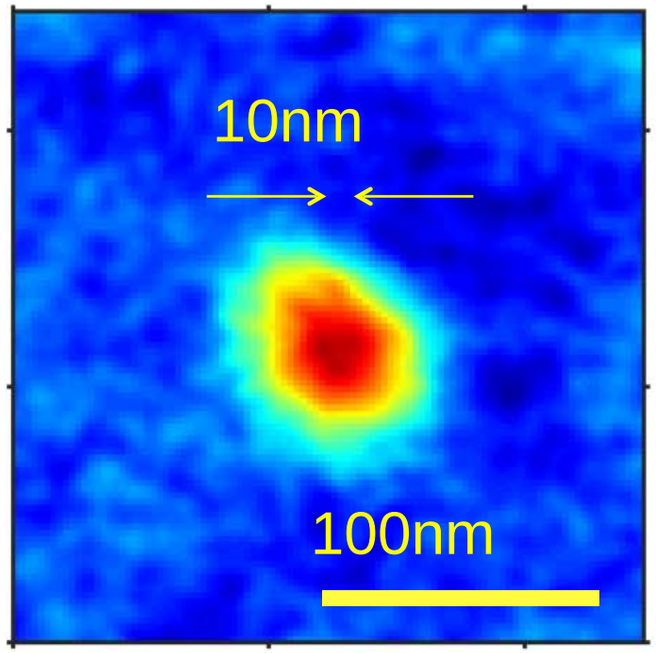

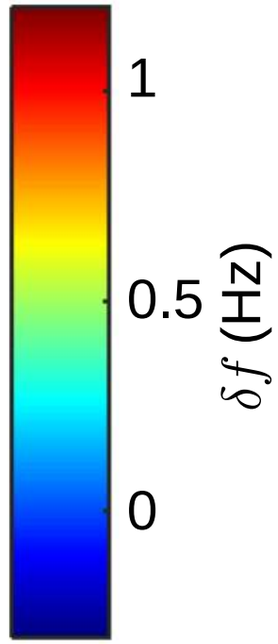

$$ICF_{\delta f,\partial H_z}(\mathbf{k})$$

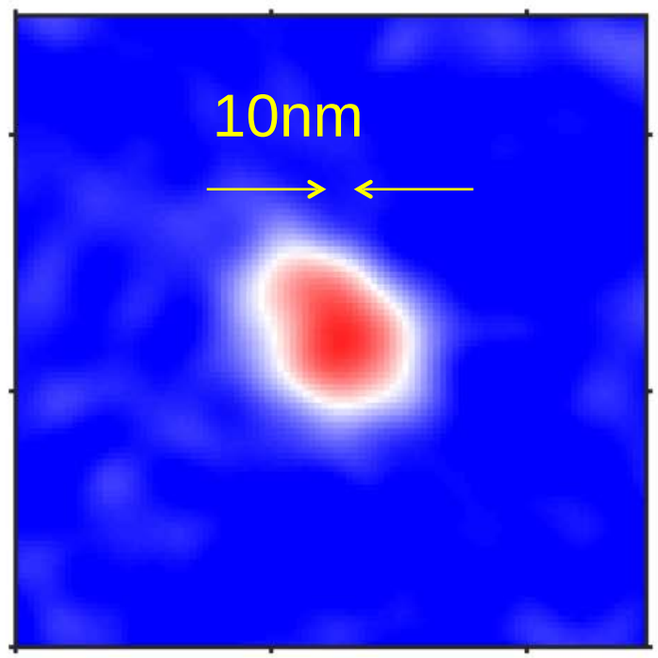

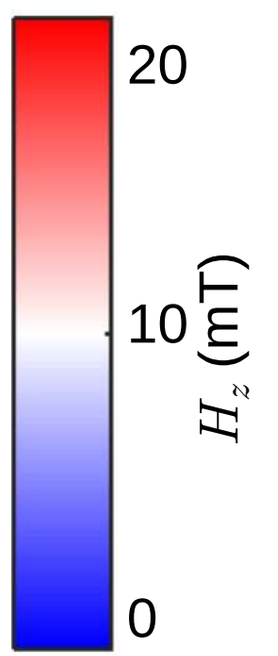

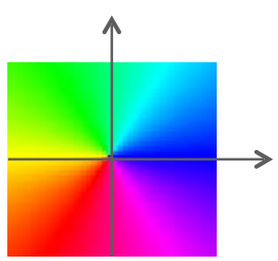

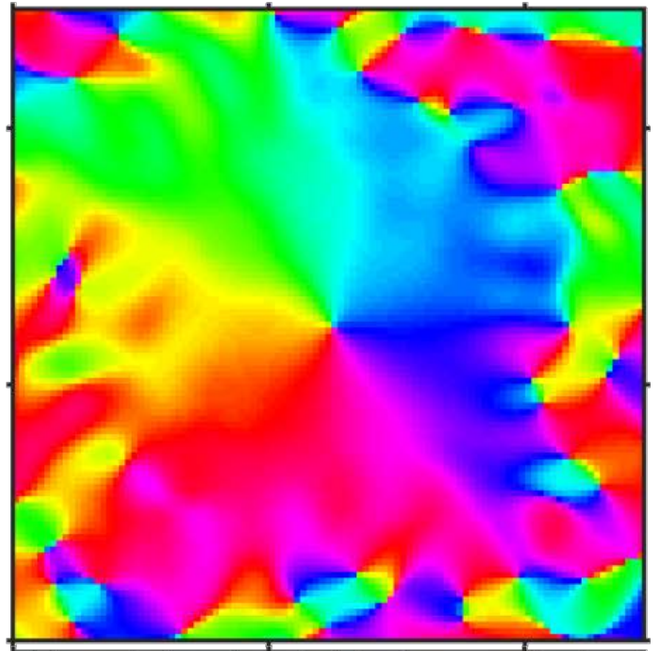

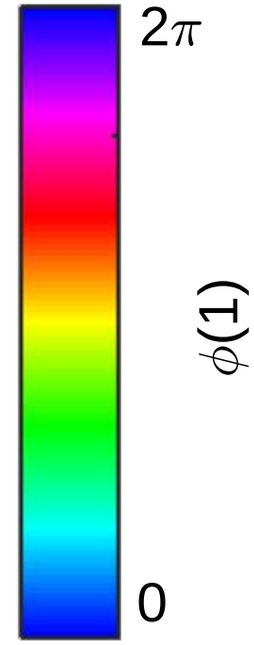

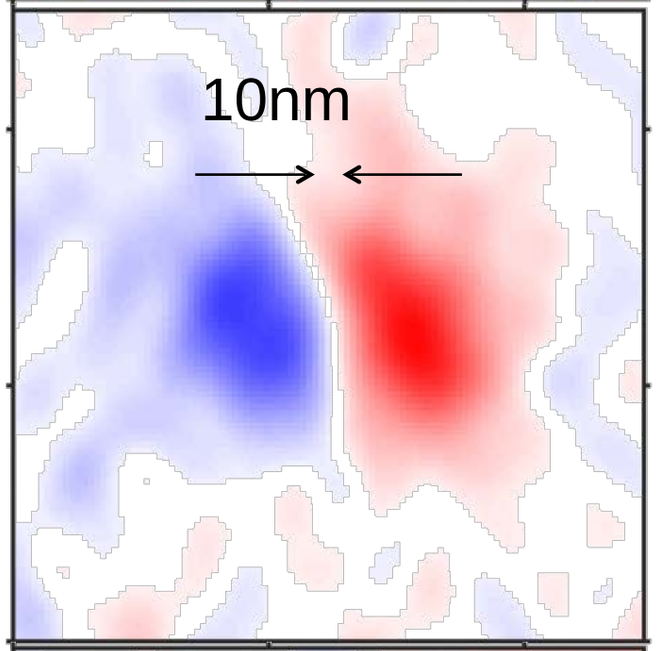

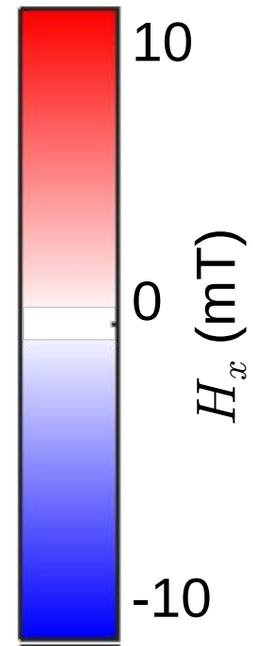

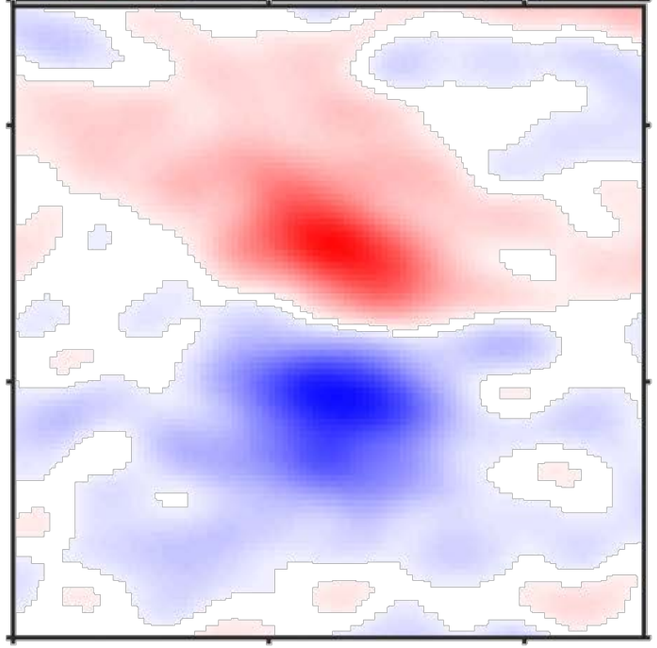

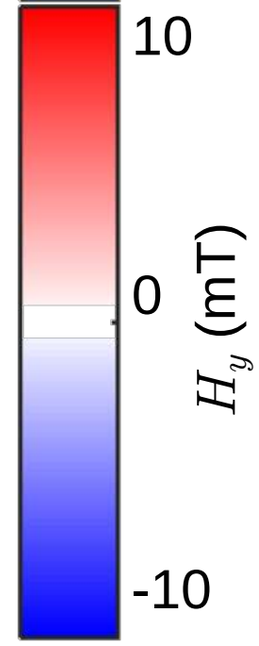

M. Bacani, M. Penedo, M.A. Marioni, and H.J. Hug et al., arXiv:1609.01615 [cond-mat]

4. Cantilever Sensors

Cantilever-based Sensors

bi-metallic	dynamic	static
Heat Source	Resonance frequency-shift	Cantilever Bending
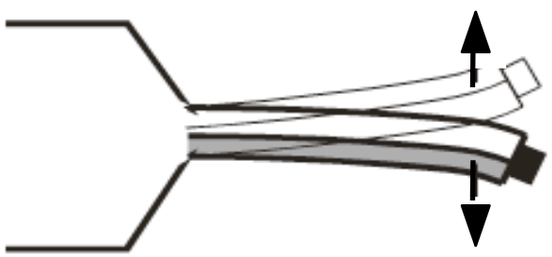	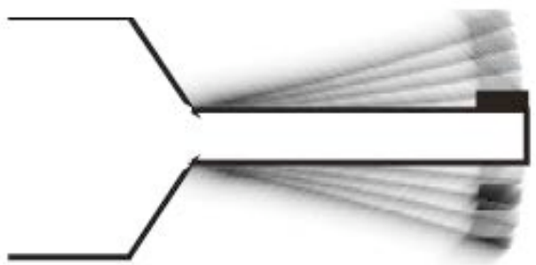	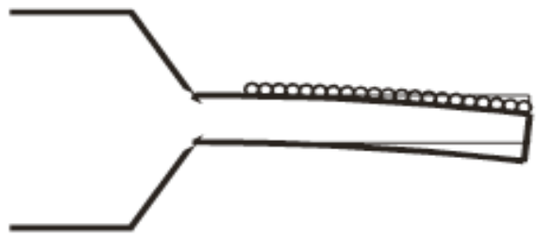
Heat Drain		
Calorimeter Pico-Joule	Microscale Pico-Gramm	Surface Tension Atto-Mol

Important: Functionalization of Cantilever Surface.

Appl. Phys. A 66, S61–S64 (1998)

Applied Physics A
Materials
Science & Processing

A chemical sensor based on a micromechanical cantilever array for the identification of gases and vapors

H.P. Lang[1,2,*], R. Berger[1,2], F. Battiston[2], J.-P. Ramseyer[2], E. Meyer[2], C. Andreoli[1], J. Brugger[1], P. Vettiger[1], M. Despont[1], T. Mezzacasa[3], L. Scandella[3], H.-J. Güntherodt[2], Ch. Gerber[1], J.K. Gimzewski[1]

[1] IBM Research Division, Zurich Research Laboratory, Säumerstrasse 4, CH–8803 Rüschlikon, Switzerland
[2] Institute of Physics, University of Basel, Klingelbergstrasse 82, CH-4056 Basel, Switzerland
[3] Paul-Scherrer-Institute, Laboratory for Micro- and Nanostructures, CH-5232 Villigen-PSI, Switzerland

Cantilever-based Chemical Nose

Principle

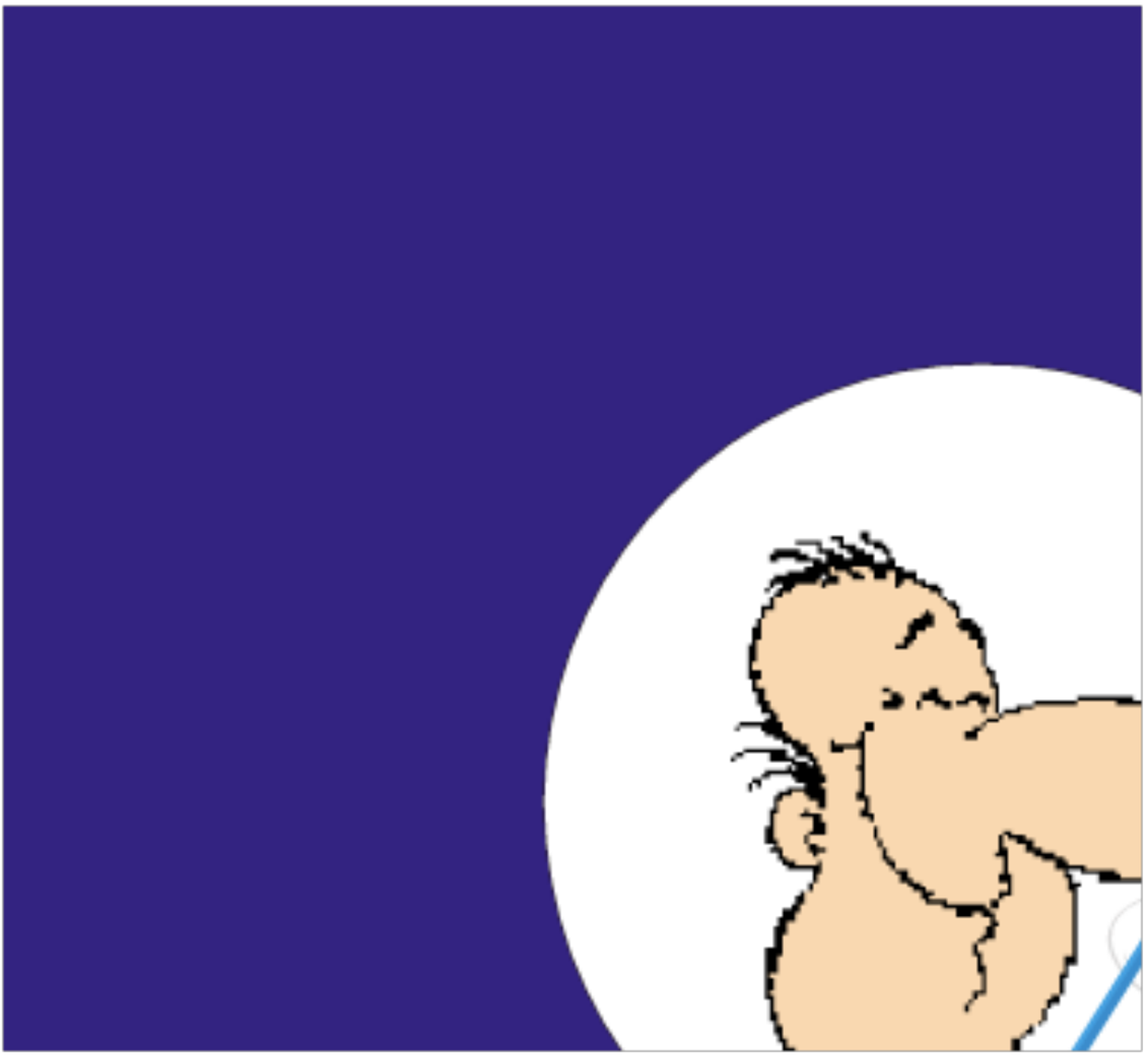

Quantitative Analysis

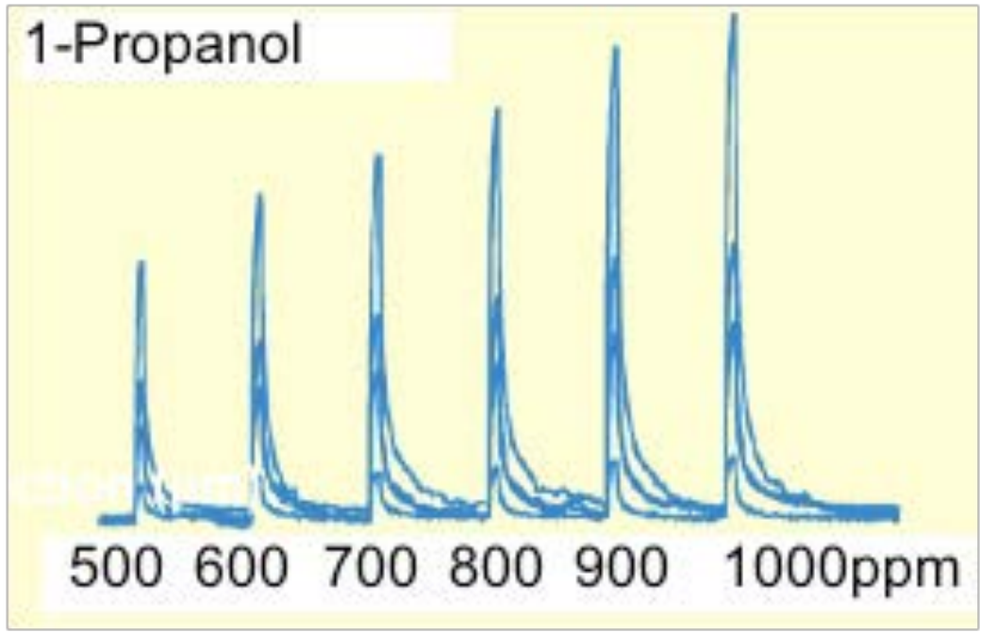

Neuronal Network Analysis

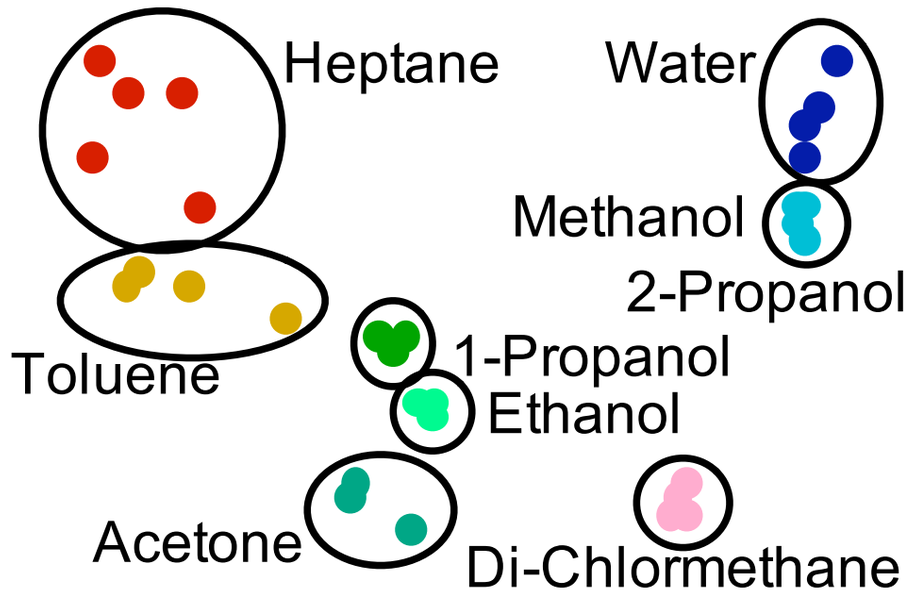

5. SFM combined with other Methods

5.1. Scanning Chemical Force Microscopy

5.1.1. Scanning Chemical Force Microscopy with X-rays

Nano-XAS: a confocal arrangement of a SPM and a STXM

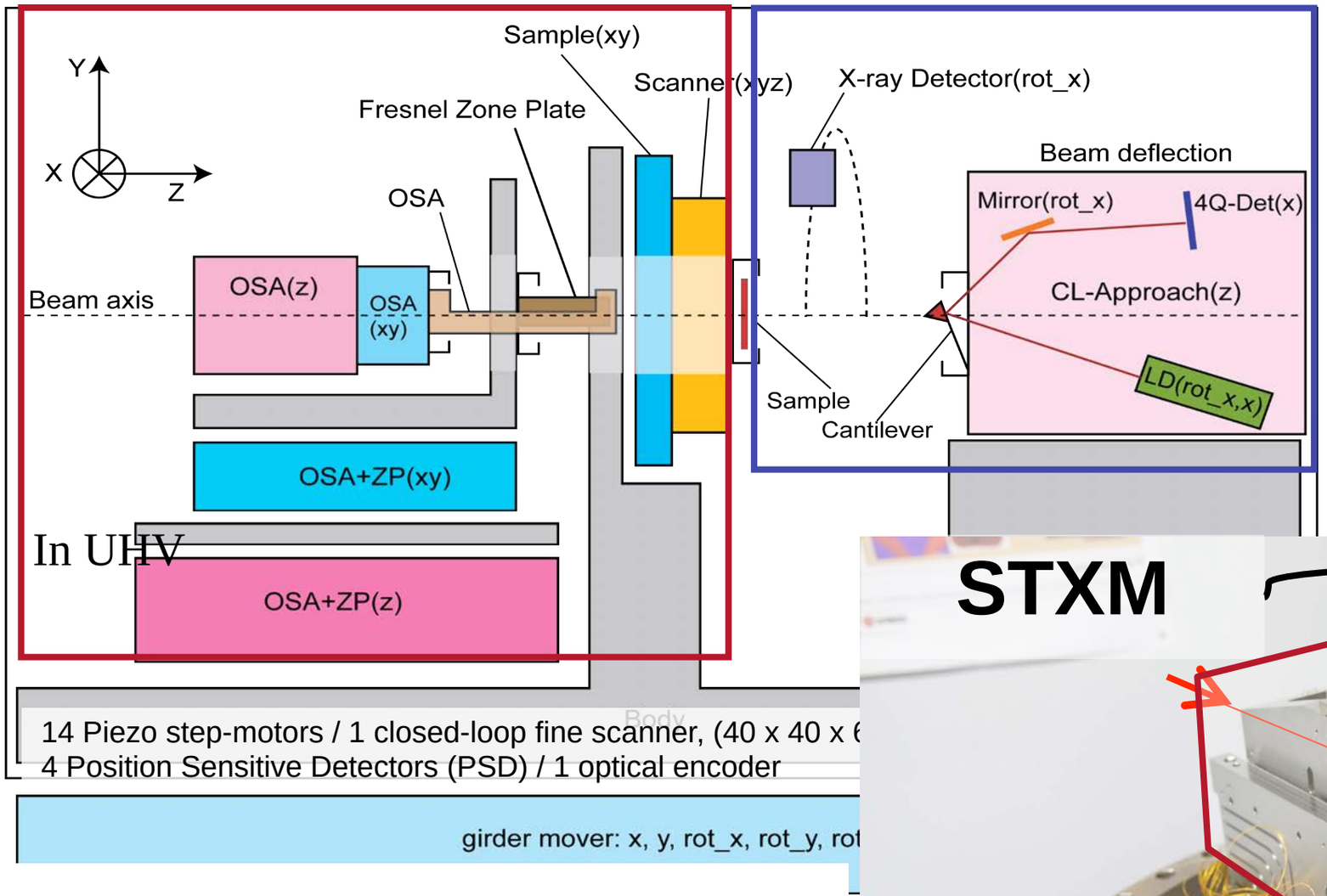

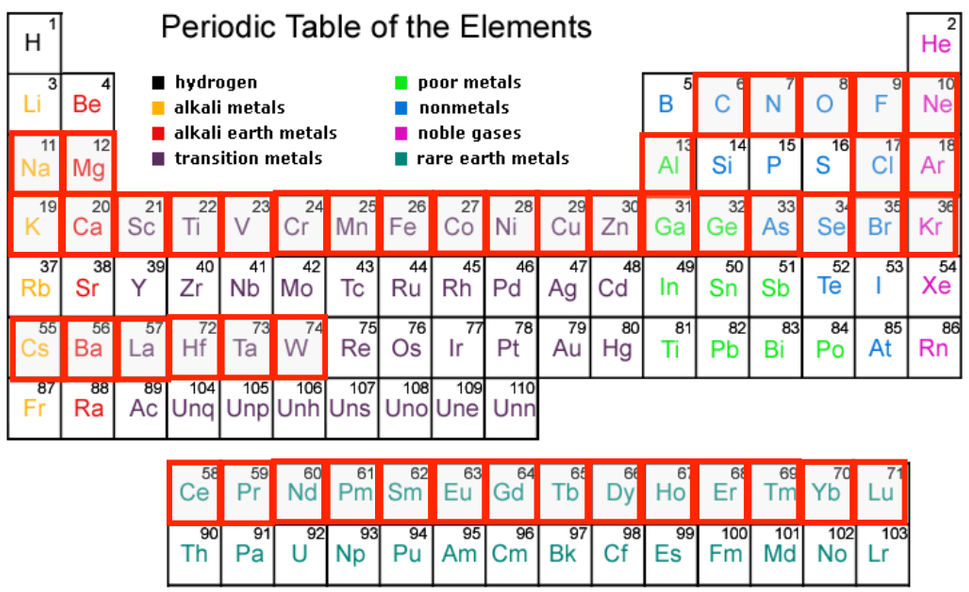

NanoXAS can be operated as a classical Scanning Probe Microscope (SPM):
Scanner range 40µm x 40µm x 6µm

and as a classical Scanning Transmission X-Ray Microscope (STXM) resolution:
~ 40nm, energy range ~270-1800eV
or
As a combined SPM ⊕ STXM

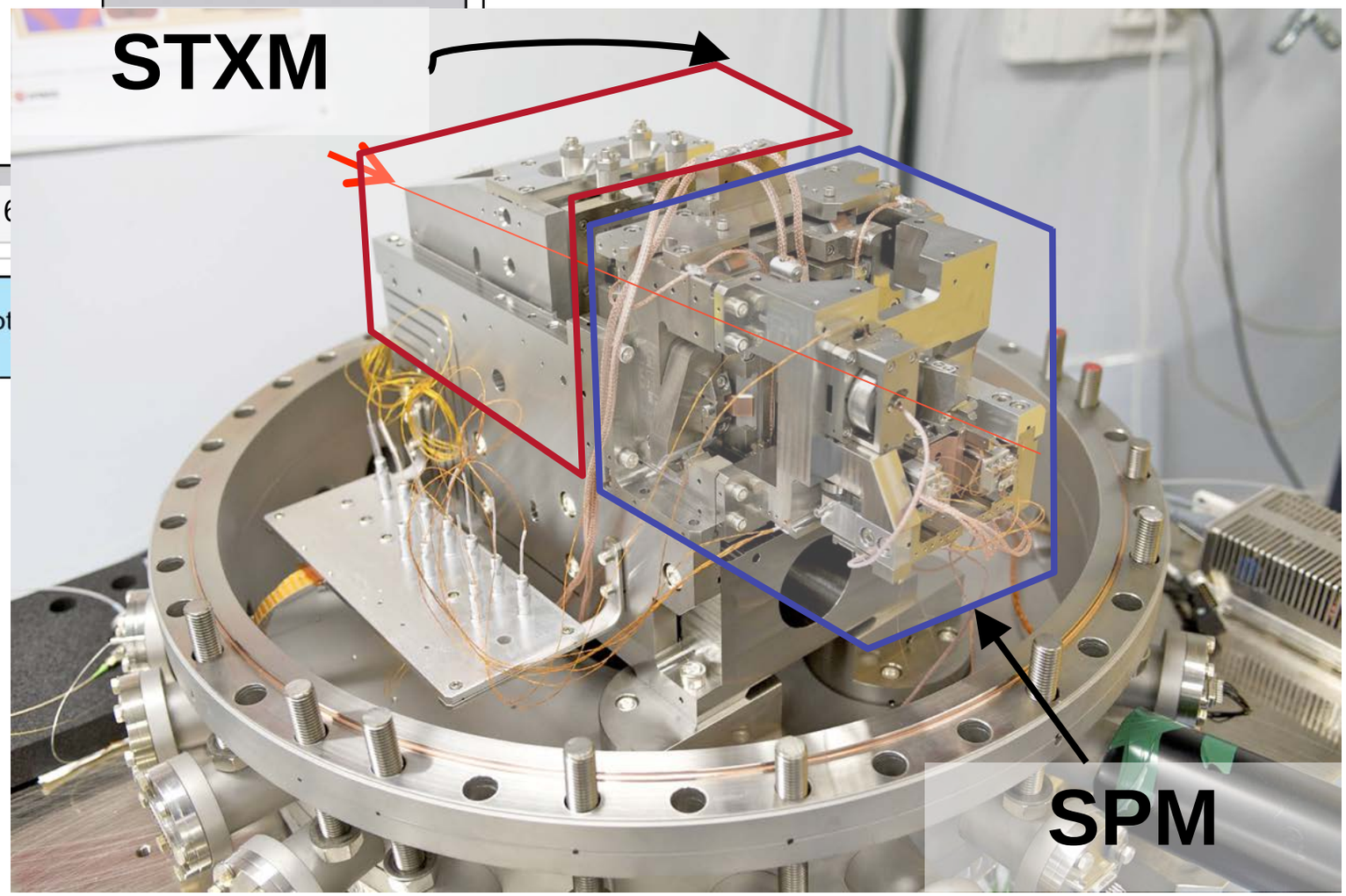

PAUL SCHERRER INSTITUT PSI
EMPA Materials Science & Technology
FAU FRIEDRICH-ALEXANDER UNIVERSITÄT ERLANGEN-NÜRNBERG

Polymer Blend imaged at different x-ray Energies

Materials: poly(3-hexylthiophene) (P3HT) and polystyrol (PS)

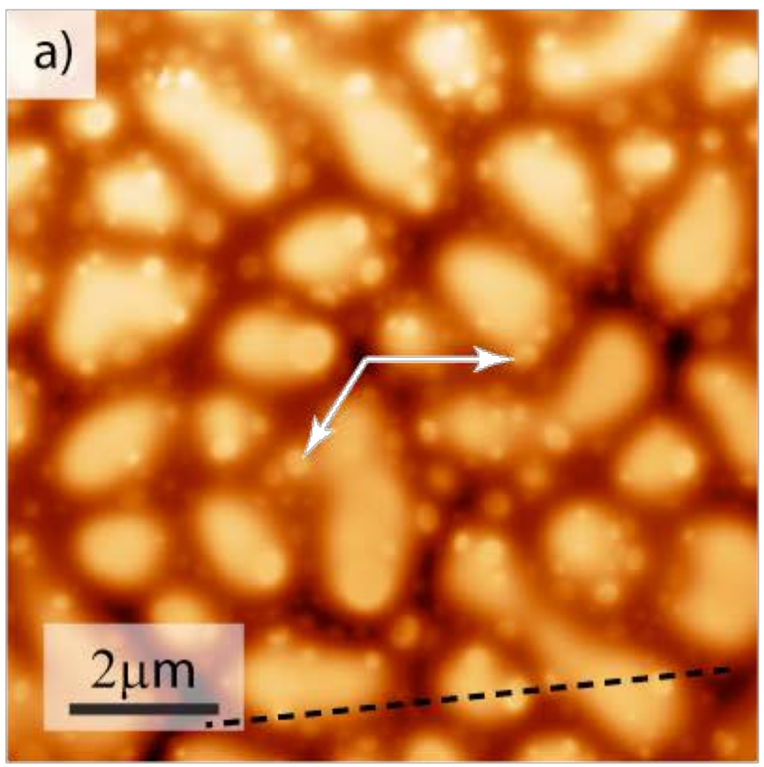

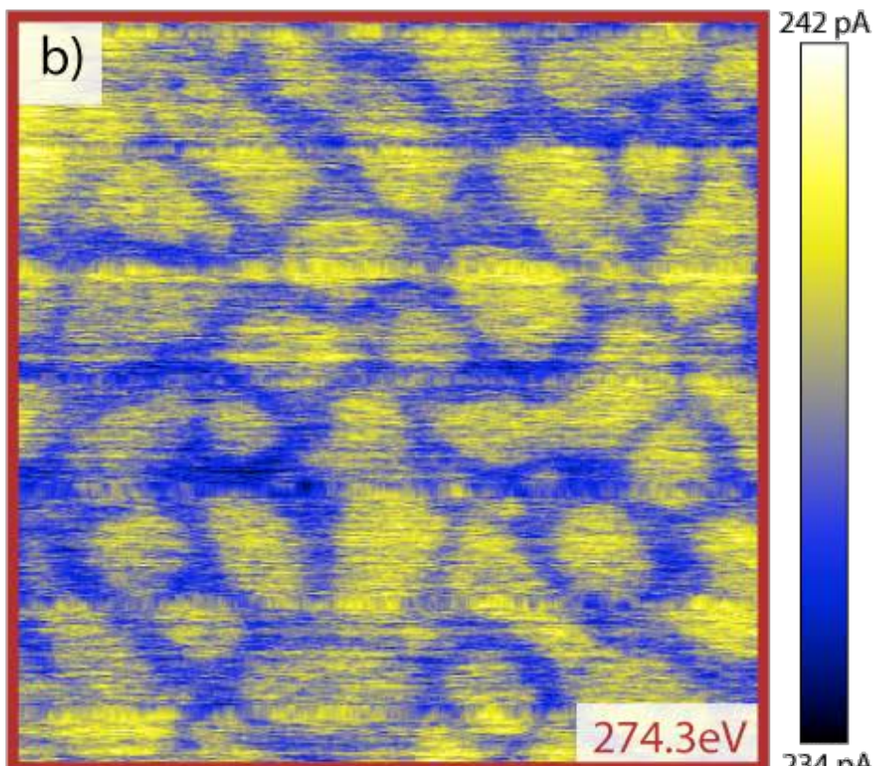

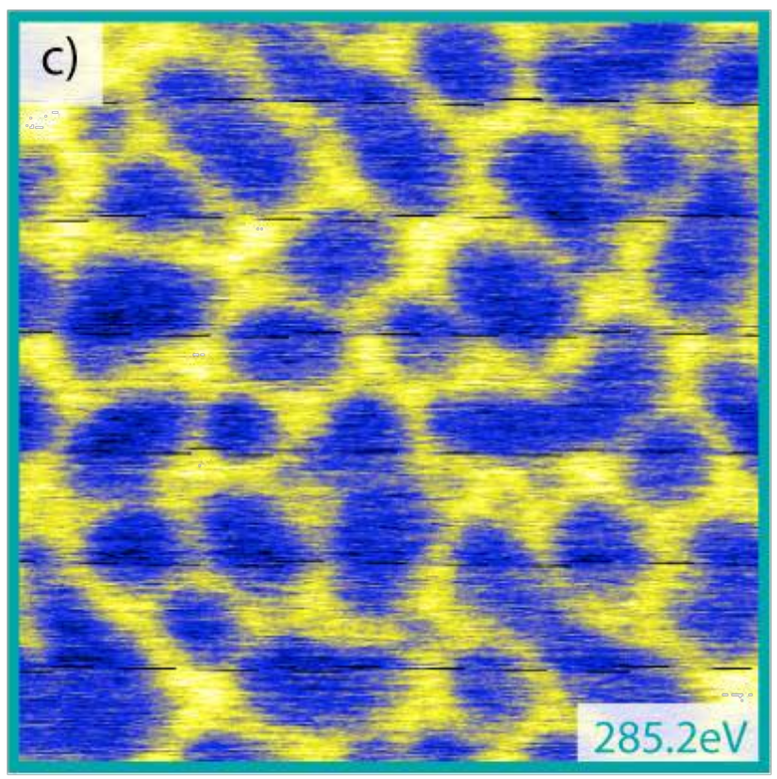

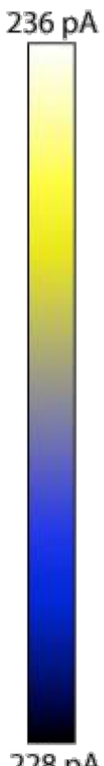

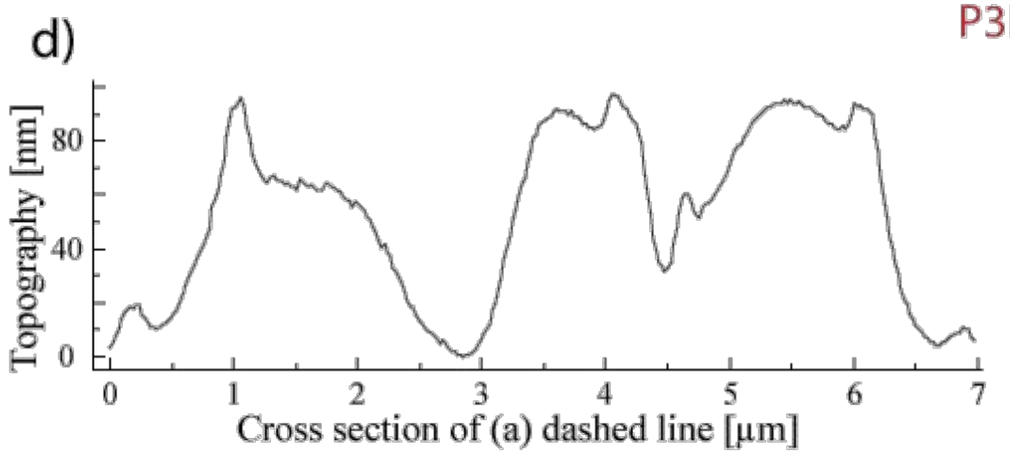

P3HT

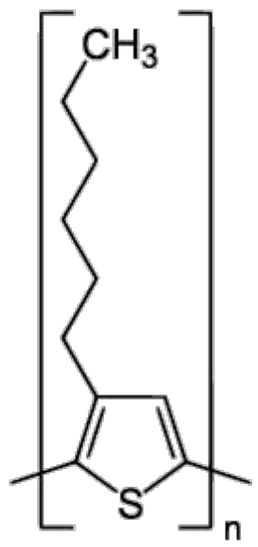

PS

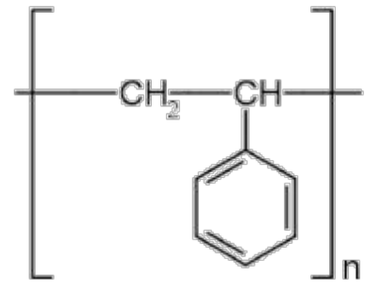

N. Pilet et al. Nanotechnology 23, 475708 (2012)

5.1.2. Scanning Chemical Force Microscopy combination with ToF-SIMS

Time-of-Flight Scanning Ion Mass Spectrometry (ToF-SIMS)

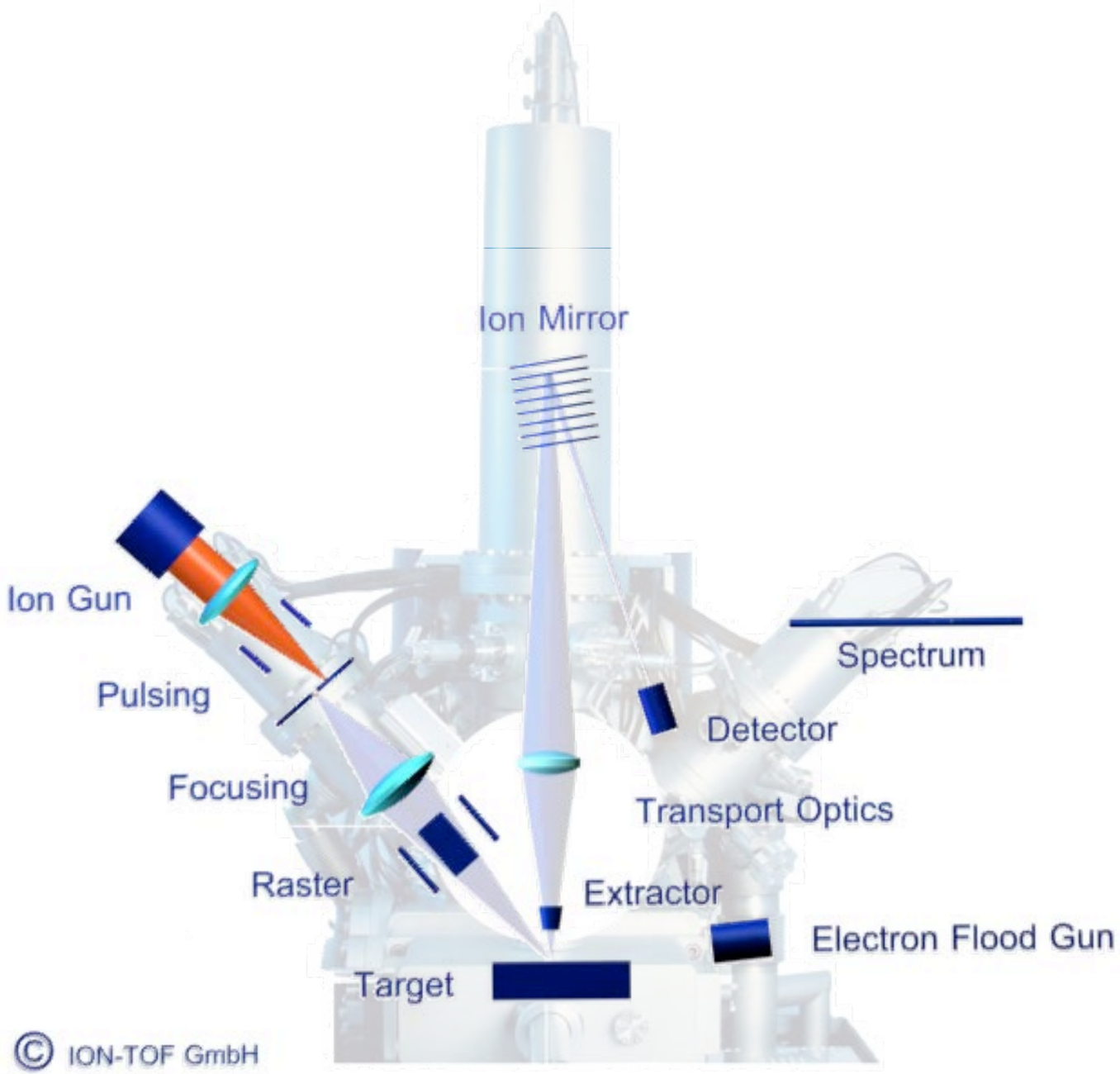

Detection of secondary ions

high sensitivity	ppm – ppb range
detect all elements & isotopes	Si, ^{29}Si, ^{30}Si,
organic and inorganic chem. information	Molecules & -fragments, atoms, clusters
small information depth	first 1-3 at. layers
lateral resolution	~ 100 nm
depth resolution	~ 1 nm
high mass resolution	> 16,000
high mass range	up to 10,000 u
parallel mass detection	

from IONTOF GmbH

Polymer Blend imaged at different x-ray Energies

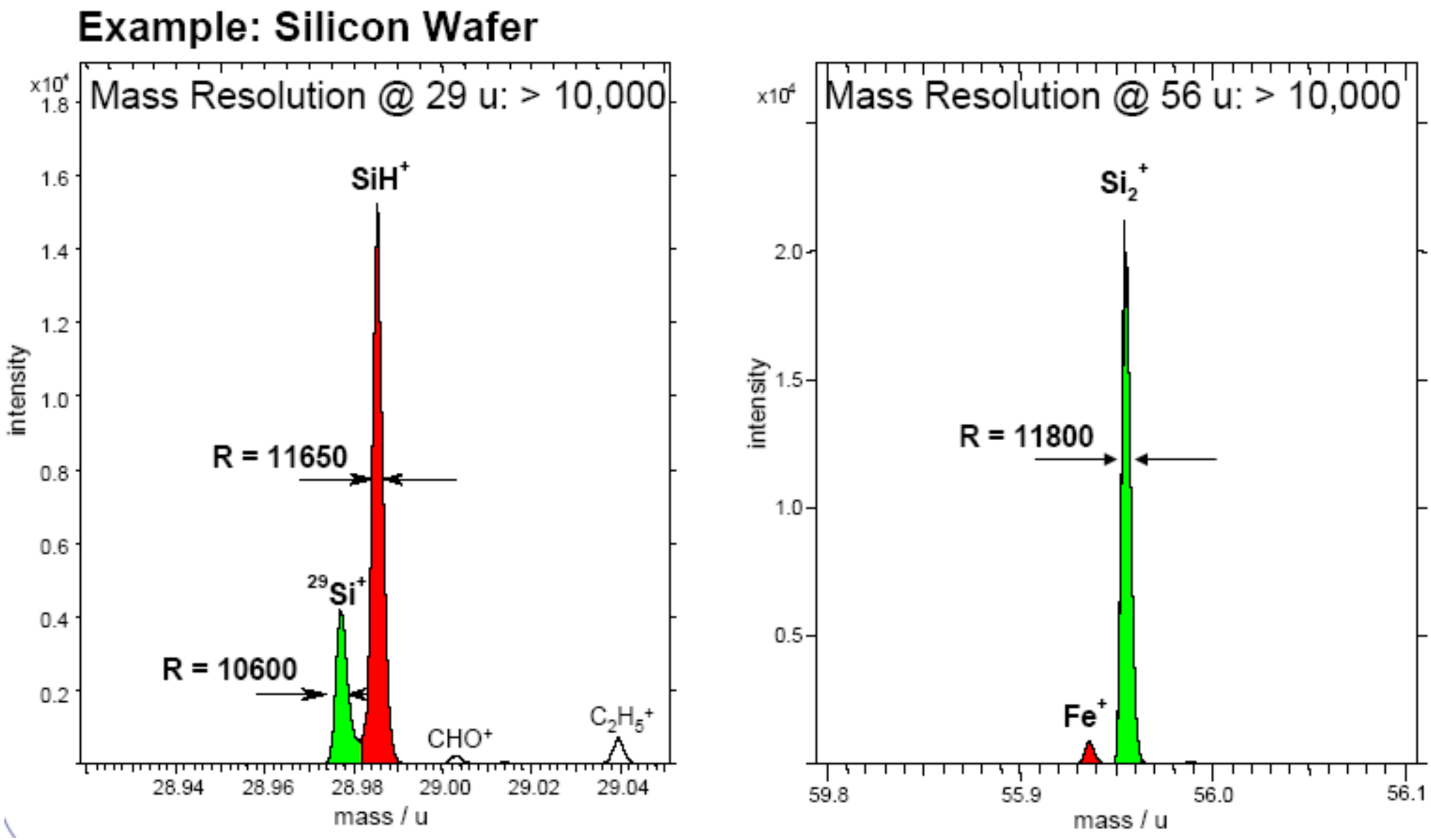

from IONTOF GmbH

3D retrospective analysis: LCD Switch

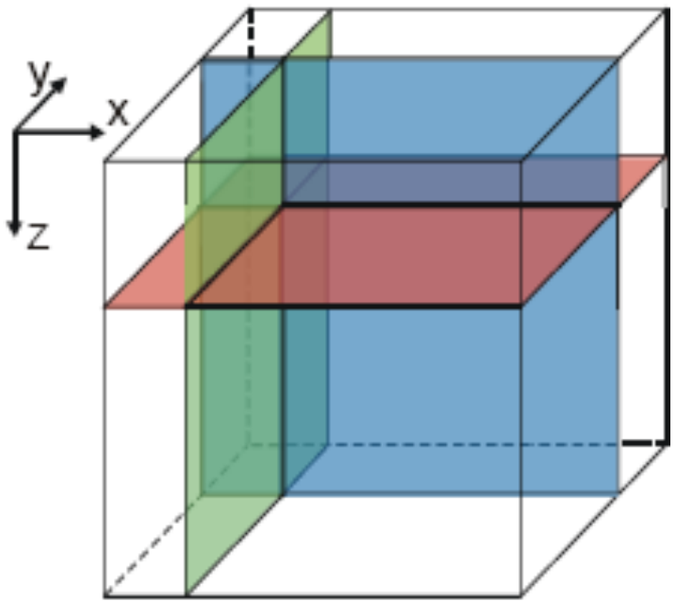

© Ion-Tof GmbH

from IONTOF GmbH

Polymer Blend imaged at different x-ray Energies

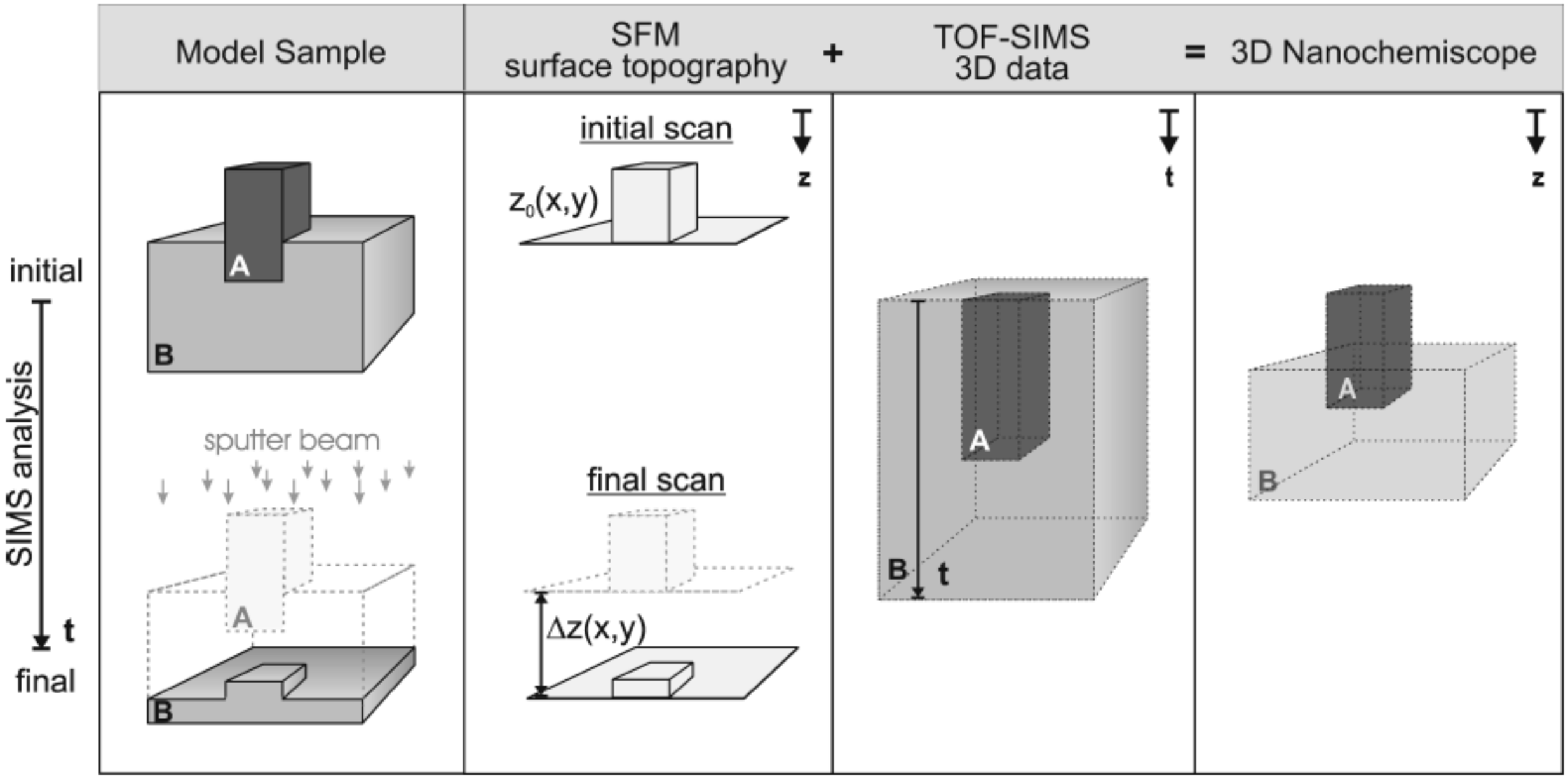

… after 4 yYears of dDevelopment

3D NanoChemicope instrument:

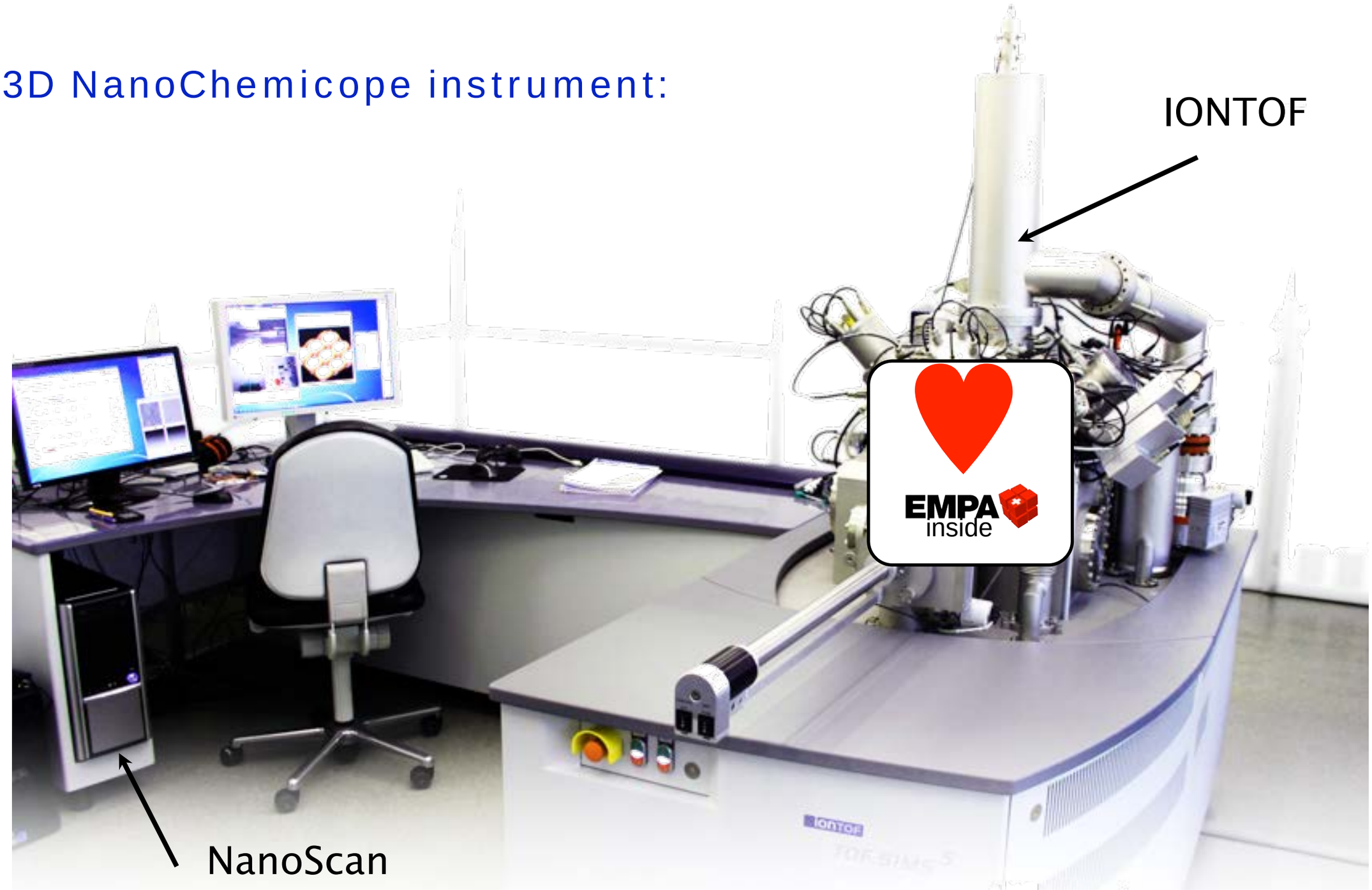

@ IONTOF laboratories

… inside the 3D-Nanochemiscope

SFM measurement position

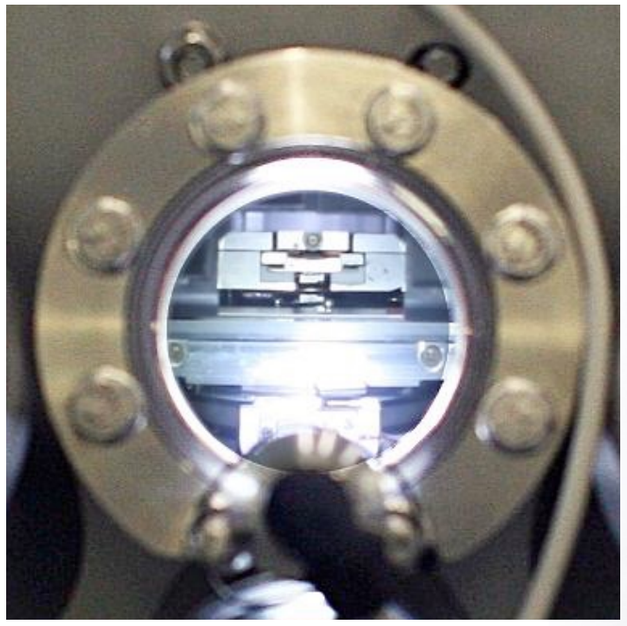

- 40s for 23cm distance, < 0.5um accuracy
- Fast coarse positioning (6mm/s)
- 20nm positioning precision

- bearing-free 5 axis XYZRT stage for ToF-SIMS and SFM operation
- Fast & precise displacement between ToF-SIMS and SFM measurement positions

ToF-SIMS meas. position

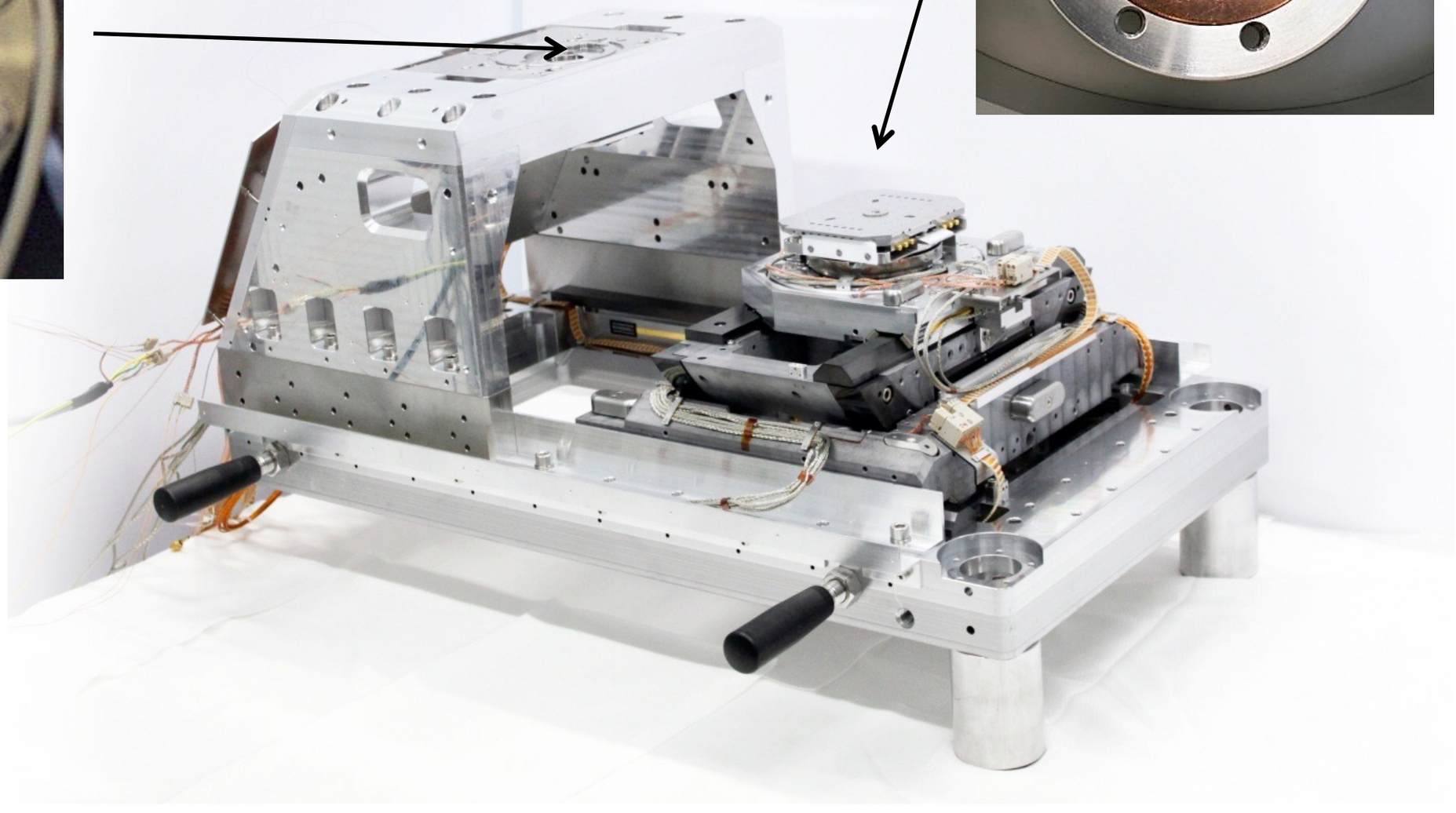

3d Reconstruction of Topography and local Surface

PMMA/Au structures on Si wafer

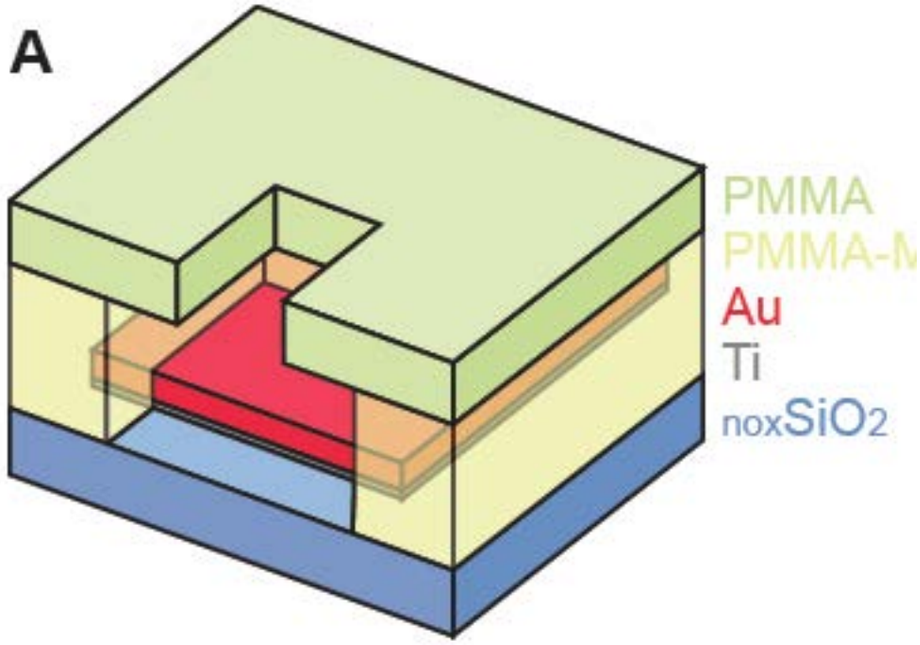

AFM topography

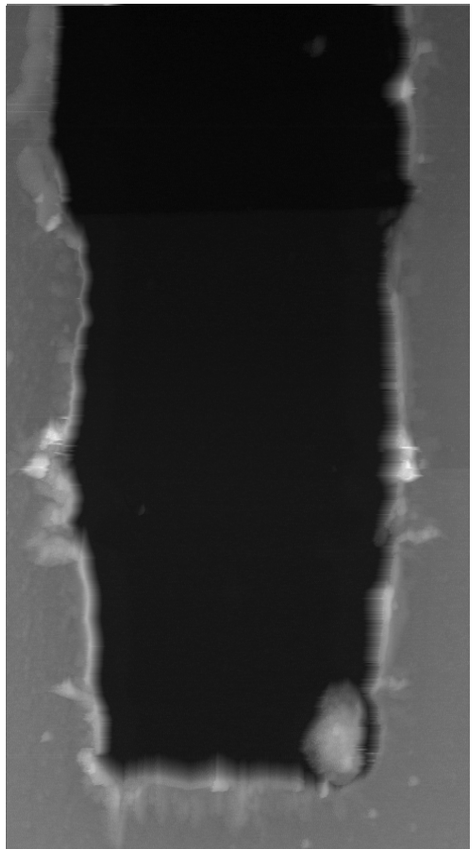

ToF-SIMS chemistry

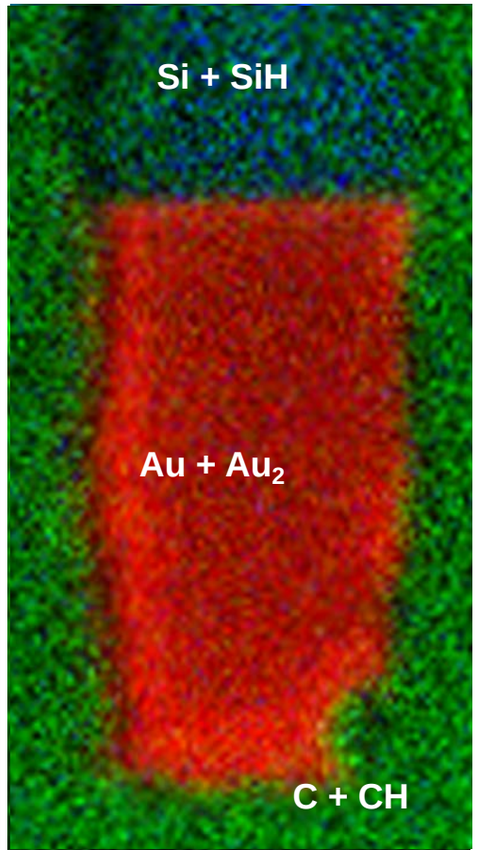

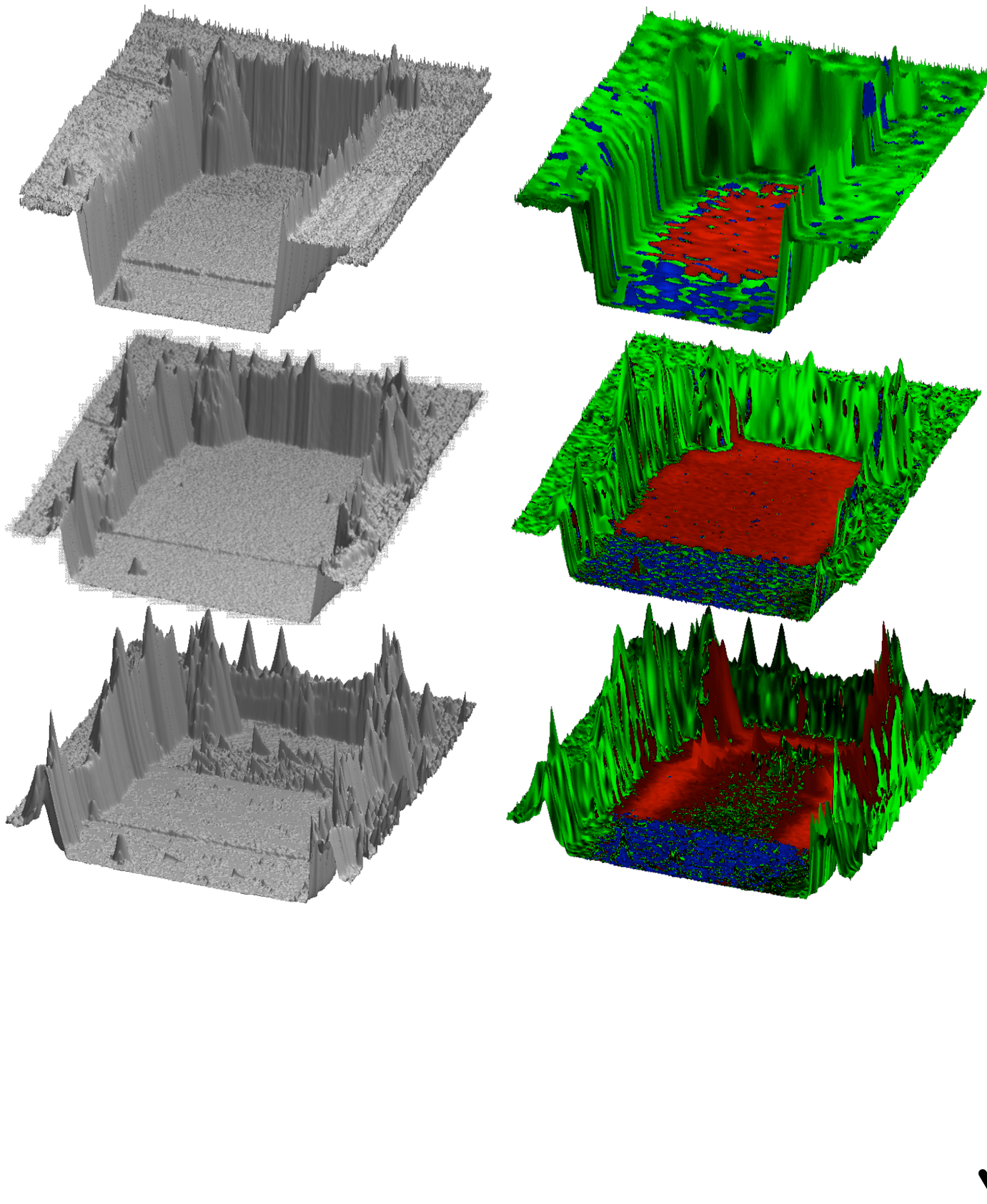

First TOF-SIMS / SPM instrument delivered

Jun 17, 2016

Fully equipped TOF.SIMS NCS with new high-end SPM option

IONTOF is delighted to announce the successful installation of our first, new TOF.SIMS NCS instrument at IMEC in Belgium. The new platform combines all the well-known options of our high-end TOF.SIMS 5 with the possibility to perform in-situ SPM measurements. The sophisticated, large area SPM unit has a scan range of up to 80 x 80 μm^2 and is ideally suited to provide high-resolution topographic information for SIMS measurements. Beside AFM, MFM, KPFM and multi-frequency modes it also supports a unique surface profiler mode which allows for fast measurements of large SIMS sputter craters. The new piezo sample stage with submicron position accuracy ensures fast and precise movement between the TOF-SIMS and the SPM measurement position.

With this new tool IONTOF now offers the ideal instrument for nano characterisation and high-performance SIMS imaging. If you would like to learn more about this fascinating new tool please feel free to contact us.

5.1.3. Scanning Force and IR Microscopy

AFM-IR: Breakthrough nanoscale infrared spectroscopy

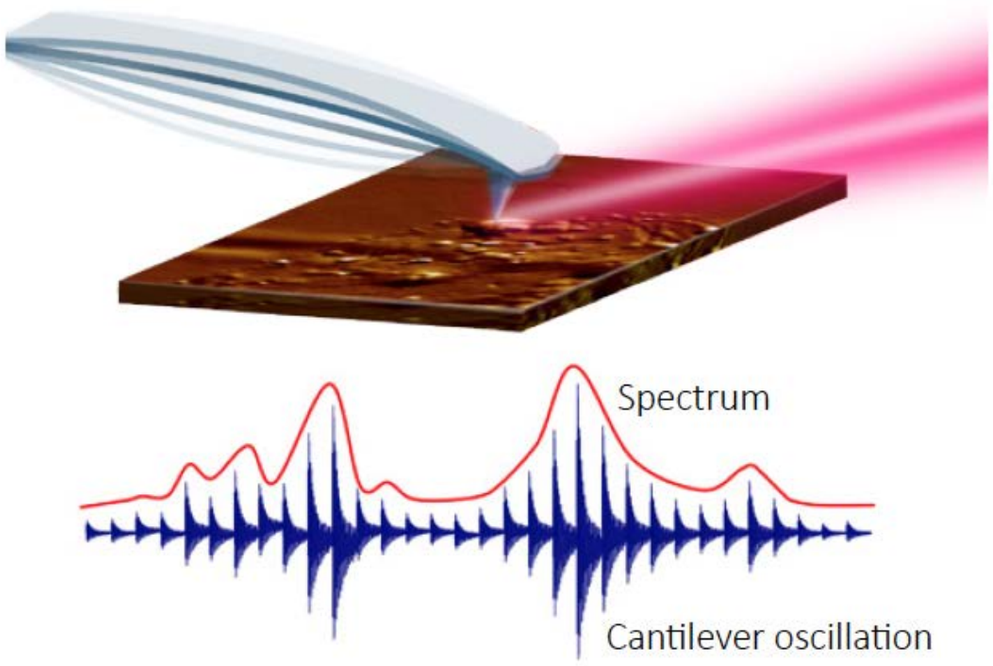

AFM-IR: How it works

Pulses of infrared laser radiation tuned to an absorbance band of a material causes an abrupt and short-lived thermal expansion. The rapid expansion excites resonant oscillation of the AFM cantilever in contact with the surface. The amplitude of the cantilever oscillation is directly proportional to the sample absorption coefficient. An AFM-IR absorption spectrum is created by measuring the cantilever oscillation amplitude while scanning the laser across the spectral range of interest. The resulting absorption spectrum is a unique chemical fingerprint of a nanoscale region of the sample under the AFM probe tip.

Results

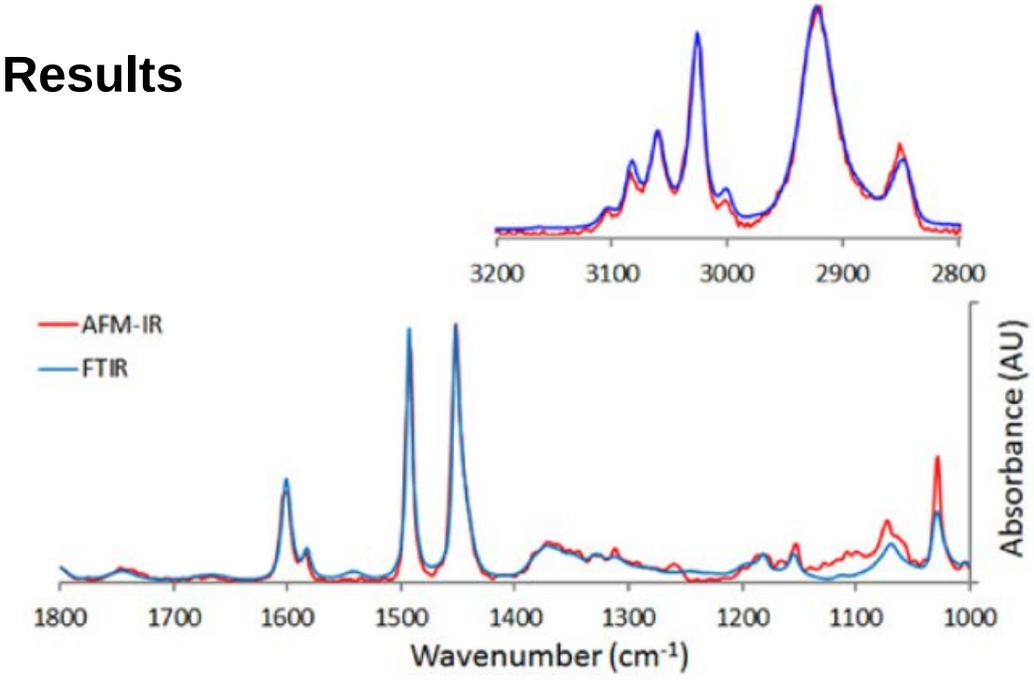

Monolayer Sensitivity

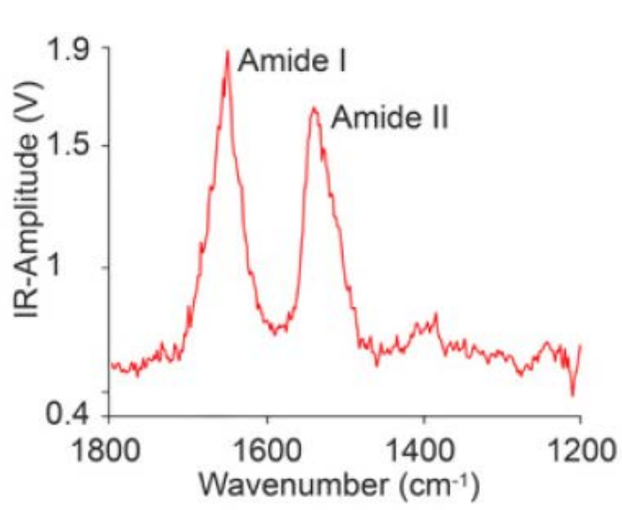

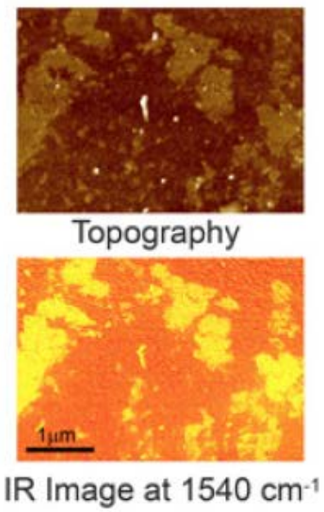

Halobacterium Salinarum deposited on a Au substrate, membrane is ~ 5 nm, thick.

ANASYS INSTRUMENTS
The nanoscale analysis company

325 Chapala Street, Santa Barbara, CA 93101 | Phone: (805) 730-3310 Fax: (805) 730-3300
http://www.anasysinstruments.com | info@anasysinstruments.com

AFM-IR: Breakthrough nanoscale infrared spectroscopy

Polymer interface chemistry

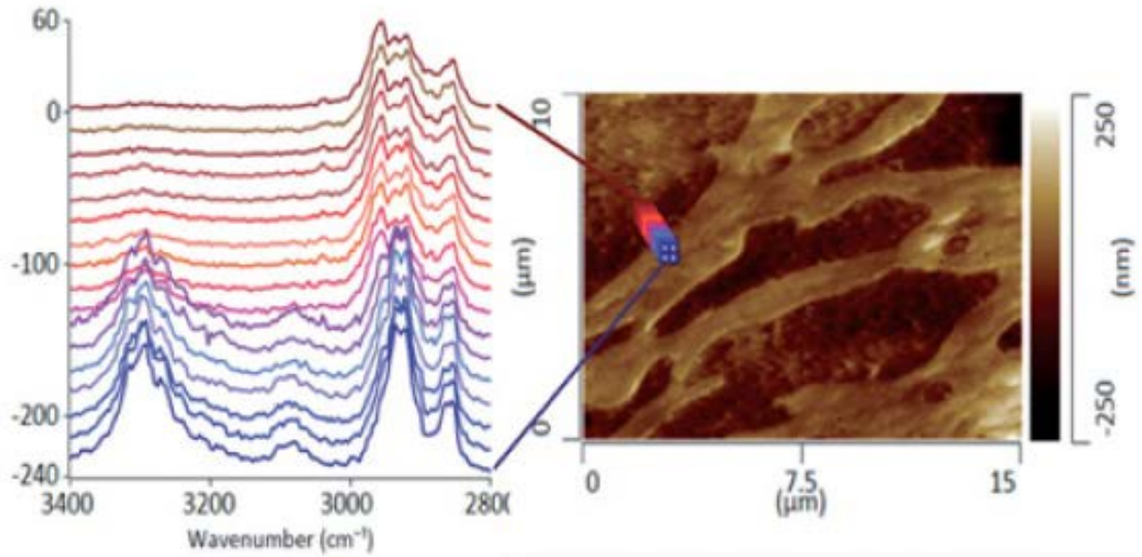

AFM-IR spectra (left) and morphology (right) of a polymer blend across a rubber/nylon interface.

Multilayer films

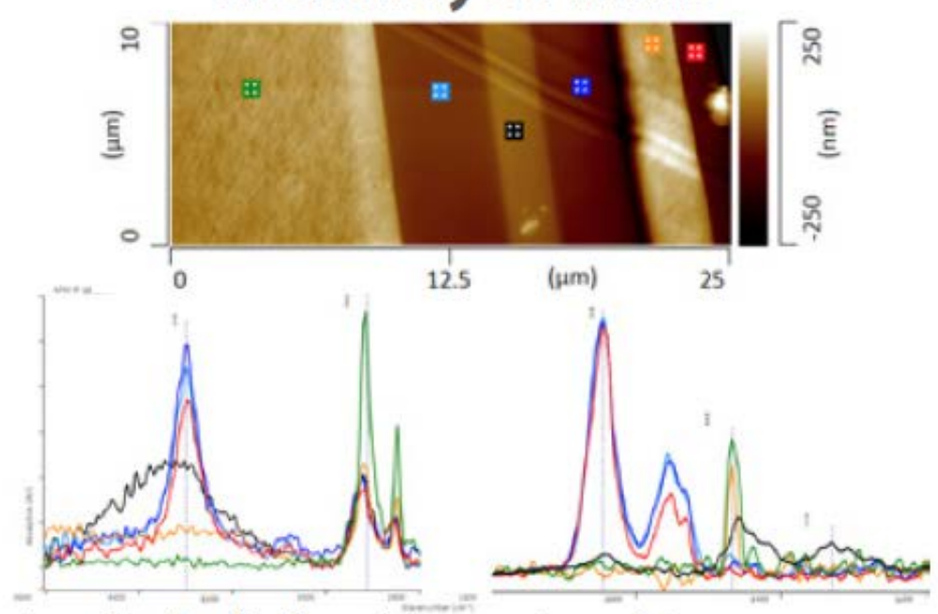

AFM-IR chemically distinguishes polyamide vs. polyethylene film components.

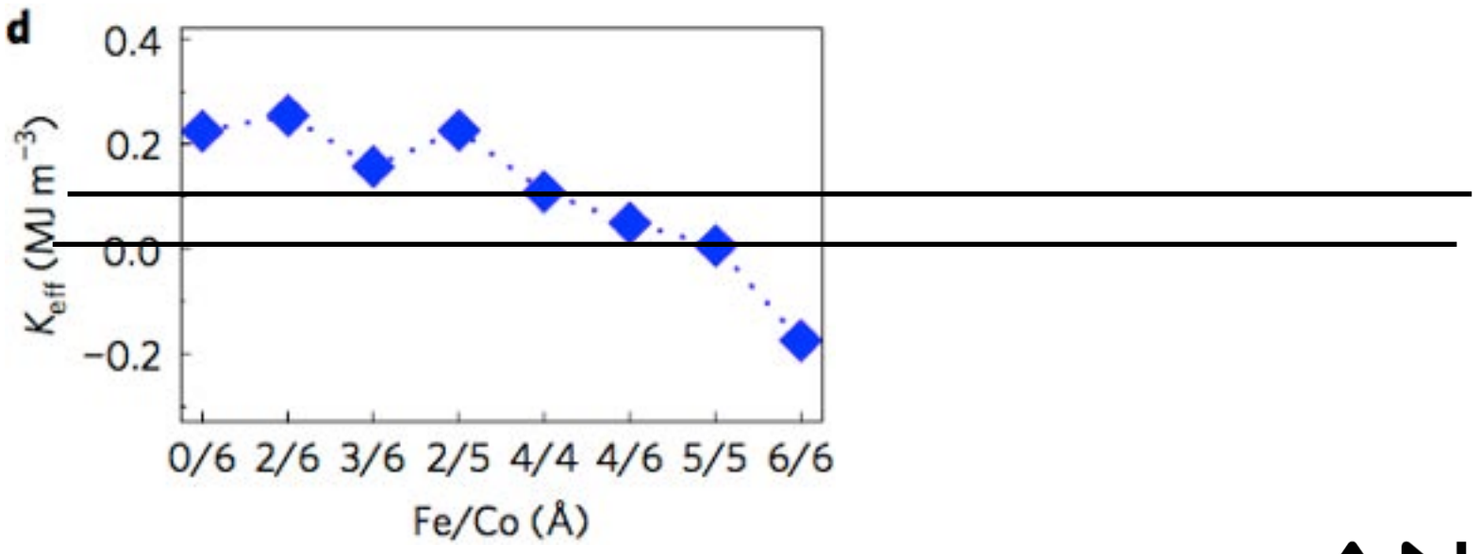

ANASYS INSTRUMENTS
The nanoscale analysis company
325 Chapala Street, Santa Barbara, CA 93101 | Phone: (805) 730-3310 Fax: (805) 730-3300
http://www.anasysinstruments.com | info@anasysinstruments.com